EU Horizon 2020 Research & Innovation Program
Digital transformation in Health and Care
SC1-DTH-06-2020
Grant Agreement No. 101016496

SimCardioTest - Simulation of Cardiac Devices & Drugs for in-silico Testing and Certification

SIM CARDIO TEST

Technical Report

D 6.1: Verification & uncertainty quantification for the use cases of WP2-4

Work Package 6 (WP6)

Verification, validation, uncertainty quantification & certification

Task Lead: UBx, France

WP Lead: MPC, France

PUBLIC

DELIVERABLE INFORMATION

Deliverable number	D6.1
Deliverable title	Verification & uncertainty quantification for the use cases of WP2-5
Description	Implementation of Verification on a selection of Models developed for the Use Cases of WP2-4
Lead authors	Romano SETZU (MPC)
Contributors	For UC1 (WP2): Yves COUDIERE (UBx) For UC2 (WP3): Oscar CAMARA (UPF) For UC3 (WP4): Beatriz TRENOR (UPV), Maria Teresa MORA (UPV)
Due date	M30
Submission date	30/06/2023 And 25/09/2025
Comments	This version, updated on 24 September 2025, includes **ANNEX A** (WP6 complement of D6.1 and D6.2) & **ANNEX B** (WP6 UC3 PK Verification), which cover the additional work carried out between M30 and M54.

Document history			
Date	**Version**	**Author(s)**	**Comments**
22/05/2023	V1	R. SETZU	First Draft
22/06/2023	V2	R. SETZU, D. FEURESTEIN, G. FAURE, M. LEGUEBE, Y. COUDIERE A. OLIVARES, J. MILL, C. ALBORS, O. CAMARA M. T. MORA, B. TRENOR, J. WELZEL, I. VAN HERCK, H. FINSBERG A. BARETTA, F. SIPS, M. GAZZIN	First consolidated draft including contributions from UC1/2/3
29/06/2023	V3	H. AREVALO	Quality Review
30/06/2023	V4	R. SETZU	Final Version
01/07/2024	V5	R. SETZU, M. BARBIER	Format editing
24/09/2025	VF	M. BARBIER	Addition of **Annexes A** (WP6 complement of D6.1 and D6.2) & **B** (WP6 UC3 PK Verification)

TABLE OF CONTENTS

EXECUTIVE SUMMARY

This report and its annexes constitute the SimCardioTest WP6 deliverable D6.1 due in June 2023 (M30). It describes all verification activities engaged for assessing the credibility of computational models developed in the frame of Use Cases 1 to 3 (cf. WP2, 3, and 4 respectively). This report is closely linked to SCT deliverable D6.2 which reports the validation activities also supporting the credibility of these same models.

Verification is conducted on one specific model per each Use Case, corresponding to a pre-selected Question of Interest (QI). All verification activities are conducted according to ASME VV40 standard guidelines. While the main document body summarizes all verification activities, the detailed technical description of this work is reported on the attached documents which are included in the annex of this document.

Some of the engaged verification activities are still ongoing at the date of this publication, and will be documented at later time once completed.

Acronyms

Table 1: List of Acronyms.

Acronym	Meaning
AF	Atrial Fibrillation
ASME	The American Society of Mechanical Engineers
Avg.	Average (abbreviation)
CEPS	Cardiac ElectroPhysiology Solver (cf. Use Case 1)
CFD	Computational Fluid Dynamic
CI	Continuous Integration
CiPA	Comprehensive in-vitro Proarrhythmia Assay (cf. Use Case 3)
COU	Context of Use
DE	Discretization Error (in Verification)
DRT	Device-Related Thrombosis
ECG	Electrocardiogram
EP-0D	0D Electrophysiology Model (cf. Use Case 3)
EP-3D	3D Electrophysiology Model (cf. Use Case 3)
EXC	ExactCure
FDA	US Food and Drug Administration
IST	INSILICOTRIALS TECHNOLOGIES SRL Also referring to the Cloud service hosting the models
LA	Left Atrium
LAAO	Left Atrial Appendage Occluder
MOTS	Modified Off-the-Shelf Software
MPC	MICROPORT CRM - SORIN CRM SAS
MV	Mitral Valve
N.A. / n.a.	Not Applicable
NCV	Numerical Code Verification
NSE	Numerical Solver Error (in Verification)
ODE	Ordinary Differential Equations
OTS	Off-the-Shelf Software

Acronym	Meaning
PK	Pharmacokinetics Model (cf. Use Case 3)
PR	Pulmonary Ridge
PV	Pulmonary Vein
QI	**Question** of Interest
QoI	**Quantity** of Interest
SCT	SimCardioTest
SQA	Software Quality Assurance (in Verification)
SRL	SIMULA RESEARCH LABORATORY AS
TAWSS	Time-Averaged Wall Shear Stress
TC	Test Condition (in Validation)
TdP	Torsade de Pointes
TS	Test Sample (in Validation)
UB / U.B.	Uncertainty Budget
UBx	Université de Bordeaux
UC	Use Case
UD	User Developed (Software)
UE	Use Error (in Verification)
UPF	UNIVERSIDAD POMPEU FABRA
UPV	UNIVERSITAT POLITECNICA DE VALENCIA
V&V, VV	Verification & Validation
VVUQ	Verification, Validation, and Uncertainty Quantification
WP	Work Package
WSS	Wall Shear Stress

Table 2: Table cell background colour-code used across the document to identify and differentiate VV40 items: Verification, Validation, Applicability.

Background Cell Colour-Code
"Light Green" for Verification Items
"Salmon" for Validation Items
"Light Blue" for Applicability Items

1. Introduction

This report and its annexes constitute the SimCardioTest WP6 deliverable D6.1 due in June 2023 (M30). It describes all verification activities engaged for assessing the credibility of computational models developed in the frame of Use Cases 1 to 3 (cf. WP2, 3, and 4 respectively). This report is closely linked to SCT deliverable D6.2 which reports the validation activities also supporting the credibility of these same models.

1.1 Normative Background

Until recently, medical device and drugs manufacturers have been lacking a harmonized framework for supporting the use of computational modelling in their regulatory submissions. For this reason the American Society of Mechanical Engineers (ASME) together with the US Food and Drug Administration (FDA) and key industry stakeholders have developed a risk-supported credibility assessment framework. The result of this joint effort is the ASME VV40 standard which has been published in 2019 [1].

ASME VV40 organizes the V&V activities in three distinct phases:

- Model Verification
- Model Validation
- Model Applicability

Model Verification comprises those activities meant to demonstrate that the numerical model accurately represents the underlying mathematical model. Model Validation comprises those activities meant to show how well the numerical model represents reality. Finally Model Applicability comprises those activities meant to show the relevance of validation activities to support the use of the numerical model in the selected context of use.

Each V&V activity listed in ASME VV40 addresses a specific credibility factor. All credibility factors contribute to the overall credibility of the numerical model. How well a credibility factor must be investigated depends on the model risk, intended as the result on the importance that the numerical model supposedly has in taking clinical decisions and the severity of clinical consequences in case the model leads to wrong decisions.

Up to this date VV40 remains to our knowledge the most appropriate document for addressing verification and validation of numerical models. Nor are we aware of other international standards addressing this topic on the process of being written.

WP6 recognizes that currently this document is the most complete and sound approach for conducting V&V activities meant to support the credibility of the computational models developed in the frame of the SimCardioTest project.

1.2 Global V&V Strategy

Running full Validation and Verification according to ASME VV40 guidance in the frame of WP6 activities has a double objective. On one hand it allows to gain credibility on the selected numerical models, and to show how a file should be built for presenting numerical models as part of official regulatory submissions of new drugs and medical devices. On the other hand it allows to benchmark the feasibility and the usability of the ASME VV40 standard itself in a real case scenario, this document being relatively young and still lacking relevant feedback from the industry on its applicability.

Due to the significant amount of work and complexity for running a complete V&V on a given numerical model according to ASME VV40 guidelines, only one model per Use Case will be addressed in the frame of WP6 activities.

The selected models will address these specific aspects:

- For Use Case 1 (WP2): Pacing leads electrical performance
- For Use Case 2 (WP3): Left Atrial Appendage Occluders (LAAO) safety
- For Use Case 3 (WP4): Drugs safety

Even if only one numerical model will be directly addressed, the V&V framework consolidated at the end of this work will be directly applicable to other numerical models. In addition, we expect that much of the V&V results are also applicable to other models in the frame of SimCardioTest project (for instance models sharing the same algorithms or relying on the same physical comparators for validation).

The following sub-sections present the V&V activities undertaken by each Use Case on the selected models.

1.2.1 Model Description

Before running any V&V activity, it is important to clarify the perimeter of the model. According to ASME VV40 guidelines, for each Use Case and for the selected numerical model the following key concepts are clarified:

- **Device/Drug Description**: the device or drug for which the numerical model is developed
- **Question of Interest**: the question concerning the device/drug safety/efficacy addressed by the selected numerical model
- **Context of Use**: the context in which the numerical model is used in the device/drug life cycle (e.g. device/drug design, validation, clinical use)
- **Model Risk**: the risk related to using the numerical model in the defined context of use

1.2.2 Model Verification

The purpose of Model Verification as intended by ASME VV40 is to demonstrate that the computational model numerical implementation is a robust and accurate representation of the mathematical model describing the phenomenon that the model aims to replicate.

Verification Credibility factors are grouped in two main areas:

- Code Verification
- Calculation Verification

Code Verification credibility factors are intended to demonstrate that the numerical model is developed and runs using robust software and hardware, and correctly implements the underlying mathematical equations which describe the model.

Calculation Verification credibility factors are intended to assess the numerical error associated with the numerical discretization of the mathematical problem, as well as with the implemented numerical solver strategy. In addition, this phase addresses how user errors are handled and possibly mitigated in both model inputs and outputs management.

Table 3 summarizes the Credibility Factors to be addressed in the frame of the computational model validation activities according to ASME VV40.

Table 3: Verification Credibility Factors (cf. ASME VV40).

Activity	Credibility Factor	VV40§	Guidance
Code Verification	Software Quality Assurance Software functions correctly and gives repeatable results in a specified Hardware/Software environment. (OTS / MOTS / UD)	5.1.1.1	Consider following steps: - Provide evidence that software works correctly (software validation, or software quality development assurance) - Installation Qualification of Hardware and Software prior running simulations - Maintenance activity vs software releases, and analysis of impact of new bugs on model prior running simulations
Code Verification	Numerical Code Verification - NCV Demonstrate correct implementation and functioning of algorithms. Compare to analytical solutions.	5.1.1.2	List key algorithms which need verification. For key algorithms: + Compare solution to analytical benchmarks OR to solution from another verified code. ++ Run grid convergence analysis vs exact solution.
Calculation Verification	Discretization Error Run spatial/temporal grid sensitivity analysis	5.1.2.1	Run grid convergence analysis and estimate discretization error.
Calculation Verification	Numerical Solver Error Run solver parameters sensitivity analysis	5.1.2.2	Example: Run Sensitivity on Simulation Convergence.
Calculation Verification	Use Error [Verify I/O controls in place]	5.1.2.3	How is it verified that simulation practitioner does not introduce errors when running the model? (key inputs and outputs verification).

1.2.3 Model Validation

The purpose of Model Validation as intended by ASME VV40 is to demonstrate that the computational model provides reliable information about the real-life phenomena it wants to represent.

Validation Credibility factors are grouped in three main areas:

- Computational Model
- Comparator
- Assessment

Computational Model credibility factors are intended to fully describe and quantify the model ability to address its question of interest. Its form, properties and conditions are addressed, as well as its inputs. The investigation includes both sensitivity analysis and uncertainty analysis of these quantities (when applicable) meant to assess the model accuracy.

Comparator credibility factors are intended to fully describe and quantify the comparator(s) used for validating the computational model. Comparators may be of different nature depending on the nature of the numerical model: pre-existing clinical literature data, in-vitro comparators, pre-clinical (animal) or clinical data. There may be one or more comparators addressing different aspects of the numerical model under investigation. Comparator uncertainties are also investigated.

Assessment credibility factors are relative to the actual comparison of the numerical model with the selected comparator. Both inputs and outputs to the comparison are taken into account in this analysis.

Table 4 summarizes the Credibility Factors to be addressed in the frame of the computational model validation activities according to ASME VV40.

NOTE: when multiple items are given for a specific credibility factor, not all of them may be applicable to the numerical model under consideration. Each Use Case will select and justify the credibility factor items to be addressed.

Table 4: Validation Credibility Factors (cf. ASME VV40).

Activity	Credibility Factor	VV40§	Guidance
Computational Model	Model Form: • Conceptual Formulation of Numerical Model • Mathematical formulation of Numerical Model Address 4 items: • Governing Equations (governing modeled phenomena) • System Configuration (Geometry of device/environment)	5.2.1.1	Evaluate Influence of Model Form Assumptions on Model Output Examples: • Scale Analysis • Sensitivity Analysis • PIRT (Phenomena Identification and Ranking Table)

Activity	Credibility Factor	VV40§	Guidance
	• System proprieties (Bio. Chem. Phys. Properties) • System conditions (boundary & initial cond.)	5.2.1.1	
Computational Model	Model Inputs Address 4 items: • Governing Equations Parameters (governing modeled phenomena) • System Configuration (Geometry of device/environment) • System proprieties (Bio. Chem. Phys. Properties) • System conditions (boundary & initial cond.)	5.2.1.2	Evaluate Model Input Sensitivities and Uncertainties
	Quantification of Sensitivities		Evaluate Sensitivities of selected inputs
	Quantification of Uncertainties		Evaluate Uncertainties of selected inputs
Comparator	Test Samples (TS) Address 4 items:	5.2.2.1	Describe Comparator (for information)
	• Quantity of TS		Covering number of samples used in comparator: • Single; few; statistically relevant
	• Range of Characteristics of TS		Covering range of each characteristic of interest across samples • Single Value; Nominal Range; Extreme Range; Full Range
	• Measurements of TS		Covering: • Characterization of Comparator Inputs • Characterization of Comparator Outputs
	• Uncertainty of TS measurements		Covering Uncertainty of tools/methods used to get measurements of test samples
Comparator	Test Conditions (TC) Address 4 items:	5.2.2.2	
	• Quantity of TC		Covering number of test conditions in comparator study: • Single; few; many
	• Range of TC		Covering range of values of test conditions: • Single Value; Nominal Range; Extreme Range; Full Range
	• Measurements of TC		Rigor in characterizing test conditions
	• Uncertainty of TC measurements		Covering Uncertainty of tools/methods used to get measurements of test conditions

Activity	Credibility Factor	VV40§	Guidance
Assessment	Equivalency of Input Parameters between Numerical Model and Comparator	5.2.3.1	Evaluate type and range of all inputs
Assessment	Output Comparison Address 4 items: • Quantity • Equivalency of Output Parameters • Rigor of Output Comparison • Agreement of Output Comparison	5.2.3.2	 How many outputs are compared: single vs multiple Type of outputs observed How the outputs are compared: visual; arithmetic difference; comparison vs. Uncertainty Evaluate the level of agreement, and state if it is satisfactory

1.2.4 Model Applicability

The ultimate purpose of verifying and validating the numerical model is to gain confidence that the model outputs can be used to make predictions on the represented medical device/drug. However, the validation space (*in primis* the comparator selected for model validation) is a limited representation of the reality which the model aims to replicate.

ASME VV40 predicates an additional analysis, referred to as applicability, meant to assess the relevance of the engaged validation activities to support the use of the numerical model for the selected context of use.

Table 5 summarizes the Credibility Factors to be addressed in the frame of the computational model applicability assessment according to ASME VV40.

Table 5: Model Applicability (cf. ASME VV40).

Activity	Credibility Factor	VV40§	Guidance
Applicability	Relevance of the Quantities of Interest QoI of Validation may be surrogate to the QoIs of COU	5.3.1	Compare QoIs of Validation vs COU: related, identical
Applicability	Relevance of the Validation Activities to the COU Proximity of Validation Points to COU	5.3.2	Compare range of Validation points vs. range of COU

1.2.5 Credibility Factors Coverage Level

According to ASME VV40, the model risk is the result of the combination of two factors:

- The ***Decision Consequence***: the clinical consequence of making a wrong decision based on a false prediction of the model
- The ***Model Influence***: the importance of the contribution of the model outcome in making clinical decisions, weighted amongst all other available inputs, such as available literature, design, in-vitro, pre-clinical and clinical information

Decision Consequence can be weighted as:

- **low**: an incorrect decision would not adversely affect patient safety or health, but might result in a nuisance to the physician or have other minor impacts
- **medium**: an incorrect decision could result in minor patient injury or the need for physician intervention, or have other moderate impacts
- **high**: an incorrect decision could result in severe patient injury or death, or have other significant impacts

Model Influence can be weighted as:

- **low**: simulation outputs from the computational model are a minor factor in the decision
- **medium**: simulation outputs from the computational model are a moderate factor in the decision
- **high**: simulation outputs from the computational model are a significant factor in the decision

Figure 1 gives a graphical representation of the Model Risk resulting from the combination of Decision Consequence and Model Influence.

Model influence	**high**	**3**	**4**	**5**
	medium	**2**	**3**	**4**
	low	**1**	**2**	**3**
		low	**medium**	**high**
		Decision consequence		

Figure 1: *Model Risk Matrix (cf. ASME VV40).*

Each of the credibility factors previously described may be investigated in several ways, each with a different level of investigation. The selected way of investigating each credibility factor may depend on several variables, such as complexity, available knowledge, or available means in the timeframe of this project.

ASME VV40 gives guidance on how to evaluate whether the credibility factors have been sufficiently investigated. For each credibility factor, a score varying from 1 to 5 is given to indicate how deeply the item has been investigated, where 1 means none or little investigation, and 5 means a thorough investigation. The scores are then compared to the model risk level as defined. Whenever a credibility factor coverage level does not match the risk level, a justification is given. This evaluation is summarized in a matrix as shown in Table 6.

Table 6: Credibility Factors Coverage Level (cf. ASME VV40). The model risk level is set to Medium (3) in this table for illustration purposes. The coverage level of the credibility factors is given an arbitrary score on a 1-to-5 scale for illustration purposes.

Model Risk					x		
Credibility Factor Coverage Level		1	2	3	4	5	
Code Verification: Software Quality Assurance	I			x			
Code Verification: Numerical Code Verification - NCV	I			x			
Calculation Verification - Discretization Error	II			x			
Calculation Verification - Numerical Solver Error	II			x			
Calculation Verification - Use Error	III			x			
Validation - Model [Form]	III			x			
Validation - Model [Inputs]	III			x			
Validation - Comparator [Test Samples]	IV			x			
Validation - Comparator [Test Conditions]	IV			x			
Validation - Assessment [Input Parameters]	IV			x			
Validation - Assessment [Output Comparison]	V			x			
Applicability: Relevance of the Quantities of Interest	V			x			
Applicability: Relevance of the Validation Activities to the COU	V			x			

1.3 Deliverables Organization

The V&V activities conducted in the frame of WP6 are summarized in two official deliverables:

- Deliverable D6.1 - Verification & uncertainty quantification for the use cases of WP2-5
- Deliverable D6.2 - Validation of the model predictions for the use cases of WP2-5

V&V activities described below are split between the two official deliverable documents as follows:

- Model Verification activities are reported in deliverable D6.1
- Model Validation activities and resulting Uncertainty Analysis are reported in deliverable D6.2
- Model Applicability is reported in deliverable D6.2

NOTE: As stated in the SimCardioTest Statement of Work, the official D6.1 deliverable title is: "Verification & uncertainty quantification for the use cases of WP2-5". The following deviations in the deliverable content with respect of this title are made:

1. Only Work Packages 2, 3, 4 develop numerical models needing V&V activities. These correspond to Use Case 1, 2 and 3 respectively. WP5 corresponds to the in-silico trial activities which will be carried out based on these numerical models.
2. Uncertainty Quantification activities are carried out according to ASME VV40 guidelines. As such, for sake of consistency with VV40, they are reported in SCT deliverable D6.2, rather than in deliverable D6.1.

For sake of clarity, the general introduction addresses both Verification and Validation activities and is identical for both deliverables. In addition, for each Use Case the Model Summary section describing the numerical model undergoing V&V is identical in both deliverables.

NOTE: Each deliverable contains several attachments detailing the technical work necessary to address specific credibility factors. The list of attachments is presented in the Appendices section.

2. Use Case 1

2.1 UC1 Model Summary

NOTE: This section is identical for both SCT deliverables D6.1 and D6.2. Refer to section 1.3 for document organization.

2.1.1 Background

The role of a cardiac pacing lead is to effectively stimulate the heart when it is deficient. Current pacemakers offer a wide range of stimulation pulse amplitudes and pulse durations to ensure that the therapy is effectively delivered. However, the higher the stimulation amplitude (and duration), the more energy is drained from the pacemaker battery, which can have an impact on the device longevity. When developing new leads, it is therefore important that the stimulation threshold remains in normal range.

2.1.2 Device Description

Medical devices addressed by the model are cardiac pacing leads. More precisely, their electrical behaviour, and interaction with the cardiac tissue is addressed.

2.1.3 Question of Interest

The Question of Interest addressed by the model is the following:

- What are the stimulation pulse characteristics (voltage amplitude in V and pulse duration in ms) required for a bradycardia lead in bipolar (tip/ring) mode to capture (stimulate) healthy cardiac tissue?

2.1.4 Context of Use

The computational model can be used to help pacing lead manufacturers when developing new products, providing information on the energy levels (pulse amplitudes and durations) required to successfully trigger action potentials and stimulate cardiac tissue.

2.1.5 Model Risk

The following considerations support the assessment of the risk associated with the numerical model.

- Decision Consequence: Low

An error in the model prediction may result in either an underestimation or an overestimation of the energy required to stimulate the cardiac tissue for a given pacing lead design. The clinician will adjust the energy in order to stimulate correctly. An overestimation of the energy by the model has no negative clinical influence on the delivered therapy, as it would result in an increase of the device battery life, which would actually be an unexpected benefit. An underestimation of the energy would have a minor clinical influence, as it would require the physician to increase the programmed therapy energy in order to achieve cardiac stimulation, resulting in a decrease of the expected battery life.

- Model Influence: Medium

Results of simulations with a new design will be systematically compared to those of previous well-established designs. In addition, pre-clinical and clinical data collected during the validation of the new lead design would contribute to corroborate the data provided by the models.

- Model Risk: 2/5 (Low-Medium)

Model Risk is based on Decision Consequence and Model Influence stated above, according to Risk Matrix in Figure 2 (cf. section 1.2.5).

Model	**high**	**3**	**4**	**5**
influence	**medium**	**2 COU**	**3**	**4**
	low	**1**	**2**	**3**
		low	**medium**	**high**
		Decision	**consequence**	

Figure 2: *Model Risk Matrix (cf. ASME VV40) evaluating the COU included in UC1.*

2.1.6 Model Description

The model aims to reproduce capture threshold detection measurements that are performed ex vivo on a healthy ventricular wedge.

The model includes the tissue and the surrounding electrolyte, the pacing circuit of the device, and a contact model between the device and the tissue. Given a pulse duration and amplitude, it computes the transmembrane voltage in the cardiac tissue, the electric potential in the tissue and electrolyte, as well as the voltage drops at the tip and ring electrodes.

Simulations are parametrized by:

- Contact properties between the leads and the tissue/electrolyte (modelled by parallel RC-circuits)
- The geometry of both the lead and computational domain
- Micro-structural description of the tissue and its electrical properties
- A model that describes ionic exchanges at the cell membranes

The contact properties are characterized by bench experiments. The geometry and microstructure of the tissue are obtained from 9.4T MR imaging. The shape of the lead is chosen among a family of designs, with the possibility of modifying several parameters (such as inter electrode distance, or radius). The ionic model is chosen from the standardized “cellML” database [2], with parameters adjusted from optical mapping data.

To compute an approximate solution of the model, we need a geometrical mesh of the domain, a spatial discretization scheme (e.g. P1 Lagrange Finite Elements), a time stepping method and an algorithm to solve large linear systems.

In Figure 3 we show the computation of the electric field created by the pacemaker in a slab of passive tissue, which will be the shape of the excitation of the cardiac tissue at the beginning of pacing.

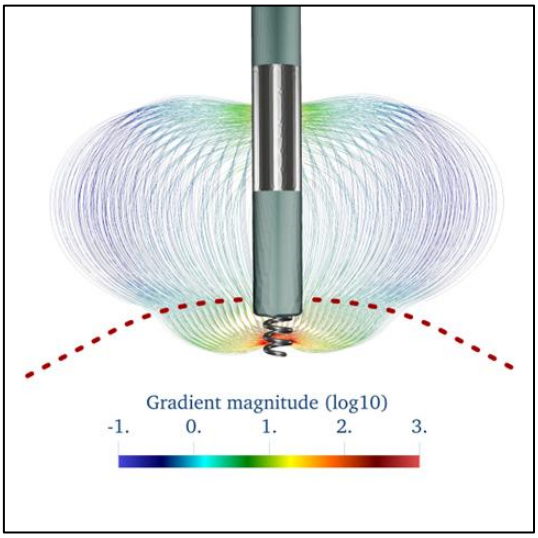

Figure 3: *Electric field generated by a pacemaker lead, computed in a computational domain representing blood and a passive tissue, above and below the dotted line, respectively.*

Computing the solution for various amplitudes and durations of stimulation allows to locate the so-called Lapicque curve, which is the threshold between capturing and non-capturing stimulations in the amplitude/duration plane (see Figure 4).

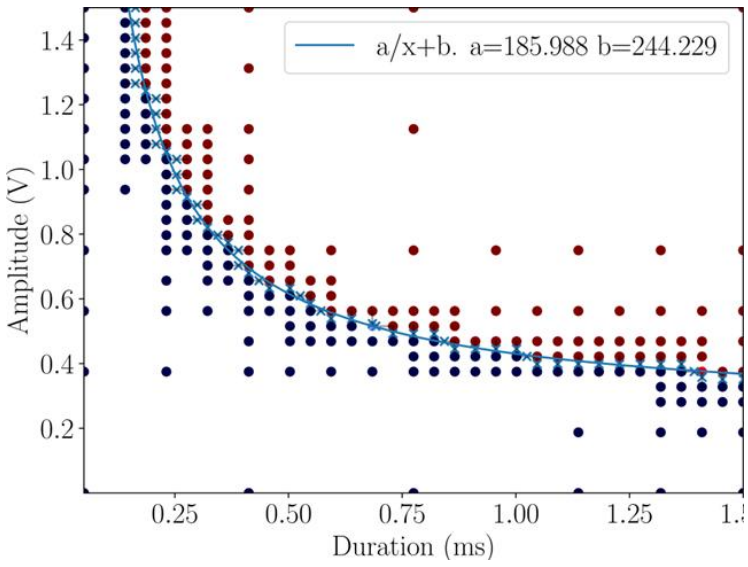

Figure 4: *Lapicque Curve obtained from the solutions of an exploratory 0D model. For each blue/red point of the diagram, ie for each pair of amplitude and duration of stimulation, the model computes the response to 5 stimulations, and evaluates whether or not an action potential was triggered after each stimulation. Blue dots are for 0 out of 5 captures, red dots are for 5 out 5 captures.*

2.2 UC1 Model Verification

2.2.1 Software Quality Assurance

2.2.1.1 CEPS Model

SQA is continuously performed while our software CEPS is being developed. A complete description of SQA activities is given in section 1.1 of annex A6.1-UC1 (UC1 Verification Annex).

2.2.1.2 IST Platform

SimCardioTest platform has been developed to host the three Use Cases developed within the project (sections 2.2.1.2, 3.2.1.2 and 4.2.1.4 respectively) and has been created in a private tenant within the InSilicoTrials's Azure account. The platform infrastructure is described in the figure below.

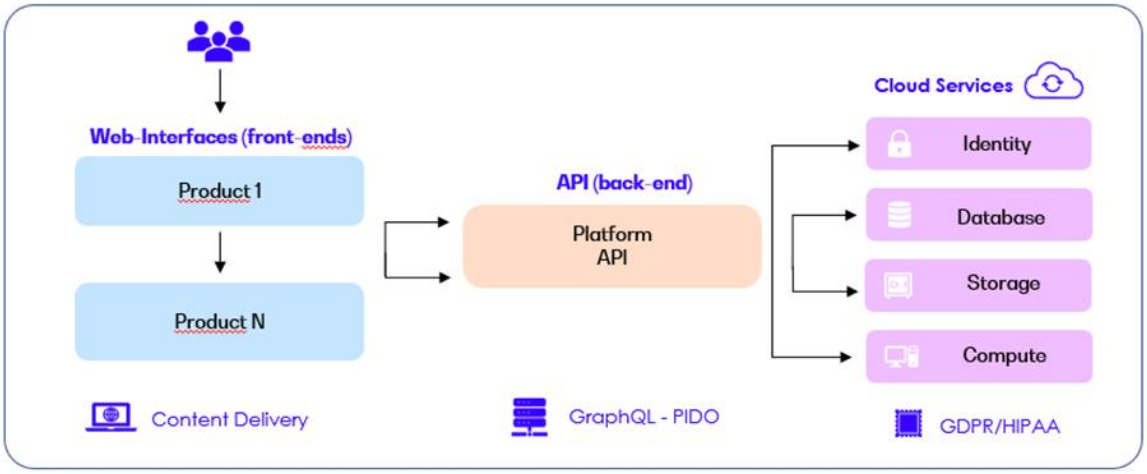

Figure 5: *InSilicoTrials platform infrastructure, applicable to UC1, UC2, and UC3.*

The architecture is split into 3 main parts:

- Front-End: VUE3 web interfaces are served through the Azure Content Delivery Network
- Back-End: ReST API layer connected to several Azure services
- Execution: handled through Azure Batch

Prior to starting the development, we analysed which cloud providers were compliant with regulations governing the pharmaceutical and healthcare industries. Microsoft Azure was selected due to its high compliance level (https://learn.microsoft.com/en-us/azure/compliance).

Azure has undergone independent third-party audits for quality management and information security, including ISO 9001 and ISO/IEC 27001 among many others. IP of model providers are protected against the downloading, copying, and changing of their models, while providing a safe environment for users to manage their own data. The whitepaper from Microsoft Azure Gxp Guidelines [3], which we've contributed to editing in the first version, highlights the compliance with the GxP. In the development of the platform, we've also followed the requests by FDA 21 CFR Part 11.

InSilicoTrials platform already embeds a variety of programming languages (e.g., C++, Python, R, Matlab) and simulation engines (e.g., NONMEM, ANSYS, Abaqus, CodeASTER, OpenFOAM) with no direct access to the solvers by the user. For the specific SimCardioTest Use Cases, we integrated the software required to run for each workflow.

Considering the need to finalize seamless integration with all partner components and to optimize performance, we are currently undergoing an architectural restructuring of the application. We will conduct end-to-end testing once we have the finalized interface in place.

Software Development

We follow the Agile SCRUM, a software development methodology that emphasizes iterative, incremental development and a flexible, collaborative approach to development. In an Agile approach, requirements and solutions evolve through the collaborative effort of cross-functional teams, and the focus is on delivering working software quickly and responding to change.

We use Jira [4], a popular project management and issue tracking tool developed by Atlassian, to track and manage tasks, bugs, and other issues that arise during software development projects.

2.2.2 Numerical Code Verification

2.2.2.1 CEPS Model

Some aspects of NCV of CEPS are treated in the same way as SQA. Examples of NCV unit tests are verifying the convergence rate of ordinary differential equation solvers. However, some NCV tasks required longer computation times, and cannot be performed on our CI setup. More details on NCV activities are described in section 1.2 of annex A6.1-UC1 (UC1 Verification Annex).

2.2.2.2 IST Platform

- Step 1A: For OTS software: standard verification benchmarks provided by software house are run on cloud machine and results are compared to expected benchmark results.
- Step 1B: For MOTS & UD software: benchmarks defined by model developers are run on cloud machine using inputs agreed with model developers, results are compared to solutions expected by model developers.
- Step 2: The model is run on cloud machines using inputs agreed with model developers, results are compared to solutions expected by models developers.

2.2.3 Discretization Error

2.2.3.1 CEPS Model

The study of the influence of discretization parameters — for instance size of the computational domain, mesh resolution, time step — on the final outputs of the model started May 30th, and will be carried out during summer 2023.

The software computing the complete cardiac model coupled to a pacemaker is not ready yet, and so is the computation of Lapicque curves. In consequence, we begin the discretization error study with computation of static electric fields generated by the pacemaker in the tissue. The process will

be automated in order to be repeated with the complete model when available. The plan is to carry out a convergence analysis on the Lapicque curves which are post-processed from the electric potential, in a similar way for reference solutions (section 2 of annex A6.1-UC1, UC1 Verification Annex). This will document the influence of the discretization error on the curves output by the solver.

2.2.3.2 IST Platform

Discretization Error analysis provided by model developer apply. The model is run on the IST platform for time and space discretization parameters agreed with model developer, and results are compared to solutions expected by model developers. In case of mismatch, an additional discretization error analysis on the cloud engine may be required.

2.2.4 Numerical Solver Error

2.2.4.1 CEPS Model

Numerical solver error can be analysed in the similar way to discretization error. Hence, the study is performed at the same time as Discretization Error (start May 30th, end by summer 2023).
Namely, we will quantify the influence of the linear algebra solver tolerances, and the order of the numerical scheme first on static electrical fields, then on the Lapicque curves.

2.2.4.2 IST Platform

Numerical Solver Error analysis provided by model developer applies. The model is run on the IST platform for numerical solver parameters agreed with model developer, and results are compared to solutions expected by model developers. In case of mismatch, an additional numerical solver error analysis on the cloud engine may be required.

2.2.5 Use Error

2.2.5.1 CEPS Model

Use error within CEPS is treated as part of SQA. More details are given in section 2.1 of annex A6.1-UC1 (UC1 Verification Annex).

2.2.5.2 IST Platform

Use error management on the IST platform is described in section 2.1 of annex A6.1-UC1 (UC1 Verification Annex).

2.3 UC1 Discussion and Future Work

The development of the coupled bidomain and pacemaker model within CEPS for computation of Lapicque curves, first of its kind to our knowledge, is undergoing a SQA protocol that is rather unusual for scientific user-developed codes at this stage of development. The setup of CI as well as systematic checking of SQ as it is written is a time-consuming process. However, it proved to be useful by helping removing bugs in complex parts of CEPS. We pushed further the scope of unit tests to ensure an excellent coverage of the code, in order to reach a good credibility factor for SQ. The testing suite for CEPS covers several aspects of Verification: basic SQ, verification of simple numerical solvers as well as control of most of the user's inputs, in addition to IST input control from the web-platform.

Numerical tests consist, whenever possible, in comparing approximated solutions to analytic one-solutions, and verifying the convergence order of the methods. When the solved problems do not have an analytic solution, such as for the cardiac bidomain problem, reference solutions were used. In addition, a manufactured problem with analytic solution was proposed to check the performances of the solver for a problem that is close to the bidomain problem.

The sensitivity analysis of the solver error to discretization and numerical solver parameters started early June 2023. We are implementing a tool that will generate convergence reports for any PDE problem implemented within CEPS, including the bidomain and pacemaker model. From these reports, critical parameters will be identified, and we will be able to make recommendations on the size of the mesh, time step and solver parameters to use to reach an error value that suits a target credibility factor.

In order to propose a completely verified pipeline for the electrophysiology QI of Use Case 1, we need to continue on developing the complete 3D coupled bidomain and pacemaker model with the same high standard of SQA as previously for the CEPS code. In addition, we need to develop a verification tool that will validate or refuse the meshes that will be generated from the web-platform user inputs. This tool will either invoke a remeshing application, or suggest new input in case the first mesh generation is not completed at all.

In conclusion, we designed all verification items described in this document to cover perfectly the credibility factor requirements. Since the model risk was evaluated to low, and the model influence to medium, the credibility factor required to answer our QI is 2 out of 5 according to the Model Risk Matrix of AMSE VV40. The high standard SQA tools as well as thorough error analysis on the quantities of interest in our COU will actually cover requirements for higher credibility factors (see Table 7).

Table 7: Verification Credibility Factors Coverage Level for Use Case 1 (cf. ASME VV40); * indicates verification activities not yet completed.

Model Risk			x			
Credibility Factor Coverage Level		1	2	3	4	5
Code Verification: Software Quality Assurance	V		x			
Code Verification: Numerical Code Verification - NCV	V		x			
Calculation Verification - Discretization Error *	V		x			
Calculation Verification - Numerical Solver Error *	V		x			
Calculation Verification - Use Error	IV		x			

2.3.1 IST Platform

For what concerns the InSilicoTrials Platform, considering the need to finalize seamless integration with all partner components and to optimize performance, we are currently undergoing an architectural restructuring of the application. We will conduct end-to-end testing once we have the finalized interface in place.

3. Use Case 2

3.1 UC2 Model Summary

NOTE: This section is identical for both SCT deliverables D6.1 and D6.2. Refer to section 1.3 for document organization.

3.1.1 Background

Atrial fibrillation (AF) is considered the most common of human arrhythmias. AF is currently seen as a marker of an increased risk of stroke since it favours thrombus formation inside the left atrium (LA). Around 99% of thrombi in non-valvular AF are formed in the left atrial appendage (LAA) [5]. LAA shapes are complex and have a high degree of anatomical variability among the population [6]. Percutaneous left atrial appendage occlusion (LAAO) can be an efficient strategy to prevent cardioembolic events in selected non-valvular AF patients, as an alternative to life-long oral anticoagulation (OAC) [7], as shown in large clinical trials (ACP Multicentre [8], EWOLUTION [9]), where LAAO procedures demonstrated non-inferiority. However, a successful implantation of LAAO devices remains a challenge in some cases, due to the complexity of LA geometry. Sub-optimal LAAO settings can lead to device-related thrombosis (DRT), i.e., a thrombus formed at the device, becoming a major concern [10] since it can lead to stroke. Based on the Virchow's triad, three factors are thought to contribute to thrombus formation: hypercoagulability, endothelial injury (replaced by a nitinol surface after LAAO) and blood stasis [11]. Related to the latter, key hemodynamic factors with demonstrated influence in thrombus formation in LAAO include (see Figure 6):

1. Occluder design and position: The geometry and characteristics of the occluder device can impact the flow patterns in the left atrium. Different occluder designs, such as shape, size, and surface properties, can influence the likelihood of thrombus formation. The position and alignment of the occluder within the left atrium can affect the flow patterns and the likelihood of thrombus formation. For instance, covering the pulmonary ridge (see Figure 7) may have a protective effect regarding DRT. Studying different occluder positions can help determining the optimal placement to minimize the DRT risk.

2. Blood flow velocity: Areas with low flow velocity or regions of recirculation may be prone to stasis and clot formation.

3. Blood viscosity: Altering the viscosity can provide insights into how changes in blood composition or conditions, such as hematocrit or temperature, affect thrombus formation. Parameters related to blood coagulation, such as platelet activation or coagulation cascade dynamics, can be simulated to understand their impact on thrombus formation.

4. Wall shear stress: Wall shear stress is the frictional force exerted by the flowing blood on the atrial wall. Low wall shear stress regions can be associated to thrombus formation. Evaluating different wall shear stress levels can help identify critical areas. Wall injuries due to abnormal stresses can also be caused by the device deployment.

To avoid blood stasis, it is crucial to properly choose the type of device and the position where the device is going to be deployed. Thus, different planning tools has emerged to find the optimal device

configuration for each patient such as the commercial products from FEOPS [12] and Pie Medical [13], or the VIDAA platform [14], developed by UPF. However, none of these solutions include functional information on blood stasis, which is key for assessing the risk of DRT. In-silico computational fluid dynamic (CFD) can help to describe and relate patient-specific LA/LAA morphology and complex hemodynamics to understand the mechanism behind thrombus formation. Moreover, computational models of the blood flow can be used to predict the effectiveness of LAAO devices, to evaluate new device designs, and to better understand clinical outcomes such as DRT.

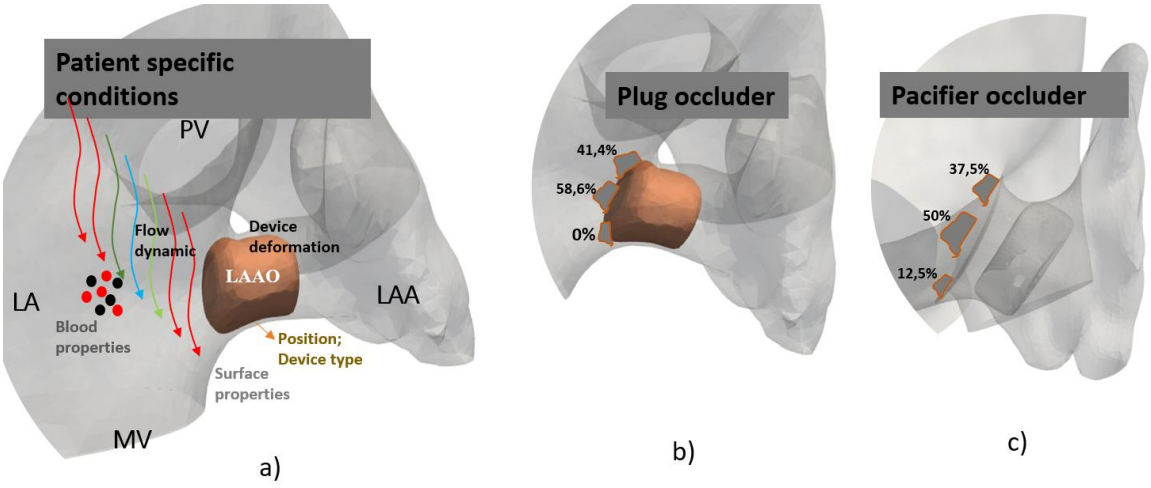

Figure 6: *a) Principal factors associated to thrombus formation, including blood properties, device type and positioning. b,c) Percentages of device-related thrombus (DRT) in different parts of the device, reported in Sedaghat et al.* ***[10]*** *for the plug- and pacifier-type of occluder devices (b and c, respectively). LAAO: left atrial appendage occluder. MV: mitral valve. PV: pulmonary veins.*

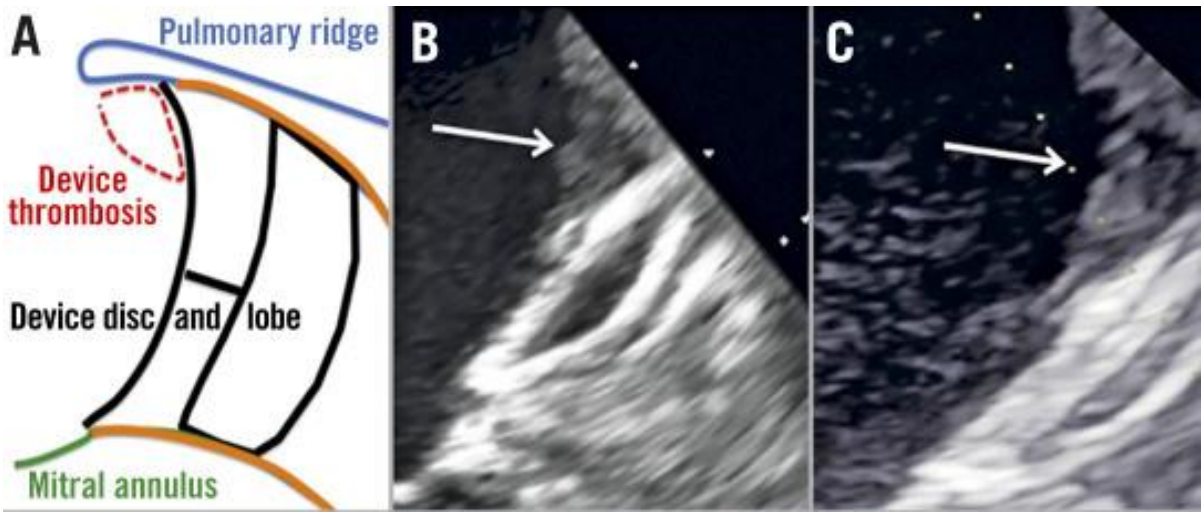

Figure 7: *Influence of covering the pulmonary ridge (PR) for avoiding device-related thrombosis, from Freixa et al.* ***[15]****. The arrows point to uncovered PR where thrombus is found after left atrial appendage occluder implantation.*

3.1.2 Device Description

Left atrial appendage closure devices (see Figure 8) are used to reduce the risk of stroke in patients with atrial fibrillation by occluding or sealing off the left atrial appendage, which is a small pouch-like structure in the heart where blood clots can form. Here are two commonly used device types:

1. Plug-Type Devices
   - Plug-type left atrial appendage occluders are designed to completely seal off the left atrial appendage (LAA). These devices typically consist of a self-expanding frame or mesh structure that fills and completely occludes the LAA, preventing blood flow into the appendage. The frame or mesh is often covered with a fabric or membrane material to enhance closure.
   - The Watchman device is an example of a plug-type occluder. It is developed by Boston Scientific, and it is a fabric-covered, self-expanding nitinol frame with fixation barbs. It is delivered through a minimally invasive procedure and placed in the left atrial appendage to block blood flow, thereby preventing blood clots from forming and potentially causing a stroke.

2. Pacifier-Type Devices
   - Pacifier-type left atrial appendage occluders, as the name suggests, partially occlude the LAA while allowing some blood flow to continue. These devices have a central channel or opening that allows limited blood flow through the LAA while reducing the risk of blood clot formation. This design is intended to maintain some physiological flow patterns and potentially reduce the risk of complications associated with complete occlusion.
   - The Amplatzer Amulet device is an example of a pacifier-type occluder. It is manufactured by Abbott and it consists of a self-expanding nitinol frame covered with a permeable polyester fabric. Similar to the Watchman, it is implanted in the left atrial appendage to close it off and reduce the risk of stroke.

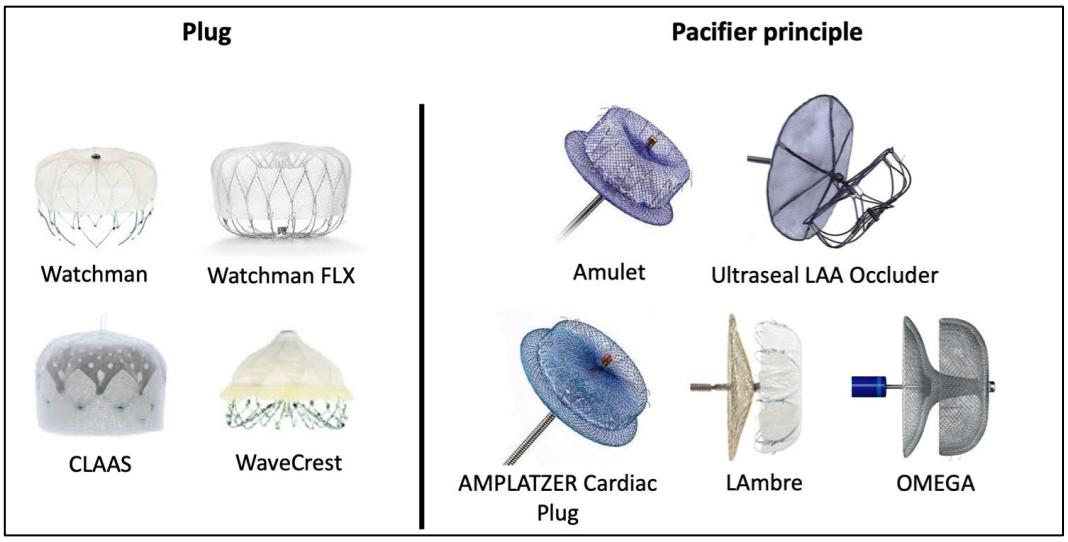

Figure 8: *Types of left atrial appendage devices, classified as plug or pacifier types. The most used devices are the Watchman and Watchman FLX (plug-type), developed by Boston Scientific (left), and the Amplatzer Amulet device (pacifier-type), manufactured by Abbott (right).*

3.1.3 Question of Interest

Several relevant questions of interest (QI) can be answered by computational fluid simulations applied to left atrial appendage occluder devices, encompassing different aspects of the device design and applicability. The different stakeholders involved in SimCardioTest, including device manufacturers, clinicians and academic partners defined multiple QIs during the project, which were ranked based on the most critical aspects to study in relation to possible adverse events during the implantation, especially regarding DRT. The QI that had the maximum level of priority and feasibility, being selected to guide the V&V exercise of Use Case 2 according to ASME VV40 guidelines, is the following:

- Does covering of the pulmonary ridge with a LAAO device (plug or pacifier) relate with the likelihood of low blood flow velocities around the device and induce the device-related thrombus (DRT)?

The QI above follows the formulation found in pioneering V&V works on cardiac devices [16] and studies the influence of device settings (type and position) in relation to DRT by measuring low blood flow velocities.

3.1.4 Context of Use

From the selected QI, two different Contexts of Use (COU), assessing the device performance, were defined. These COUs have different level of influence on the decision of whether the covering of the pulmonary ridge (PR) with the LAAO device is equivalent to or better than placing it deeper into the LAA (i.e., with an uncovered PR). In both cases, the computational model is used to assess blood flow velocities near the device. The performed evaluations are based on two different cohorts, depending on the COU. In the first COU, pre-operative and follow-up imaging data from twenty patients who underwent LAAO has been used, half of them suffering DRT. The second COU is based on a set of two patient-specific geometries obtained from clinical cases: one suffer from AF, and the other acts as a control case.

- **COU1** - Performance evaluation with computational fluid simulations only. Computational modelling is used to identify low blood flow velocities near the device, placed in a proximal or distal position (e.g., covering or not the PR) with both device types (i.e., plug and pacifier). There is no supporting data from in-vitro testing available for assessing the performance of the occluder devices.

- **COU2** - Performance evaluation with computational fluid simulations and in-vitro data. In addition to in-silico experiments, in-vitro testing is conducted to create additional evidence on whether the covering of the PR is critical for DRT with both types of device.

3.1.5 Model Risk

The following considerations support the assessment of the risk associated with the numerical model.

- Decision Consequence: Medium

Based on VV40 guidelines, both COUs have a Medium consequence since the intended users are engineers from manufacturers, using computational fluid simulations and in-vitro testing experiments to optimize the design of next-generation occluder devices and provide better implantation guidelines to prevent DRT. If simulations and experiments are incorrect (i.e., under- or over-estimating the risk of DRT), they could lead to sub-optimal design of new devices and recommendations, potentially increasing abnormal events after implantation such as device embolization, DRT or peri-device leaks.

- Model Influence for COU 1: High
- Model Influence for COU 2: Medium

Based on VV40 guidelines, COU1 has a High influence because the computational model results are the only ones informing the decision. COU2 has a Medium influence because supporting data from in-vitro testing complement the computational modelling studies.

- Model Risk for COU 1: 4/5 (Medium-High)
- Model Risk for COU 2: 3/5 (Medium-Medium)

Model Risk is based on Decision Consequence and Model Influence stated above, according to Risk Matrix in Figure 9 (cf. section 1.2.5).

Model influence	**high**	**3**	**4 COU1**	**5**
	medium	**2**	**3 COU2**	**4**
	low	**1**	**2**	**3**
		low	**medium**	**high**
		Decision consequence		

Figure 9: *Model Risk Matrix (cf. ASME VV40) evaluating the COU1 and COU2 included in UC2.*

3.1.6 Model Description

Simulating blood flow in the left atrium with an implanted occluder device can indeed facilitate the identification of the parameters that may contribute to thrombus formation. By conducting blood flow simulations with the occluder device in place, researchers can explore the impact of various factors, such as the shape or position of the device, on flow characteristics and the potential for

thrombus formation. The initial step involves processing patient-specific medical images to extract a three-dimensional model, followed by the building of an appropriate 3D volumetric mesh. In COU1, for each left atrial geometry, the two studied device positions (covering and uncovering the pulmonary ridge) have been previously defined. In COU2, fluid simulations from two patients are compared with an in-vitro setup. The blood flow magnitude and directions will serve as the primary parameters evaluated in the current V&V study, for detecting blood stagnation zones around the LAAO device.

As a previously required step for VV40 analysis of flow simulations with LAAO devices, verification and validation experiments to assess the credibility of blood flow simulations in the left atria without a device are also required. In SimCardioTest, we performed the largest VV40 study available in literature for such type of simulations, testing several numerical parameters in mesh and time-step convergence analysis, as reported in SCT deliverable D3.2, and recently published [17]. This study contributed to identify most of the numerical parameters to be used in fluid simulations of the left atria. The rest of the document will mainly focus on the complementary VV40 experiments performed on simulations including LAAO devices.

3.2 UC2 Model Verification

3.2.1 Software Quality Assurance

3.2.1.1 Ansys Model

The computational model uses an off-the-shelf (OTS) software, ANSYS Fluent [14], [6]. The following is an example of gradation of activities from VV40 guidelines, listed from lowest to highest credibility, that reflects the rigor of SQA:

A) No SQA procedures are documented
B) SQA procedures from the vendor are referenced
C) A supplier audit is conducted with the vendor to confirm that quality procedures are conducted and documented during the software development process
D) Benchmark verification test cases, provided by the vendor, are run on the user's computer platform. The results are compared to vendor results and documented

Software Quality Assurance (SQA) procedures from ANSYS are available [18]. Quality procedures were conducted and documented during the software development process, following the guidelines for ISO 9001 certification. ANSYS have roughly 270 formal verification test cases benchmarks [19], basically using bench-top set-ups and synthetic experiments with known and fully-controlled analytical solutions.

The evaluation of hardware infrastructure and software tools prior to running simulations was verified for the following hardware configurations:

- A regular PC (Core i9 10900 / 2.8 GHz - vPro - RAM 32 GB - SSD 1 TB)
- UPF cluster (Rocky Linux, 32 nodes, with 48-64 processors/nodes)
- Oracle cluster (Linux, AMD 64 cores processor)

Stable and permanent licenses of ANSYS Academic Research CFD 2022 (5 tasks), not requiring maintenance, were run. The main conclusion of this analysis was that the results were reproducible if the user follows the protocols and the mathematical assumptions described in the protocols, independently of employing a stand-alone PC or a cluster (see Figure 10). Therefore, this credible factor has the maximum level of rigor **(D)**.

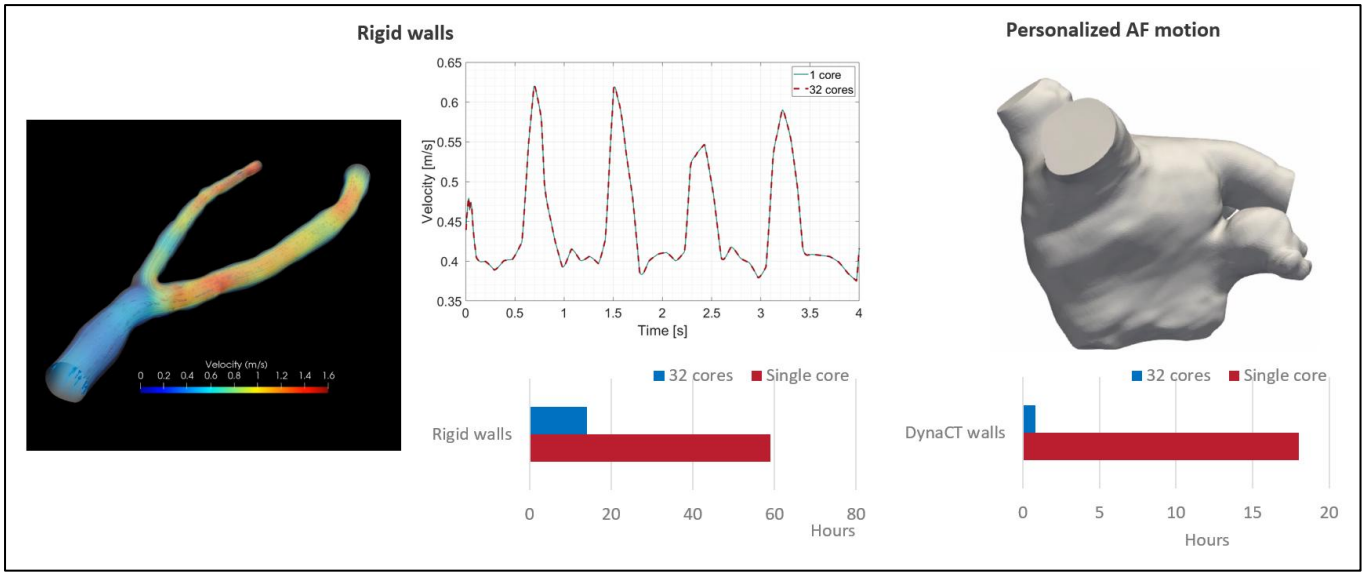

Figure 10: *Trials with different numbers of cores used for solving fluid simulations, providing insight into the performance and scalability of the system. In both examples displayed in the figure, a fluid simulation with rigid walls on a vascular structure (left), and a left atria with moving walls (right), the obtained results show a reduction of the running time by a factor of 20 when using 32 cores, while the value of the velocity magnitude is not affected, proving robustness of the solver.*

3.2.1.2 IST Platform

SimCardioTest platform has been developed to host the three Use Cases developed within the project (sections 2.2.1.2, 3.2.1.2 and 4.2.1.4 respectively) and has been created in a private tenant within the InSilicoTrials's Azure account. The platform infrastructure is described in the figure below.

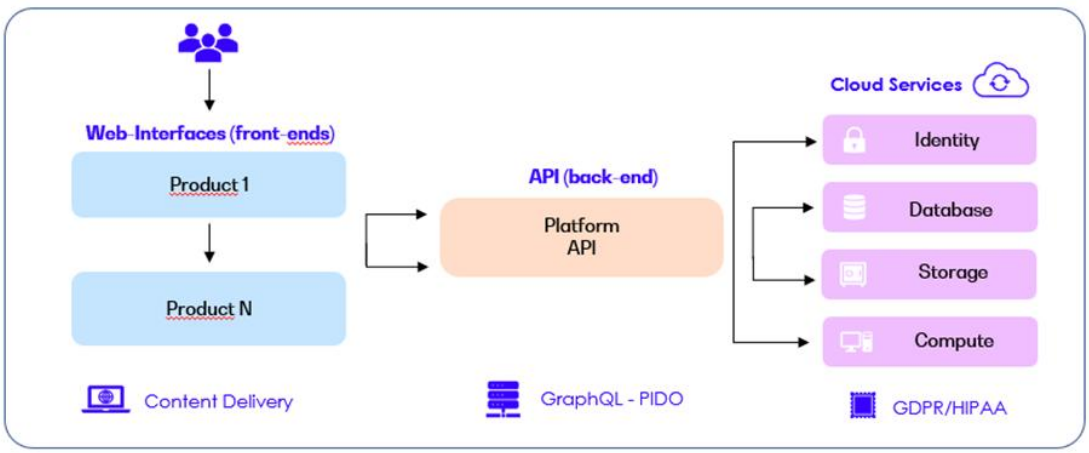

Figure 11: *InSilicoTrials platform infrastructure, applicable to UC1, UC2, and UC3.*

NOTE: Unlike Use Cases 1 and 3, Use Case 2 model results are pre-calculated and hosted in UC3 proprietary servers. IST platform fetches model results already calculated by UC2 model developers via an Internet connection, according to final user inputs. Even if UC2 computational algorithm is not implemented in IST's cloud resources but instead accessed through API, the UC3 web interface is built as for the other UCs. This means that the user cannot notice this technicality from the platform interface: for the user, all UCs are actually on the platform.

The architecture is split into 3 main parts:

- Front-End: VUE3 web interfaces are served through the Azure Content Delivery Network
- Back-End: ReST API layer connected to several Azure services
- Execution: handled through Azure Batch

Prior to starting the development, we analysed which cloud providers were compliant with regulations governing the pharmaceutical and healthcare industries. Microsoft Azure was selected due to its high compliance level (https://learn.microsoft.com/en-us/azure/compliance).

Azure has undergone independent third-party audits for quality management and information security, including ISO 9001 and ISO/IEC 27001 among many others. IP of model providers are protected against the downloading, copying, and changing of their models, while providing a safe environment for users to manage their own data. The whitepaper from Microsoft Azure Gxp Guidelines [3], which we've contributed to editing in the first version, highlights the compliance with the GxP. In the development of the platform, we've also followed the requests by FDA 21 CFR Part 11.

InSilicoTrials platform already embeds a variety of programming languages (e.g., C++, Python, R, Matlab) and simulation engines (e.g., NONMEM, ANSYS, Abaqus, CodeASTER, OpenFOAM) with no direct access to the solvers by the user. For the specific SimCardioTest Use Cases, we integrated the software required to run for each workflow.

Considering the need to finalize seamless integration with all partner components and to optimize performance, we are currently undergoing an architectural restructuring of the application. We will conduct end-to-end testing once we have the finalized interface in place.

Software Development

We follow the Agile SCRUM, a software development methodology that emphasizes iterative, incremental development and a flexible, collaborative approach to development. In an Agile approach, requirements and solutions evolve through the collaborative effort of cross-functional teams, and the focus is on delivering working software quickly and responding to change.

We use Jira [4], a popular project management and issue tracking tool developed by Atlassian, to track and manage tasks, bugs, and other issues that arise during software development projects.

3.2.2 Numerical Code Verification

3.2.2.1 Ansys Model

The following scale is used to guide the code verification activities in the LAAO use case:

A) NCV is not performed

B) The numerical solution is compared to an accurate benchmark solution from another verified code

C) Discretization error is quantified by comparison to an exact solution, and a grid convergence study was carried out to show the numerical solution asymptotically approaches the exact solution as the discretization is refined. However, the observed order of accuracy is not quantified

D) In addition to the quantification of discretization error and the execution of a grid convergence study, the observed order of accuracy is quantified and compared to theoretical order of accuracy. Or the code has been externally verified

The numerical code verification (NCV) of equations and algorithms available in ANSYS Fluent, being a commercial and widely-used computational fluid dynamics (CFD) software tool, have been extensively performed. The verification experiments have involved comparing numerical results obtained from Fluent simulations with known analytical solutions or benchmark experimental data. By conducting such verification studies, the software developers can ensure that Fluent accurately solves the governing equations of fluid flow and provides reliable results. The process fulfils the ASME VV20 guidelines; the benchmarks can be consulted and tested [19].

Additionally, in SimCardioTest we performed benchmark analysis tests to compare the commercial ANSYS solution with fluid simulation results provided by the Open-Source Oasis solver, developed by Simula SRL partners. Similar results were obtained by the two solvers in classical benchmark analytical experiments, as can be seen in Figure 12 and

Table 8. Therefore, this credible factor will have the maximum level of rigor **(D)**.

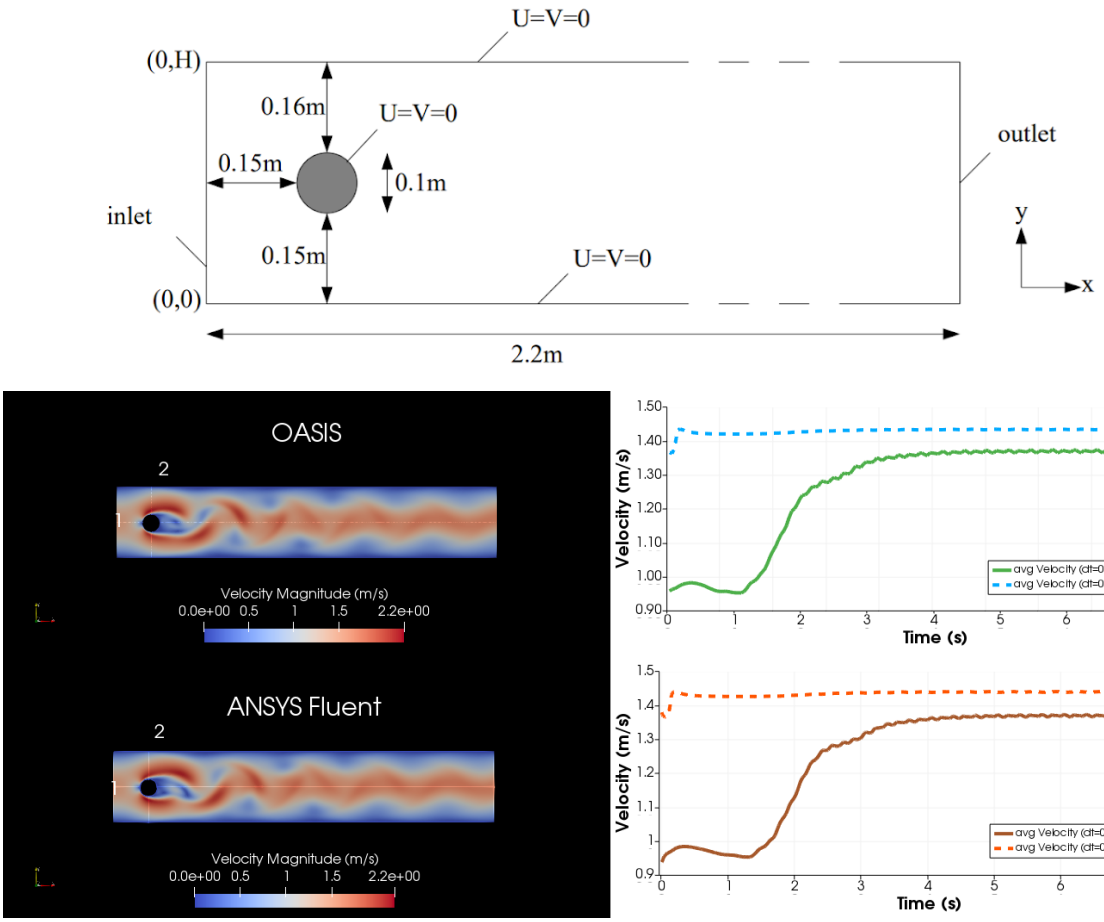

Figure 12: *Classical benchmark experiment with fully-known analytical solution for evaluating numerical code verification of commercial ANSYS fluent and open-source Oasis solvers. 2D tests analysing flow around a cylinder with a circular cross-section and boundary conditions described in Schäfer et al.* ***[20]****. Avg: average.*

Table 8: Quantitative results from benchmark experiments shown in Figure 6 obtained with ANSYS Fluent and Oasis. Green indicates differences below 5% at pressure drop of simulation results compared to benchmark's ground-truth.

ANSYS Fluent				Oasis				Schafer, M. et al. 1996		
Space	dt	ΔP	Error	Space	dt	ΔP	Error	Space	dt	ΔP
[*10^3 elem]	[s]	[Pa]	[%]	[*10^3 elem]	[s]	[Pa]	%	[*10^3 elem]	[s]	[Pa]
8	0.02	2.35	-	8	0.02	2.66	-	-	-	-
8	0.01	2.58	4.8	8	0.01	2.58	4.8	8.7	dt	2.46
8	0.005	2.43	-	8	0.005	2.64	-	-	-	-
28	0.02	2.43	2.8	32	0.02	2.79	11	29	2dt	2.50
28	0.01	2.46	0.8	32	0.01	2.49	0.4	29	dt	2.48
28	0.005	2.57	-	32	0.005	2.46	-	-	-	-

3.2.2.2 IST Platform

- Step 1A: For OTS software: standard verification benchmarks provided by software house are run on cloud machine and results are compared to expected benchmark results.
- Step 1B: For MOTS & UD software: benchmarks defined by model developers are run on cloud machine using inputs agreed with model developers, results are compared to solutions expected by model developers.
- Step 2: The model is run on cloud machines using inputs agreed with model developers, results are compared to solutions expected by models developers.

3.2.3 Discretization Error

3.2.3.1 Ansys Model

A grid/mesh convergence study was performed to estimate spatial discretization error when having left atrial meshes including an occluder device. The adapted gradation of activities, listed from lowest to highest credibility, that reflects the rigor of the discretization error analysis is the following:

A) No grid or time-step convergence analysis was performed to estimate the discretization error

B) Applicable grid or time-step convergence analysis were performed and their respective convergence behaviours were observed to be stable, but the discretization error was not estimated

C) Applicable grid or time-step convergence were performed and discretization error was estimated

Credibility level **(C)** is chosen from the gradation of activities reflecting the rigor of the discretization error analysis, based on the risk associated with the selected COUs. To achieve this level, mesh sensitivity studies were conducted with a focus on refining the mesh in regions of interest, i.e., around the occluder device, using boundary layers, as can be seen in Figure 13. The mesh verification studies were conducted directly evaluating the primary quantities of interest, blood flow velocities and wall shear stress, both analysed around the LAAO device.

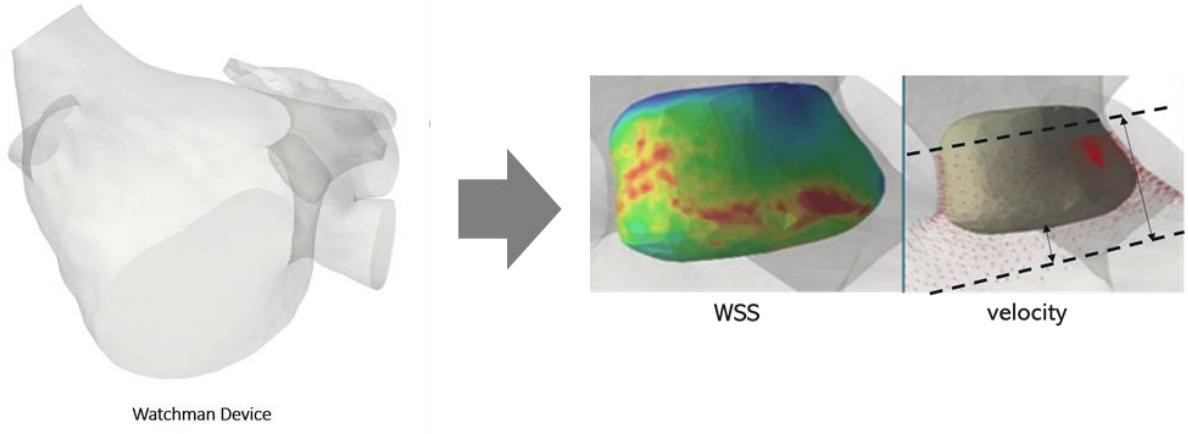

Figure 13: *Left atrial model domain. Evaluation zone around a plug-type device (Watchman). Wall shear stress (WSS) evaluated in the occluder surface (left) and the velocity in the fluid volume around the device (right).*

Spatial and time discretization were also verified (see Table 9 and Figure 14), again focusing on the two quantities of interest (i.e., average velocities and WSS around the device). Simulation data were analysed during the second simulated beat. Table 9 shows the obtained errors when increasing the time-step from a high resolution one (equal to 0.001 s), demonstrating how critical it is to carefully select an appropriate time-step that balances computational efficiency and accuracy. Smaller time-steps generally provide more accurate results but come at the cost of increased computational resources and longer simulation times. The reported error values suggest that Δt = 0.01 s and Δt = 0.005 s were within an acceptable range (5-7%) for the analysis, while larger time steps led to unacceptable errors.

Table 9: Time convergence study for a plug-type occluder device. WSS: wall shear stress.

Time Step convergence Δt [s]	0.1	0.05	0.01	0.005	0.001
with Plug Device (Δx = 1.83)					
Average WSS [Pa]	0.9823	1.3514	1.655	1.6685	1.680
Errors based on WSS [%]	41%	19.64%	1.4%	0.6%	-
Average velocity magnitude [m/s]	0.09511	0.06532	0.0721	0.0733	0.07723
Errors based on velocity [%]	23%	15%	6.6%	5%	-

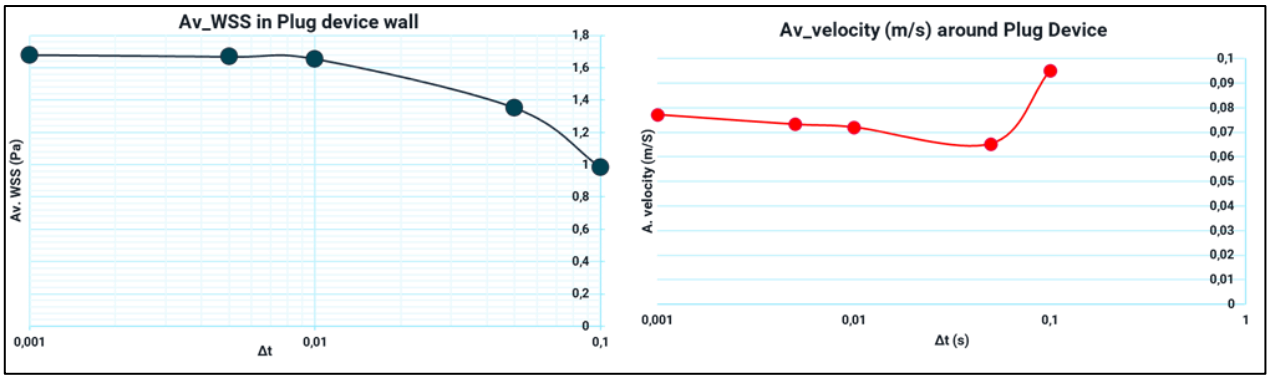

Figure 14: *Convergence trends when analysing time-step in the two quantities of interest around the left atrial appendage occluder device: average velocities and wall shear stress (WSS).*

Table 10 shows the quantification of convergence trends in the mesh convergence study. It can be observed that around 1 M mesh elements ensure robust estimations of the quantities of interest under analysis. Additionally, we also investigated the impact of adding boundary layers in the mesh with an occluder device since it has been shown to improve the accuracy of wall-related metrics such as WSS on fluid simulations. This was also the case in the performed experiments, as shown in Figure 15, where a comparison of the WSS distribution with and without boundary layers is displayed.

Table 10: Mesh convergence study for a plug-type occluder device. WSS: wall shear stress.

Mesh Convergence h =Δx [mm]	3.17	2.44	1.83	1.55
with Plug Device (simulation→ Δt = 0.01s)	150k	320k	750k	1.5M
Avg. WSS [Pa]	1.040	1.204	0.853	0.892
Errors [%]	17%	34.5%	4.5%	-
Avg. Velocity Magnitude [m/s]	0.0475	0.0778	0.0721	0.0732
Errors [%]	35%	6.2%	1.5%	-

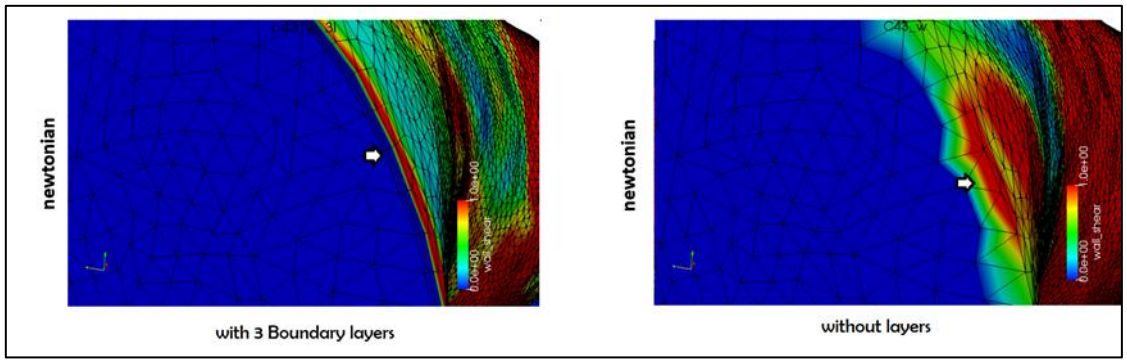

Figure 15: *Distribution of wall shear stress (WSS) in a Newtonian fluid model with (left) and without (right) boundary layers. The WSS distribution presents some artifacts in the latter scenario.*

3.2.3.2 IST Platform

Not applicable for UC2. IST platform fetches model results already calculated by UC2 model developers via an Internet connection.

3.2.4 Numerical Solver Error

3.2.4.1 Ansys Model

The adapted gradation of activities, listed from lowest to highest credibility, that reflects the rigor of the numerical solver error analysis is the following:

A) No solver parameter sensitivity was performed

B) No solver parameter sensitivity was performed. Solver parameters were established based on values from a previously verified computational model

C) Problem-specific sensitivity study was performed on solver parameters, confirming that changes in simulation results due to changes in the solver parameters were negligible relative to the model accuracy goal

Credibility level **(C)** is chosen from the gradation of activities reflecting the rigor of the sensitivity of numerical solver, since we have performed a sensitivity analysis modifying one of the most critical

parameter that we found in the previous VV40 experiment with fluid simulations without occluder devices (see SCT deliverable D3.2), namely the number of simulated cardiac beats.
Figure 16 represents the changes along different cardiac beats around the LAAO device for the time-averaged wall shear stress (WSS), the average WSS and the blood flow velocities. The stability of the obtained results suggests that the analysed flow characteristics and parameters remain consistent and reproducible over multiple cardiac cycles.

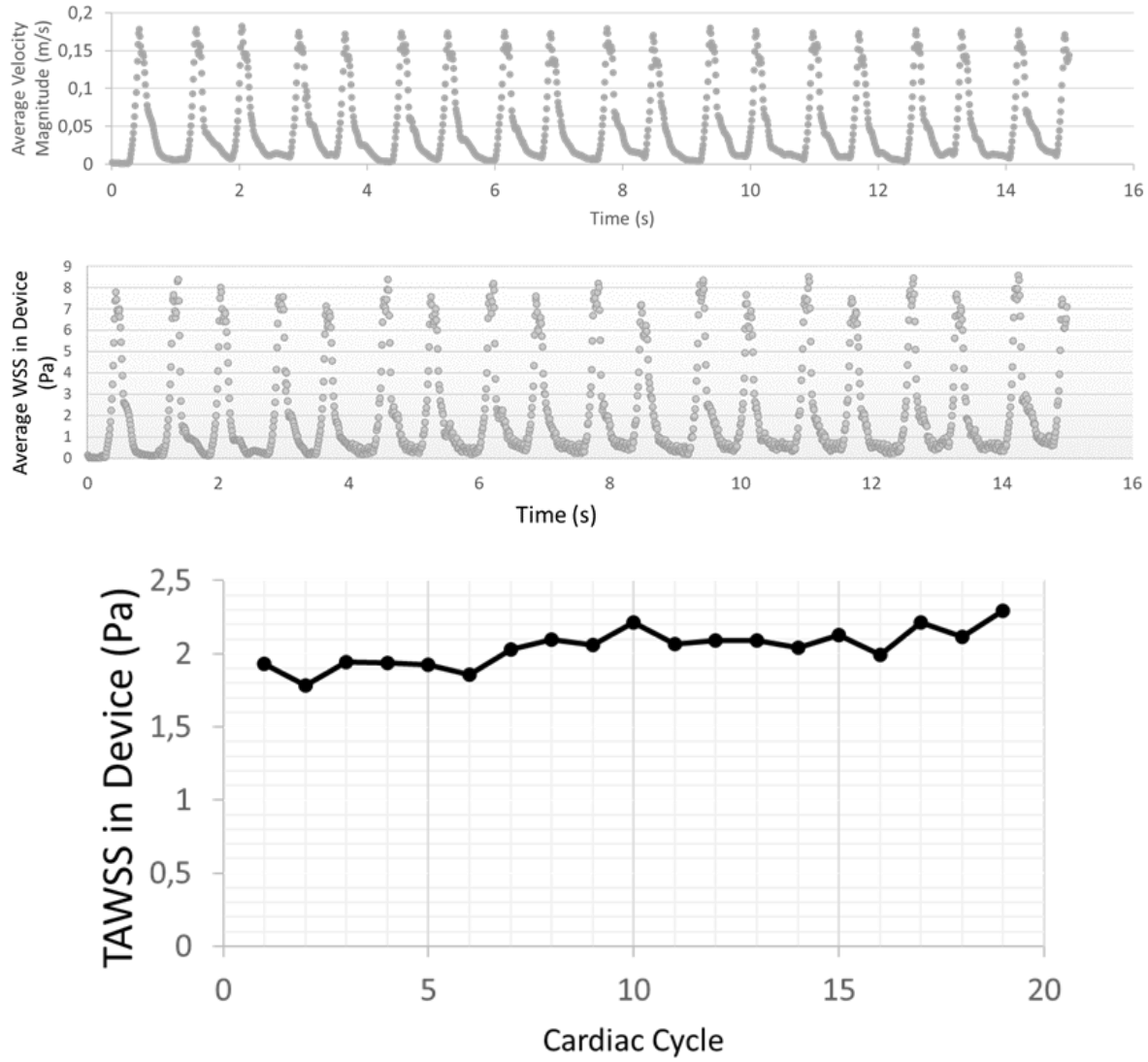

Figure 16: *Visualization of the time-averaged wall shear stress (TAWSS), WSS and average velocity around the left atrial appendage occluder device during 19 cardiac beats.*

3.2.4.2 IST Platform

Not applicable for UC2. IST platform fetches model results already calculated by UC2 model developers via an Internet connection.

3.2.5 Use Error

3.2.5.1 Ansys Model

The adapted gradation of activities for this credibility factor is the following:

A) Inputs and outputs are not verified

B) Key inputs and outputs are verified by the practitioner

C) Key inputs and outputs are verified by internal peer review

D) Key inputs and outputs are verified by reproducing important simulations as part of an external peer review

User errors typically arise from human factors and can be mitigated through appropriate training, meticulous attention to detail, and adherence to standardized in-silico protocols. The processing of medical images, which also depends on the image resolution of the available data, is a pivotal stage to build patient-specific three-dimensional models. Errors in this stage can accumulate and have a non-negligible impact in the modelling process. We have then performed experiments to analyse the key inputs and outputs (see Figure 17) in the developed modelling pipeline, evaluating the influence of critical model parameters and the correct application of the modelling approach, as well as the accurate interpretation of the results. As a result, our credibility level is classified as **(B)**.

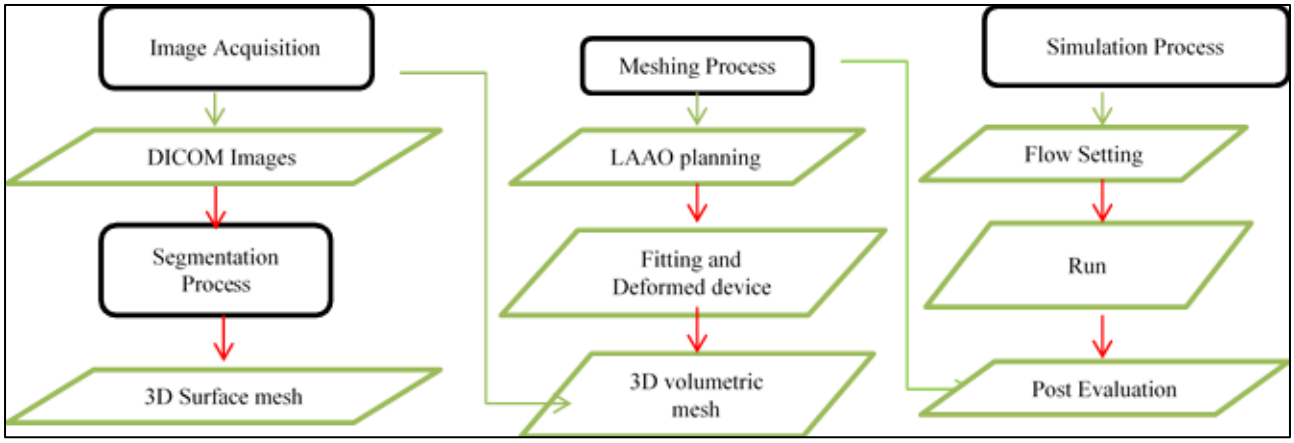

Figure 17: *Scheme of the developed modelling pipeline in Use Case 2, which represents each step where user error can occur. Inside the process, the results (green box) need to be checked.*

Outlined below are the measures undertaken to guarantee the aforementioned credibility of the model. The modelling pipeline comprises four key stages:

- Image Acquisition
- Image Segmentation
- Pre-Processing and Meshing
- Simulation Setup

Following the completion of each step, a thorough examination of both the inputs and outputs is conducted to ensure the absence of any errors.

Image Acquisition

The image acquisition protocol was meticulously designed and implemented by physicians to obtain high-resolution images and comprehensive visualization of the entire left atrial structure, which is essential for conducting fluid simulations in the left atria. Consequently, for COU1, three-dimensional cardiac CT images were captured using a 64-slice dual Source CT system (e.g., Siemens Definition, Siemens Medical Systems, Forchheim, Germany), featuring isotropic voxel sizes ranging from 0.37 to 0.5 mm and dimensions of 512 x 512 x [270-403] slices. Contrast agent was administered to facilitate accurate extraction of the targeted anatomy, specifically the left atrium. The protocol entails a biphasic injection approach, where 1mL/kg of Iomeprol 350mg/mL (Bracco, Milan, Italy) was infused at a rate of 5mL/s, followed by a 1mL/kg flush of saline at the same rate. Prior to the study, approval from the Institutional Ethics Committee of the hospital as obtained, and informed consent was provided by all participating patients.

In the case of COU2, two retrospective cardiac-gated computed tomography angiography images, one from a healthy individual and another from a patient with atrial fibrillation (AF), were acquired from Hospital de la Santa Creu i Sant Pau (Barcelona, Spain), following approval from the institutional Ethics Committee and obtaining informed consent from the patients. To capture dynamic movement in the CT scans, images were obtained using a Somatom Force scanner (Siemens Healthineers, Erlangen, Germany) with a biphasic contrast injection protocol, resulting in a slice thickness of 2 mm without overlapping. In the control case, full cardiac phase reconstruction was performed at every 1% interval of the cardiac cycle, except for the 34% to 48% interval, which was not acquired. For the AF patient, images were acquired at every 5% interval of the cardiac cycle (from 0% to 99% of the R-R interval). The left atria in both cases were segmented from the dynamic CT images using semi-automatic tools available in Slicer 4.10.11.

Image Segmentation

The first step involved ensuring the complete capture and visualization of the LA structure, which serves as the input for our simulation. Subsequently, for COU1, LA segmentation was performed on pre-procedural CT images using image processing techniques such as region growing and thresholding (with a mask intensity range of 300-2045). The segmentation process was carried out manually by two skilled biomedical engineers experienced in this task. Following that, an expert with extensive knowledge of LA simulations and anatomy carefully examined and selected the best segmentation for each case. In COU2, a similar process was employed, with the segmentation and assessment being conducted by the same experienced individual. However, the level of risk associated with COU2 was comparatively lower. From all the frames captured during a cardiac cycle, the first frame (frame 0) was chosen for simulation purposes, while the remaining frames were used to validate the movement over time.

Pre-Processing and Meshing

The binary masks derived from the CT images were further processed using semi-automatic tools available in Slicer 4.10.11. This enabled the reconstruction of patient-specific surface meshes both

before and after occlusion, employing the flying edges algorithm within Slicer. Furthermore, the occluder devices implanted in the patients, as seen in the post-CT images, were manually segmented to replicate their real configuration in the in-silico environment.

As the characterization of the LAA is not feasible in the post-occlusion CT scans, the reconstructed device was placed within the pre-occlusion mesh to simulate the LAAO configuration. To achieve this, a fiducial-based registration technique was performed between the pre- and post-LAAO meshes using Meshlab v2021-07. This registration involved manually selecting an average of eight landmarks in the PVs, LAA ostium, and MV annulus. The registration process was guided by rotations and translations, without altering the scale. This meticulous manual process, overseen by an expert in LA anatomy, ensured an accurate registration.

Subsequently, the web-based VIDAA platform was utilized to simulate the deployment of the device in the pre-LAAO mesh using computer-aided design (CAD) models, with the segmented device serving as a reference. The device segmentation allowed for identifying its size, type, and location from the post-CT images, which were then used to select the corresponding CAD model for deployment in the pre-CT LA geometry. The implementation of CAD models was necessary due to the limited spatial resolution of the CT scans, particularly in the plug device, where only the metallic structure was visible. Furthermore, the attachments of the plug-type device were removed after device compression to reduce computational costs. To determine the appropriate size for this configuration, recommendations based on anatomical measurements were incorporated within the VIDAA platform, following guidelines provided by device manufacturers [21]. To ensure the integrity of the mesh and prevent manual errors that could affect the quality of COU1, Meshlab and Meshmixer were employed to conduct a thorough quality check.

Finally, a 3D Delaunay refinement algorithm with Netgen tetrahedra quality optimization from Gmsh 4.5.4 software was employed to generate volumetric meshes for the fluid domain. The tetrahedral volumetric mesh resolution, consisting of 12 x 105 elements, adhered to recent publications proposed by [22] and sensitivity studies [6], [23] in the field. Finally, to ensure a reliable volumetric mesh, one of the key inputs for our simulations, meeting the minimum requirements, a mesh quality check was performed to identify and correct elements with orthogonal quality below 0.1 and negative cell volumes. Additionally, in cases where we need to extract movement from the LA, which serves as another input for COU2 in our simulations, the segmentation of all frames was carefully reviewed by an expert.

Simulation Setup

Python scripts were developed to establish a connection with ANSYS Fluent, facilitating the automation of processes to enhance efficiency and eliminate potential manual errors. Nevertheless, once the case is configured, the modeller meticulously verified that all the inputs were properly defined within ANSYS Fluent.

3.2.5.2 IST Platform

- For User defined input parameters: Lower-upper bounds are checked automatically by the interface. A webpage will recap all data entered by the user, and ask confirmation before

running the model on the cloud. Final user will be responsible of demonstrating that inputs were correct.

- For hard-coded input parameters: a peer review with model developers will ensure that parameters are correctly implemented on the cloud. Disclaimer exists in platform: "IST not responsible for the use of the outputs".
- For output parameters: IST to demonstrate that the model outputs are correctly reported in generated report (output to the user). Final user will be responsible that outputs are relayed and used correctly.

3.3 UC2 Discussion and Future Work

The verification of computational fluid simulations including left atrial appendage occluder devices is a complex and arduous task, requiring a thorough analysis of the modelling parameters and available data, as well as a large amount of computational resources. Prior to including LAAO devices, it is necessary to perform verification studies without it, to identify the most critical parameters in fluid simulations of the left atria. This prior step helps reducing the amount of experiments required when a LAAO device is included. Within SimCardioTest, we conducted the largest verification analysis of fluid simulations in the left atria available in the literature, as it was reported in SCT deliverable D3.2, and recently published in Khalili et al. [17].

The first step of the VV40 guidelines is to define the question of interest. Simulations can be used to answer different questions within the same application, and selecting the most relevant ones is not trivial. For doing so, all stakeholders (i.e., device manufacturers, clinicians, academics) need to be involved. The QI that was finally selected for Use Case 2 includes one of the most critical factors in LAAO device deployment, i.e., the presence of device-related thrombus, in relation with some key device settings that are chosen during the intervention. If simulations are credible, they could help to assess the influence of some device configuration settings (e.g., type, positioning) in the covering of the pulmonary ridge and its relation with DRT.

The definition of the context of use is another critical step in the VV40 guidelines, once the QI has been defined. The selection of the COU highly depends on the available sources of data. In Use Case 2, we have defined two different contexts of use, based on the availability or not of in-vitro testing experiments. The main reason is related to validation since it would be difficult to conduct experiments comparing fluid simulations with in-vitro testing data in large cohorts of cases and scenarios (see SCT deliverable D6.2). The first COU (COU1), only involves fluid simulations, allowing the generation of large cohorts such as the ones needed for in-silico trials. As only fluid simulations are used, the influence of the model is higher, but the large variability of the population is captured. The second COU (COU2), incorporates in-vitro testing experiments, producing data to be compared with simulation results, thus reducing the influence of the model.

Table 11 summarizes the verification credibility factor coverage in the model risk analysis for the two selected COUs. Coverage level determined in section 2.2 was converted in a 1-to-5 scale for consistency with section 1.2.5. It is important to emphasize that the initial gradation of activities for each credibility level has been adapted following available VV40 examples based on stents, due to the similarity with the use case based on LAAO devices.

Table 11: Verification Credibility Factors Coverage Level for Use Case 2 - COU1 and COU2 (cf. ASME VV40); * indicates validation activities not yet completed.

Model Risk					COU2	COU1	
Credibility Factor Coverage Level		1	2	3	4	5	
Code Verification: Software Quality Assurance	V			x	x		
Code Verification: Numerical Code Verification - NCV	V			x	x		
Calculation Verification - Discretization Error	V			x	x		
Calculation Verification - Numerical Solver Error	V			x	x		
Calculation Verification - Use Error *	III			x	x		

For verification, both COUs have the same credibility factor coverage. Regarding the Software Quality Analysis (SQA), the task was facilitated by the use of a commercial software, ANSYS Fluent, since there are several public documents on the experiments performed by the company to cover this item. To reach a higher level of credibility, we performed additional experiments based on classical benchmark studies with analytical solutions, comparing simulation results provided by ANSYS fluent and an open-source fluid solver, Oasis, developed by SIMULA SRL. Both solvers provided equivalent simulation outcomes, contributing to increase the confidence on the developed modelling pipeline.

The discretization error was analysed with classical spatial and time convergence experiments. They were complementary to the ones reported in SCT deliverable D3.2 since now the analysis was focused around the region of interest, i.e., the device, rather than evaluating the quantities of interest (i.e., blood flow velocities and WSS) in the whole left atria. The main conclusions drawn from the experiments is that blood flow velocities around the occluder device are not largely affected (< 5 % error) with meshes around 750 k elements (edges of 1.83 mm) and using time-steps lower than 0.01 s. For ensuring convergence, the recommendation then is to use meshes of at least 1 M elements and a minimum time-step of 0.01 s. Additional experiments could be run with finer grid discretization (e.g., 6 M, 24 M, 50 M mesh elements) but the associated computational cost is prohibitive (i.e., weeks of simulations) in relation to the model risk of the selected COUs. It is important to emphasize that these results are not in contradiction with the conclusions derived from the grid discretization analysis performed on fluid simulations in the LA without occluder devices (see SCT deliverable D3.2), which recommended the use of 10 M mesh elements for obtaining numerically robust simulation results. The main difference is that the analysed quantities of interest were different (e.g., ECAP, OSI in the entire LA, rather than blood flow velocities around the device, without considering a specific QI and the selected COUs; the sensitivity analysis described in this deliverable is tailored for properly answering the selected QI. Moreover, high-resolution modelling configurations will not make sense for processing the large cohorts of patient-specific cases required for in-silico clinical trials, and when other potential sources of errors in the patient-specific modelling pipeline (e.g., user errors such as image segmentation, availability of personalized boundary conditions) would have a larger impact on the final results. Finally, we found that adding boundary layers in the meshing process was beneficial for the studied quantities of interest.

We analysed the influence of the number of simulated cardiac beats as part of the numerical solver error study. Blood flow velocities and WSS distributions were consistent from the second cardiac beat. Additionally, other modelling parameters could be studied to increment the level of credibility

of this factor, such as analysing the convergence tolerance (i.e., residuals) or parameters of the dynamic mesh approach available in ANSYS Fluent for incorporating left atrial wall mechanics.

Finally, we have thoroughly investigated user errors, detailing the different steps that could influence the simulation results, especially the ones related to the building of patient-specific meshes from medical data. In the current version of the modelling pipeline, inputs and outputs of the different modelling steps are manually checked by experts, ensuring the required level of credibility for the simulations. However, works is needed to fully automatize these steps (e.g., mesh building and refinement), which after being analysed, would increase the level of credibility of this factor. On the other hand, there will not be any negative consequence on the initial in-silico trial scenario (see SCT deliverable D3.1) we have designed, which is based on an already available virtual population of simulations, previously run and manually checked.

In conclusion, we have performed the more comprehensive verification analysis of fluid simulations with LAAO devices up to date, perfectly complementing our previous VV40 studies without devices. We have identified the critical modelling parameters in relation with the selected QI and COUs, studying their influence on the quantities of interest to establish the credibility level of all important factors in the VV40 guidelines. Additional uncertainty studies could be beneficial for increasing some credibility levels, but it will not be critical for the work in SimCardioTest due to the defined model risk.

3.3.1 IST Platform

For what concerns the InSilicoTrials Platform, considering the need to finalize seamless integration with all partner components and to optimize performance, we are currently undergoing an architectural restructuring of the application. We will conduct end-to-end testing once we have the finalized interface in place.

4. Use Case 3

4.1 UC3 Model Summary

NOTE: This section is identical for both SCT deliverables D6.1 and D6.2. Refer to section 1.3 for document organization.

4.1.1 Background

Safety pharmacology studies evaluate cardiac risks induced by drugs. Since Torsade de Pointes (TdP), a well-known malignant arrhythmia, was related to pharmacological effects, regulatory guidelines have looked for biomarkers able to identify arrhythmogenic effects of drugs in order to withdraw them from the development process. Consequently, research efforts to ensure the safety of new molecules have become time-consuming and expensive for drug developers, delaying the release of new medicines into the market. Besides, initial tests focused on hERG (human ether-à-go-go related gene) activity and in vitro repolarization assays limited the development of potentially beneficial compounds, and the increasing attrition rate urged the design of new strategies.

The first initiative to include in-silico models was the Comprehensive in-vitro Proarrhythmia Assay (CiPA), which proposed integrating drug effects obtained in-vitro into a cardiomyocyte model to

predict TdP risk. Furthermore, the continuous development of new models opens the possibility to personalize computer simulations to optimize drug therapy.

4.1.2 Drug Description

Drugs are chemical compounds that exert a therapeutic action by modulating physiology. Besides the therapeutic effects, undesirable secondary effects can alter the normal functioning of different organs, including the heart.

Some molecules can modulate cardiac function by interacting with cellular mechanisms. Specifically, molecules that induce critical changes in ion channel permeability alter myocyte electrical activity, causing changes in heart rhythm with potentially fatal consequences. For this reason, drug developers need to perform safety pharmacology tests to evaluate drug candidates.

Before reaching cardiac tissue, drugs undergo a series of processes inside the body from its administration, including a distribution phase. Pharmacokinetics describes all these steps inside a living organism until the complete elimination of the substance, but interactions between each chemical compound and each organism differ. Pharmacokinetic processes are influenced by many external variables such as gender, age, weight, and previous pathologies, and the analysis of all the contributors is needed to determine the better therapeutic dose and route of administration.

Integrating pharmacokinetics and electrophysiology studies in drug assessment allows a more complete and personalized evaluation of the proarrhythmic risk by including the dosage and specific characteristics of the patient.

4.1.3 Question of Interest

The Question of Interest addressed by the model is the following:

- What is the maximum concentration/dose regimen of a drug to assure TdP-related safety in a population of healthy subjects?

4.1.4 Context of Use

A human electrophysiological (EP) model with pharmacokinetics (PK) can be used at early phases of drug development to obtain biomarkers that guide in selecting drugs and doses without TdP-risk for each subpopulation (male/ female/ age). This computational model is not intended to replace in vitro or animal experiments but to enrich and complement them by predicting additional outcomes. The goal of the in-silico trials is to help in designing clinical trials, to reduce the number of participants and protect them from suffering malignant arrhythmogenic events.

TdP-risk index is a metric obtained from a single or a set of electrophysiological biomarkers. By using appropriate threshold values, it performs a binary classification (safe/unsafe).

Quantities of Interest (QoI)

To obtain TdP-risk index, we considered action potential duration (APD90) and QT interval as the main indicators. Secondary biomarkers were calculated to improve predictions.

4.1.5 Model Risk

The following considerations support the assessment of the risk associated with the numerical model.

- Decision Consequence: Medium

An incorrect prediction with the computational model can have a risk on the development of the clinical trial if torsadogenic concentrations were administered. Low concentrations, on the other hand, do not have negative electrophysiological consequences.

- Model Influence: Medium

The model will complement preclinical and non-clinical (animal) experimental data and will help to design and refine the inclusion criteria and dosage in posterior clinical trials. In vitro and in vivo tests will still be required, but the number of participants in clinical trials as well as malignant arrhythmogenic events can be reduced. Therefore, the model will act as a complementary approach in determining safe drug concentrations.

- Model Risk: 3/5 (Medium-Medium)

Model Risk is based on Decision Consequence and Model Influence stated above, according to Risk Matrix in Figure 18 (cf. section 1.2.5).

Model influence	**high**	**3**	**4**	**5**
	medium	**2**	**3 COU**	**4**
	low	**1**	**2**	**3**
		low	**medium**	**high**
		Decision consequence		

Figure 18: *Model Risk Matrix (cf. ASME VV40) evaluating the COU included in UC3.*

4.1.6 Model Description

The computational model for proarrhythmia risk prediction integrates the following steps:

- Pharmacokinetics
- Heart electrophysiology
- Cardiac mechanics

One particular aspect of this in-silico strategy we propose for drug assessment is the inclusion of patient characteristics to optimize predictions.

The model pipeline initiates with drug pharmacokinetics, which consists of obtaining the plasmatic concentration following a specific compound dosage. This concentration is used as the input of the cellular model to simulate the drug effect on myocyte electrophysiology based on the interaction of the pharmacological molecule with ion channels. The last step of the computational model is to simulate and predict the electrophysiological activity in the whole heart.

Verification activities were evaluated separately in each computational model because the tools were developed independently.

4.2 UC3 Model Verification

4.2.1 Software Quality Assurance

4.2.1.1 PK Model

As a part of ExaMed which is a Software Medical Device, SQA procedures of ExaTwin/Papi follow the ISO/IEC 62304 norm. ExaTwin is a web service installed on ExactCure servers and accessed from third-party application (eg. IST platform) through the PAPI service. See details in annex A6.1-UC3-PK (UC3 PK Verification Annex), Software Quality Assurance section.

4.2.1.2 EP-0D Model

Main SQA procedures to install and use the computational model were specified and documented. The mathematical model is implemented in MATLAB, which means that algorithms, solvers, and built-in functions are backed by MathWorks. Developers can easily obtain repeatable results on different computers, including IST platform, which is the tool to which the end user will have access. See details in annex A6.1-UC3-0D (UC3 0D Verification Annex), Software Quality Assurance section.

4.2.1.3 EP-3D Model

Installation and use of the Simcardems software for 3D simulations of cardiac tissue were specified in GitHub documentation. Continuous integration methods and testing were implemented in main dependencies and Simcardems software itself. Developers can obtain repeatable results on different system architectures, including IST platform, which is the tool to which the end user will have access. See details in annex A6.1-UC3-3D (UC3 3D Verification Annex), Software Quality Assurance section.

4.2.1.4 IST Platform

SimCardioTest platform has been developed to host the three Use Cases developed within the project (sections 2.2.1.2, 3.2.1.2, and 4.2.1.4 respectively) and has been created in a private tenant within the InSilicoTrials's Azure account. The platform infrastructure is described in the figure below.

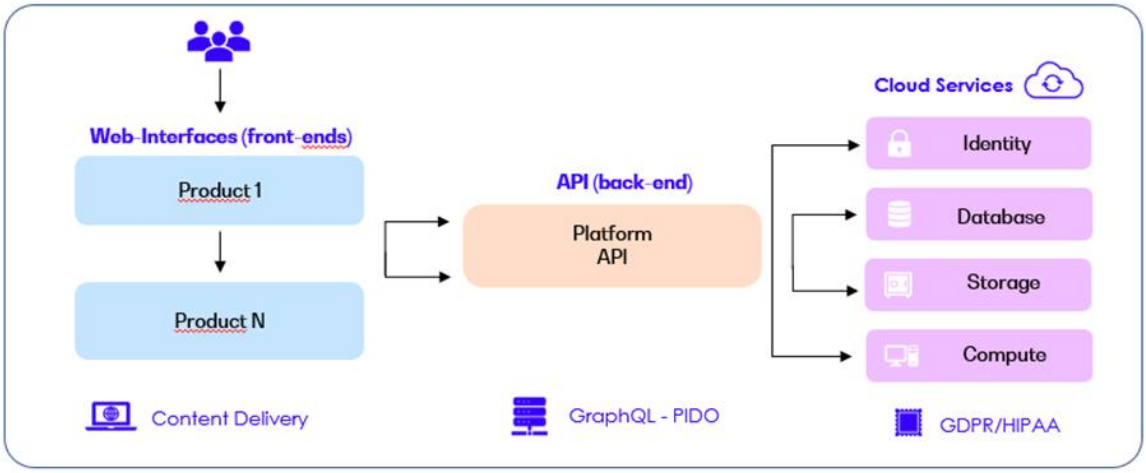

Figure 19: *InSilicoTrials platform infrastructure, applicable to UC1, UC2, and UC3.*

The architecture is split into 3 main parts:

- Front-End: VUE3 web interfaces are served through the Azure Content Delivery Network
- Back-End: ReST API layer connected to several Azure services
- Execution: handled through Azure Batch

Prior to starting the development, we analysed which cloud providers were compliant with regulations governing the pharmaceutical and healthcare industries. Microsoft Azure was selected due to its high compliance level (https://learn.microsoft.com/en-us/azure/compliance).

Azure has undergone independent third-party audits for quality management and information security, including ISO 9001 and ISO/IEC 27001 among many others. IP of model providers are protected against the downloading, copying, and changing of their models, while providing a safe environment for users to manage their own data. The whitepaper from Microsoft Azure Gxp Guidelines [3], which we've contributed to editing in the first version, highlights the compliance with the GxP. In the development of the platform, we've also followed the requests by FDA 21 CFR Part 11.

InSilicoTrials platform already embeds a variety of programming languages (e.g., C++, Python, R, Matlab) and simulation engines (e.g., NONMEM, ANSYS, Abaqus, CodeASTER, OpenFOAM) with no direct access to the solvers by the user. For the specific SimCardioTest Use Cases, we integrated the software required to run for each workflow.

Considering the need to finalize seamless integration with all partner components and to optimize performance, we are currently undergoing an architectural restructuring of the application. We will conduct end-to-end testing once we have the finalized interface in place.

Software Development

We follow the Agile SCRUM, a software development methodology that emphasizes iterative, incremental development and a flexible, collaborative approach to development. In an Agile

approach, requirements and solutions evolve through the collaborative effort of cross-functional teams, and the focus is on delivering working software quickly and responding to change.

We use Jira [4], a popular project management and issue tracking tool developed by Atlassian, to track and manage tasks, bugs, and other issues that arise during software development projects.

4.2.2 Numerical Code Verification

4.2.2.1 PK Model

PK models are systems of ordinary differential equations (ODEs) programmed in a proprietary user-friendly language that ExactCure system (ExaTwin) parses and solves when simulating a drug intake scenario. ODEs are solved numerically, and calibration involves numerical algorithms.

Numerical Code Verification has been performed in 2 steps:

- Algorithms verification (ODE, root solving)
- Drug simulation pipeline verification against benchmarks

The details are described in annex A6.1-UC3-PK (UC3 PK Verification Annex), Numerical Code Verification section.

An illustrative example of this process is shown in Figure 20 where the graph shows a good agreement between analytical and numerical solutions of drug concentration with time.

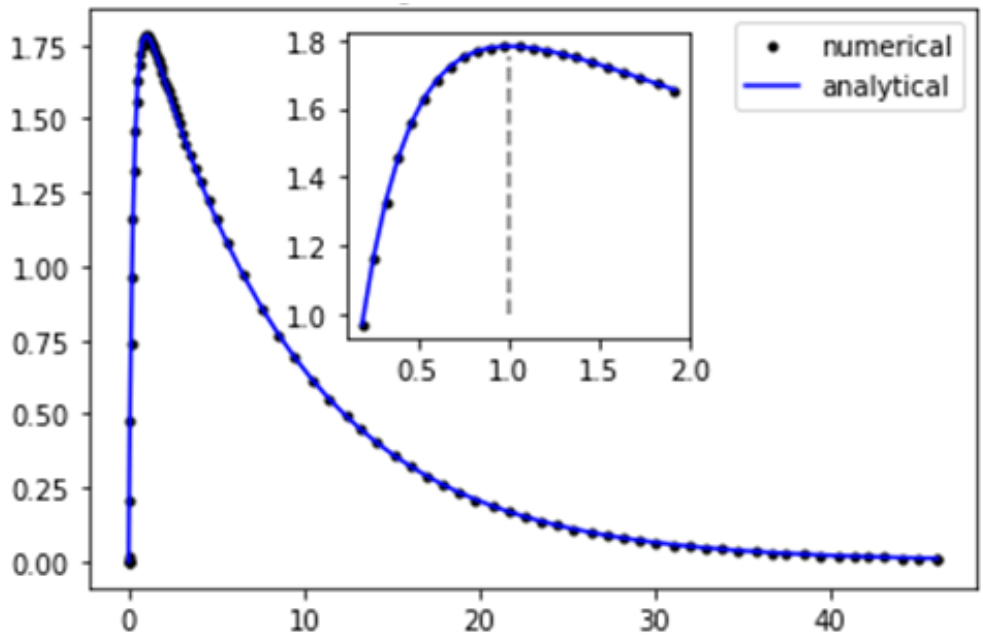

Figure 20: *Simulation output against analytical solution. 1 compartment, linear model. Concentration in mg/L, vs time in hours.*

4.2.2.2 EP-0D Model

In the absence of an accurate benchmark solution, the numerical solution was qualitatively compared with electrophysiological signals (action potential, calcium transient and isometric twitch). Other published codes were also used as comparators.

Figure 21 shows the main electrophysiological outputs used to verify the correct implementation of equations, i.e. an expected shape of the AP, intracellular Ca2+ concentration transient and the characteristic isometric twitch.

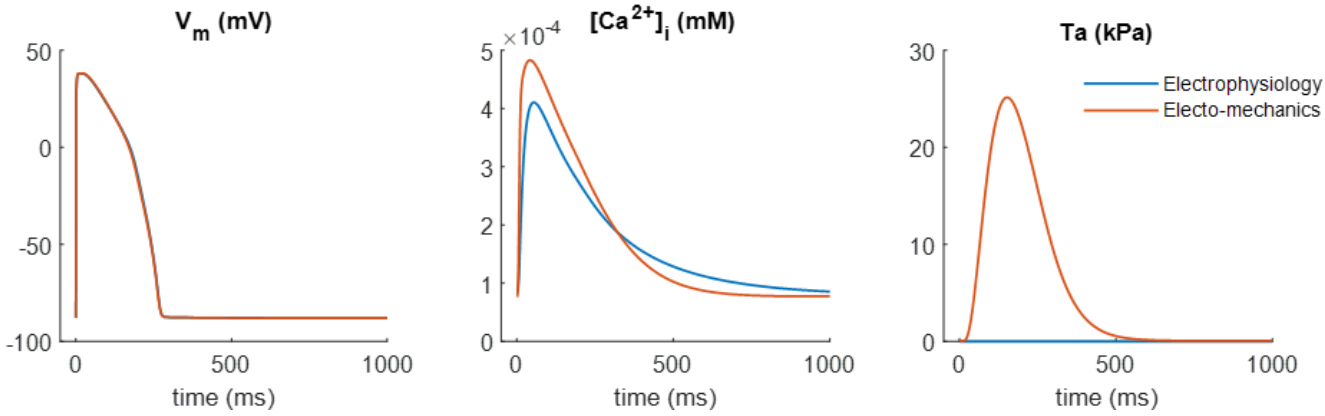

Figure 21: *Qualitative comparison of cellular outputs of two models.*

See details in annex A6.1-UC3-0D (UC3 0D Verification Annex), Numerical Code Verification section.

4.2.2.3 EP-3D Model

The model and required packages/modules were compared with published code and benchmarks for individual model components. The numerical solution was qualitatively compared with electrophysiological signals/biomarkers, as well as direct comparison with EP-0D model in this pipeline. See details in annex A6.1-UC3-3D (UC3 3D Verification Annex), Numerical Code Verification section.

4.2.2.4 IST Platform

- Step 1A: For OTS software: standard verification benchmarks provided by software house are run on cloud machine and results are compared to expected benchmark results.
- Step 1B: For MOTS & UD software: benchmarks defined by model developers are run on cloud machine using inputs agreed with model developers, results are compared to solutions expected by model developers.
- Step 2: The model is run on cloud machines using inputs agreed with model developers, results are compared to solutions expected by models developers.

4.2.3 Discretization Error

4.2.3.1 PK Model

No spatial discretization applies, drug time courses are solved with an adaptive time-step. See details in annex A6.1-UC3-PK (UC3 PK Verification Annex), Discretization and Numerical Solver Error section.

4.2.3.2 EP-0D Model

A stabilization test was performed to minimize errors and ensure model accuracy. A time-step convergence test was not performed because the cellular model was solved with a variable step size. Spatial discretization did not apply in this case. See details in annex A6.1-UC3-0D (UC3 0D Verification Annex), Discretization and Numerical Solver Error section.

4.2.3.3 EP-3D Model

The 3D model used two different discretizations: spatial and temporal. Both discretizations have been tested around the default values to assess time- and mesh-step convergence in a 3D slab of size 3x7x20 mm (see Figure 22). See details in annex A6.1-UC3-3D (UC3 3D Verification Annex), Discretization Error section.

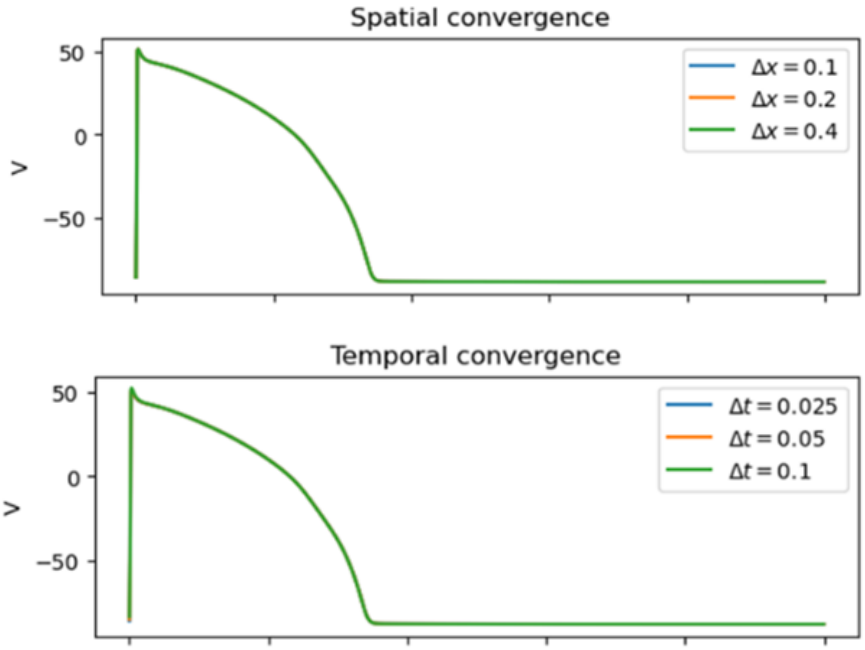

Figure 22: *Resulting traces of action potential (V) in a specific node of the 3D slab after performing spatial and temporal convergence tests.*

4.2.3.4 IST Platform

Discretization Error analysis provided by model developer applies. The model is run on the IST platform for time and space discretization parameters agreed with model developer, and results are compared to solutions expected by model developers. In case of mismatch, an additional discretization error analysis on the cloud engine may be required.

4.2.4 Numerical Solver Error

4.2.4.1 PK Model

ODE solver was verified against benchmarks, and a convergence analysis by reducing solver tolerances was performed.

Root solving algorithm was verified against benchmarks, and a convergence analysis was performed.

Solver parameters cannot be changed from the drug simulation interface, convergence analysis at this level will be performed in a future work.

We performed a Parameters estimation verification and a Maximum concentration verification for each molecule available from the public interface and in scope of H2020/SimCardioTest; Figure 23 shows an example. The maximum concentration after one drug intake and at steady state. were extracted numerically. Similarly, we used the model parameters to compute the theoretical maximum concentration after one drug intake and at steady state, and the results were compared.

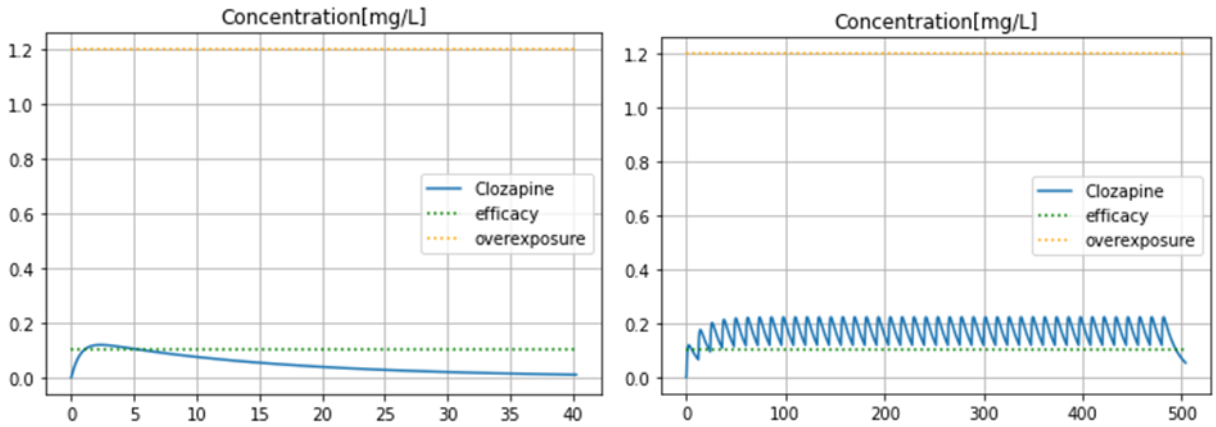

Figure 23: *Numerical simulation with a male patient, clozapine is administered orally every 12 hours with a dose of 100mg, for a period of 20 days (where steady state is practically obtained).*

See details in annex A6.1-UC3-PK (UC3 PK Verification Annex), Discretization and Numerical Solver Error section.

4.2.4.2 EP-0D Model

Although solver parameters were established based on initial values used by the original computational model, we compared the computational cost between different solver options, and analysed the effects of varying convergence tolerances.

Figure 24 shows an example of action potential duration (APD90) stabilization using different tolerances.

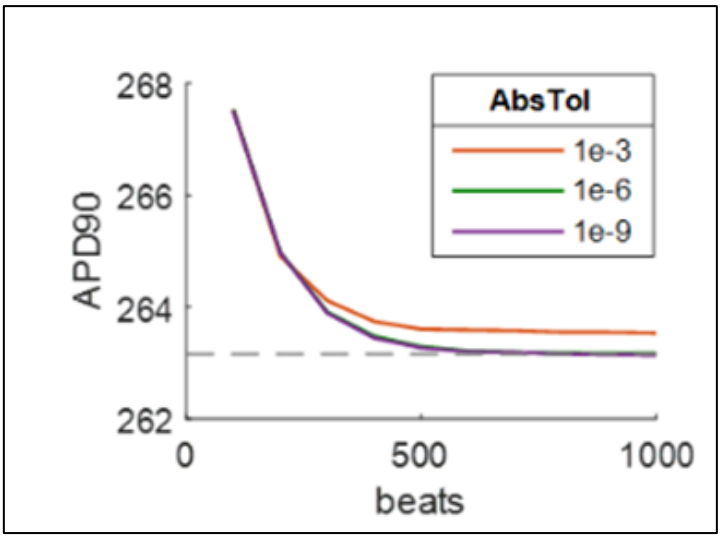

Figure 24: *Effect of absolute tolerance error on convergence.*

See details in annex A6.1-UC3-0D (UC3 0D Verification Annex), Discretization and Numerical Solver Error section.

4.2.4.3 EP-3D Model

Not Applicable. Users in IST platform will not be able to change the settings for the solver and default values will be used.

4.2.4.4 IST Platform

Numerical Solver Error analysis provided by model developer applies. The model is run on the IST platform for numerical solver parameters agreed with model developer, and results are compared to solutions expected by model developers. In case of mismatch, an additional numerical solver error analysis on the cloud engine may be required.

4.2.5 Use Error

4.2.5.1 PK Model

Several input checks are setup to prevent use error, from peer review of model inputs to automatic input checks on interfaces (internal and external). See details in annex A6.1-UC3-PK (UC3 PK Verification Annex), Use Error section.

4.2.5.2 EP-0D Model

Key inputs and outputs were verified by internal peer review. See details in annex A6.1-UC3-0D (UC3 0D Verification Annex), Use Error section.

4.2.5.3 EP-3D Model

Model inputs are required to be the correct type. This is automatically tested in the software and results in a warning or error for incorrect use. See details in annex A6.1-UC3-3D (UC3 3D Verification Annex), Use Error section.

4.2.5.4 IST Platform

- For User defined input parameters (control of drugs, doses, IC50 values, etc.): Lower-upper bounds are checked automatically by interface. A webpage will recap all data entered by the user, and ask confirmation before running the model on the cloud. Final user will be responsible of demonstrating that inputs were correct.
- For hard-coded input parameters: a peer review with model developers will ensure that parameters are correctly implemented on the cloud. Disclaimer exists in platform: "IST not responsible for the use of the outputs".
- For output parameters: IST to demonstrate that the model outputs are correctly reported in generated report (output to the user). Final user will be responsible that outputs are relayed and used correctly.

4.3 UC3 Discussion and Future Work

The credibility on the predictive capability of the computational model for proarrhythmic assessment required Verification actions of at least intermediate rigor because the tool was considered to have a medium risk level for the defined COU.

Table 6 shows that the score planned to be achieved by verification activities is equal or larger than III, according to the general gradation of credibility factors and the rationale behind each item, as explained in previous sections. Each credibility factor is the combination of the different actions taken for each of the three individual models that comprise the computational application for drug evaluation, and the final score represents the most restrictive level.

Table 12: Verification Credibility Factors Coverage Level for Use Case 3 (cf. ASME VV40); * indicates verification activities not yet completed.

Model Risk					x		
Credibility Factor Coverage Level		1	2	3	4	5	
Code Verification: Software Quality Assurance	III			x			
Code Verification: Numerical Code Verification - NCV *	IV			x			
Calculation Verification - Discretization Error *	III			x			
Calculation Verification - Numerical Solver Error *	III			x			
Calculation Verification - Use Error *	IV			x			

The future work for each of the models and the IST platform is as follows:

4.3.1 PK Model

Concerning PK models, next steps in Verification will include:

- Completion of the molecule scope (not all models have been verified yet)
- Sensitivity analysis of model outputs to solver parameters
- Convergence analysis and drug simulation interface level

4.3.2 EP 0D Model

High level verification activities were possible on the cellular electrophysiological model due to the use of a standard software application and the simplicity to control calculation error. Therefore, no

future verification work is expected. Indeed, we also included the evaluation of the electromechanical version of the model for future use.

4.3.3 EP 3D Model

The electrophysiological tissue model and Simcardems software are verified and changes in the code are continuously reported on the open source GitHub page. This automatic continuous integration and reporting will verify minor updates in the software. In future use of the model, additional features will be added to the software such as electromechanics and generation of ECG signals. These features will require the same verification steps as currently applied to the software.

4.3.4 IST Platform

Concerning verification activities on the platform, next steps will include the integration of EP-3D Model and verification tests (code verification, calculation verification, use error).
Finally, in case updated versions of model codes will be integrated on the platform, new verification tests will be performed. Also, after finalization of seamless integration of all components and architectural restructuring of the application, we will conduct end-to-end testing.

5. Conclusion

This report and its annexed documents constitute the SimCardioTest WP6 deliverable D6.1 due in June 2023 (M30). It described all verification activities engaged for assessing the credibility of computational models developed in the frame of Use Cases 1 to 3 (cf. WP2, 3, and 4 respectively). This report is closely linked to SCT deliverable D6.2 which reports the validation activities also supporting the credibility of the models.

Verification was conducted on one specific model per each Use Case, corresponding to a pre-selected Question of Interest (QI). All verification activities are conducted according to ASME VV40 standard guidelines. Some of the engaged verification activities are still ongoing at the date of this publication, and will be documented at later time once completed.

For what concerns Use Case 1, the verification activities that were planned and are currently being completed were designed to provide a high level of credibility of the software and numerical methods. Even if the model risk evaluated with respect to the ASME VV40 standard is low, we made great effort to setup Continuous Integration and Software Quality Assurance tools that are not frequently used in the applied mathematics scientific community. Although it is time consuming, this process helped us in developing a good quality solver for the complete 3D model of pacemaker and cardiac tissue, which should be available during summer 2023. Together with the convergence and sensitivity tests we are currently running, we will be able to propose electrophysiology software that stands out thanks to the rigorous framework the SimCardioTest project requires.

For what concerns Use Case 2, we have performed the more comprehensive verification analysis of fluid simulations with LAAO devices up to date, perfectly complementing our previous VV40 studies without devices. We have identified the critical modelling parameters in relation with the selected QI and COUs, studying their influence on the quantities of interest to establish the credibility level of all important factors in the VV40 guidelines. Additional uncertainty studies could be beneficial for

increasing some credibility levels, but it will not be critical for the work in SimCardioTest due to the defined model risk.

For what concerns Use Case 3, completed verification activities provide the appropriate credibility required by the application tool developed to assess the torsadogenic risk of drugs. Computational models and the final cloud platform were verified following VV40 standards, assuring software quality and reporting errors along the whole pipeline. Furthermore, results reproducibility and user error control by the IST platform guarantees that the tool for client use will perform as the initial model but by means of a simple graphical interface.

6. Bibliography

[1] V&V40, "Assessing Credibility of Computational Modeling Through Verification and Validation: Application to Medical Devices," ASME, New York, 2018.

[2] "cellML database," [Online]. Available: https://models.cellml.org/electrophysiology.

[3] "Microsoft Azure Gxp Guidelines Whitepaper," [Online]. Available: https://azure.microsoft.com/mediahandler/files/resourcefiles/microsoft-azure-gxp-guidelines-april/Microsoft%20Azure%20GxP%20Guideline%20(FINAL)%20July%202020.pdf.

[4] "Jira," [Online]. Available: https://www.atlassian.com/software/jira.

[5] A. Cresti, M. García-Fernández, H. Sievert and others, "Prevalence of extra-appendage thrombosis in non-valvular atrial fibrillation and atrial flutter in patients undergoing cardioversion: a large transoesophageal echo study," *EuroIntervention,* vol. 15(3), p. e225–e230, 2019.

[6] M. Pons, J. Mill, A. Fernandez-Quilez and others, "Joint Analysis of Morphological Parameters and In Silico Haemodynamics of the Left Atrial Appendage for Thrombogenic Risk Assessment," *Journal of interventional cardiology,* 2022.

[7] A. Sedaghat and G. Nickenig, "Letter by Sedaghat and Nickenig Regarding Article, "device-Related Thrombus after Left Atrial Appendage Closure: Incidence, Predictors, and Outcomes," *doi:10.1161/CIRCULATIONAHA.118.036179,* 2019.

[8] J. Saw, A. Tzikas, S. Shakir and others, "Incidence and clinical impact of device-associated thrombus and peri-device leak following left atrial appendage closure with the amplatzer cardiac plug," *JACC: Cardiovascular Interventions,* vol. 10, p. 391–399, 2017.

[9] L. V. Boersma, B. Schmidt, T. R. Betts and others, "Implant success and safety of left atrial appendage closure with the watchman device: peri-procedural outcomes from the ewolution registry," *European heart journa,* vol. 37, p. 2465–2474, 2016.

[10] A. Sedaghat and others, "Device-Related Thrombus After Left Atrial Appendage Closure: Data on Thrombus Characteristics, Treatment Strategies, and Clinical Outcomes From the EUROC-DRT-Registry," *Circulation. Cardiovascular interventions,* Vols. 14,5, no. e010195, 2021.

[11] I. Chung and G. Y. Lip, "Virchow's triad revisited: Blood constituents," *Pathophysiology of Haemostasis and Thrombosis,* vol. 33, no. doi:10.1159/00008384, p. 449–454, 2003.

[12] O. D. Backer, X. Iriart, J. Kefer and others, "Impact of computational modeling on transcatheter left atrial appendage closure efficiency and outcomes," *JACC: Cardiovascular Interventions,* vol. 16, no. doi:10.1016/j.jcin.2023.01.008, p. 655–666, 2023.

[13] J. Saw, J. P. Lopes, M. Reisman and H. G. Bezerra, "CT Imaging for Percutaneous LAA Closure," *Cham: Springer International Publishing,* no. doi:10.1007/978-3-319-16280-5, p. 117–132, 2016.

[14] A. M. Aguado, A. L. Olivares, E. Silva and others, "In silico optimization of left atrial appendage occluder implantation using interactive and modeling tools," *Frontiers in physiology,* vol. 10, p. 237, 2019.

[15] X. Freixa and others, "Pulmonary ridge coverage and device-related thrombosis after left atrial appendage occlusion," *EuroIntervention : journal of EuroPCR in collaboration with the Working Group on Interventional Cardiology of the European Society of Cardiology,* vol. 16(15), no. doi:10.4244/EIJ-D-20-00886, pp. e1288-e1294, 2021.

[16] A. Santiago, C. Butakoff, B. Eguzkitza and others, "Design and execution of a verification, validation, and uncertainty quantification plan for a numerical model of left ventricular flow after lvad implantation," *PLoS computational biology,* vol. 18, no. e1010141, 2022.

[17] E. Khalili, C. Daversin-Catty, A. Olivares and others, "On the importance of fundamental computational fluid dynamics towards a robust and reliable model of left atrial flows: Is there more than meets the eye?," *arXiv:2302.01716 [physics.flu-dyn],* 2023.

[18] ANSYS, "Software quality assurance," 2015. [Online]. Available: https://www.ANSYS.com/company-information/quality-assurance.

[19] ANSYS, "Benchmark verification test case," 2005. [Online]. Available: https://www.ANSYS.com/it-solutions/benchmarks-overview.

[20] M. Schäfer, S. Turek, S. Durst and others, "Benchmark Computations of Laminar Flow Around a Cylinder. In: Hirschel, E.H. (eds) Flow Simulation with High-Performance Computers II. Notes on Numerical Fluid Mechanics (NNFM), vol 48. Vieweg+Teubner Verlag," no. DOI: https://doi.org/10.1007/978-3-322-89849-4_39.

[21] C. Albors and others, "Sensitivity Analysis of Left Atrial Wall Modeling Approaches and Inlet/Outlet Boundary Conditions in Fluid Simulations to Predict Thrombus Formation," *In: , et al. Statistical Atlases and Computational Models of the Heart. Regular and CMRxMotion Challenge Papers. STACOM 2022. Lecture Notes in Computer Science, Springer, Cham.,* vol. 13593, no. DOI: https://doi.org/10.1007/978-3-031-23443-9_17.

[22] K. Korsholm and J. Nielsen-Kudsk, "The Art of Planning a Left Atrial Appendage Closure: Will Computational Modeling Simplify the Intervention?," *JACC Adv.,* vol. 1 (5), no. https://doi.org/10.1016/j.jacadv.2022.100138, 2022.

[23] J. Mill, V. Agudelo, A. Olivares and others, "Sensitivity analysis of in silico fluid simulations to predict thrombus formation after left atrial appendage occlusion," *Mathematics,* vol. 9(18), p. 2304, 2021.

7. Appendices

Detailed implementation of the verification activities and results can be found in the annex documents listed in Table 13.

Table 13: List of Attachments.

Reference	Title
A6.1-UC1	Use Case 1 Verification Annex
A6.1-UC2	Use Case 2 Verification Annex
A6.1-UC3-PK	Use Case 3 PK Verification Annex
A6.1-UC3-PK-IST *	Use Case 3 PK Verification Annex - IST Integration
A6.1-UC3-0D	Use Case 3 0D Verification Annex
A6.1-UC3-3D	Use Case 3 3D Verification Annex

* NOTE: Only Use Case 3

added on 25 September 2025:

ANNEX A (WP6 complement of D6.1 and D6.2)

ANNEX B (WP6 UC3 PK Verification), which cover the additional work carried out between M30 and M54

This project received funding from the European Union's Horizon 2020 research and innovation program under grant agreement No 101016496

EU Horizon 2020 Research & Innovation Program
Digital transformation in Health and Care
SC1-DTH-06-2020
Grant Agreement No. 101016496

SimCardioTest - Simulation of Cardiac Devices & Drugs for in-silico Testing and Certification

Technical Report

D6.1-UC1: Use Case 1 Verification Annex

Work Package 6 (WP6)
Verification, validation, uncertainty quantification & certification

Annex Lead: UBx, France
Task Lead: UBx, France
WP Lead: MPC, France

PUBLIC

Document history			
Date	**Version**	**Author(s)**	**Comments**
25/06/2023	V1	M. LEGUEBE	Template, SQA elements
21/06/2023	V2	M. LEGUEBE	Ready for consolidation
23/06/2023	V3	R. SETZU	Format consolidation
29/06/2023	V4	H. AREVALO	Quality Review
30/06/2023	V5	R. SETZU	Final Version
01/07/2024	V6	R. SETZU, M. BARBIER	Format editing

TABLE OF CONTENTS

EXECUTIVE SUMMARY

This document is an annex of SimCardioTest deliverable D6.1 and was elaborated for Use Case 1 in the context of the assessment of cardiac pacing leads. It contains the technical details for the verification of the UC1 numerical model and the verification activities performed by InSilicoTrials during the integration of the aforementioned model in the cloud platform of SimCardioTest project.

Acronyms

Table 1: List of Acronyms.

Acronym	Meaning
CEPS	Cardiac ElectroPhysiology Solver
CI	Continuous Integration
ODE	Ordinary Differential Equation
PDE	Partial Differential Equation
SCT	SimCardioTest
SQA	Software Quality Assurance

1. Code Verification

1.1 Software Quality Assurance

1.1.1 Presentation of CEPS

CEPS (Cardiac ElectroPhysiology Solver) is one of the user-developed applications of by the Inria team Carmen. It is a modular high-performance computing software for performing numerical simulations in cardiac electrophysiology. Some of CEPS features include:

- Management of geometries represented by meshes in 3D, 2D or 1D (volumes, surfaces, trees)
- Model simulation of cellular electrophysiology
- Calculating the tissue propagation of the action potentials in the cardiac geometries
- Calculation of extra-cardiac potentials
- Time approximation methods in order 2, 3 and 4 specific to electrocardiography

CEPS is designed to run on massively parallel architectures, and to make use of state-of-the-art and well known computing libraries to achieve realistic and complex heart simulations.

CEPS is publicly available to use and contribute, under the LGPL-v3 Licence. It relies on the following dependencies:

- An MPI implementation, such as openMpi [1] for parallel communications
- Eigen [2], for small linear algebra operations
- PETSc [3], version 3.14 or higher, for solving large sparse linear systems in parallel
- CxxTest [4], for the unit tests
- At least one of the mesh partitioning libraries: ParMETIS [5], PTScotch [6]
- VTK [7], for standard data I/O

CEPS has regularly benefited from engineering support and an environment of good programming practices since the first stages of development in 2011. Continuous Integration (CI) has been set up (section 1.1.2) for CEPS in 2017, and Software Quality Assurance (SQA) has been pushed further for the SimCardioTest project by running code analysis through the SonarQube platform (section 1.1.3).

1.1.2 Continuous Integration and Unit Tests

Since early development, CEPS embarks on a suite of unit tests designed to ensure the good execution of the program. These unit tests are themselves small programs that are intended to cover small portions of the main code, and are supposed to pass (succeed) even if modifications are brought to other sections of the code.

Initially, the tests can be run on demand on the developer's machine. As CEPS was migrated onto Inria's instance of Gitlab, we setup Continuous Integration machines on which the unit tests are run each time the code is updated on the repository, thus automating the testing procedure. A message is sent every time an update from a developer leads to a failing build-and-test pipeline (Figure 1).

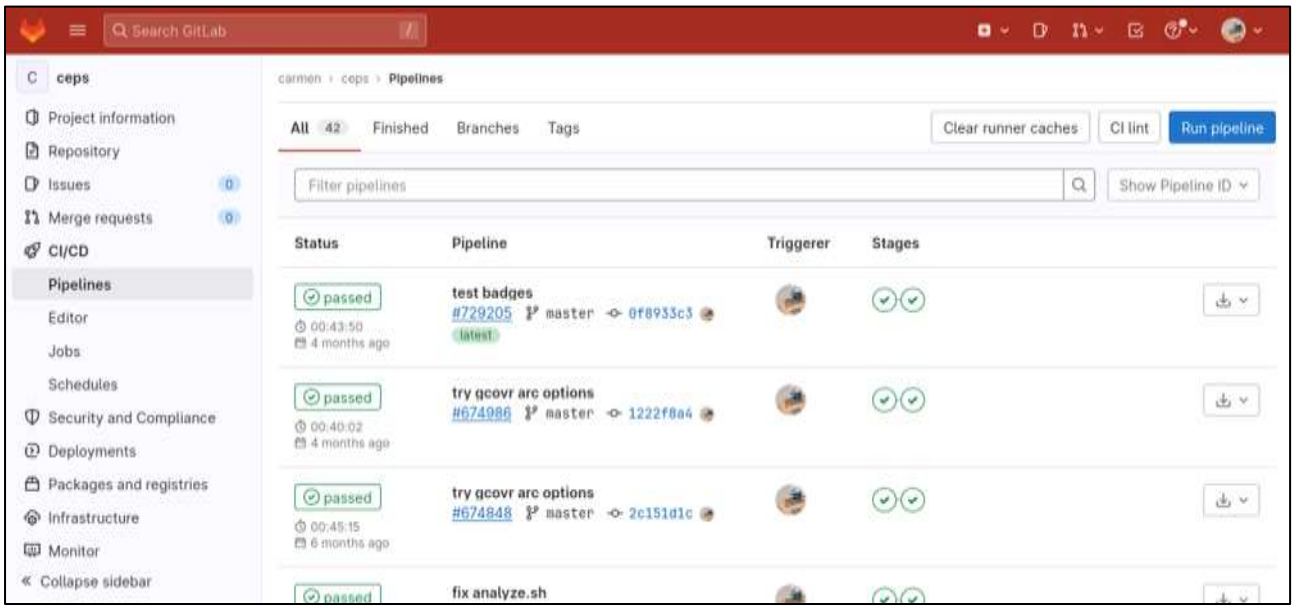

Figure 1: *Gitlab build and testing pipelines for CEPS.*

At the time of writing, the testing suite of CEPS is made of 360 unit tests. Each unit test can perform one or several of the following tasks:

- Verification that the code runs without crashing in normal conditions
- Verification that the code stops when wrong inputs are given to the program or internally, categorized as Use Error
- Verification of the accuracy of the results (or NCV Numerical Code Verification). These tests are discussed specifically in section 1.2 of this document

There are around 250 unit tests that are dedicated to non-NCV tasks. We do not give an exhaustive list of the tested items. To cite a few, tests range from very basic elements, such as verification of automatic deduction of type variable, character string manipulation tools, to more complex program units, such as mesh partitioning or management of data arrays in parallel.

1.1.3 Analysis of Code using SonarQube

Beyond running unit tests, additional analysis can be performed on demand during development, and automatically at each update on the Gitlab repository. For this, we wrote an analysis script that invokes the following tools:

- **cppcheck**, which runs a syntactic analysis of static code. The list of checked elements can be found on cppcheck documentation [8]
- **gcovr**, which tracks the lines of code through which the unit tests have passed, and in which states they were passed through (conditional loops, etc.)
- **valgrind**, which tracks memory leaks that could lead to forced program interruption during execution

We then send the analysis logs from these tools to Inria's instance of the SonarQube linter. This platform regroups the results and produces an interactive report of issues that were detected. The issues are raised with respect to a set of ~5,800 C++ rules that were selected by the Experimental Development branch of Inria. Rules originate from various C++ analysis tools and SonarQube own set of rules [9]. Issues can then be tracked and resolved by developers to produce clean code (Figure 2).

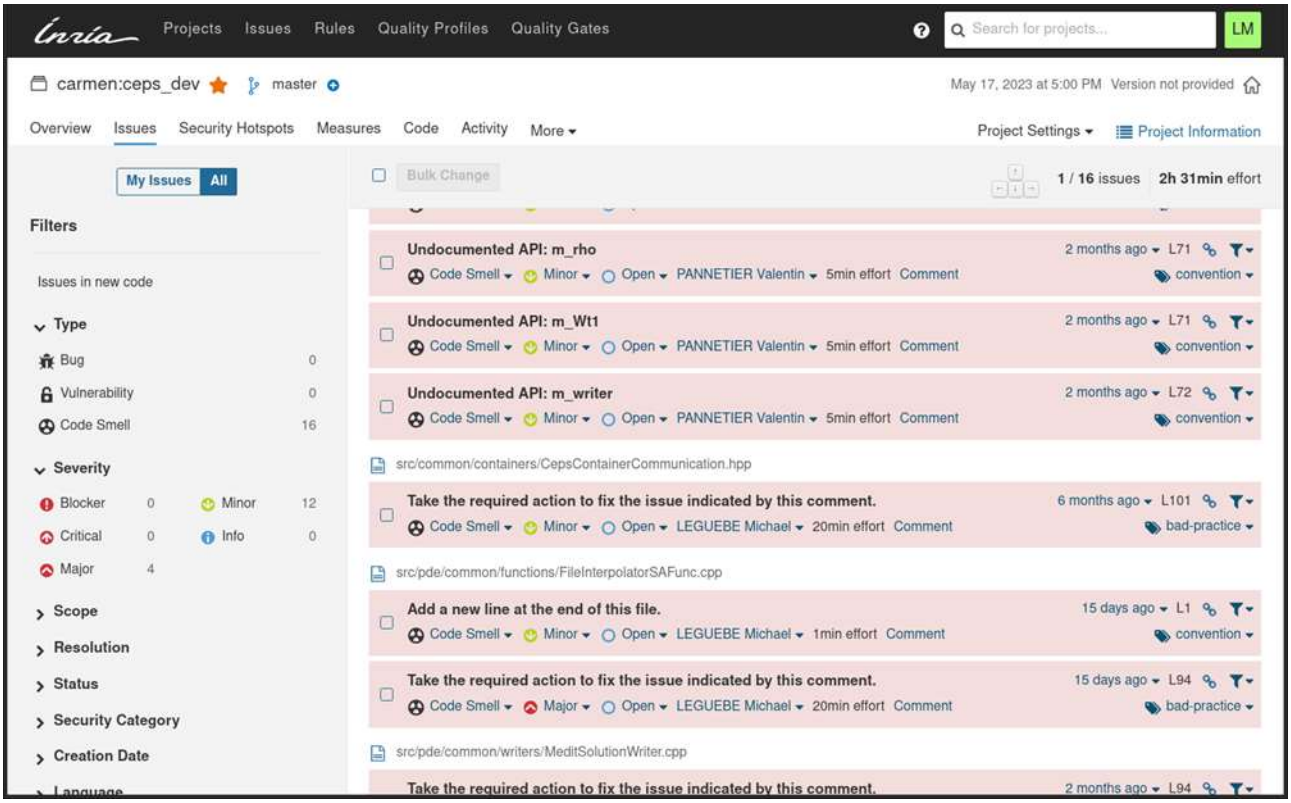

Figure 2: *SonarQube issue tracker allows to affect, inspect and eventually mark as resolved all problems that were detected by analysis tools.*

In addition, several measures are displayed by SonarQube for each source file. For example, we can monitor which lines were not covered by tests, which may be the source of bugs (Figure 3).

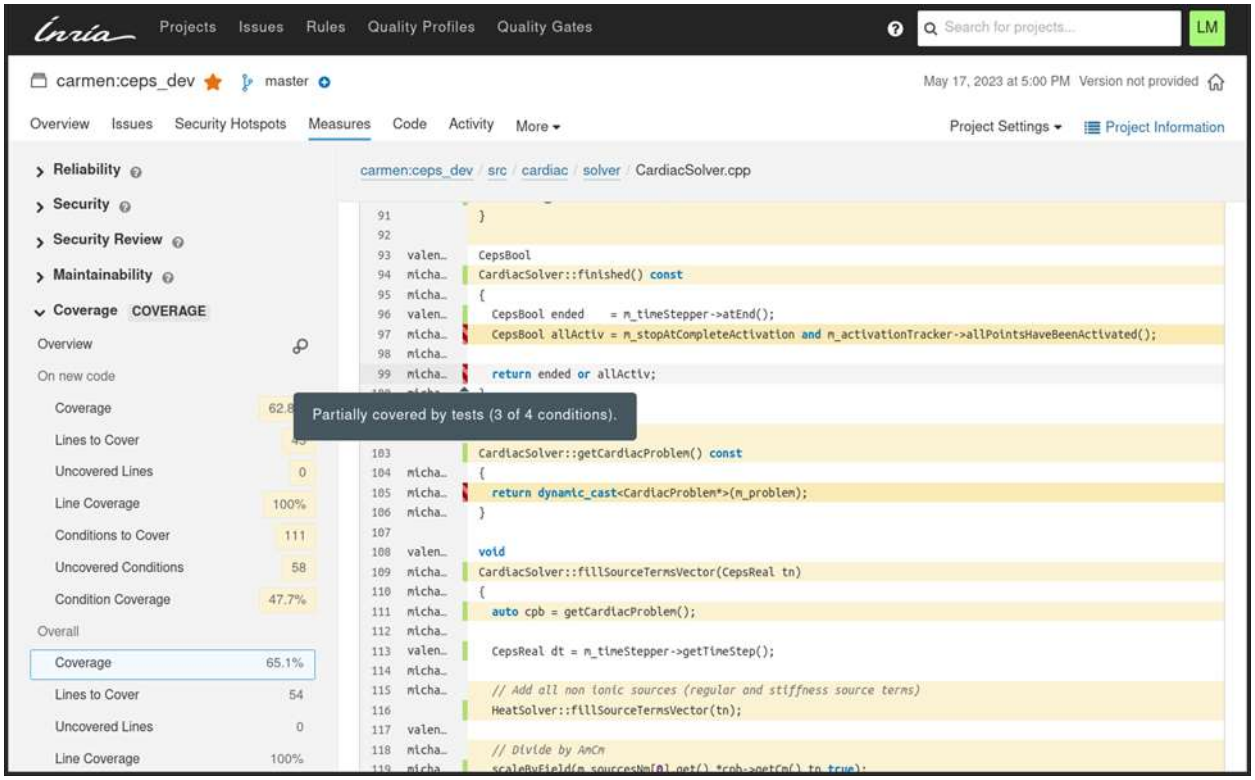

Figure 3: *SonarQube coverage report for a single file highlights the lines that were not covered or partially covered by unit tests.*

Finally, SonarQube defines the notion of Quality Gate: it consists in fulfilling several criteria. For CEPS, the criteria are the following (Figure 4):

- All unit tests must pass
- Coverage of the code by unit tests must be greater than 80% (CEPS: 89.3%)
- There should be less than 3% of duplicated code (CEPS: 0.5 %)
- Maintainability must be rated A, i.e. evaluated time to fix issues should be less than 5% development time (as guessed by SonarQube, CEPS: less than 0.1%)

Reliability must be rated A, i.e. no bugs should be found by SonarQube. However, this does not prevent bugs, and the unit tests are designed to eliminate most of them. These ratings are exported as badges that are displayed on the main web page of CEPS (Figure 5).

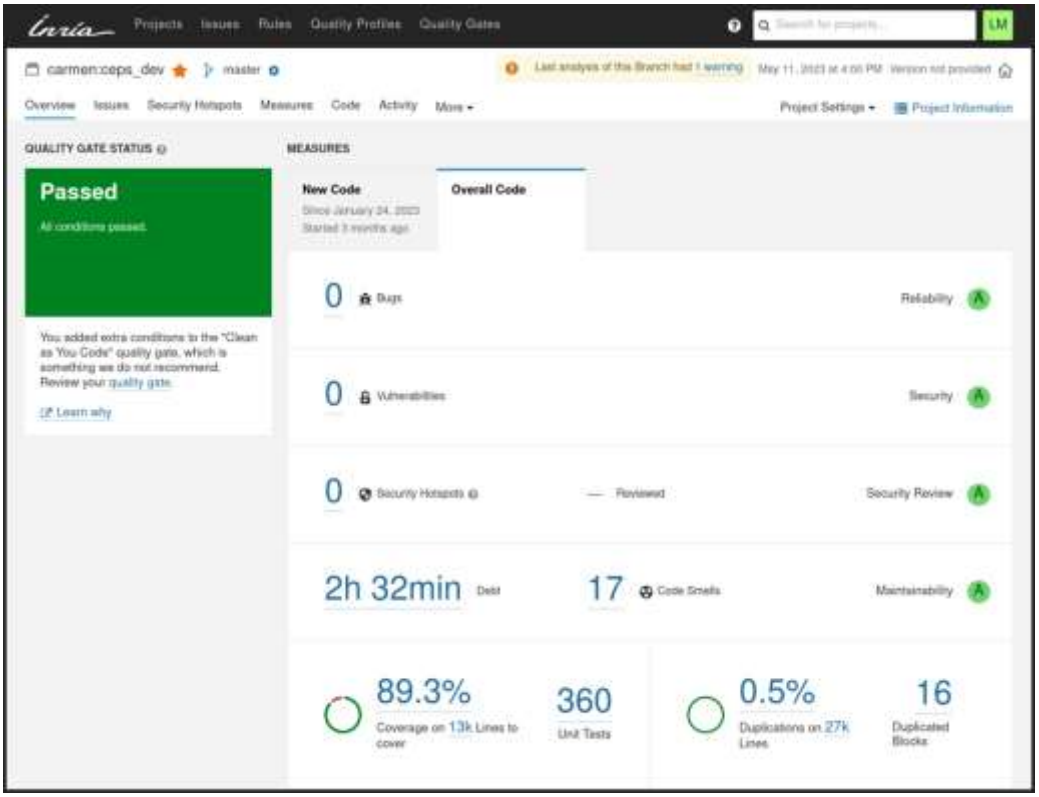

Figure 4: *SonarQube checks that CEPS passes the Quality Gate we defined.*

Figure 5: *SonarQube badges for CEPS before the SCT project (2020, top) and current status (bottom).*

1.2 Numerical Code Verification

1.2.1 NCV on CEPS

Around 100 of the 360 unit tests of CEPS are dedicated to verification of numerical schemes that are available. They usually consist in using a numerical method to approximate a solution of a simple problem or a quantity, and comparing the result with an analytic (manufactured) solution.

Tested numerical algorithms are

- Lagrange polynomial interpolation of scalar quantities
- Integration of quantities in time
- Quadrature methods for finite elements
- ODE solvers

These tools are not computationally intensive, so we can run complete convergence tests within the time limit of a unit test (5 seconds). When possible, we check that the order of convergence is reached.

Thorough convergence tests of partial differential equation solvers (Laplacian equation, heat equation, reaction-diffusion equation) require very large meshes and very small time steps, and so cannot be run on CI machines. The developer must check and report the convergence of any new implemented problem or method, including a reference convergence curve. Convergence is measured with respect to the exact solution in L-inf, L1 and L2 norms in space, and in L1 and L2 norms in time as well as the value at the final time. We are currently defining an automated protocol that generates the convergence reports.

Then, as unit test for PDE solvers, a point of the convergence study must be reproduced, up to a small tolerance. This amounts to run only one computation using a reasonably fine mesh and time step, instead of a series.

For cardiac problems, which have no analytic solution, error can be measured with respect to a reference solution generated on very fine mesh, with very small time steps, and the methods of highest order available (currently P1 Lagrange finite elements with Rush Larsen 4 ODE solvers). Errors are measured with the same metrics as above. A series of non-regression tests can be executed on demand by the user (for example after installation) to ensure that the solvers generate activation maps that reproduce a precomputed reference map, up to a small tolerance. Maps are generated for each cardiac PDE, and a selection of numerical parameter sets.

2. Calculation Verification

2.1 Use Error

2.1.1 Use Error on InSilicoTrials Platform

The user interacts with the cloud-based platform through the Input Interface (by inserting input parameters) and through the Results Interface (by viewing and downloading simulation outputs). Therefore, the error associated with potential human errors (e.g., errors that occur when entering model input parameters on the web interface) needs to be assessed. In the following paragraphs, we describe the tests and actions taken to mitigate the risks of use error.

2.1.1.1 Input Interface

Input lower and upper limits are checked automatically by the interface for every field. Warnings appear when the user types a number that is outside the boundaries. Examples are illustrated in Figure 6.

Figure 6: *InSilicoTrials platform - example of input lower and upper limits automatic check.*

To demonstrate that the user inputs inserted in the webpage are correctly submitted to the simulation workflow of each of the 3 sub-pipelines, we performed some tests by inserting specific values in the fields on the web interface, and verified that the values collected by the system and passed to the calculation were the same.

2.1.1.2 Test Sub-pipeline 1 - Energy thresholds

Pictures in Figure 7, Figure 8, and Figure 9 show the input interfaces of the sub-pipeline "Energy threshold".

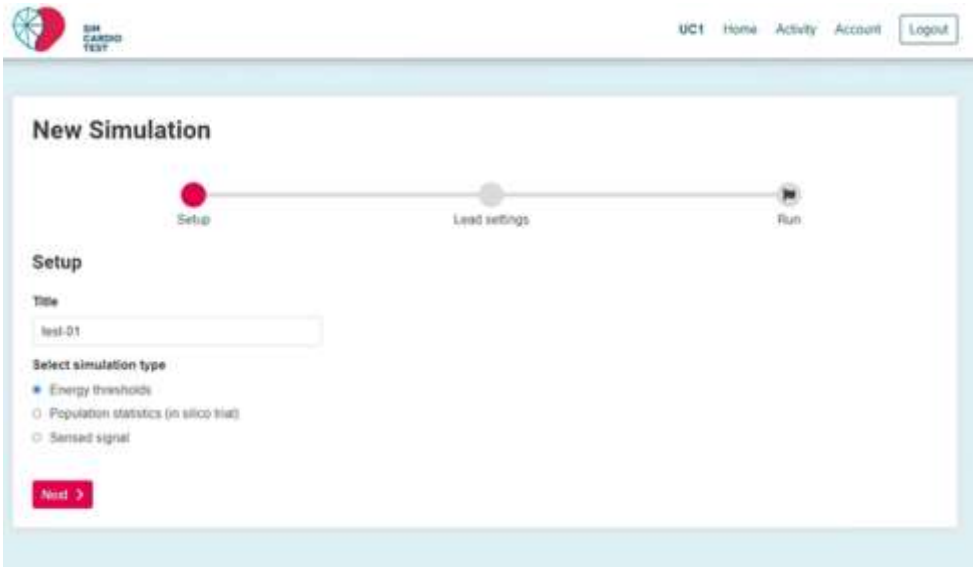

Figure 7: *InSilicoTrials - Sub-pipeline 1 - Energy thresholds - Setup.*

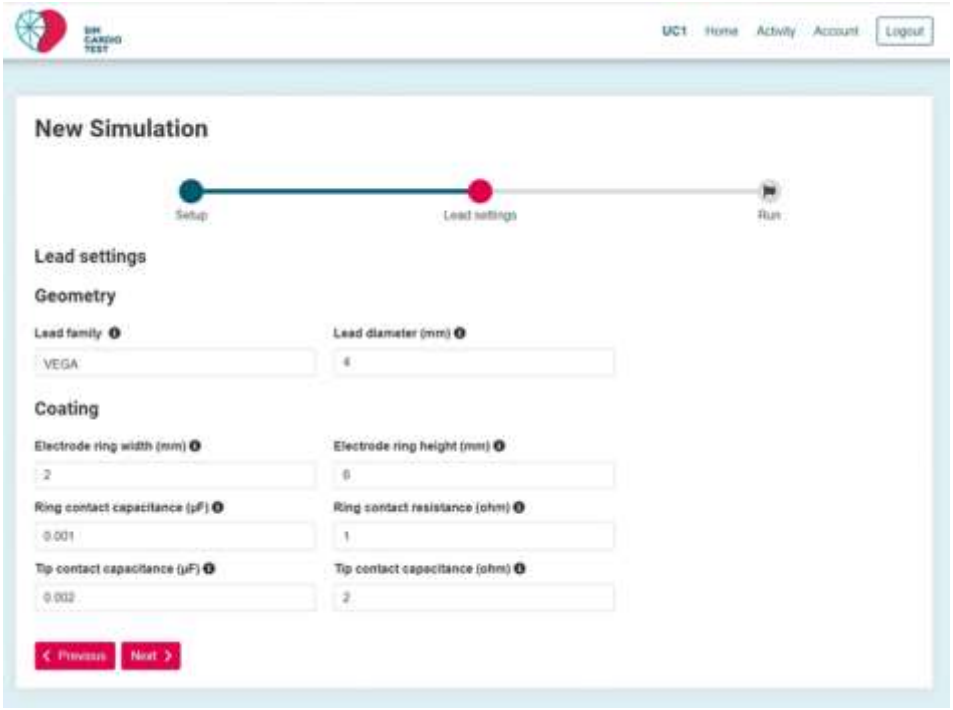

Figure 8: *InSilicoTrials - Sub-pipeline 1 - Energy thresholds - Lead Settings.*

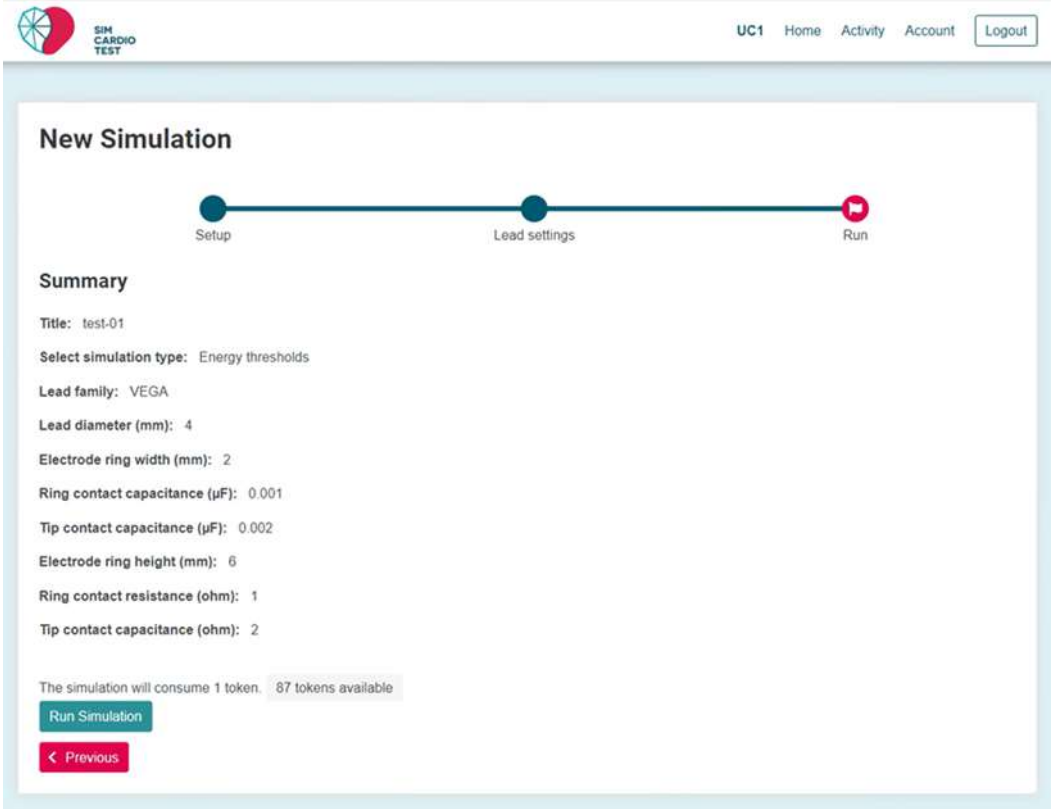

Figure 9: *InSilicoTrials - Sub-pipeline 1 - Energy thresholds - Run.*

A webpage at the end of the input submission shows the summary of all data entered by the user and notifies the user in case any information is missing before allowing the user to run the model on the cloud. After clicking on the "Run Simulation" button, an input.json file is created and stored in the corresponding repository in the dedicated environment (simcardiotest-uc1) created on Microsoft Azure (see Figure 10).

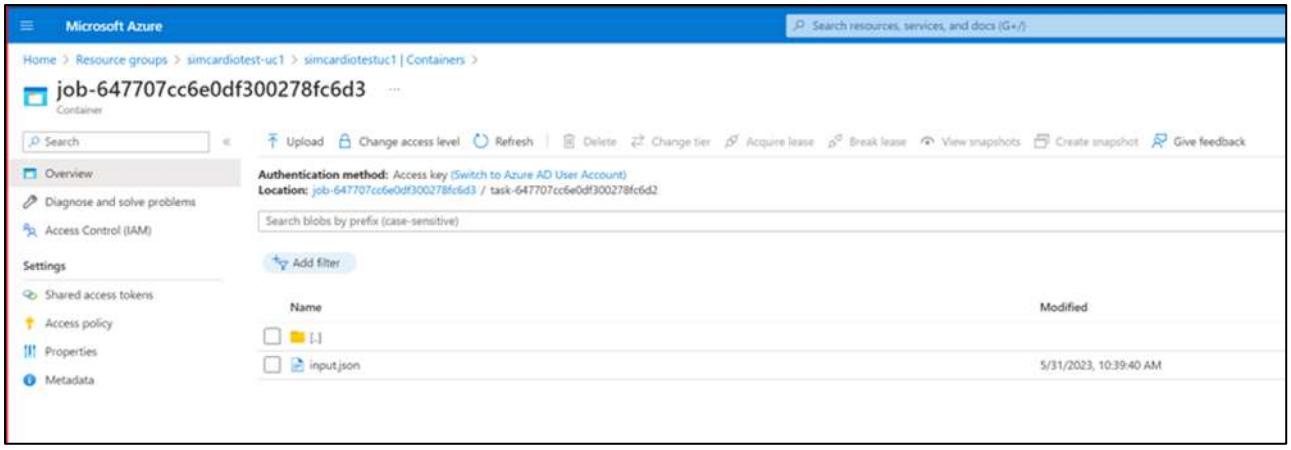

Figure 10: *InSilicoTrials - Sub-pipeline 1 - input.json file created and stored in the corresponding repository in the dedicated environment (simcardiotest-uc1) created on Microsoft Azure.*

The file contains the list of variables displayed on the web interface, and values correspond to the ones inserted by the user, meaning that the tests has passed (see Figure 11).

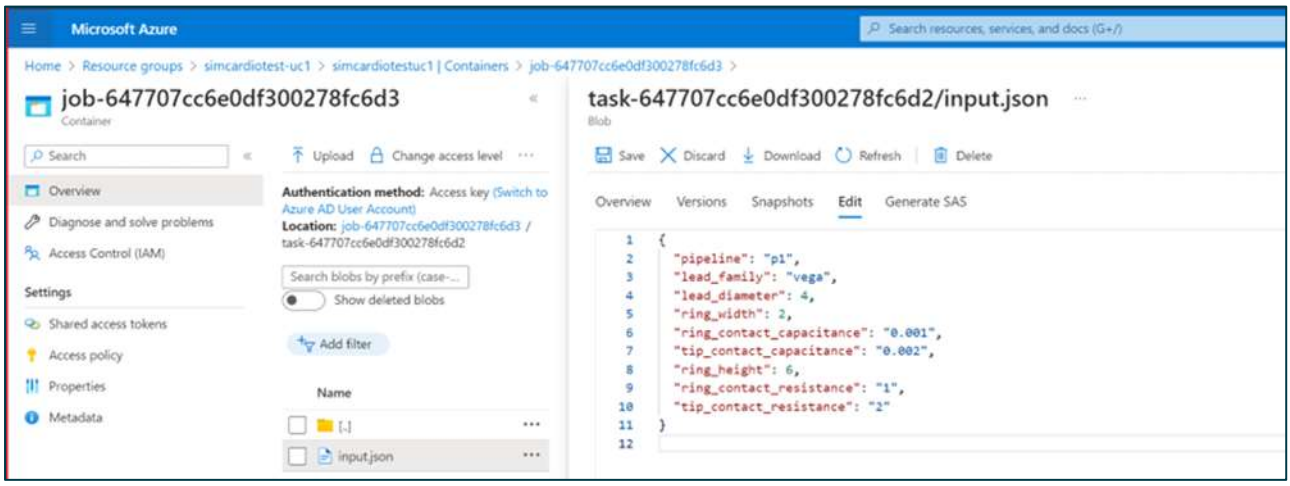

Figure 11: *InSilicoTrials - Sub-pipeline 1 - input.json file content displaying the list of input variables inserted by the user.*

2.1.1.3 Test Sub-pipeline 2 - Population Statistics

Pictures in Figure 12, Figure 13, Figure 14, and Figure 15 show the input interfaces of the sub-pipeline “Population statistics (in-silico trial)”.

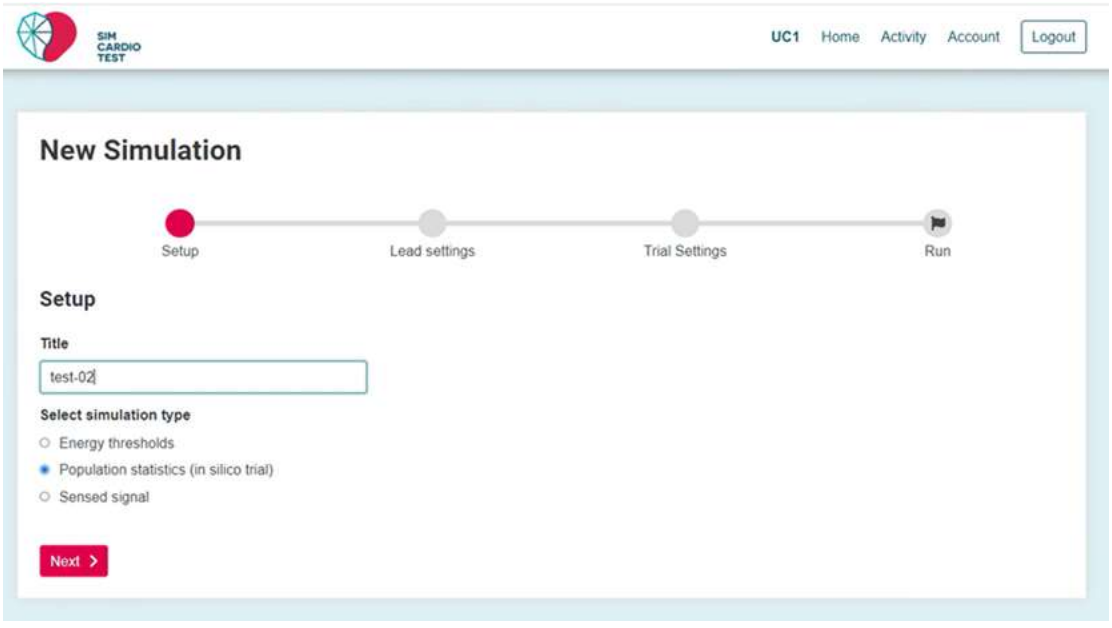

Figure 12: *InSilicoTrials - Sub-pipeline 2 - Population Statistics - Setup.*

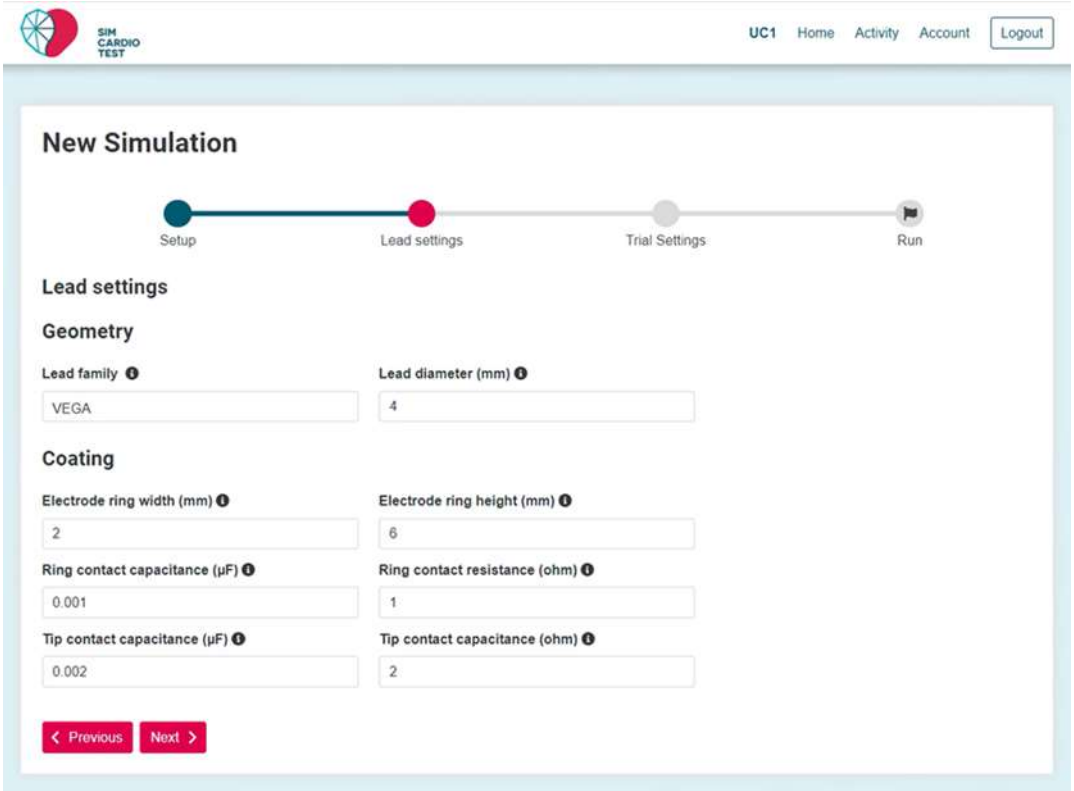

Figure 13: *InSilicoTrials - Sub-pipeline 2 - Population Statistics - Lead Settings.*

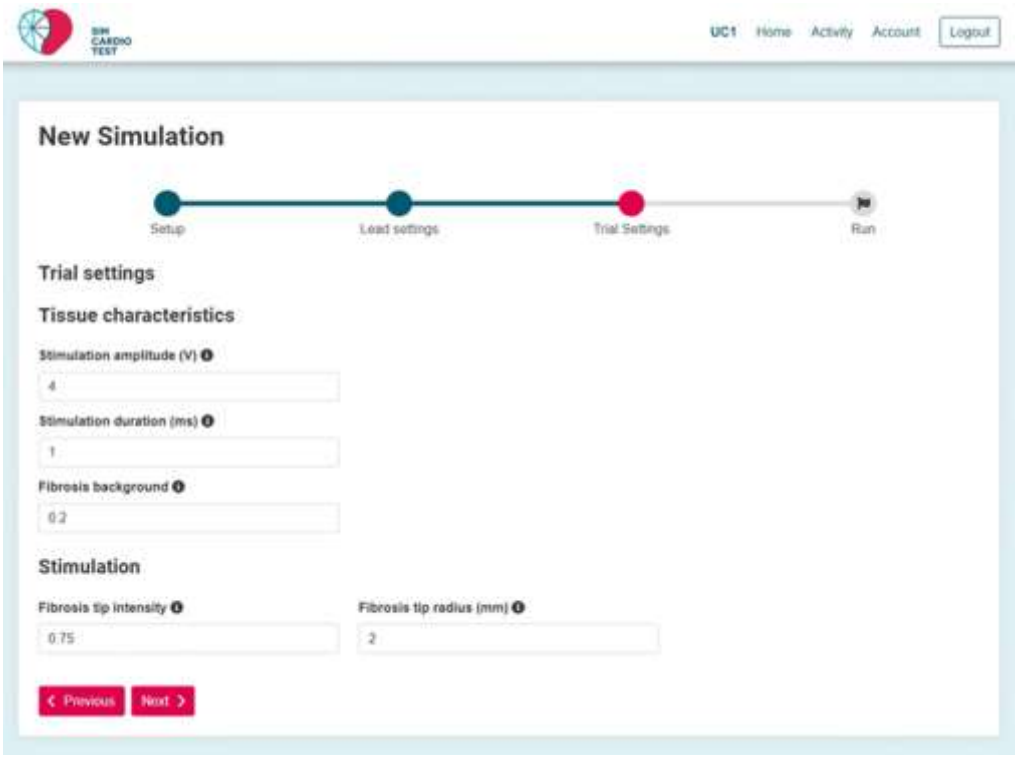

Figure 14: *InSilicoTrials - Sub-pipeline 2 - Population Statistics - Trial Settings.*

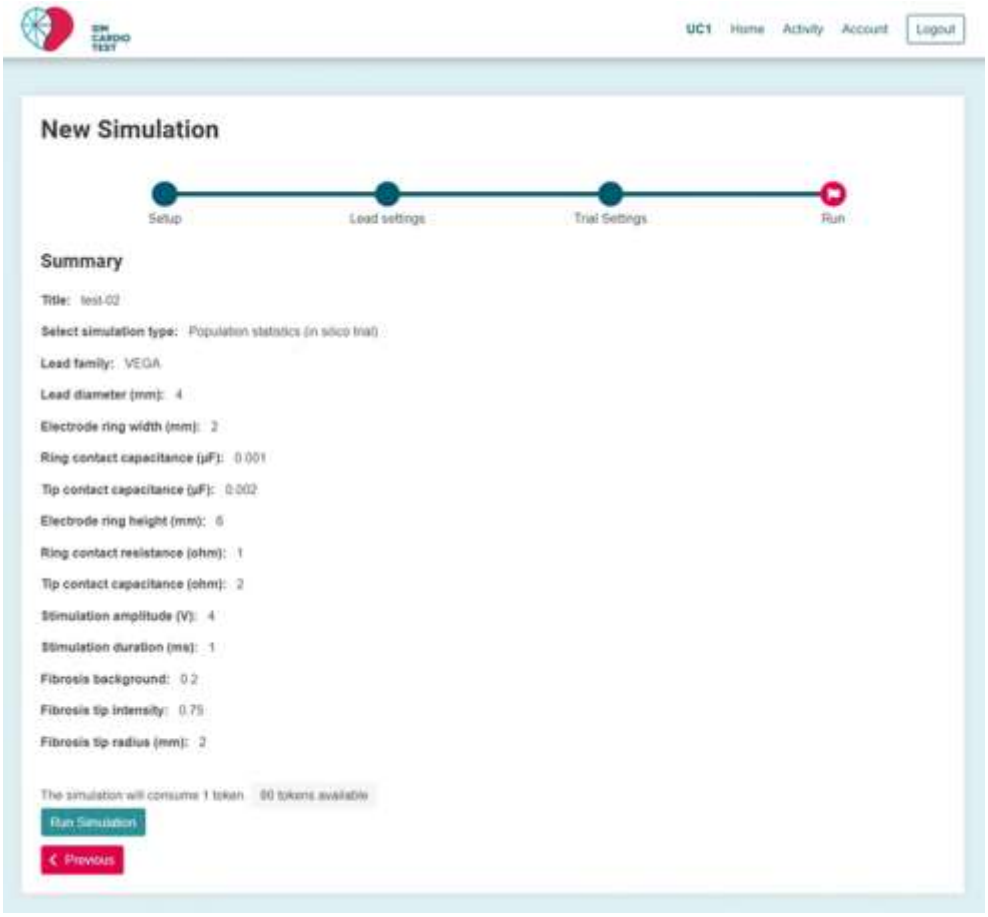

Figure 15: *InSilicoTrials - Sub-pipeline 2 - Population Statistics - Run.*

After clicking on the "Run Simulation" button, an input.json file is created and stored in the corresponding repository in the dedicated environment (simcardiotest-uc1) created on Microsoft Azure (see Figure 16).

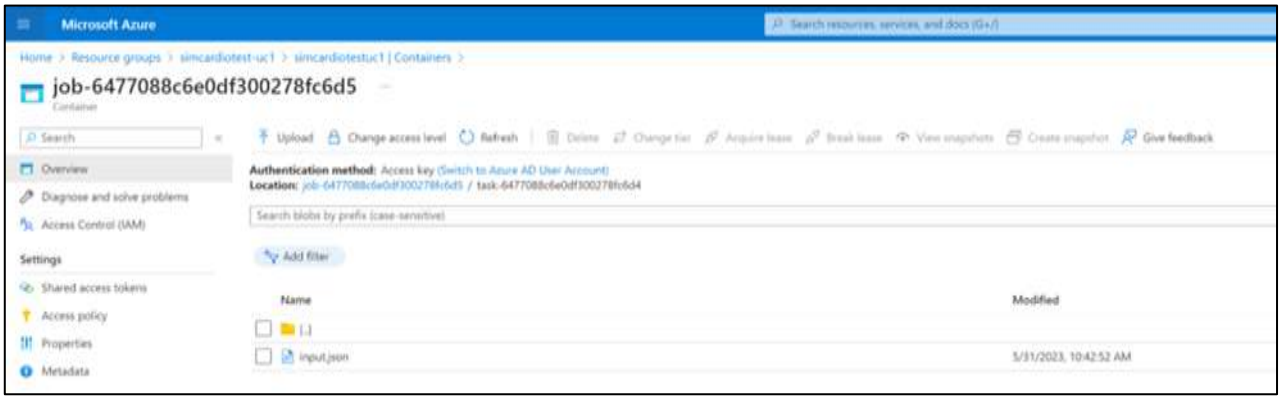

Figure 16: *InSilicoTrials - Sub-pipeline 2 - input.json file created and stored in the corresponding repository in the dedicated environment (simcardiotest-uc1) created on Microsoft Azure.*

The file contains the list of variables displayed on the web interface, and values correspond to the ones inserted by the user, meaning that the test has passed (see Figure 17).

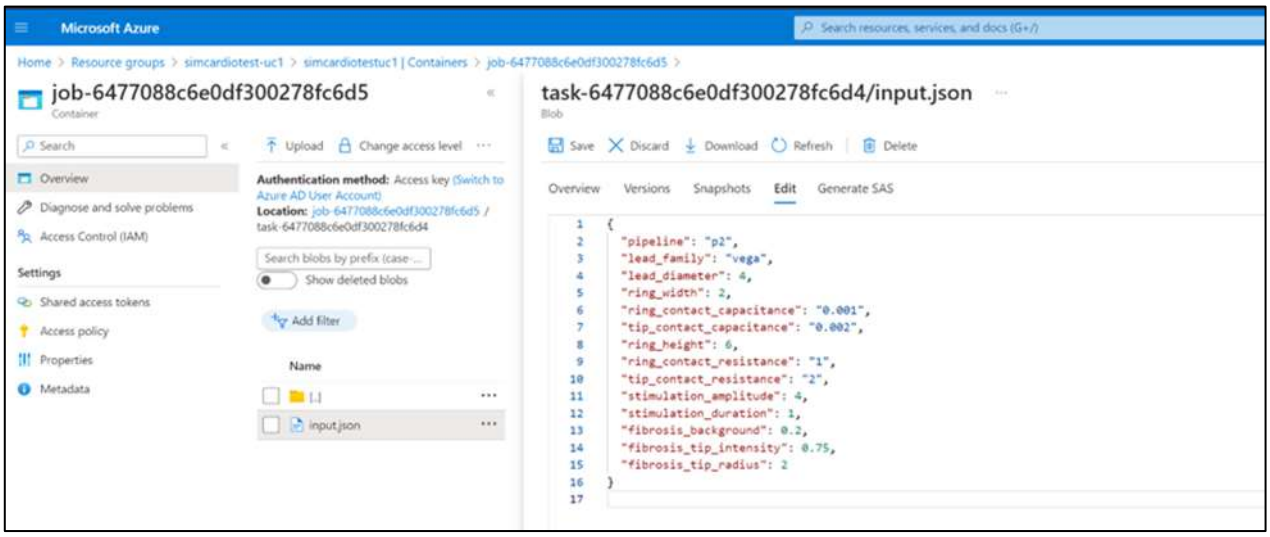

Figure 17: *InSilicoTrials - Sub-pipeline 2 - input.json file content displaying the list of input variables inserted by the user.*

2.1.1.4 Test Sub-pipeline 3 - Sensed signal

Pictures in Figure 18, Figure 19, and Figure 20 show the input interfaces of the sub-pipeline “Sensed signal”.

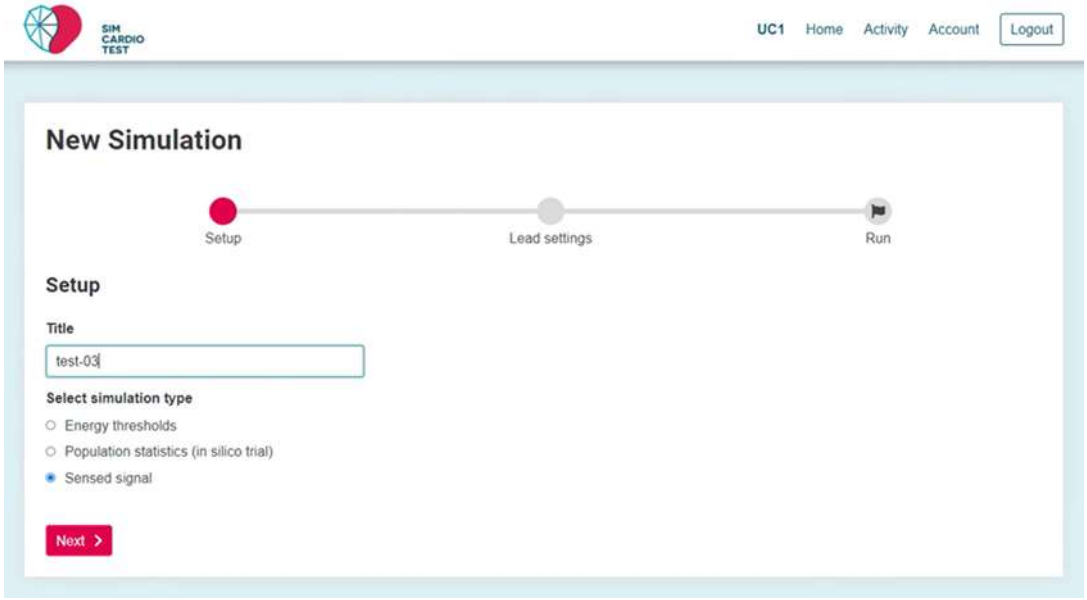

Figure 18: *InSilicoTrials - Sub-pipeline 3 - Sensed Signal - Setup.*

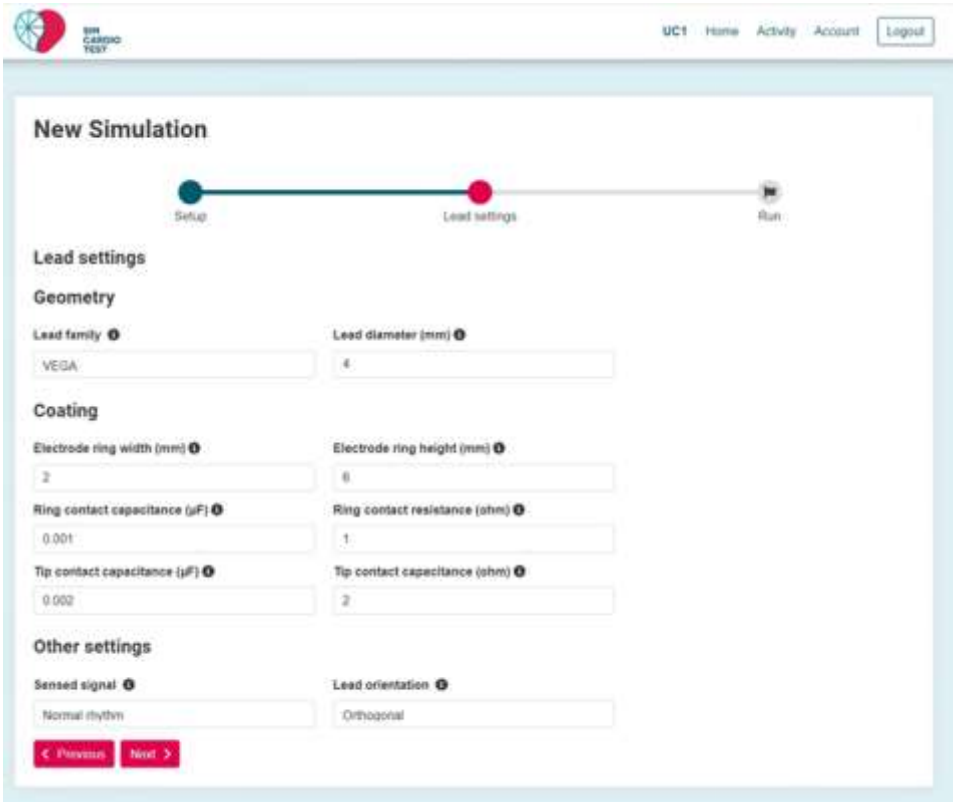

Figure 19: *InSilicoTrials - Sub-pipeline 3 - Sensed Signal - Lead Settings.*

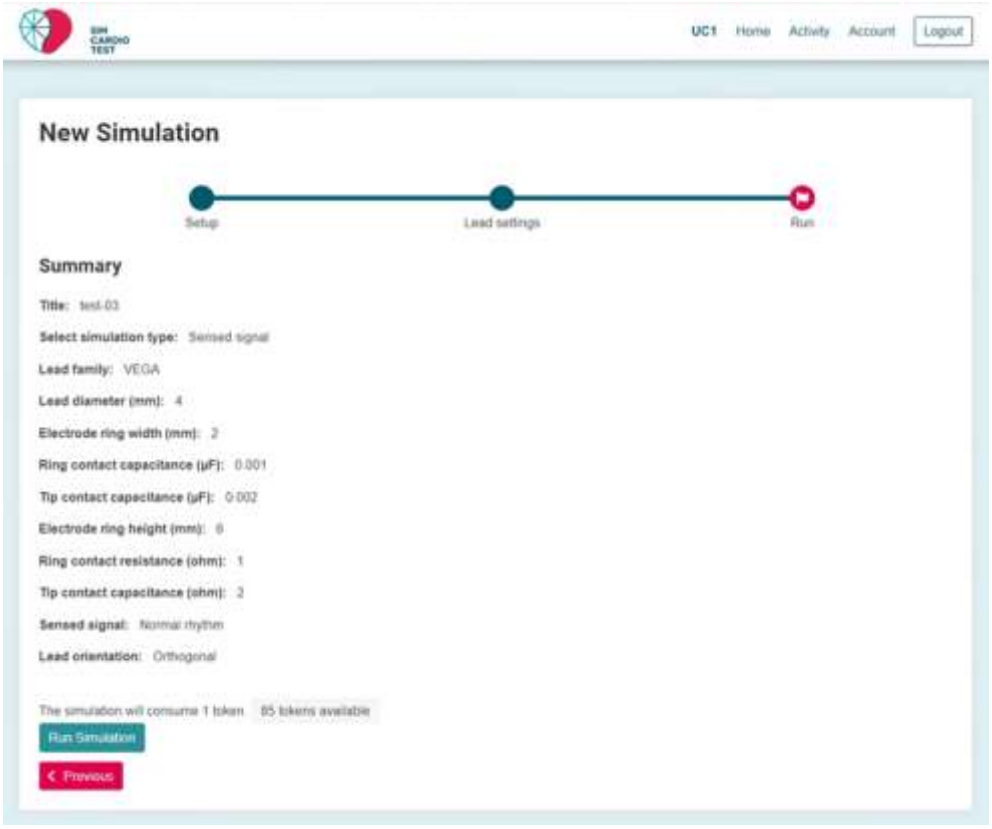

Figure 20: *InSilicoTrials - Sub-pipeline 3 - Sensed Signal - Run.*

After clicking on the “Run Simulation” button, a new job is created and an input.json file is created and stored in the corresponding repository in the dedicated environment (simcardiotest-uc1) created on Microsoft Azure (see Figure 21).

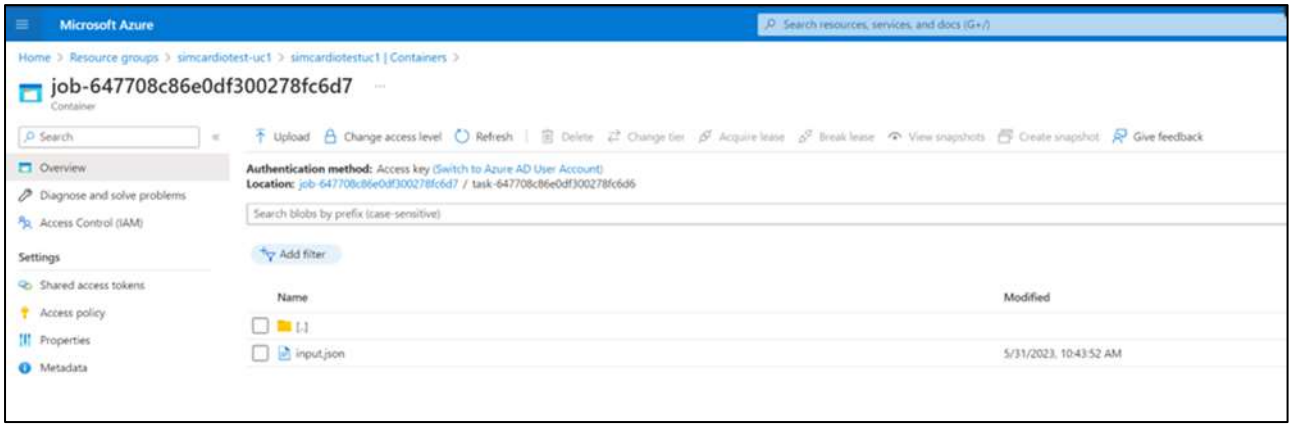

Figure 21: *InSilicoTrials - Sub-pipeline 3 - input.json file created and stored in the corresponding repository in the dedicated environment (simcardiotest-uc1) created on Microsoft Azure.*

The file contains the list of variables displayed on the web interface, and values correspond to the ones inserted by the user, meaning that the test has passed (see Figure 22).

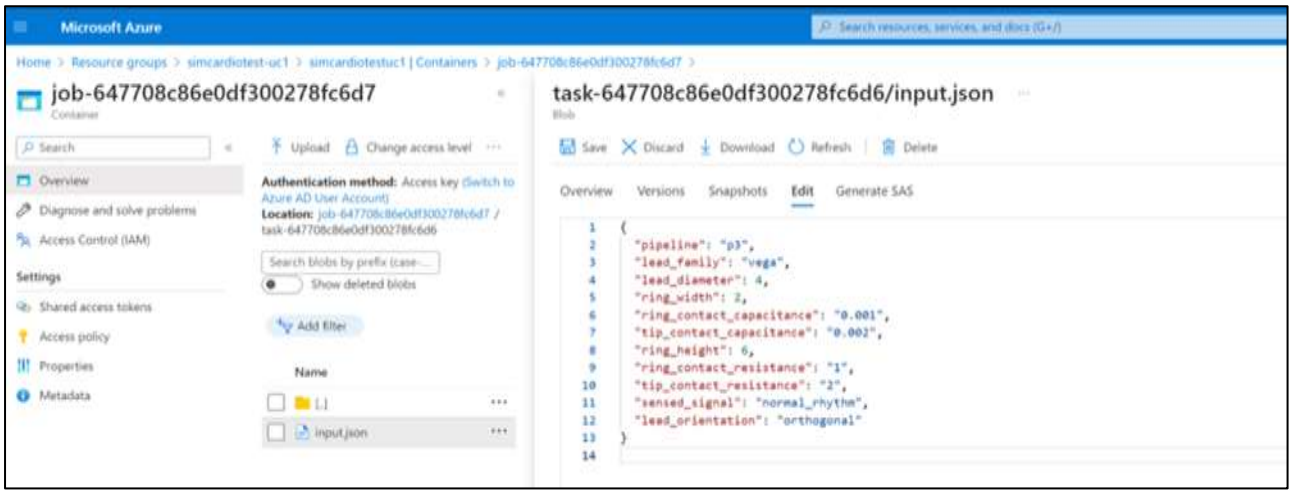

Figure 22: *InSilicoTrials - Sub-pipeline 3 - input.json file content displaying the list of input variables inserted by the user.*

The .json file is passed to the model, which uses the parameter values to run the simulation.

Final user will be responsible of demonstrating that inputs were correct.

3. Conclusion

This document is an annex of SimCardioTest deliverable D6.1, and reports technical details relative to the verification of the numerical model developed for Use Case 1. General conclusions relative to the verification of UC1 numerical model are reported in main deliverable D6.1.

4. Bibliography

[1] "openMpi," [Online]. Available: https://www.open-mpi.org/software/ompi/v4.0/.

[2] "Eigen," [Online]. Available: http://eigen.tuxfamily.org/index.php?title=Main_Page.

[3] "PETSc," [Online]. Available: https://www.mcs.anl.gov/petsc/download/index.html.

[4] "CxxTest," [Online]. Available: https://sourceforge.net/projects/cxxtest/files/cxxtest/.

[5] "ParMETIS," [Online]. Available: http://glaros.dtc.umn.edu/gkhome/metis/parmetis/download.

[6] "PTScotch," [Online]. Available: https://www.labri.fr/perso/pelegrin/scotch/.

[7] "VTK," [Online]. Available: https://vtk.org/download/.

[8] "cppcheck documentation," [Online]. Available: https://sourceforge.net/p/cppcheck/wiki/ListOfChecks/.

[9] "SonarQube Set of Rules," [Online]. Available: https://github.com/SonarOpenCommunity/sonar-cxx/wiki/CXX-Rules.

[10] V&V40, Assessing Credibility of Computational Modeling Through Verification and Validation: Application to Medical Devices, New York: ASME, 2018.

This project received funding from the European Union's Horizon 2020 research and innovation program under grant agreement No 101016496

EU Horizon 2020 Research & Innovation Program
Digital transformation in Health and Care
SC1-DTH-06-2020
Grant Agreement No. 101016496

SimCardioTest - Simulation of Cardiac Devices & Drugs for in-silico Testing and Certification

Technical Report

D6.1-UC2: Use Case 2 Verification Annex

Work Package 6 (WP6)
Verification, validation, uncertainty quantification & certification

Annex Lead: UPF, Spain
Task Lead: UBx, France
WP Lead: MPC, France

PUBLIC

Document history			
Date	**Version**	**Author(s)**	**Comments**
21/06/2023	V1	A. OLIVARES	First Draft
23/06/2023	V2	R. SETZU	Format consolidation
29/06/2023	V3	H. AREVALO	Quality Review
30/06/2023	V4	R. SETZU	Final Version
01/07/2024	V5	R. SETZU, M. BARBIER	Format Editing

TABLE OF CONTENTS

EXECUTIVE SUMMARY

This document is an annex of SimCardioTest deliverable D6.1 and was elaborated for Use Case 2 in the context of the assessment of right atrial appendage occluders. It contains the technical details for the verification of the UC2 numerical model and the verification activities performed by InSilicoTrials during the integration of the aforementioned model in the cloud platform of SimCardioTest project.

Acronyms

Table 1: List of Acronyms.

Acronym	Meaning
SCT	SimCardioTest

1. Calculation Verification

1.1 Discretisation Error

1.1.1 Software and Model Description

CFD simulations were performed using Oasis, an open-source library solving the Navier-Stokes equations using the Finite Element method, based on the FEniCS computing platform, which has been rigorously and successfully verified and validated. Oasis is a high-performance computing implementation of a segregated, space/time centred, incremental pressure correction scheme. All details of this study in Khalili et al [1].

1.1.2 Boundary Conditions and Modelling Assumptions

We applied a generic waveform at the pulmonary veins (PVs), where the flow rate was scaled with respect to cross-sectional area and prescribed as parabolic velocity profile. We applied a normal cardiac output of 5.5 $Lmin^{-1}$. We assumed rigid walls and an open mitral valve, where the pressure was set to zero. At the outlet boundary, we also used a back-flow stabilization for the velocity. Blood was modelled as an incompressible and Newtonian fluid with constant density of ρ = 1060 kg/m3 and dynamic viscosity of μ =0.0035 Pa*s.

1.1.3 Mesh Convergence Study

We investigated the effect of spatial resolution on the 12 cases of the cohort by using six different meshes varying from 100k to 26M tetrahedral elements to cover the span of used mesh resolutions in the literature (Table 2).

Table 2: Effect of Spatial Resolution.

Millions of elements	x (mm)	Nodes per Volume $1/mm^3$
0.1	2.4	300-1000
0.4	1.8	1200-4300
0.8	1.2	2500-8600
3.2	0.9	10000-34000
6.4	0.6	20000-68000
26	0.4	82000-28000

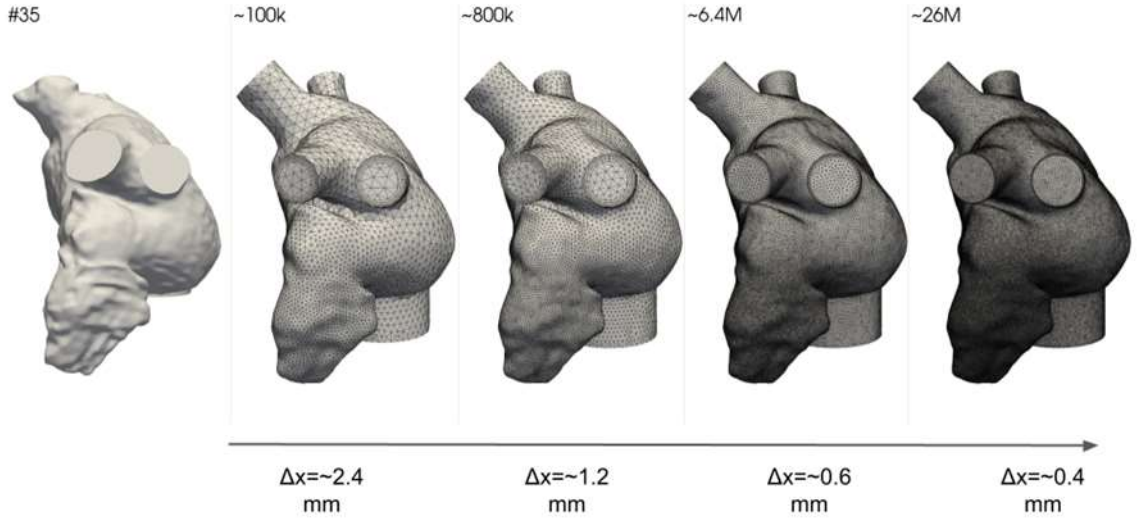

Figure 1: *The leftmost shows the initial model (case 35) before smoothing and mesh generation. On the right, it shows four different meshes; 100k, 800k, 6.4M, and 26M elements. Meshes with 400k and 3.2M elements are not presented for the sake of simplicity.*

1.1.4 Time Convergence Study

Following the results of the mesh resolution study, we investigated the sensitivity to temporal resolution on three selected cases that showed high, medium, and low sensitivity to mesh resolution (case number 4, 26, and 192). We used 6.4M element mesh and varied the time-steps per cardiac cycle from 1250, 2500, 5000, 10000 to 20000, which corresponds to Δt = 0.8 ms, 0.4 ms, 0.2 ms, 0.1 ms and 0.05 ms. The corresponding calculated range of Courant–Friedrichs–Lewy (CFL) numbers in the domain was CFL$\approx$ 0.4 – 0.025.

1.1.5 Mesh Convergence Study

First, we focus on qualitative results for three representative cases (i.e., number 4, 26, and 192), in which the WSS quantitatively showed low, medium, and high sensitivity to mesh resolution (cf. Figure 2). These cases are also qualitatively presented for time convergence and combined effects to enable a thorough visual comparison among the results. Figure 3 shows isovelocity surfaces (in the range of [0.18-0.22] m/s), WSS, OSI, RRT, and ECAP for 100k, 800k, 6.4M, and 26M element meshes, respectively. The hemodynamic indices are presented separately for LA and LAA. For the coarse meshes with 100k elements, the flow patterns are difficult to interpret and the flows are not smooth or can be reflective of numerical artefacts. In contrast, we can observe that the higher resolution meshes captures more detailed and complex flow structure. Refining the mesh leads to phenotypically different WSS patterns with different regions with the highest values, especially for the meshes larger than 6.4M. These effects are relatively pronounced in the LAA for the regions near the ostium. By definition, OSI is arguably more sensitive to mesh resolution than WSS. By refining the mesh, different OSI patterns and high/low regions appear. Differences are less pronounced in the LAA, however, there are noticeable differences for case 26 for finer meshes compared to coarser ones. Similarly, RRT and ECAP show different patterns and high/low regions on the higher resolution meshes. Although it is difficult to visually observe the differences in the LAA compared to the LA, quantitative results (cf. Figure 3) suggests that differences are still high in the LAA.

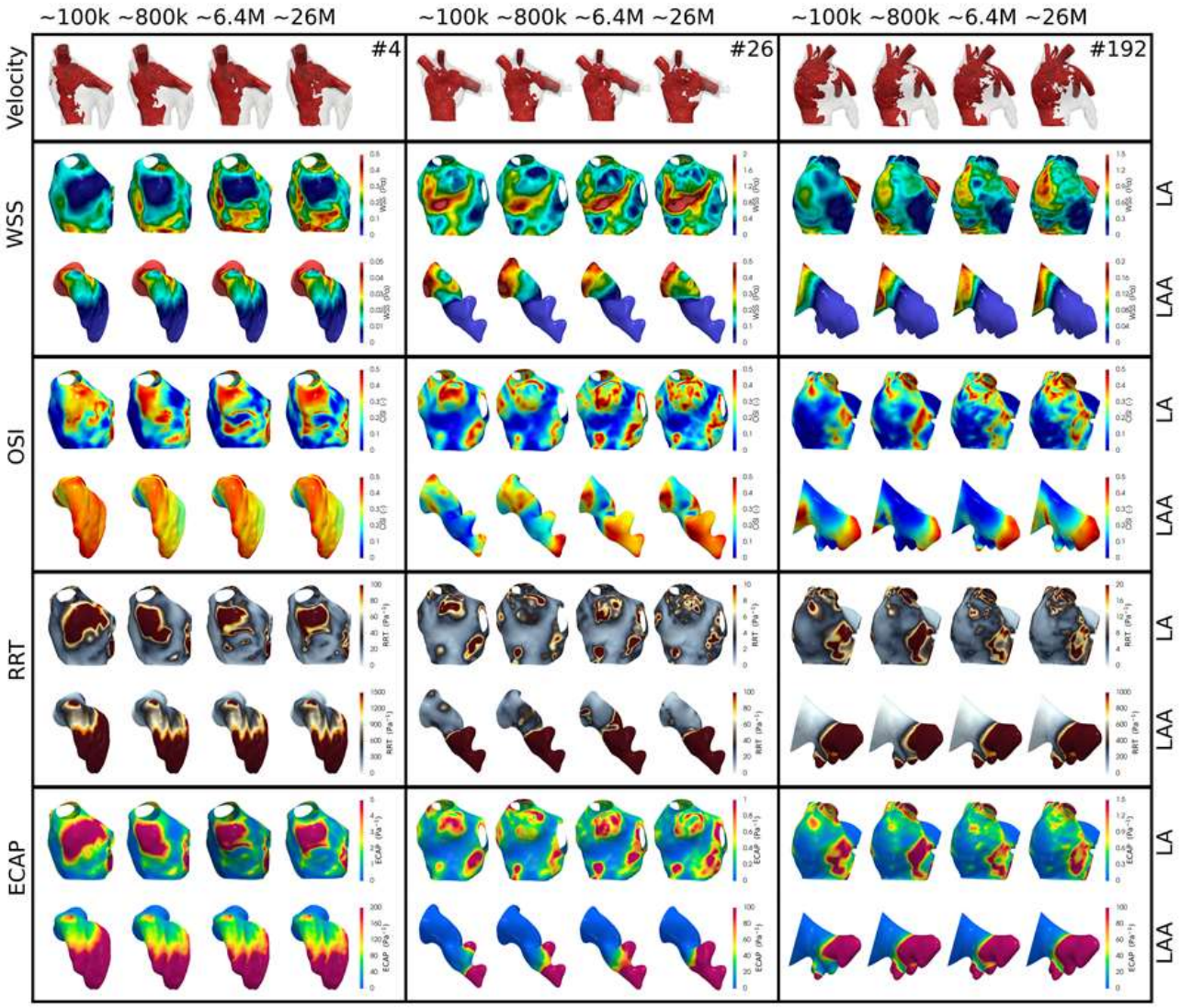

Figure 2: *Qualitative impact of mesh resolution (100k, 800k, 6.4M, and 26M elements) on cases 4, 26 and 192. Results of 400k and 3.2M element mesh are not presented for the sake of simplicity. For each case, the first row compares isovelocity surfaces (in the range of [0.18-0.22] m/s), the second and third rows compare time averaged wall shear stress (WSS) in the left atrium (LA) and left atrial appendage (LAA), respectively, the fourth and fifth rows show oscillatory shear index (OSI) in LA and LAA, respectively, sixth and seventh rows present relative residence time (RRT) and finally eighth and ninth rows present endothelial cell activation potential (ECAP) results.*

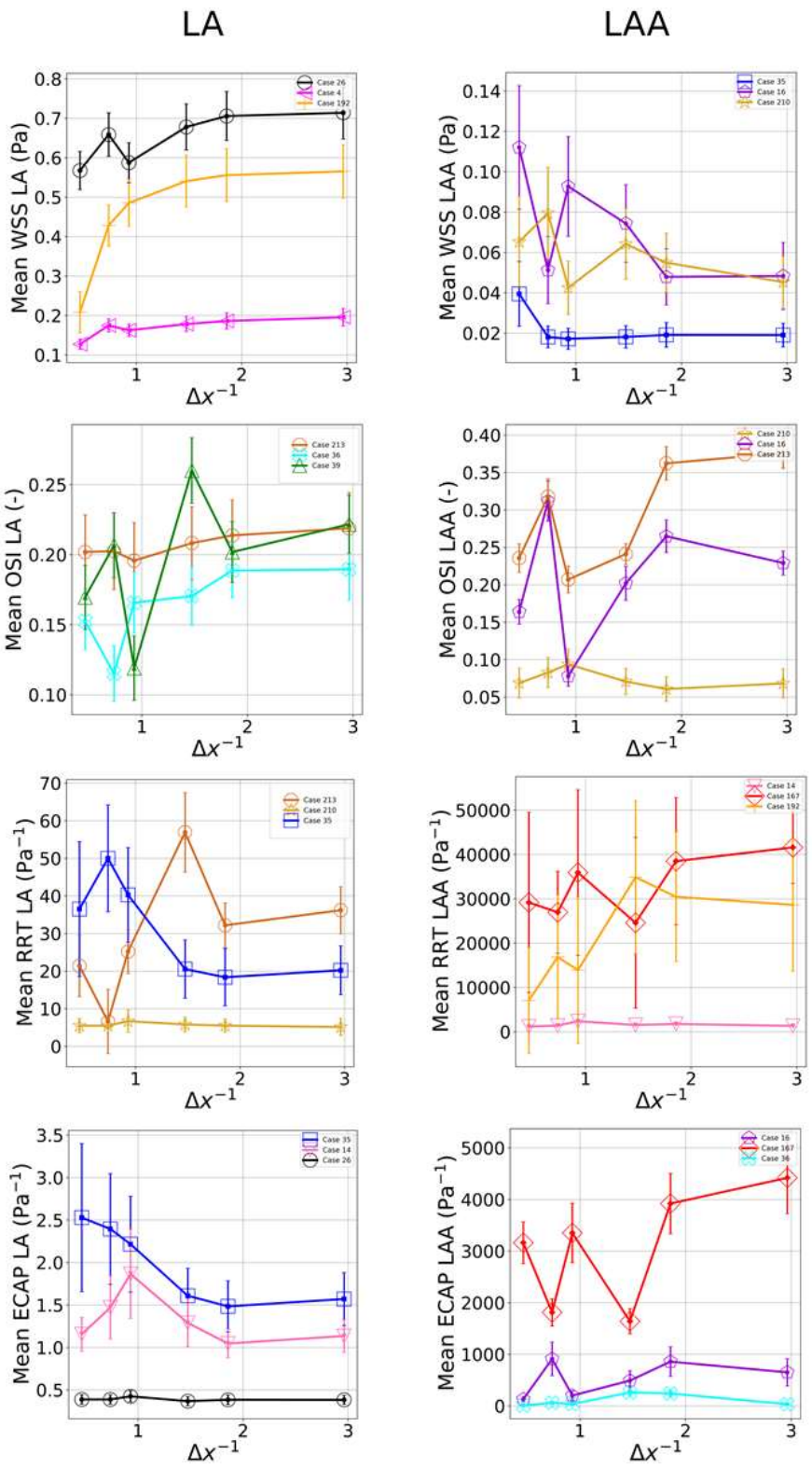

Figure 3: *Quantitative results of mesh convergence study of time averaged wall shear stress (WSS), oscillatory shear index (OSI), relative residence time (RRT), and endothelial cell activation potential (ECAP) in left atrium (LA) and left atrial appendage (LAA) separately. Representative cases of high, medium, and low sensitivity of each hemodynamic indices are separately presented for the LA and the LAA. ⊿x =~2.4, ~1.2, ~0.6, and ~0.4 mm corresponds to meshes of 100k, 3.2M, 6.4, and 26M elements.*

We identified three different pheno- typical behaviours in the results, which we classified as:

1. High variability between mesh resolutions with a staggered pattern
2. Lower variability but high errors between fine and coarse meshes
3. Inconsiderable/low variability with a smooth pattern.

A subset of the representative quantitative results is shown in Figure 3. The hemodynamic indices have been independently computed for the LA and the LAA. The average relative errors of all cases for WSS values between 800k element mesh (median value as shown in Table 3) and 26M element mesh (as a reference) are 16 $\pm$ 34% and 45 $\pm$ 49% in the LA and the LAA, respectively. However, we can see in the LA of case 192 (cf. top left in Figure 2), a WSS value of 0.21 $\pm$ 0.02 Pa on the 100k element mesh that increases to 0.57 $\pm$ 0.05 Pa on 26M element mesh, (i.e., 270% increase, with a 63% $\pm$ 22 relative error), which classified as number (2).

Moreover, there is a higher dependency of WSS to mesh resolutions in the LAA for cases 16 and 210. For case 16, WSS values show a staggered pattern as classification number (1), shifting from 0.05 $\pm$ 0.01 Pa to 0.09 $\pm$ 0.02 Pa and to a converged value of 0.04 $\pm$ 0.02 Pa, on the 400k, 800k, and 6.4M element mesh, respectively, which is 100% variability.

In contrast, case 26 shows classification number (3), where relative errors of WSS in the LAA stays below 5% between meshes of 800k and 26M elements. The average relative errors of all cases for OSI are 12 $\pm$ 0.1% and 30 $\pm$ 0.2% in the LA and the LAA, respectively. However, we can see that OSI is more sensitive to mesh resolutions both in the LA and the LAA.

Case 39 in the LA shows classification number (1), where the OSI value shifts from 0.12 $\pm$ 0.018 to 0.26 $\pm$ 0.016 and to 0.2 $\pm$ 0.014 on 800k, 3.2M and 6.4M element mesh, respectively.

The OSI value in the LAA for case 213 also increases 170% from 0.21 $\pm$ 0.01 to 0.37 $\pm$ 0.01 on the 800k and 26M element mesh, respectively.

RRT also shows high sensitivity to mesh resolution even though he average relative errors of all cases are 27 $\pm$ 0.4% and 74 $\pm$ 0.6% in the LA and LAA, respectively. For instance, it can be seen that for case 35 in the LA that classified as number (2), the RRT value 35.5% $\pm$ 19 Pa−1 on the 100k element mesh, reduces to 20.22 $\pm$ 8 Pa−1 on the 26M element mesh, (i.e., 180% drop, with a 81% $\pm$ 137 relative error). For case 167, the RRT value in the LAA shows a staggered pattern with variability range of 10-80% between the meshes of 100k to 26M elements.

Although ECAP shows relatively high sensitivity to mesh resolution particularly in the LAA, the average relative errors of all cases are 22 $\pm$ 2.7% and 66 $\pm$ 0.5% in the LA and the LAA, respectively. The ECAP value in the LAA for case 167 varies highly, shifting from 3327 $\pm$ 440 Pa−1 to 1836 $\pm$ 521 Pa−1, and 3904 $\pm$ 0.02 Pa−1 on the 800k, 3.2M, and 6.4M element mesh, respectively. There is not a clear convergence of ECAP magnitudes for case 167 in the LAA, up to mesh 26M elements due to a high variance of differences 14 $\pm$ 8% – 221 $\pm$ 43%. To compare the results with some points of reference as presented in Section 4.1, the averaged WSS value over all cases for 26M elements mesh is 0.44 $\pm$ 0.12 Pa and 0.036 $\pm$ 0.06 Pa in the LA and LAA, respectively. For OSI, the

averaged value of all cases for 26M elements mesh is 0.21±0.11 and 0.24±0.09 in the LA and the LAA, respectively. And the averaged of normalized RRT and ECAP with respect to mean values for 26M elements are 0.93 ± 0.21 and 1.05 ± 0.48 in the LA, and 1.1 ± 0.16 and 0.92 ± 0.52 in the LAA.

1.1.6 Time Convergence Study

Figure 4 shows the qualitative results for isovelocity surfaces (in the range of [0.18-0.22] m/s), WSS, OSI, RRT, and ECAP in the LA and LAA separately. To concisely present the results, only simulations at 1250, 2500, 5000 and 10000 time-steps per cardiac cycle are presented. Although there are small changes in flow patterns in cases 26 and 192 by refining temporal resolution, relatively indistinguishable flow changes can be seen for case 4. This is reflected on the WSS results as well, where case 26 and 192 show slightly different patterns in the LA, and amplified levels in the regions near ostium in the LAA.

The latter suggests that fundamental flow changes occur in the LA, which affects the inflow to the LAA. OSI also shows sensitivity in cases 26 and 192, where different patterns can be seen in the LA. Differences are noticeable in the LAA as well, especially for case 26. RRT and ECAP in the LA show different patterns in the region near the ostium where there is low WSS and high OSI. Although it is difficult to find the qualitative differences in the LAA, quantitative results (cf.Figure 5) suggest that there are high differences in RRT and ECAP in the LAA, especially for case. The quantitative results of WSS, OSI, RRT, and ECAP in the LA and LAA for cases 4, 26, and 192 are separately presented in Figure 4. Although WSS values in the LA are robust to the temporal resolutions relatively for all three cases, WSS value in the LAA for case 26 decreases from 0.075 ± 0.012 Pa at 1250 time-steps/cycle to 0.05 ± 0.1 at 10000 time-steps/cycle which is a 50% decline, relative error of 50 ± 0.2%. However, OSI shows more sensitivity particularly in the LAA, where for case
26, it shifts from 0.23 ± 0.01 to 0.2 ± 0.01, and to converged value of 0.32 ± 0.01, at 1250, 2500, and 20,000 time-steps/cycle, respectively, 30% variability. However, overall variability below 5% are generally obtained in the LA and LAA at time-steps larger than 5000 per cardiac cycle. Similar behaviour can be seen for RRT and ECAP where variability exists noticeably in the LAA. For case 192, RRT values in the LAA varies roughly from 55269 ± 15300 at 5000 time-steps/cycle to 40078 ± 21767 at 10,000 time-steps/cycle, and to 27772±10171 at 20,000 time-steps/cycle, indicating 200% overall decrease. ECAP values in the
LAA for case 26 show 30% variability, shifting from 404 ± 85 at 5000 time-steps/cycle to 311 ± 70 at 10000 time-steps/cycle to even 352 ± 75 at 20000 time-steps/cycle, relative error of 12 ± 0.1%.

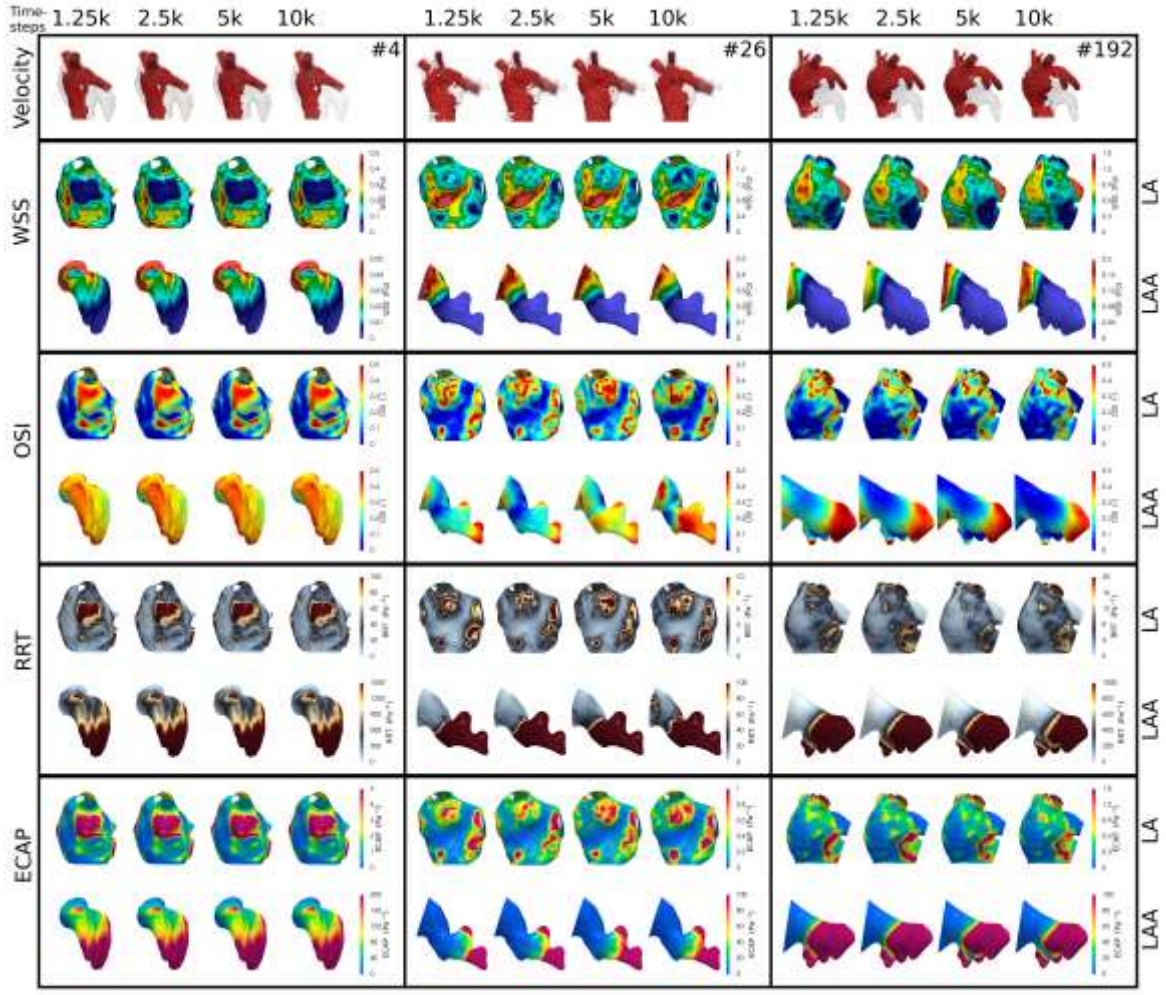

Figure 4: *Qualitative results at 1250, 2500, 5000 and 10,000 time-steps per cardiac cycle for cases 4, 26, and 192 in the LA and the LAA separately. For each case, the first row compares isovelocity surfaces (in the range of [0.18- 0.22] m/s), the second and third rows compare time averaged wall shear stress (WSS), the fourth and fifth rows show oscillatory shear index (OSI), sixth and seventh rows present relative residence time (RRT) and finally eighth and ninth rows show endothelial cell activation potential (ECAP) in the left atrium (LA) and left atrial appendage (LAA) separately.*

1.1.7 Combined Solution Strategies

Figure 6 shows isovelocity surfaces (in the range of [0.18-0.22] m/s) and maps of WSS, OSI, RRT, and ECAP in the LA and LAA separately, for high and normal resolution solvers (HR and NR, respectively) simulations. All NR simulations show smoother flows in contrast to the HR simulations, which show complex flows with fine structures. This can be seen clearly for cases 26 and 192, where flows have fundamentally different phenotypes. HR simulations show different WSS patterns and high/low regions compared to the NR ones in the LA, the differences in the LAA can mainly be observed in the regions near the ostium. HR simulations also predict different OSI patterns both in the LA and LAA compared to NR, which is in alignment with the observed different flow behaviours. The differences in RRT and ECAP are obvious in the LA for all three cases.

However, it needs a closer look to observe the differences in the LAA, especially for RRT. Figure 6 highlights the quantitative results/statistics between NR and HR simulations for WSS, OSI, RRT, and

ECAP in the LA and LAA separately. WSS values in the LA and LAA show a robust correlation (i.e., R^2=0.93 and 0.81, respectively), averaged relative errors of all cases are 21%±6% and 14%±11%, respectively. Although WSS patterns are qualitatively different in Figure 5, the domain-averaged values show relatively small difference. OSI in both LA and LAA was highly affected and highlights a poor correlation (i.e., R^2=0.63 and 0.55, respectively), particularly in the LAA where the averaged relative error of all cases is 44% ± 21%. The RRT and ECAP indicate poor correlation in the LAA as well (i.e., R^2=0.63 and 0.61, respectively) in contrast to the LA. The averaged relative errors of all cases in the LAA are 64%±18% and 56%±23%. Note that a logarithmic scale for RRT and ECAP is used in Figure 6.

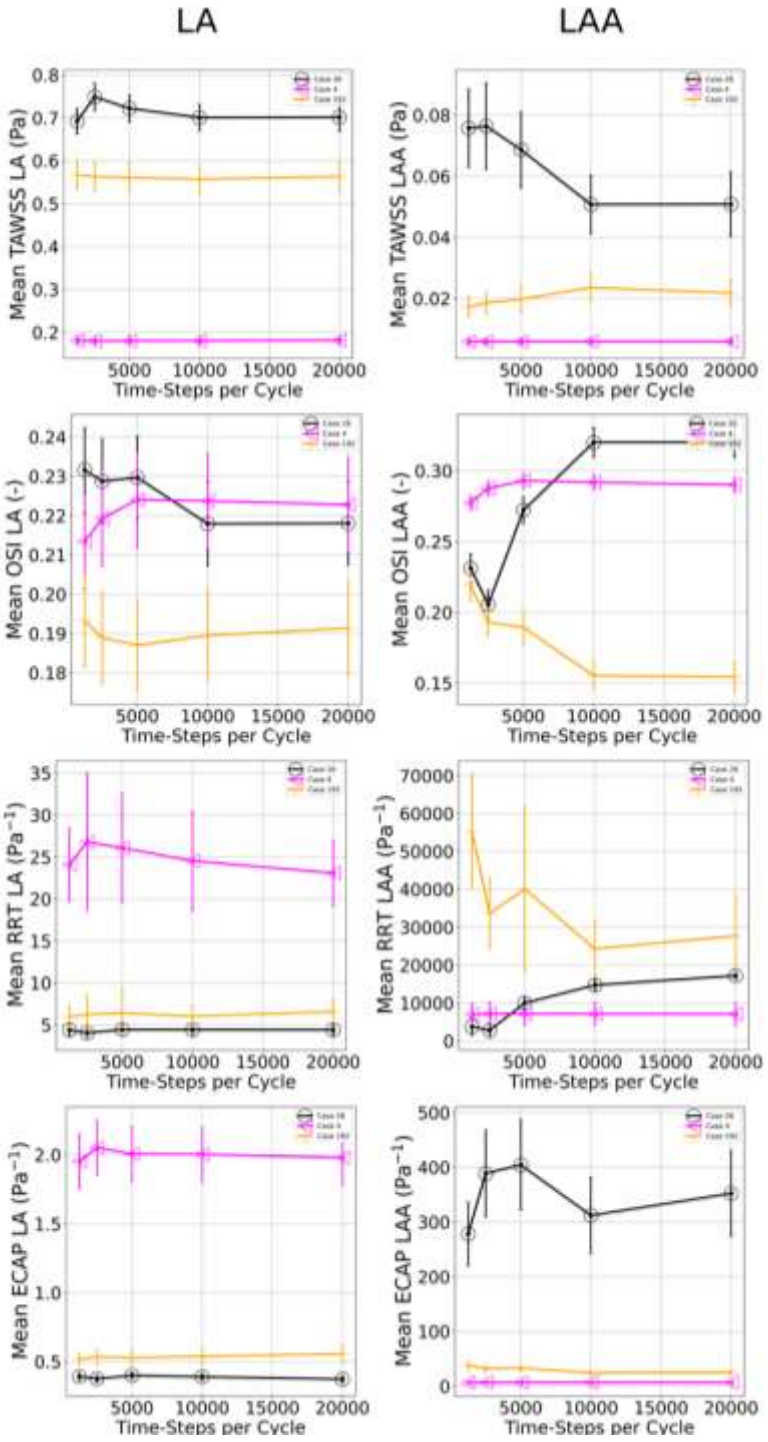

Figure 5: *Quantitative results of time averaged wall shear stress (WSS), oscillatory shear index (OSI), relative residence time (RRT), and endothelial cell activation potential (ECAP) in the left atrium (LA) and the left atrial appendage (LAA) for cases 4, 26 and 192 at 1250, 2500, 5000, 10000 and 20000 time-steps per cardiac cycle.*

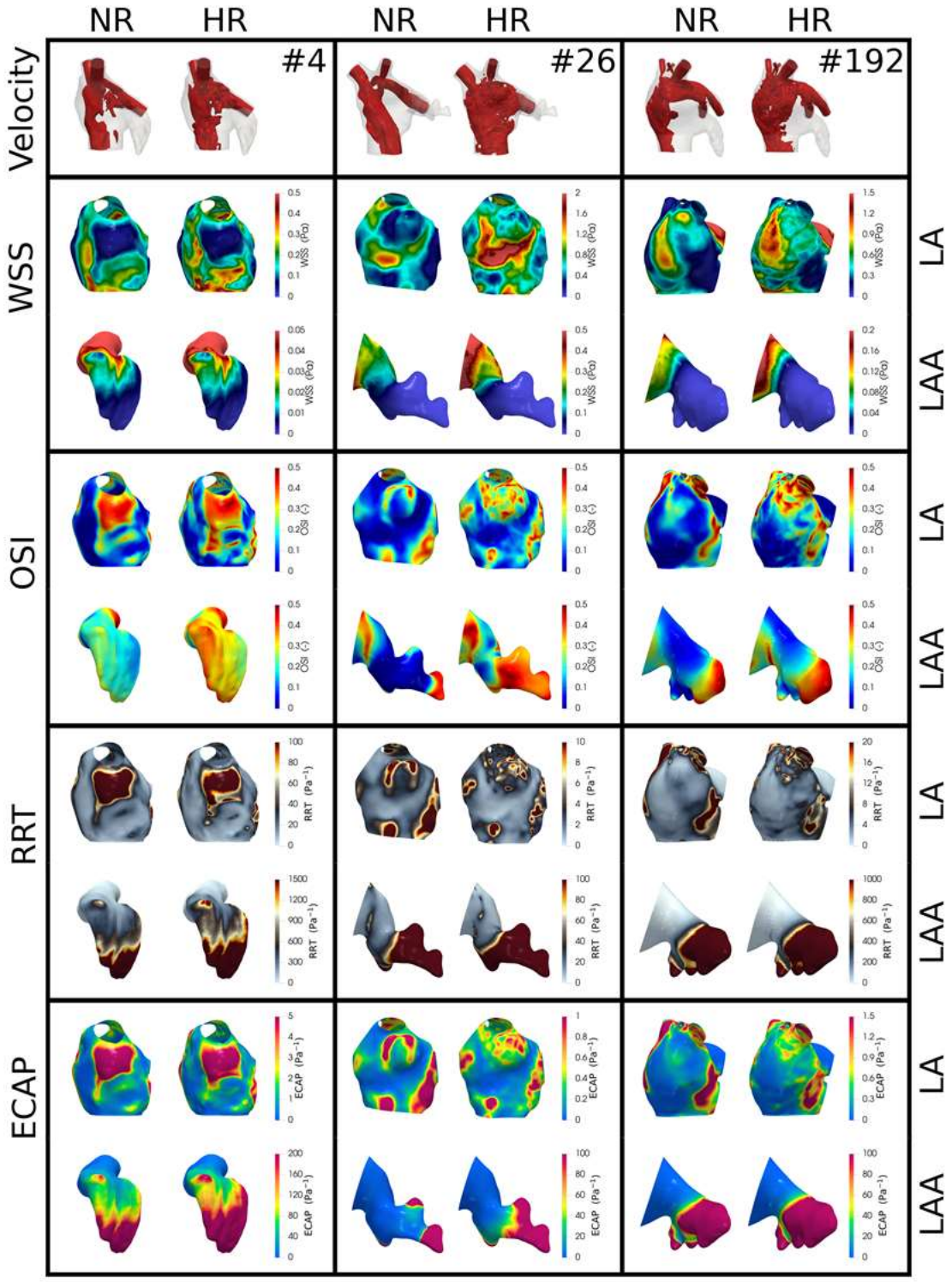

Figure 6: *Qualitative results of HR and NR simulations for cases 4, 26, and 192 in the left atrium (LA) and the left atrial appendage (LAA) separately. For each case, the first row compares isovelocity surfaces (in the range of [0.18-0.22] m/s), the second and third rows compare time averaged wall shear stress (WSS), the fourth and fifth rows show oscillatory shear index (OSI), sixth and seventh rows present relative residence time (RRT) and finally eighth and ninth rows present endothelial cell activation potential (ECAP).*

1.1.8 Conclusion

In this convergence study, we have presented a sensitivity analysis of spatial resolution, temporal resolution, and solver accuracy to assess the importance of modelling choices for predicting flows and hemodynamic indices in the left atria. It seems that there is indeed more than meets the eye. More specifically, there seems to be a profound sensitivity of modelling choices on predicting atrial flows, but also rank ordering of metrics, even on intermediate spatial/temporal resolutions, which could impact conclusions, depending on the question of interest and the context of use.

The main limitations of this study related with the verification D6.1, are:

- No devices included: The study lacks the inclusion of devices or components that could impact the fluid dynamics. This limitation may reduce the realism of the model
- The study does not include a comparison of the magnitude of velocity between the simulated results and experimental or reference data. This comparison is crucial to validate the accuracy of the model and verify if the simulated velocities align with expected or measured values
- Rigid wall assumption: The model assumes a rigid wall, which neglects the effects of wall compliance or flexibility
- Generic conditions with the mitral valve (MV) open under pressure equal to zero: The conditions used in the study are generic and may not accurately represent the specific physiological conditions or scenarios of interest

1.2 Use Error on InSilicoTrials Platform

The user interacts with the cloud-based platform through the Input Interface (by inserting input parameters) and through the Results Interface (by viewing and downloading simulation outputs).
Therefore, the error associated with potential human errors (e.g., errors that occur when entering model input parameters on the web interface) needs to be assessed.
In the following paragraphs, we describe the tests and actions taken to mitigate the risks of use error.

1.2.1 Input Interface

Input lower and upper limits are checked automatically by interface for every field. Warnings appear when the user types a number that is outside the boundaries. Examples are illustrated in the Figure 7.

Figure 7: *InSilicoTrials - example of input lower and upper limits automatic check.*

A webpage at the end of the input submission shows the summary of all data entered by the user and notifies the user in case any information is missing before allowing the user to run the model on the cloud. To demonstrate that the user inputs inserted in the webpage are correctly submitted to the simulation workflow, we performed a test by inserting specific values in the fields on the web interface, and verified that the values collected by the system and passed to the calculation were the same.

Final user will be responsible of demonstrating that inputs were correct.

The workflow guides the user along following web interfaces requiring inputs from the user as shown in the screenshots of Figure 8, Figure 9, and Figure 10.

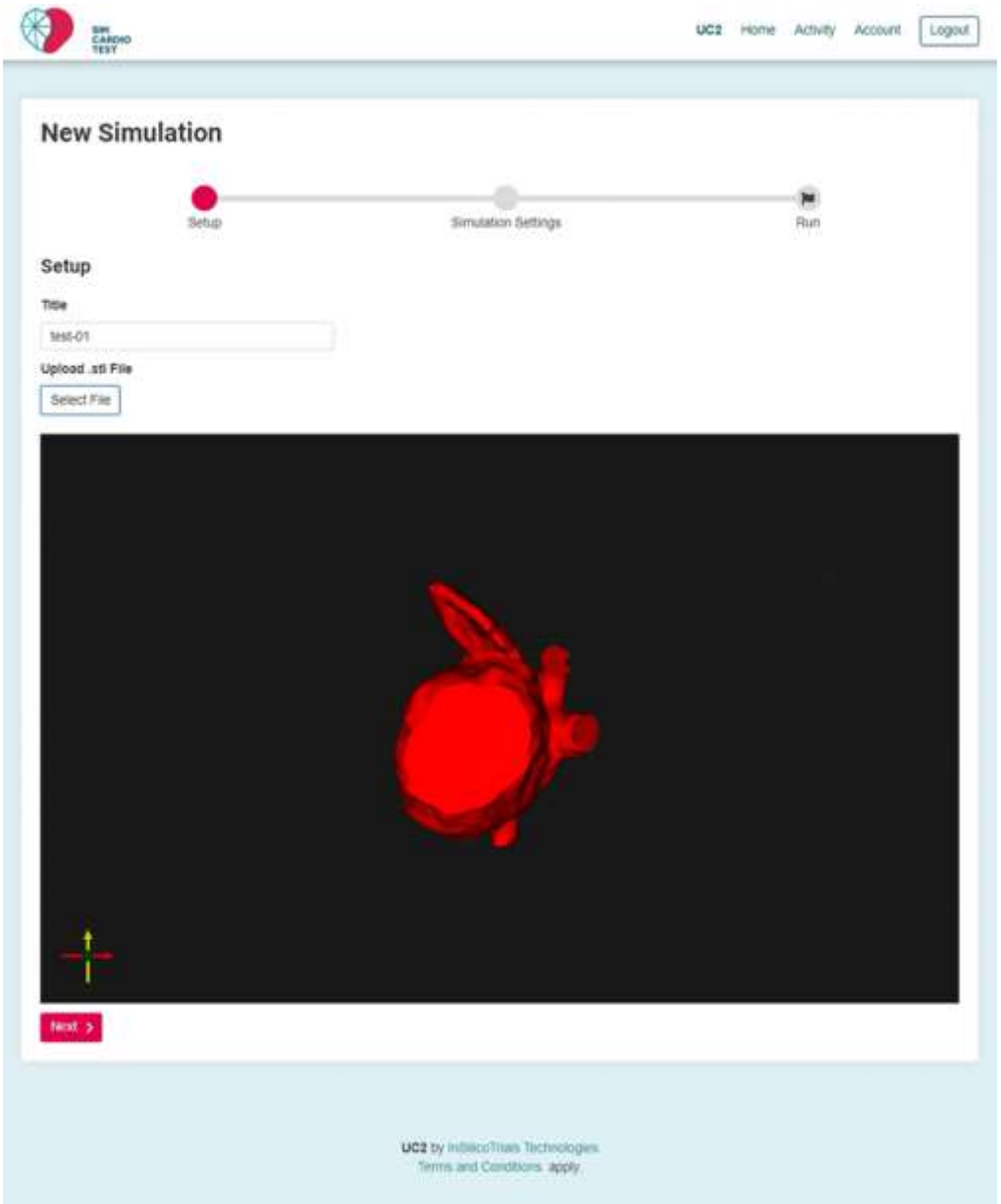

Figure 8: *InSilicoTrials - New Simulation - Setup.*

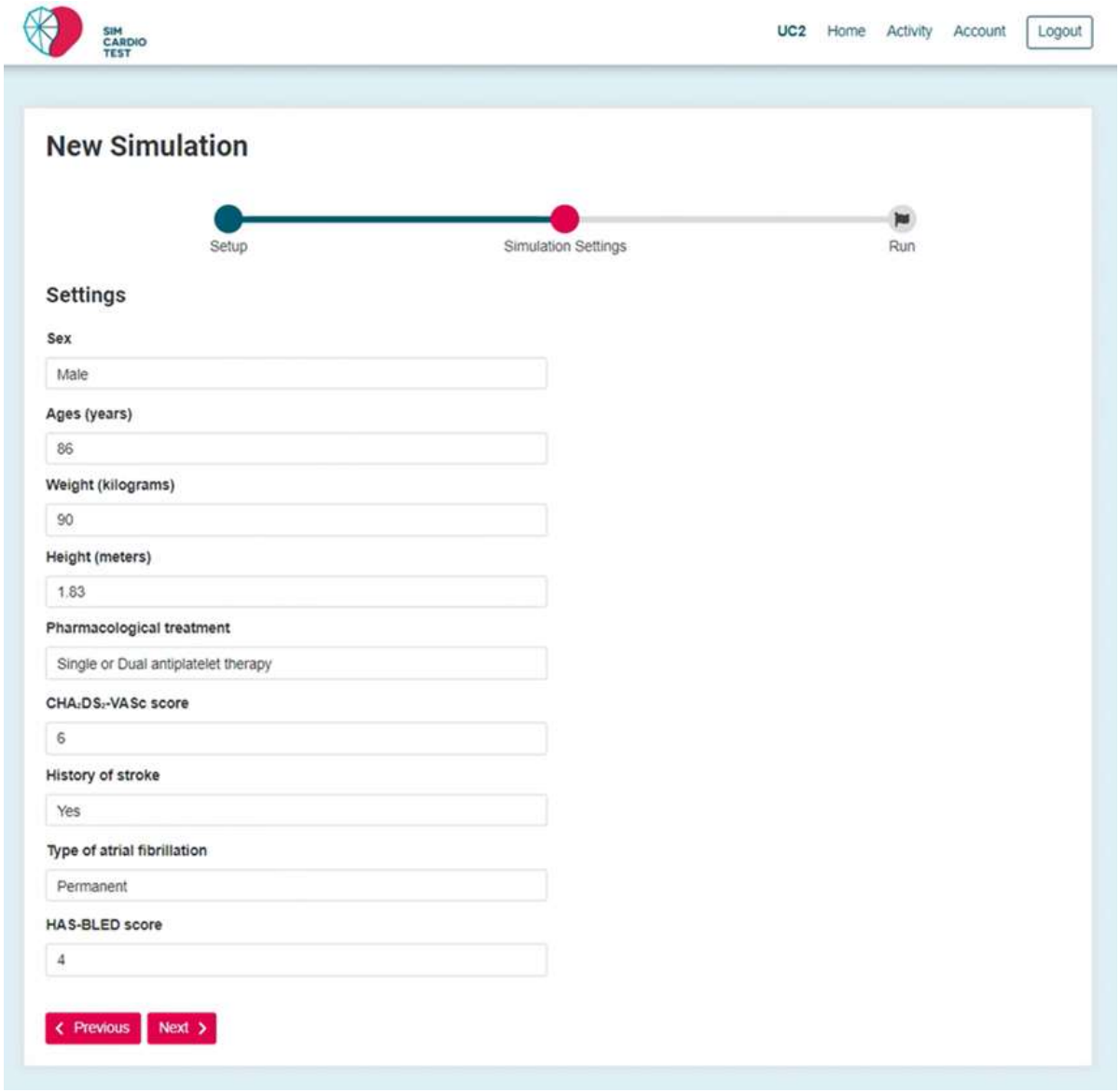

Figure 9: *InSilicoTrials - New Simulation - Simulation Settings.*

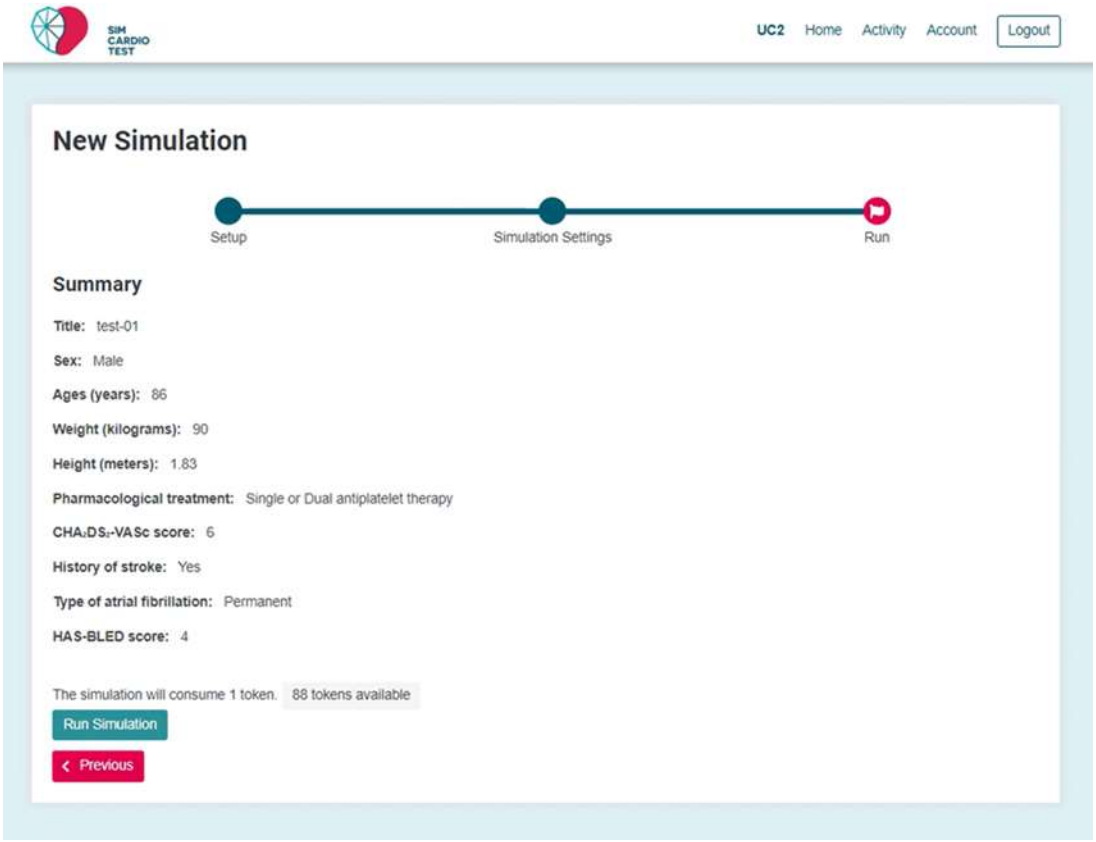

Figure 10: *InSilicoTrials - New Simulation - Run.*

After clicking on the "Run Simulation" button, an input.json file is created and stored in the corresponding repository in the dedicated environment (simcardiotest-uc2) created on Microsoft Azure (see Figure 11).

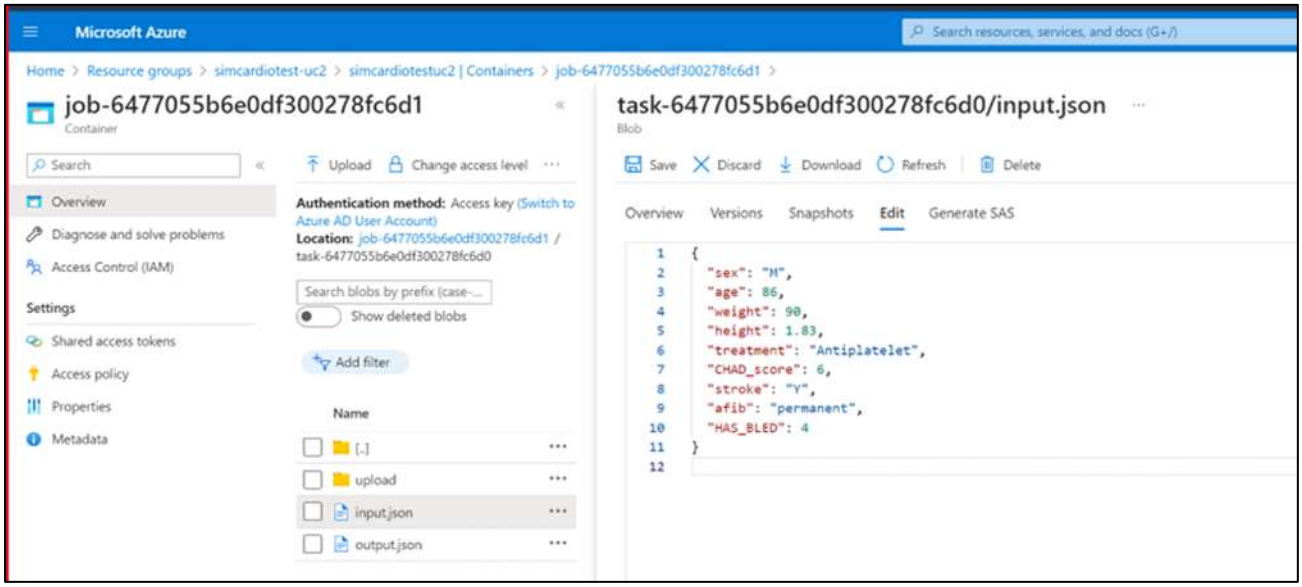

Figure 11: *InSilicoTrials - input.json file created and stored in the corresponding repository in the dedicated environment (simcardiotest-uc2) created on Microsoft Azure.*

The file contains the list of variables displayed on the web interface, and values correspond to the ones inserted by the user, meaning that the test has passed.

The uploaded .stl file is also stored in the same repository (see Figure 12).

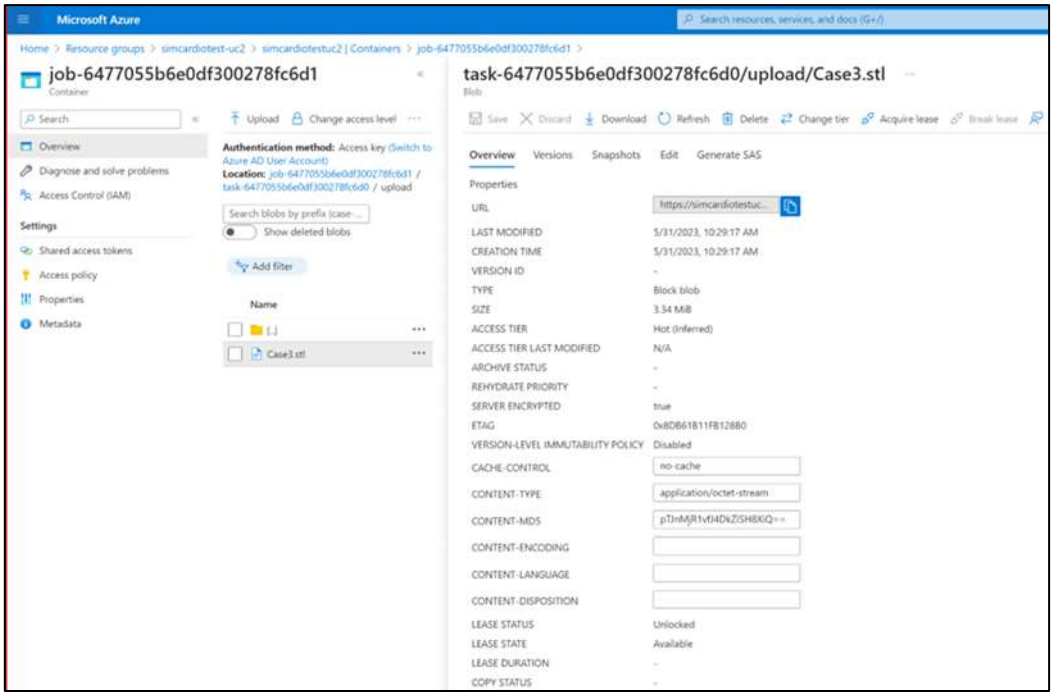

Figure 12: *InSilicoTrials - .stl file updated and store in the IST repository.*

2. Conclusion

This document is an annex of SimCardioTest deliverable D6.1, and reports technical details relative to the verification of the numerical model developed for Use Case 2. General conclusions relative to the verification of UC2 numerical model are reported in main deliverable D6.1.

3. Bibliography

[1] E. Khalili, C. Daversin-Catty, A. Olivares and others, "On the importance of fundamental computational fluid dynamics towards a robust and reliable model of left atrial flows: Is there more than meets the eye?," *arXiv:2302.01716 [physics.flu-dyn],* 2023.

[2] V&V40, Assessing Credibility of Computational Modeling Through Verification and Validation: Application to Medical Devices, New York: ASME, 2018.

This project received funding from the European Union's Horizon 2020 research and innovation program under grant agreement No 101016496

EU Horizon 2020 Research & Innovation Program
Digital transformation in Health and Care
SC1-DTH-06-2020
Grant Agreement No. 101016496

SimCardioTest - Simulation of Cardiac Devices & Drugs for in-silico Testing and Certification

SIM CARDIO TEST

Technical Report

D6.1-UC3-PK: Use Case 3 PK Verification Annex

Work Package 6 (WP6)

Verification, validation, uncertainty quantification & certification

Annex Lead: UPV, Spain
Task Lead: UBx, France
WP Lead: MPC, France

PUBLIC

Document history			
Date	**Version**	**Author(s)**	**Comments**
07/06/2023	V1	J. WELZEL	Final version prior consolidation
23/06/2023	V2	R. SETZU	Format consolidation
29/06/2023	V3	H. AREVALO	Quality Review
30/06/2023	V4	R. SETZU	Final version
01/07/2024	V5	R. SETZU M. BARBIER	Format editing

TABLE OF CONTENTS

EXECUTIVE SUMMARY

This document is an annex of SimCardioTest deliverable D6.1 and was elaborated for Use Case 3 in the context of drug safety assessment. It contains the technical details for the verification of the PK models in scope.

Acronyms

Table 1: List of Acronyms.

Acronym	Meaning
PK	Pharmacokinetic
IST	InSilicoTrials
SCT	SimCardioTest
TdP	Torsade de pointes

1. Code Verification

1.1 Software Quality Assurance

ExactCure simulation service is composed of ExaTwin, the computation-dedicated component, and PAPI, the public interface. The simulation service is part of a Software Medical Device, ExaMed. As such, its life cycle follows all software quality activities to guarantee conformity with ISO/IEC 62304 norm on Software Medical Devices.
In particular, this means the following:

- Complete life cycle management: definition, analysis, development, release, maintenance, end-of-life.
- Risk management
- Quality Management system
- Process-driven development and release, with traceability and including change management, using:
    - JIRA, Agile Project Management Issue tracking
    - Git, version control system
    - Bitbucket, a CI/CD platform to automate testing and deployment
- Multi-environment management, for development, testing and production.
- Software Verification, following the declared architecture and functionalities:
    - Unit testing of software units
    - Integration testing of software elements
    - End-to-end testing of the system
    - Code reviews, use of software quality tools performing static code analysis (coding style, test coverage, code complexity)
- Documentation (in-code of external) about interfaces, usages, methodologies

This SQA is detailed in the Technical Folder of the Medical Device.

About installation & environments

ExaTwin is a software medical device that is accessible only with an API and is not distributed.
ExactCure has installed PAPI/ExaTwin on the following machines:

- Production environment
    - Intel(R) Xeon(R) CPU E5-2673 v4 @ 2.30GHz
    - 16Go RAM
    - 32 GB temporary storage
    - Max IOPS 6400
- Pre-production (Plive) environment
    - Intel(R) Xeon(R) Platinum 8171M CPU @ 2.60GHz
    - 8Go RAM
    - 16 GB temporary storage
    - Max IOPS 3200

Both are on Ubuntu 18.04 Operating System.

1.2 Numerical Code Verification

1.2.1 Verification Plan

PK models are systems of ordinary differential equations (ODEs) with a calibration layer relating model parameters to patient covariates and other data. These model features are described in a proprietary user-friendly language that ExactCure system (ExaTwin) parses and solves when simulating a drug intake scenario.
ODEs are solved numerically, and calibration may involve numerical inversions to infer parameters. The numerical algorithms are based on SciPy's library.

A simulation request is a drug intake scenario applied to the drug model and patient, requested to an API (ExactCure public API or internal ExaTwin API).

A complete NCV requires following tasks:

1. Verifying off-the-shelf (SciPy) numerical algorithms used for ODEs and inversions.
2. Verifying that model features are correctly parsed and simulated.
3. Verifying that any drug intake scenario is properly considered (call to database, administration details) and simulated from the public interface.

Remark: In essence, ExaTwin inside ExactCure system is a generic PK simulator, and the verification tasks #2 and #3 would perform tests on all possible model features in all kinds of scenarios. We report here only individual verification for each PK model and expected drug intake scenarios. A generic verification of the drug simulation pipeline on the full model/molecule scope will be performed for December 2023.
Note also that ExaTwin contains a certain number of unit tests already guaranteeing a good level of verification. What is missing is global and systematic pipeline verification, on a practically exhaustive set of use-cases.

1.2.2 ODE Solver Algorithm

One of the key algorithms of ExaTwin simulation functionality is the ODE solver. SciPy, the widely used and sound numerical package for Python language, is integrated in the simulation algorithm, which uses the solve_ivp routine. SciPy has strong support from the scientific computing community, institutional partners and leading companies [1].

The explicit method "RK45" is a method of order O(h4) with an error estimator of order O(h5) and is the recommended default solver for non-stiff problems. PK models are most of the time non-stiff. Quoting Wikipedia: "*Runge-Kutta-Fehlberg Method 45 performs well with most ODE systems, and it is indicated as the first choice of solver. By performing one extra calculation, the error in the solution can be estimated and controlled by using the higher-order embedded method that allows for an adaptive stepsize to be determined automatically.*"

The discretization (stepsize) is controlled through the user-input tolerances "atoll" and "rtol", combined into Tol = atol + rtol * abs(y), where rtol controls a relative accuracy (number of correct digits), while atol controls absolute accuracy (number of correct decimal places). Default values are 1e-3 for rtol and 1e-6 for atol.

The RK45 solver implementation has been verified on several use-cases, for example (see Figure 1):

- Oral drug PK model: a linear, constant coefficient and scalar differential equation
- Riccati equation: a non-linear, constant coefficient and scalar differential equation

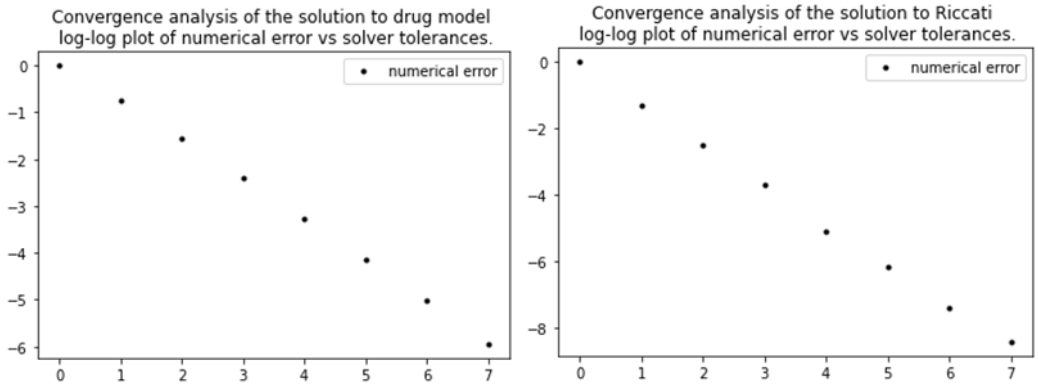

Figure 1: *Convergence analysis shows that, as solver tolerances decrease, the numerical error converges to zero (thus, the numerical solution converges to the analytical solution).*

Same convergence has been observed on other differential problems. This provides strong evidence about the capacity of the routine to solve (non-stiff) initial value problems, as required for PK model simulation.

1.2.3 Inversion Algorithm

Model parameters may be known through drug concentration curve features ("non-compartmental data"), for example AUC (Area Under the Curve), Cmax (max concentration) etc. ExaTwin is able to solve a combination of such data to infer model parameters. It proceeds by numerically inverting the relationship "parameters → NC data", using classical root-solving algorithms provided by SciPy in the routine *root_scalar()*.
We have verified Bisection and Brent. Both conformed to expectations with respect to their documentation and are suitable for use in ExaTwin and parameter estimation.

1.2.3.1 Bisection

Bisection is the most classic root-finding algorithm. It is a robust iterative algorithm that halves the bracketing of the root each step. Using 3 simple benchmarks, we studied the convergence properties (see Figure 2).

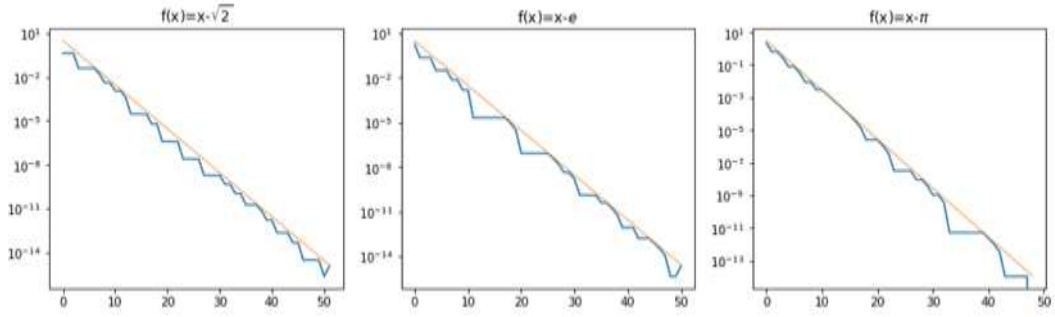

Figure 2: *Bisection convergence properties with 3 simple benchmarks functions.*

As expected, Bisection obeys a linear convergence scheme to the theoretical solution. Moreover, we checked that the implementation was robust enough against limit cases.

1.2.3.2 Brent

Brent's method combines root bracketing, interval bisection, and inverse quadratic interpolation. We studied the convergence properties on two benchmark functions that are differentiable with root zero but a different slope around it (see Figure 3).

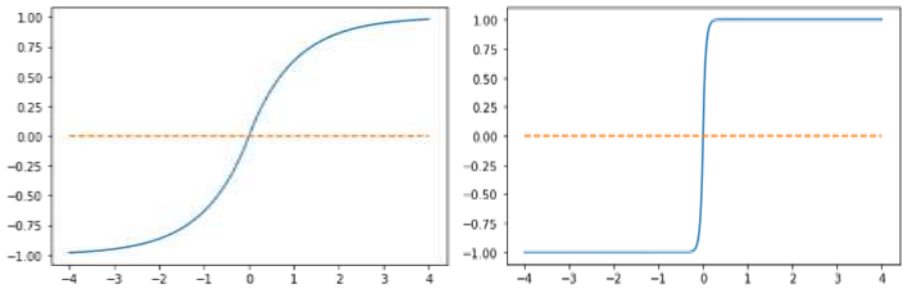

Figure 3: *Brent convergence properties with 2 simple benchmarks functions.*

Convergence to the root is displayed in Figure 4:

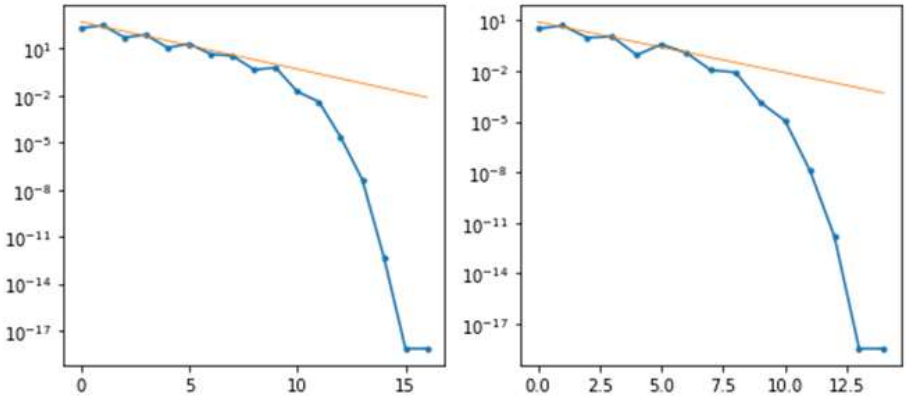

Figure 4: *Brent converge to the root with 2 simple benchmarks functions.*

As expected, Brent follows a super-linear convergence scheme for such well-behaved function and the terminal accuracy corresponds to the expected accuracy (1e-16).

1.2.4 Simulation from ExaTwin

We show here, on two relevant examples, that the ODE solving, the parameters calibration, and the drug intake scenario are all properly combined in ExaTwin simulation endpoint. These examples are PK models for which analytical solutions are known, and we compare the simulated concentration curve with the theoretical one.

To perform the simulation at ExaTwin level, we simply create an API request directly from a Python Notebook to a version of ExaTwin installed locally, and we store results. Computations from analytical formulae and plotting are done in the same Notebook.

First example is single-compartment model with linear absorption and elimination processes and respective rates ka and ke. Drug concentration is the drug quantity x1 in the central compartment divided by the so-called distribution volume V. The solution after a single drug intake D at t=0 is well-known in pharmacokinetics. In particular, the time at which the concentration is maximum is given by:

$$Tmax = (\ln(ka)-\ln(ke)) / (ka-ke)$$

The elimination half-time is given by:

$$T1/2=\ln(2)/ke$$

Now, we run the numerical simulation with the following input data:

- Scenario data: dose is 100 at t=0, meaning x0(t=0) = D
- Model parameters: ka and ke are inferred from the following observation data: concentration maximum should occur 1 hour after the drug intake, and the elimination half-time is 4 hours. Distribution volume is 50.0, bioavailability is 1.0.
- Ordinary differential system of the model, encoded in the request "model" section:
  - x0_dot = -ka*x0
  - x1_dot = +ka*x0 – ke*x1
- output is x1/V

Plotting the analytical solution on the same graph, we see that this numerical simulation conforms to expectations (see Figure 5).

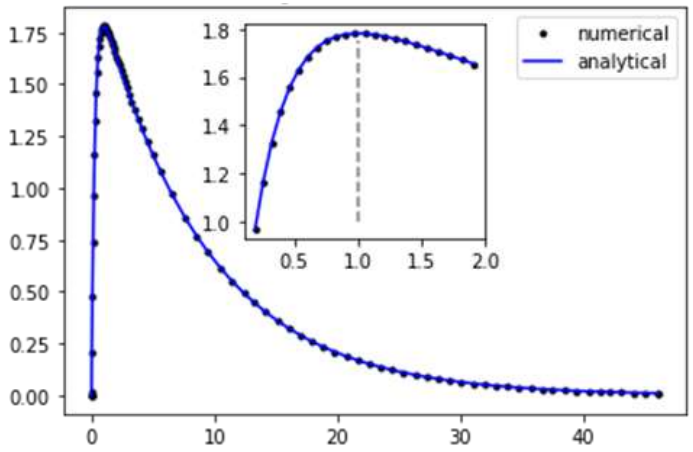

Figure 5: *Simulation output against analytical solution. 1 compartment, linear model. Concentration in mg/L, vs time in hours.*

We reproduce this verification with a slightly more complicated model. Kinematically, the model has two compartments and is fully linear. Calibration will be trivial. We run the numerical simulation with the following input data:

- Scenario data: dose is 100 at t=0
- Model parameters: ka=1.0, ke=0.25, and intercompartmental rates are k12=k21=0.2. Distribution volume is 50.0, bioavailability is 1.0

- Ordinary differential system of the model:
  - x0_dot = -ka*x0
  - x1_dot = +ka*x0 – ke*x1 + k21*x2 – k12*x1
  - x2_dot = - k21*x2 + k12*x1

We have again a match with the analytical solution (see Figure 6).

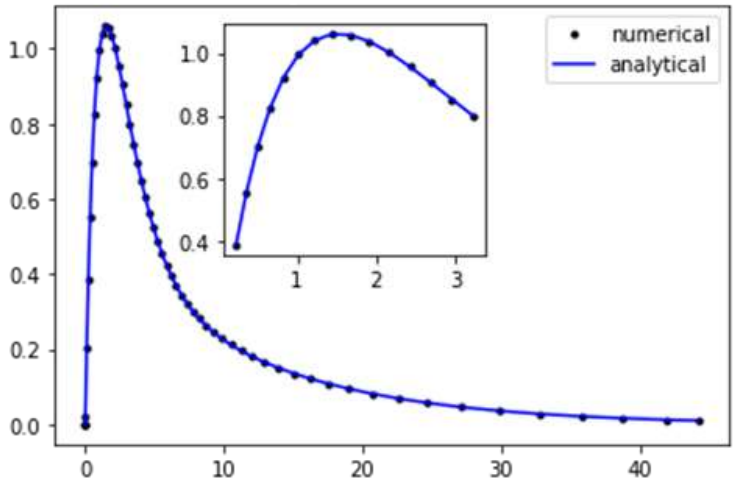

Figure 6: *Simulation output against analytical solution. 2 compartments, linear model. Concentration in mg/L, vs time in hours.*

This concludes the verification that a simulation request, at the level of ExaTwin, correctly integrates model parsing and numerical algorithms to solve a drug intake simulation. As said in the verification plan, exhaustive testing is scheduled for a later stage.

1.2.5 Simulation from the Public Interface

To verify the simulation functionality at the system level, in conditions reflecting its use for Use-Case 3, we need to perform simulations from PAPI, the public interface. We have requested the Plive environment, with the same access rights as IST.
We display the simulation of Clozapine (CIS= 67513540) on two patient profiles in Figure 7 and Figure 8 respectively, and simulation of Escitalopram (CIS=67219535) in Figure 9.

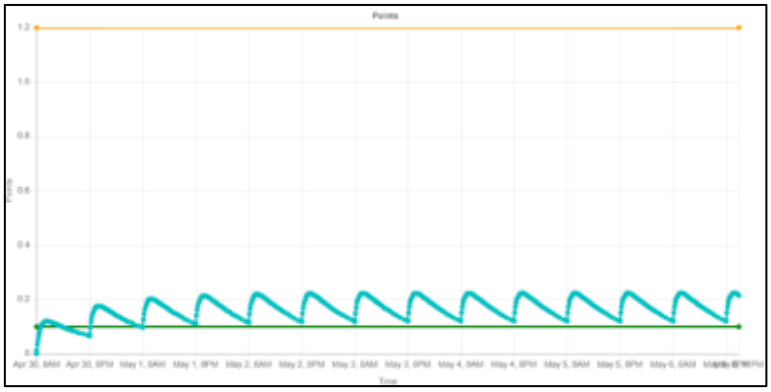

Figure 7: *PAPI simulation: clozapine, male patient, 100mg twice daily.*

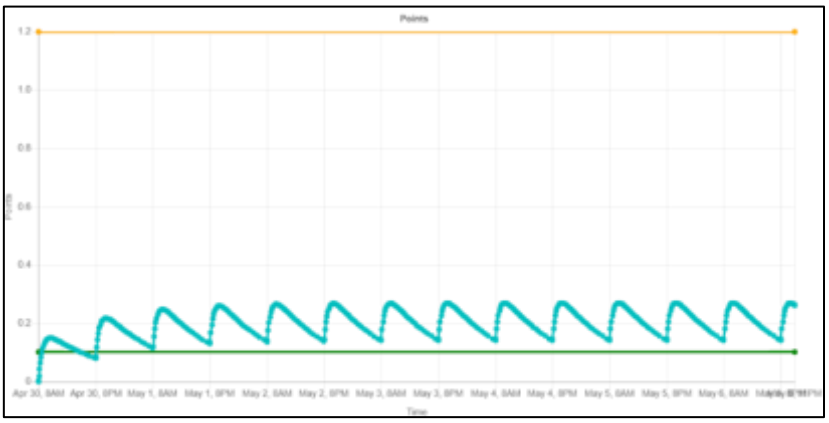

Figure 8: *PAPI simulation: clozapine, female patient, 100mg twice daily.*

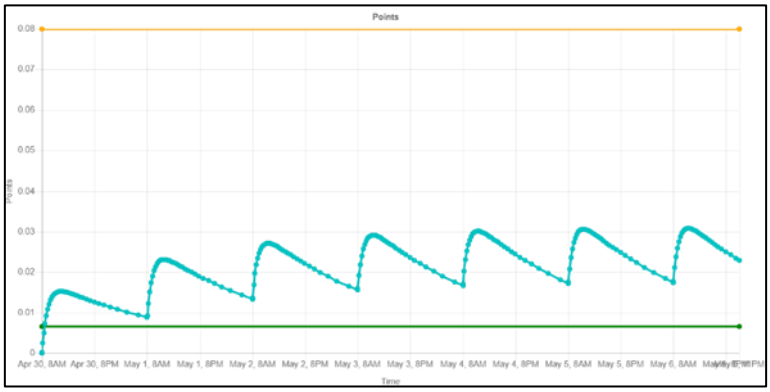

Figure 9: *PAPI Simulation: Escitalopram, standard patient, 15mg daily.*

This shows that PAPI correctly integrates ExaTwin simulation on the expected drug scope and that the interface responds to user inputs (drug, patient, administration). Note that those simulations match exactly what is obtained by requesting ExaTwin directly, as one can see from graphs in the Calculation Verification step.

Next sections will show simulation results of actual PK models for molecules in scope of Use-Case 3, making sure that for those models, the software and numerical code is accurate.

2. Calculation Verification

2.1 Discretisation Error

There is no spatial discretization in the numerical model, only temporal discretization to simulate the time-course of drug concentrations. Analysis of the associated numerical error is reported in the next section.

2.2 Numerical Solver Error

Recalling characteristics of the ODE solver, ExaTwin uses by default an adaptive solver based on RKF45 method. Accuracy in the numerical solving is controlled by user-input tolerances that loosely

speaking, bounds the difference between the numerical solution and the exact solution on any time interval. However, the public interface as well as the model definition do not allow to change these tolerances, which are fixed to their default values (1e-06 and 1e-06 for relative and absolute tolerances). The same is true for the inversion algorithms.

Convergence analysis will not be performed but we will report the numerical accuracy on the simulation output compared to known solutions.

An update of ExaTwin is planned where the numerical setup of the model (selected algorithms and tolerances) will be set and used in simulations. When available, the verification will include convergence analysis.

We perform a Parameters estimation verification and a Maximum concentration verification for each molecule available from the public interface and in scope of H2020/SimCardioTest.
Note that administration scenarios may not be therapeutically correct on the treatment duration. They are chosen so that the concentration curve attains a steady state in order to compare with theoretical concentrations accurately.

2.2.1 Clozapine

2.2.1.1 Parameters Estimation Verification

Covariates: sex_m is used, which is derived from the higher-level sex covariates. If the subject gender is male, then sex_m is True and valued to 1, else sex_m is False and valued to 0.
Parameters encoded in the model are:

- Bioavailability F = 1.0
- Lag Tlag = 0.0
- Absorption rate Ka = 1.24+(0.13*sex_m)
- Clearance Cl = 39.9+(8*sex_m)
- Distribution volume V = 564+(155*sex_m)
- Elimination rate Ke is Cl/V

Subjects:

- Subject 1: Male
- Subject 2: Female

Results are presented in Table 2 and Table 3.

Table 2: Parameters calibration values for subject 1, clozapine.

Parameter	Calibrated	Expected	Calib. Error
F	1.0	1.0	0.0
Tlag	0.0	0.0	0.0
Ka (subject 1)	1.37	1.37	0.0
Cl (subject 1)	47.9	47.9	0.0

Parameter	Calibrated	Expected	Calib. Error
V (subject 1)	719.0	719.0	0.0
Ke (subject 1)	0.066620	0.066620	0.0

Table 3: Parameters calibration values for subject 2, clozapine.

Parameter	Calibrated	Expected	Calib. Error
Ka (subject 2)	1.24	1.24	0.00
Cl (subject 2)	39.9	39.9	0.
V (subject 2)	564.0	564.0	0.0
Ke (subject 2)	0.070744	0.070744	0.0

Calibration matches expectations perfectly on these patients.

2.2.1.2 Maximum Concentration Verification

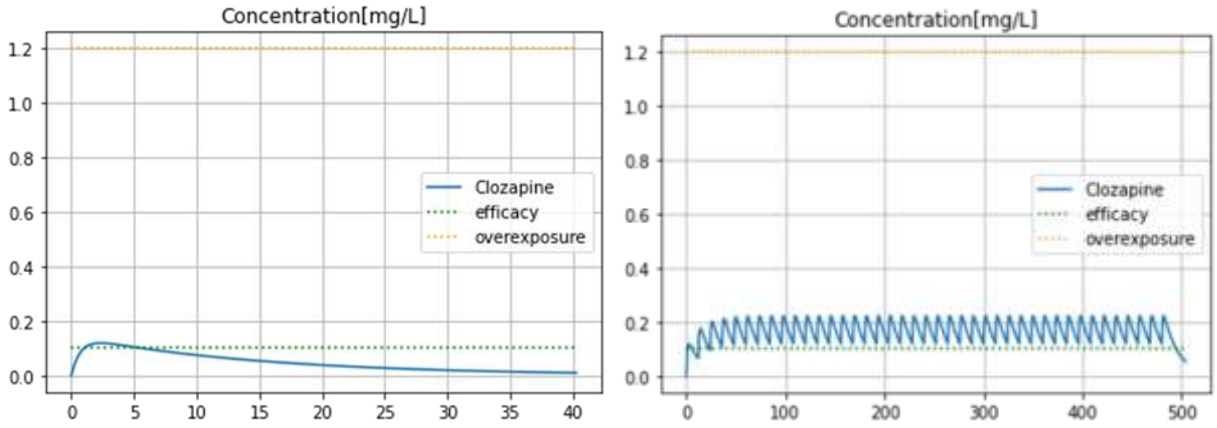

Figure 10: *Numerical simulation with a male patient, clozapine is administered orally every 12 hours with a dose of 100mg, for a period of 20 days (where steady state is practically obtained).*

We extract numerically the maximum concentration after one drug intake and at steady state. Similarly, we use the model parameters to compute the theoretical maximum concentration after one drug intake and at steady state. Table 4 displays results.

Table 4: Results of numerical vs theoretical max concentrations comparison test for clozapine.

Value \ Scenario	Single dose	Repeated admin
Numerical max concentration	0.119165	0.223206
Theoretical max concentration	0.119166	0.223209
Numerical Error	1e-06	3e-06

We see a match at the order of 10^{-6} on the maximum concentration in both scenarios.

2.2.2 Chlorpromazine

2.2.2.1 Parameters Estimation Verification

Covariates: weight, glomerular filtration rate (GFR)
Base parameters encoded in the model are:

- Bioavailability F = 0.32
- Distribution volume V = 1470
- Lag Tlag = 0.0
- Elimination half-time T12 = 30
- Time of maximum concentration Tmax = 2.5

Calibration step will infer Ke and Ka from numerical inversion of T12 and Tmax data. If we compute T12 and Tmax with calibrated parameters and compare with original values, we can measure the calibration error.

On subject 1, a standard patient (weight=70, GFR=100), we have values in Table 5.

Table 5: Parameters calibration values for subject 1, chlorpromazine.

Parameter-Data	Calibration	Expected	Calib Error
Ke	0.0231049	/	/
Ka	1.75522	/	/
T12	30.0	30	0.0
Tmax	2.49999	2.5	1e-14

For non-standard weight ($\neq$70) or GFR ($\neq$100), there is an additional calibration step. On subject 2, with weight = 140 and GFR = 50, we have values in Table 6.

Table 6: Parameters calibration values for subject 2, chlorpromazine.

Parameter	Calibrated	Expected	Calib Error
V (subject 2)	2940.0	2940.0	0.0
Ke (subject 2)	0.023047	0.023047	0.0

Calibration matches expectations perfectly on these patients.

2.2.2.2 Maximum Concentration Verification

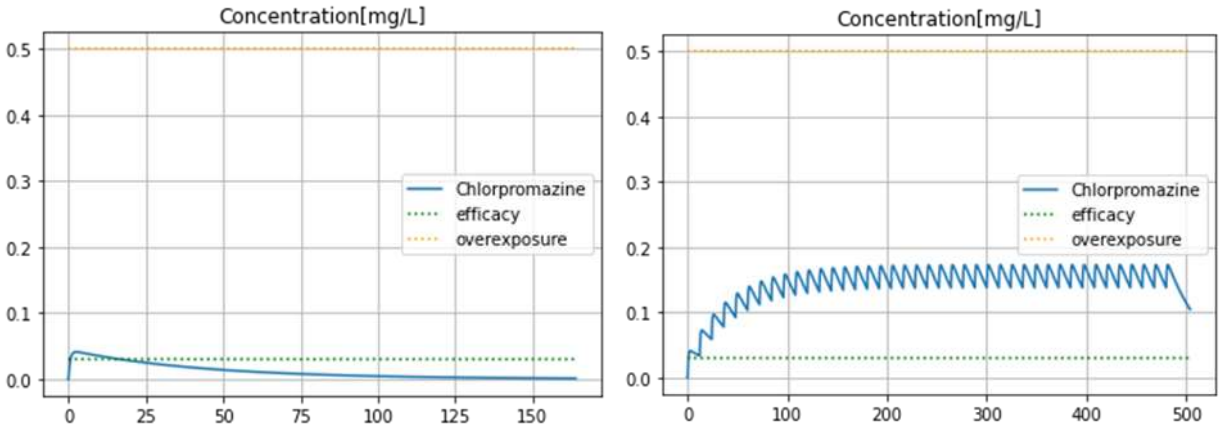

Figure 11: *Numerical simulation with a patient with GFR=100 and weight=70, chlorpromazine is administered orally every 12 hours with a dose of 200mg, for a period of 20 days (where steady state is practically obtained).*

Results on maximal concentration are reported in Table 7.

Table 7: Results of numerical vs theoretical max concentrations comparison test for chlorpromazine.

Value \ Scenario	Single dose	Repeated admin
Numerical max concentration	0.041092	0.172946
Theoretical max concentration	0.041093	0.172951
Numerical error	1e-06	4e-06

We see a match at the order of 10^{-6} on the maximum concentration in both scenarios.

2.2.3 Escitalopram

2.2.3.1 Parameters Estimation Verification

Covariates: weight, age, body mass index (BMI), CYP2C19 mutation status.
Parameters encoded in the model are:

- Bioavailability F = 1.0
- Lag Tlag = 0.0
- Absorption rate Ka = 0.80
- Clearance CL = 26.0 * power(age/40,-0.336)*power(weight/76,0.333)
- Distribution volume V = 947.0 * power(BMI/27,1.11)
- Elimination rate Ke is Cl/V

For non-standard CYP2C19 mutation status, there is an additional calibration step: The clearance Cl must be adjusted by a factor of 0.762.

Subjects:

- Subject 1: Standard (weight = 70, age = 40, BMI = 25, default CYP2C19 mutation status)
- Subject 2: Subject 1 with "poor" CYP2C19 mutation status

Results are reported in Table 8 and Table 9.

Table 8: Parameters calibration values for subject 1, escitalopram.

Parameter	Calibrated	Expected	Calib Error
F	1.0	1.0	0.0
Tlag	0.0	0.0	0.0
Ka	0.80	0.80	0.0
Cl	25.297643	25.297643	0.0
V	869.460007	869.4600075	2e-13
Ke (subject 1)	0.0290958	0.0290958	1e-17

Table 9: Parameters calibration values for subject 2, escitalopram.

Parameter	Calibrated	Expected	Calib Error
Ke (subject 2)	0.022171	0.022171	1e-17

Calibration matches expectations perfectly on these patients.

2.2.3.2 Maximum Concentration Verification

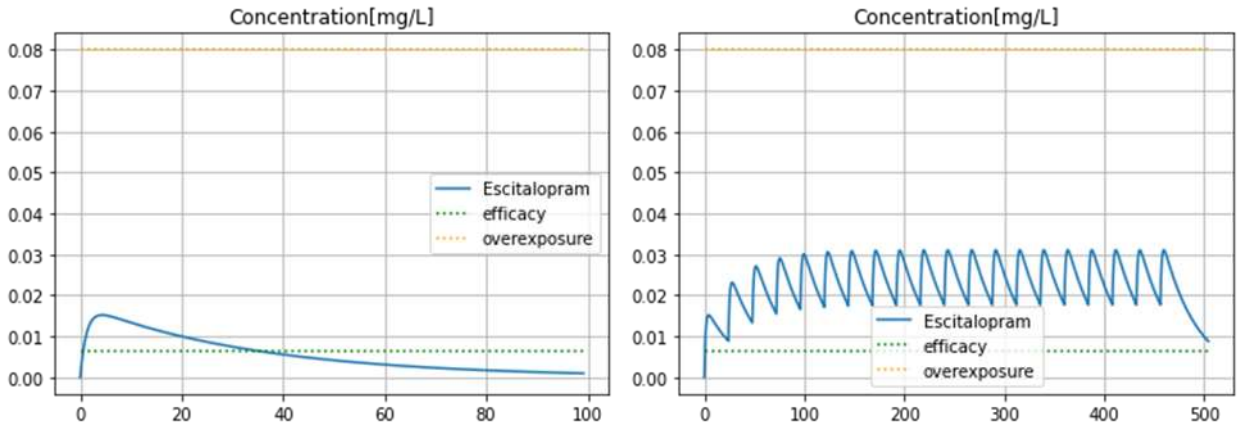

Figure 12: *Numerical simulation with a patient with age = 40, weight = 70, BMI = 25 and CYP2C19 at "extensive", Escitalopram is administered orally every 24 hours with a dose of 15mg, for a period of 20 days (where steady state is practically obtained).*

Results on maximal concentration are reported in Table 10.

Table 10: Results of numerical vs theoretical max concentrations comparison test for escitalopram.

Value \ Scenario	Single dose	Repeated admin
Numerical max concentration	0.015222	0.031083
Theoretical max concentration	0.015223	0.031088
Numerical error	9e-07	5e-06

We see a match at the order of 10^{-6} on the maximum concentration in both scenarios.

2.2.4 Risperidone

2.2.4.1 Parameters Estimation Verification

Covariates: weight, age and glomerular filtration rate (GFR)
Parameters encoded in the model are:

- Bioavailability F = 1.0
- Lag Tlag = 0.235
- Absorption rate Ka = 0.239
- Clearance CL = (4.66 * power(weight/70,0.75) + 0.00831*GFR) * power(age/18.1,-0.172)
- Distribution volume V1 = 137*weight/70
- Distribution volume V1 = 86.8*weight/70
- Intercompartmental clearance Q = 1.35
- Elimination rate Ke is Cl/V
- Intercompartmental transfer rates are K12=Q/V1 and K21=Q/V2

Subjects:

- Subject 1: standard patient (weight=70, age=40, GFR=90)
- Subject 2: non-standard patient (weight=100, age=60, GFR=50.0)

Results are shown in Table 11 and Table 12.

Table 11: Parameters calibration values for subject 1, risperidone.

Parameter	Calibrated	Expected	Calib Error
F	1.0	1.0	0.00
Tlag	0.235	0.235	0.
Ka	0.239	0.239	0.0
Q	1.35	1.35	0.0
Cl (subject 1)	4.718403	4.7184030	2e-14

Parameter	Calibrated	Expected	Calib Error
V1 (subject 1)	137.0	137.0	0.0
V2 (subject 1)	86.8	86.8	0.0
Ke (subject 1)	0.034440	0.034440	2e-16
K12 (subject 1)	0.009854	0.009854	0.0
K21(subject 1)	0.015552	0.015552	0.0

Table 12: Parameters calibration values for subject 2, risperidone.

Parameter	Calibrated	Expected	Calib Error
Cl (subject 2)	5.293074	5.293074	3e-14
V1 (subject 2)	195.714285	195.714285	2e-14
V2 (subject 2)	124.0	124.0	0.0
Ke (subject 2)	0.027044	0.02704490	1e-16
K12 (subject 2)	0.006897	0.00689781	1e-18
K21 (subject 2)	0.010887	0.01088709	0.0

Calibration matches expectations perfectly on these patients.

2.2.4.2 Maximum Concentration Verification

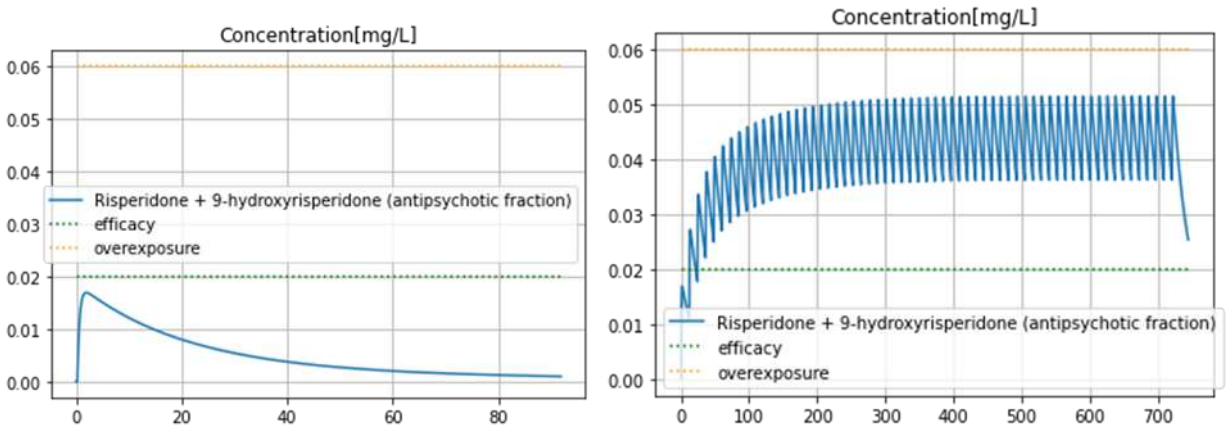

Figure 13: *Numerical simulation with a patient with weight=70, age=40 and GFR=90, Risperidone is administered orally every 12 hours with a dose of 2.5mg, for a period of 30 days (where steady state is practically obtained).*

Results on maximal concentration are shown in Table 13.

Table 13: Results of numerical vs theoretical max concentrations comparison test for risperidone.

Value \ Scenario	Single dose	Repeated admin
Numerical max concentration	0.0169259	0.051555

Value \ Scenario	Single dose	Repeated admin
Theoretical max concentration	0.016926	0.051561
Numerical Error	8e-07	6e-06

We see a match at the order of 10^{-6} on the maximum concentration in both scenarios.

2.2.5 Carvedilol

2.2.5.1 Parameters Estimation Verification

Covariates: weight, smoker status
Parameters encoded in the model are:

- Bioavailability F = 1.0
- Lag Tlag = 0
- Absorption rate Ka = 0.81
- Clearance CL = 10 + 0.434*weight + 29.9 * smoker
- Distribution volume V = 832
- Elimination rate Ke is Cl/V

Subjects:

- Subject 1: Standard (weight = 70, non-smoker)
- Subject 2: Weight=100, smoker (smoker=1)

Table 14: Parameters calibration values for subject 1, carvedilol.

Parameter	Calibrated	Expected	Calib Error
F	1.0	1.0	0.0
Tlag	0.0	0.0	0.0
Ka	0.81	0.81	0.0
Cl (subject 1)	40.379999	40.38	5e-15
V	832.0	832.0	0.0
Ke (subject 1)	0.0485336	0.04853365384615384	0.0

Table 15: Parameters calibration values for subject 2, carvedilol.

Parameter	Calibrated	Expected	Calib Error
Cl (subject 2)	83.3	83.3	0.0
Ke (subject 2)	0.100120	0.100120	0.0

Calibration matches expectations perfectly on these patients.

2.2.5.2 Maximum Concentration Verification

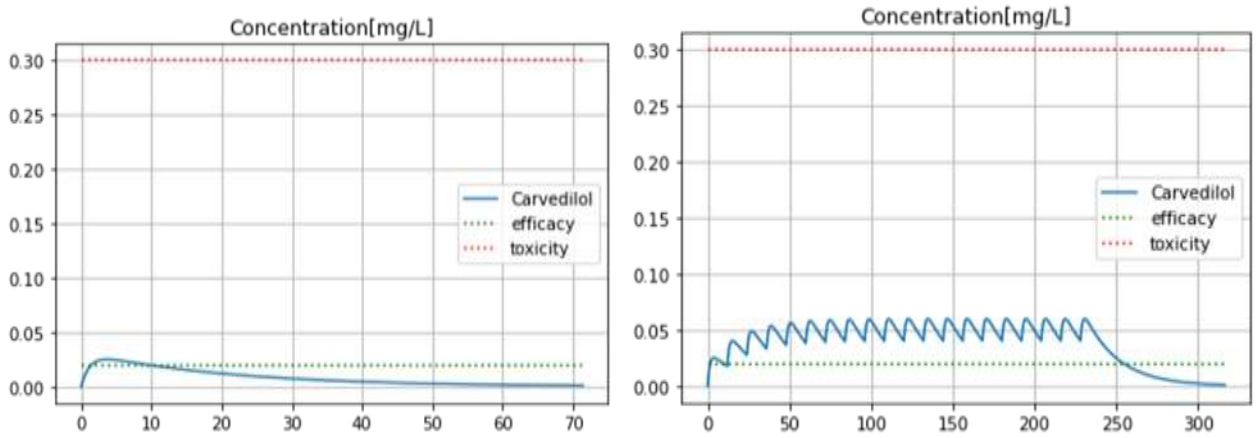

Figure 14: *Numerical simulation with a patient with weight=70 and not smoker, Carvedilol is administered orally every 12 hours with a dose of 25mg, for a period of 10 days (where steady state is practically obtained).*

Results on maximal concentration are shown in Table 16.

Table 16: Results of numerical vs theoretical max concentrations comparison test for carvedilol.

Value \ Scenario	Single dose	Repeated admin
Numerical max concentration	0.025107	0.059925
Theoretical max concentration	0.025113	0.059931
Numerical Error	5e-06	6e-06

We see a match at the order of 1e-06 on the maximum concentration in both scenarios.

2.2.6 Clarithromycine

2.2.6.1 Parameters Estimation Verification

Covariates: weight, glomerular filtration rate (GFR)
Base parameters encoded in the model are:

- Bioavailability F = 0.55
- Distribution volume V = 210
- Lag Tlag = 0.0
- Elimination half-time T12 = 3.8
- Time of maximum concentration Tmax = 1.7

Calibration step will infer Ke and Ka from numerical inversion of T12 and Tmax data. If we compute T12 and Tmax with calibrated parameters and compare with original values, we can measure the calibration error.

On subject 1, a standard patient (weight=70, GFR=100), we have the values shown in Table 17.

Table 17: Parameters calibration values for subject 1, clarithromycine.

Parameter	Calibrated	Expected	Calib Error
Ke	0.182407	/	/
Ka	1.367335	/	/
T12	3.799999	3.8	4e-16
Tmax	1.700000	1.70	3e-14

For non-standard weight or GFR, there is an additional calibration step. On subject 2, with weight = 140 and GFR = 30, we have the values shown in Table 18.

Table 18: Parameters calibration values for subject 2, clarithromycine.

Parameter	Calibrated	Expected	Calib Error
V (subject 2)	420.0	420.0	0.0
Ke (subject 2)	0.060802	0.060802	0.0

Calibration matches expectations perfectly on these patients.

2.2.6.2 Maximum Concentration Verification

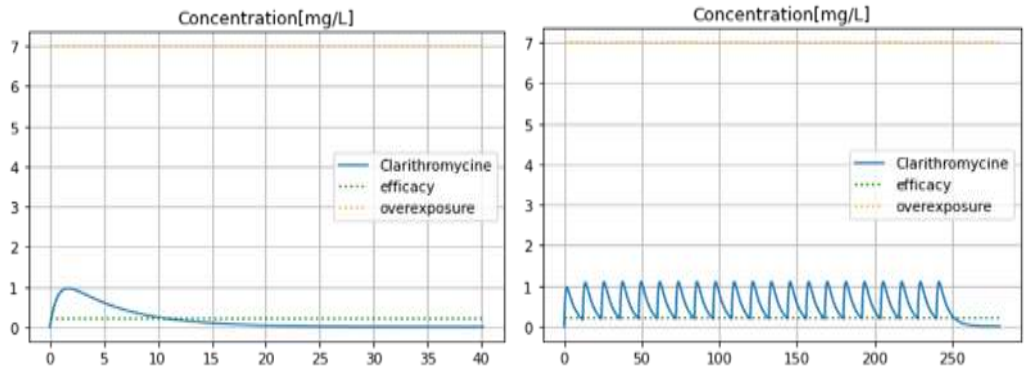

Figure 15: *Numerical simulation with a patient with weight=70 and GFR=100, Clarithromycine is administered orally every 12 hours with a dose of 500mg, for a period of 20 days (where steady state is practically obtained).*

Results on maximal concentration are shown in Table 19.

Table 19: Results of numerical vs theoretical max concentrations comparison test for Clarithromycine.

Value \ Scenario	Single dose	Repeated admin
Numerical max concentration	0.960148	1.101381
Theoretical max concentration	0.960377	1.101523
Numerical Error	2e-04	1e-04

We see a match at the order of on the maximum concentration in both scenarios.

2.2.7 Disopyramide

2.2.7.1 Parameters Estimation Verification

Covariates: weight, glomerular filtration rate (GFR)
For the oral route and immediate release form, base parameters encoded in the model are:

- Bioavailability F = 0.95
- Distribution volume V = 52.5
- Lag Tlag = 0.0
- Elimination half-time T12 = 6.3
- Time of maximum concentration Tmax = 1.5

Calibration step will infer Ke and Ka from numerical inversion of T12 and Tmax data. If we compute T12 and Tmax with calibrated parameters and compare with original values, we can measure the calibration error.

On subject 1, a standard patient (weight=70, GFR=90), we have values in Table 20.

Table 20: Parameters calibration values for subject 1, disopyramide.

Parameter	Calibrated	Expected	Calib Error
Ke	0.110023	/	/
Ka	2.064732	/	/
T12	6.300000	6.3	3e-15
Tmax	1.5000000	1.50	2e-14

For non-standard weight or GFR, there is an additional calibration step. On subject 2, with weight = 140 and GFR = 60, we have values in Table 21.

Table 21: Parameters calibration values for subject 2, disopyramide.

Parameter	Calibrated	Expected	Calib Error
V (subject 2)	105.0	105.0	0.0
Ke (subject 2)	0.078850	0.078850	0.0

For the oral route and controlled release form, base parameters encoded in the model are:

- Bioavailability F = 0.95
- Distribution volume V = 52.5
- Lag Tlag = 0.0
- Time of maximum concentration Tmax = 4.5

Calibration matches expectations perfectly on these patients.

2.2.7.2 Maximum Concentration Verification

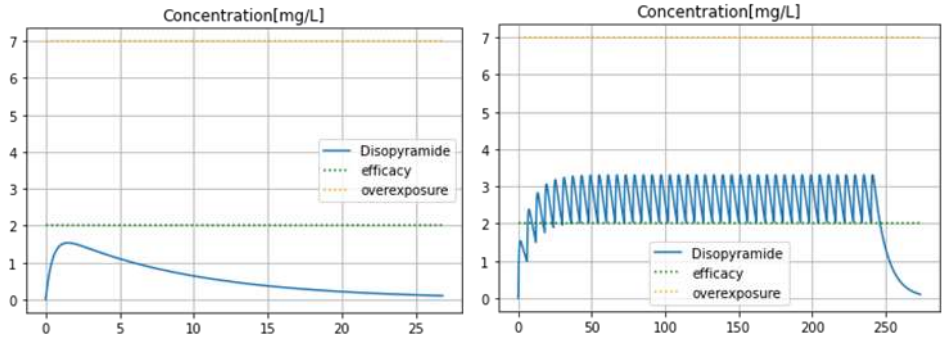

Figure 16: *Numerical simulation with a patient with weight=70 and GFR=90, Disopyramide is administered orally in immediate release form every 6 hours with a dose of 100mg, for a period of 10 days (where steady state is practically obtained).*

Results on maximal concentration are reported in Table 22.

Table 22: Results of numerical vs theoretical max concentrations comparison test for disopyramide.

Value \ Scenario	Single dose	Repeated admin
Numerical max concentration	1.533733	3.307138
Theoretical max concentration	1.534230	3.307674
Numerical Error	5e-04	5e-04

We see a match at the order of 1e-04 on the maximum concentration in both scenarios.

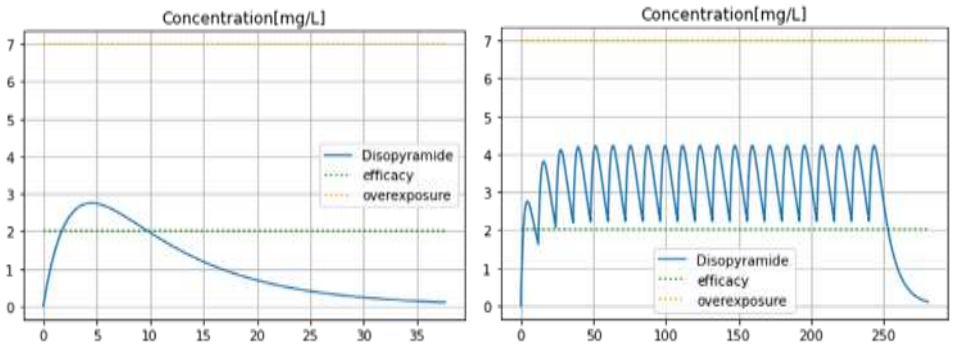

Figure 17: *Numerical simulation with a patient with weight=70 and GFR=90, Disopyramide is administered orally in controlled release form every 12 hours with a dose of 250mg, for a period of 10 days (where steady-state is practically obtained).*

Results on maximal concentration are reported in Table 23.

Table 23: *Results of numerical vs theoretical max concentrations comparison test for Disopyramide.*

Value \ Scenario	Single dose	Repeated admin
Numerical max concentration	2.754124	4.230352
Theoretical max concentration	2.757292	4.230405
Numerical Error	3e-03	5e-05

We see a match at the order of 1e-03 on the maximum concentration in the single dose scenario and 1e-05 in the repeated administration scenario.

2.2.8 Domperidone

2.2.8.1 Parameters Estimation Verification

Covariates: weight, glomerular filtration rate (GFR)
For the oral route and syrup form, base parameters encoded in the model are:

- Bioavailability F = 0.88
- Distribution volume V = 378.59
- Lag Tlag = 0.0
- Elimination half-time T12 = 8.0
- Time of maximum concentration Tmax = 0.9

Calibration step will infer Ke and Ka from numerical inversion of T12 and Tmax data. If we compute T12 and Tmax with calibrated parameters and compare with original values, we can measure the calibration error.

On subject 1, a standard patient (weight=70, GFR=100), we have values in Table 24.

Table 24: Parameters calibration values for subject 1, domperidone.

Parameter	Calibrated	Expected	Calib Error
Ke	0.086643	/	/
Ka	4.467518	/	/
T12	8.0	8.0	0.0
Tmax	0.899999	0.90	1e-15

For non-standard weight or GFR, there is an additional calibration step. On subject 2, with weight = 140 and GFR = 30, we have values in Table 25.

Table 25: Parameters calibration values for subject 2, domperidone.

Parameter	Calibrated	Expected	Calib Error
V (subject 2)	105.0	105.0	0.0
Ke (subject 2)	0.078850	0.078850	0.0

For the oral route and immediate release form, base parameters encoded in the model are:

- Bioavailability F = 0.831
- Distribution volume V = 378.59
- Lag Tlag = 0.0
- Time of maximum concentration Tmax = 1.20

On subject 1, a standard patient (weight=70, GFR=100), we have values in Table 26.

Table 26: Parameters calibration values for subject 1, domperidone.

Parameter	Calibrated	Expected	Calib Error
Ke	0.086643	/	/
Ka	3.055809	/	/
Tmax	1.199999	1.20	1e-14

For non-standard weight or GFR, there is an additional calibration step which is identical to the immediate release case before.

Calibration matches expectations perfectly on these patients.

2.2.8.2 Maximum Concentration Verification

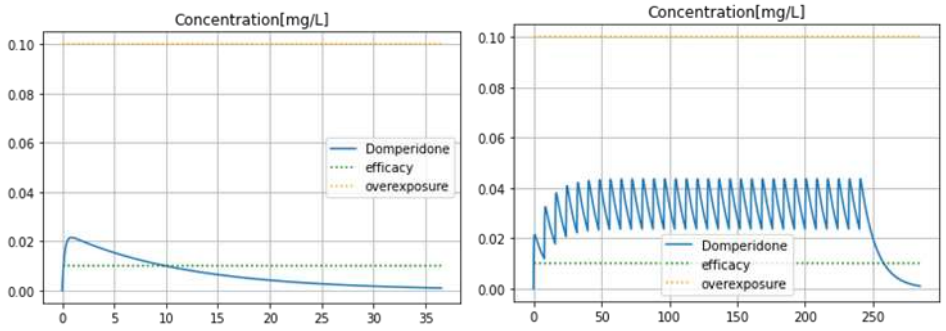

Figure 18: *Numerical simulation with a patient with weight=70 and GFR=100, Domperidone is administered orally in syrup form every 8 hours with a dose of 10mg, for a period of 10 days (where steady state is practically obtained).*

Results on maximal concentration are shown in Table 27.

Table 27: Results of numerical vs theoretical max concentrations comparison test for Domperidone.

Value \ Scenario	Single dose	Repeated admin
Numerical max concentration	0.021497	0.043585
Theoretical max concentration	0.021500	0.043594
Numerical Error	3e-06	9e-06

We see a match at the order of 1e-06 on the maximum concentration in both scenarios.

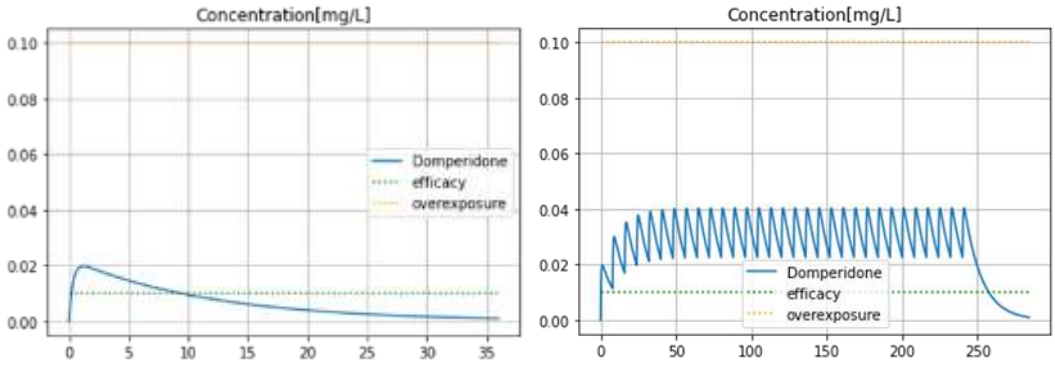

Figure 19: *Numerical simulation with a patient with weight=70 and GFR=100, Disopyramide is administered orally in controlled release form every 8 hours with a dose of 10mg, for a period of 10 days (where steady state is practically obtained).*

Results on maximal concentration are shown in Table 28.

Table 28: Results of numerical vs theoretical max concentrations comparison test for Domperidone.

Value \ Scenario	Single dose	Repeated admin
Numerical max concentration	0.019778	0.040366
Theoretical max concentration	0.019782	0.040373
Numerical Error	4e-06	6e-06

We see a match at the order of 1e-06 on the maximum concentration in both scenarios.

2.2.9 Droperidol

2.2.9.1 Parameters Estimation Verification

Covariates: None
Parameters encoded in the model are:

- Bioavailability F = 1.0
- Lag Tlag = 0
- Absorption rate Ka = 10.0
- Clearance CL=41.9
- Distribution volume V1 = 73.6
- Distribution volume V2 = 79.8
- Intercompartmental clearance Q = 71.5
- Elimination rate Ke is Cl/V
- Intercompartmental transfer rates are K12=Q/V1 and K21=Q/V2

Subject 1: Standard (weight = 70)

Results are shown in Table 29.

Table 29: Parameters calibration values for subject 1, droperidol.

Parameter	Calibrated	Expected	Calib Error
F	1.0	1.0	0.0
Tlag	0.0	0.0	0.0
Ka	10.0	10.0	0.0
Q	71.5	71.5	0.0
Cl	41.9	41.9	0.0
V1	73.60	73.60	0.0
V2	79.8	79.80	0.0
Ke	0.569293	0.569293	0.0
K12	0.971467	0.971467	0.0
K21	0.8959899	0.895989	0.0

Calibration matches expectations perfectly.

2.2.9.2 Maximum Concentration Verification

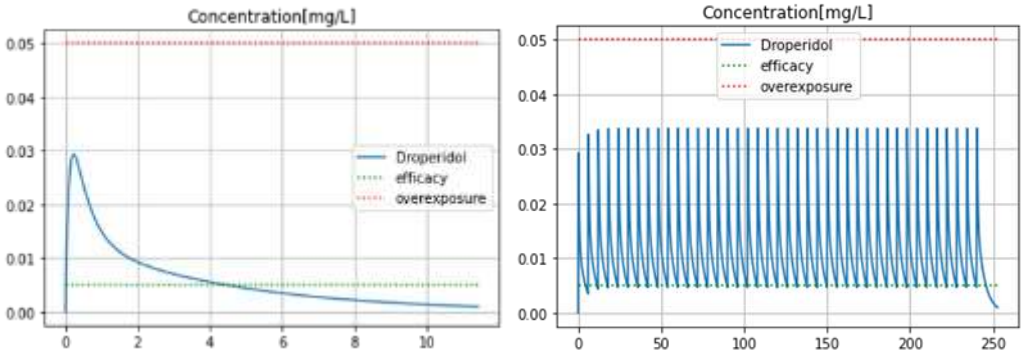

Figure 20: *Numerical simulation with a patient with weight=70, Droperidol is administered in intra-muscular route every 6 hours with a dose of 3mg, for a period of 10 days (where steady state is practically obtained).*

Results on maximal concentration are shown in Table 30.

Table 30: Results of numerical vs theoretical max concentrations comparison test for Droperidol.

Value \ Scenario	Single dose	Repeated admin
Numerical max concentration	0.029310	0.033755
Theoretical max concentration	0.029321	0.033755
Numerical Error	1e-05	4e-08

We see a match at the order of 1e-05 on the maximum concentration in the single dose scenario and 1e-08 in the repeated administration scenario.

2.2.10 Flecainide

2.2.10.1 Parameters Estimation Verification

Covariates: weight
For the oral route and syrup form, base parameters encoded in the model are:

- Bioavailability F = 0.90
- Distribution volume V = 581.0
- Lag Tlag = 0.0
- Elimination half-time T12 = 14.0
- Time of maximum concentration Tmax = 2.40

Calibration step will infer Ke and Ka from numerical inversion of T12 and Tmax data. If we compute T12 and Tmax with calibrated parameters and compare with original values, we can measure the calibration error.

On subject 1, a standard patient (weight=70, GFR=100), we have values in Table 31.

Table 31: Parameters calibration values for subject 1, flecainide.

Parameter	Calibrated	Expected	Calib Error
Ke	0.049510	/	/
Ka	1.459318	/	/
T12	14.0	14.0	0.0
Tmax	2.400000	2.40	5e-14

For non-standard weight, there is an additional calibration step. On subject 2, with weight = 140, we have values in Table 32.

Table 32: Parameters calibration values for subject 2, flecainide.

Parameter	Calibrated	Expected	Calib Error
V (subject 2)	1162.0	1162.0	0.0

For the oral route and immediate release form, base parameters encoded in the model are:

- Bioavailability F = 090
- Distribution volume V = 581.0
- Lag Tlag = 2.5
- Time of maximum concentration Tmax = 23.0

On subject 1, a standard patient (weight=70), we have values in Table 33.

Table 33: Parameters calibration values for subject 1, flecainide.

Parameter	Calibrated	Expected	Calib Error
Ke	0.049510	/	/
Ka	0.048057	/	/
Tmax	22.999999	23	1e-11

For non-standard weight, there is an additional calibration step which is identical to the immediate release case before.

Calibration matches expectations perfectly on these patients.

2.2.10.2 Maximum Concentration Verification

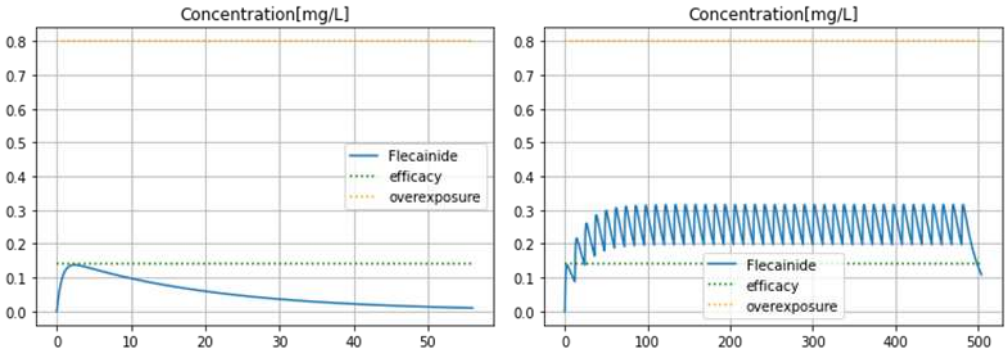

Figure 21: *Numerical simulation with a patient with weight=70, Flecainide is administered orally in immediate release form every 12 hours with a dose of 100mg, for a period of 20 days (where steady state is practically obtained).*

Results on maximal concentration are shown in Table 34.

Table 34: Results of numerical vs theoretical max concentrations comparison test for Flecainide.

Value \ Scenario	Single dose	Repeated admin
Numerical max concentration	0.137531	0.315845
Theoretical max concentration	0.137550	0.315845
Numerical Error	2e-05	3e-07

We see a match at the order of 1e-04 on the maximum concentration in both scenarios.

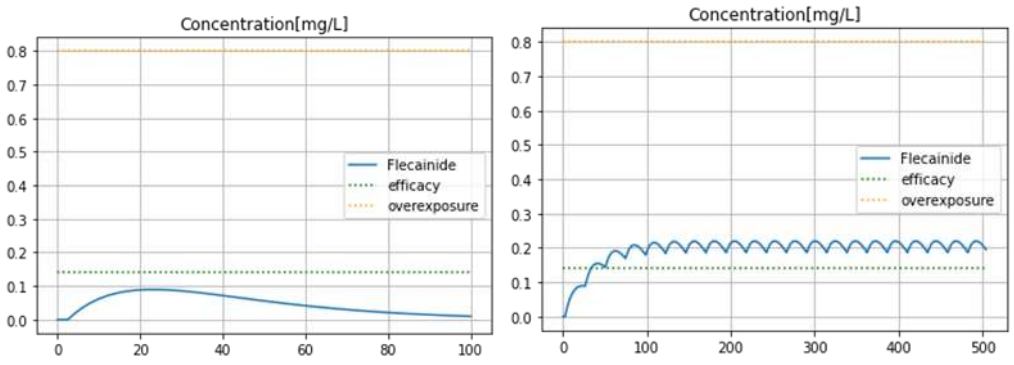

Figure 22: *Numerical simulation with a patient with weight=70, Flecainide is administered orally in controlled release form every 24 hours with a dose of 200mg, for a period of 20 days (where steady state is practically obtained).*

Results on maximal concentration are shown in Table 35.

Table 35: Results of numerical vs theoretical max concentrations comparison test for Flecainide.

Value \ Scenario	Single dose	Repeated admin
Numerical max concentration	0.089676	0.219461
Theoretical max concentration	0.089824	0.220423
Numerical Error	1e-04	1e-03

We see a match at the order of 1e-04 on the maximum concentration in the single dose scenario and 1e-03 in the repeated administration scenario.

2.2.11 Metronidazole

2.2.11.1 Parameters Estimation Verification

Covariates: weight
For the oral route and syrup form, base parameters encoded in the model are:

- Bioavailability F = 1.0
- Distribution volume V = 45.50
- Lag Tlag = 0.0
- Elimination half-time T12 = 9.0
- Time of maximum concentration Tmax = 1.0

Calibration step will infer Ke and Ka from numerical inversion of T12 and Tmax data. If we compute T12 and Tmax with calibrated parameters and compare with original values, we can measure the calibration error.

On subject 1, a standard patient (weight=70, GFR=100), we have values in Table 36.

Table 36: Parameters calibration values for subject 1, metronidazole.

Parameter	Calibrated	Expected	Calib Error
Ke	0.077016	/	/
Ka	4.036010	/	/
T12	9.0	9.0	0.0
Tmax	0.999999	1.0	1e-14

For non-standard weight, there is an additional calibration step. On subject 2, with weight = 140, we have values in Table 37.

Table 37: Parameters calibration values for subject 2, metronidazole.

Parameter	Calibrated	Expected	Calib Error
V (subject 2)	91.0	91.0	0.0

For the oral route and immediate release form, base parameters encoded in the model are:

- Bioavailability F = 0.70
- Distribution volume V = 45.50
- Lag Tlag = 0.0
- Time of maximum concentration Tmax = 4.0

On subject 1, a standard patient (weight=70), we have values in Table 38.

Table 38: Parameters calibration values for subject 1, metronidazole.

Parameter	Calibrated	Expected	Calib Error
Ke	0.0770163	/	/
Ka	0.583102	/	/
Tmax	4.000000	4.0	1e-13

For non-standard weight, there is an additional calibration step which is identical to the immediate release case before.

Calibration matches expectations perfectly on these patients.

2.2.11.2 Maximum Concentration Verification

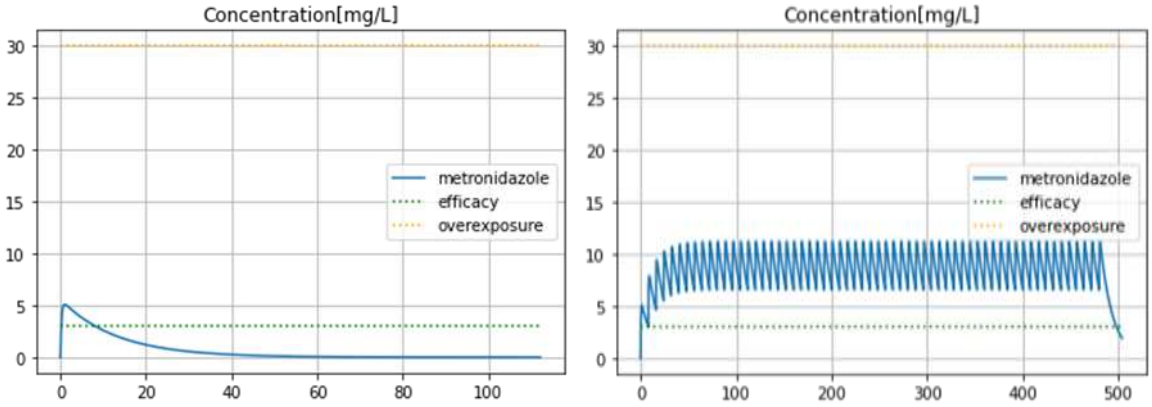

Figure 23: *Numerical simulation with a patient with weight=70, Metronidazole is administered orally in tablet form every 8 hours with a dose of 250mg, for a period of 20 days (where steady state is practically obtained).*

Results on maximal concentration are shown in Table 39.

Table 39: Results of numerical vs theoretical max concentrations comparison test for metronidazole.

Value \ Scenario	Single dose	Repeated admin
Numerical max concentration	5.086579	11.228237
Theoretical max concentration	5.087223	11.228255
Numerical Error	6e-04	2e-05

We see a match at the order of 1e-03 on the maximum concentration in the single dose scenario and 1e-05 in the repeated administration scenario.

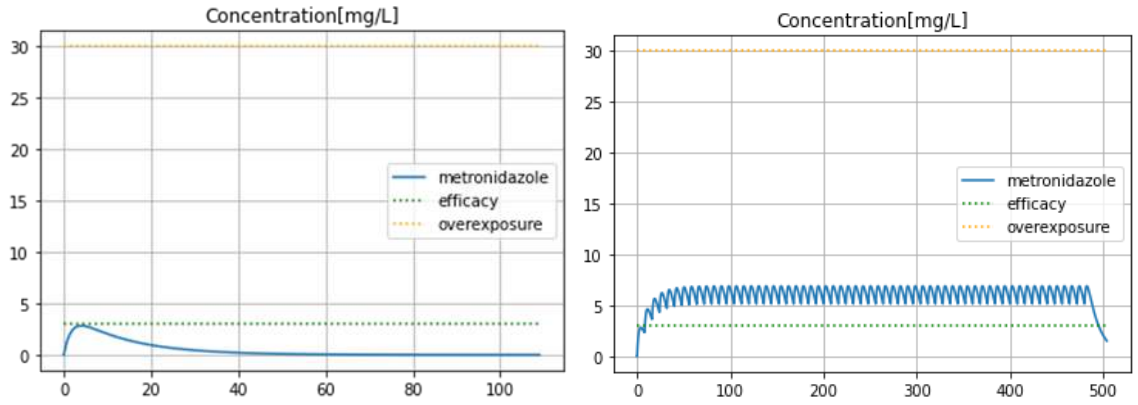

Figure 24: *Numerical simulation with a patient with weight=70, Metronidazole is administered orally in solution form every 8 hours with a dose of 250mg, for a period of 20 days (where steady state is practically obtained).*

Results on maximal concentration are shown in Table 40.

Table 40: Results of numerical vs theoretical max concentrations comparison test for metronidazole.

Value \ Scenario	Single dose	Repeated admin
Numerical max concentration	2.824809	6.904372
Theoretical max concentration	2.826412	6.905676
Numerical Error	2e-03	1e-03

We see a match at the order of 1e-03 on the maximum concentration in both scenarios.

2.2.12 Mexiletine

2.2.12.1 Parameters Estimation Verification

Covariates: weight
Parameters encoded in the model are:

- Bioavailability F = 1.0
- Lag Tlag = 0
- Absorption rate Ka = 3.1
- Clearance CL= 0.38*weight
- Distribution volume V = 5.3*weight
- Elimination rate Ke is Cl/V

Subjects:

- Subject 1: Standard, weight = 70
- Subject 2: Weight = 100

Results in Table 41 and Table 42.

Table 41: Parameters calibration values for subject 1, mexiletine.

Parameter	Calibrated	Expected	Calib Error
F	1.0	1.0	0.0
Tlag	0.0	0.0	0.0
Ka	3.1	3.1	0.0
Cl (subject 1)	26.6	26.6	0.0
V (subject 1)	371.0	371.0	0.
Ke (subject 1)	0.071698	0.071698	0.0

Table 42: Parameters calibration values for subject 2, mexiletine.

Parameter	Calibrated	Expected	Calib Error
Cl (subject 2)	38.0	38.0	0.0
V (subject 2)	530.0	530.0	0.0
Ke (subject 2)	0.071698	0.071698	0.0

Calibration matches expectations perfectly on these patients.

2.2.12.2Maximum Concentration Verification

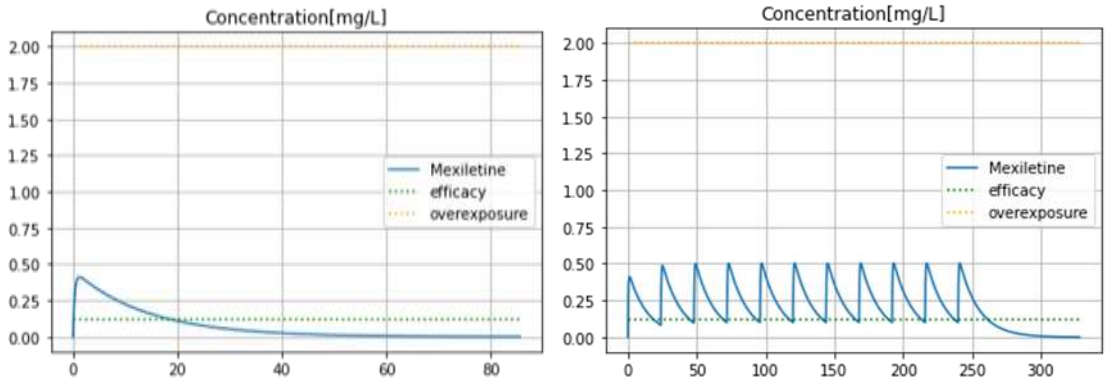

Figure 25: *Numerical simulation with a patient with weight=70, Mexiletine is administered orally in immediate release form every 24 hours with a dose of 167mg, for a period of 10 days (where steady state is practically obtained).*

Results on maximal concentration are shown in Table 43.

Table 43: Results of numerical vs theoretical max concentrations comparison test for mexiletine.

Value \ Scenario	Single dose	Repeated admin
Numerical max concentration	0.411726	0.503706
Theoretical max concentration	0.411729	0.503801
Numerical Error	3e-06	1e-04

We see a match at the order of 1e-06 on the maximum concentration in the single dose scenario and 1e-04 in the repeated administration scenario.

2.2.13 Nicorandil

2.2.13.1 Parameters Estimation Verification

Covariates: weight
Parameters encoded in the model are:

- Bioavailability F = 0.75
- Lag Tlag = 0
- Absorption rate Ka = 1.41
- Clearance CL= 26.3 *1.94 *power(weight/70,0.75)
- Distribution volume V1 = 18.1 *1.39 *(weight/70)
- Distribution volume V2 = 24.1 *4.06 *(weight/70)
- Intercompartmental clearance Q = 71.6 *0.519 *power(weight/70,0.75)
- Elimination rate Ke is Cl/V
- Intercompartmental transfer rates are K12=Q/V1 and K21=Q/V2

Subjects:

- Subject 1: Standard, weight = 70
- Subject 2: Weight = 100

Results are shown in Table 44 and Table 45.

Table 44: Parameters calibration values for subject 1, Nicorandil.

Parameter	Calibrated	Expected	Calib Error
F	0.75	0.75	0.0
Tlag	0.0	0.0	0.0
Ka	1.41	1.41	0.0
Cl (subject 1)	51.021999	51.022	3e-14
V1 (subject 1)	25.159000	25.159	2e-14
Ke (subject 1)	2.027982	2.027982	3e-15
Q (subject 1)	37.160399	37.1604	4e-15
V2 (subject 1)	97.845999	97.846	1e-14
K12 (subject 1)	1.477022	1.477022	2e-15
K21 (subject 1)	0.379784	0.379784	1e-16

Table 45: Parameters calibration values for subject 2, mexiletine.

Parameter	Calibrated	Expected	Calib Error
Cl (subject 2)	66.670536	66.670536	4e-14
V1 (subject 2)	35.941428	35.941428	3e-14
Ke (subject 2)	1.854977	1.85497	3e-15
Q (subject 2)	48.557559	48.557559	3e-14
V2 (subject 2)	139.78	139.78	1e-14
K12 (subject 2)	1.351019	1.351019	2e-15
K21 (subject 2^2)	0.347385	0.347385	2e-16

Calibration matches expectations perfectly on these patients.

2.2.13.2 Maximum Concentration Verification

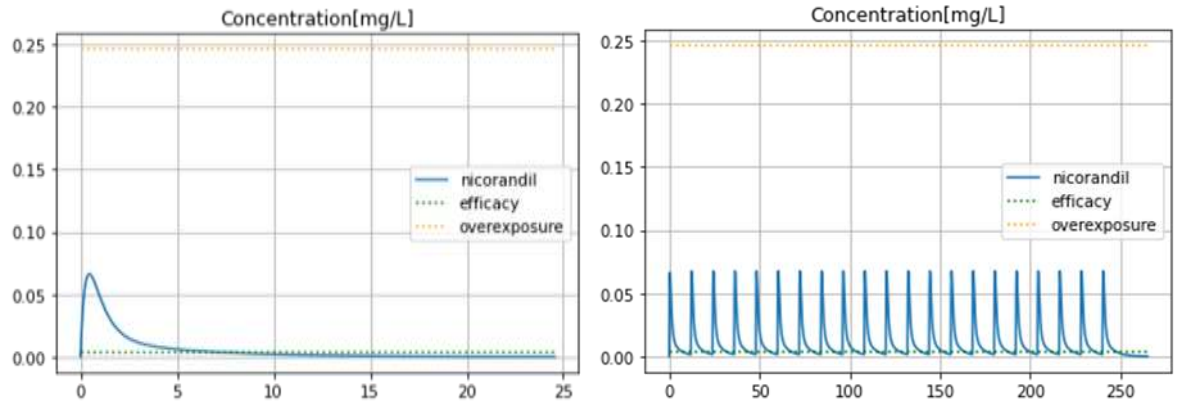

Figure 26: *Numerical simulation with a patient with weight=70, Nicorandil is administered orally in immediate release form every 12hours with a dose of 10mg, for a period of 10 days (where steady state is practically obtained).*

Results on maximal concentration are shown in Table 46.

Table 46: Results of numerical vs theoretical max concentrations comparison test for nicorandil.

Value \ Scenario	Single dose	Repeated admin
Numerical max concentration	0.066330	0.067574
Theoretical max concentration	0.066331	0.067707
Numerical Error	6e-07	1e-04

We see a match at the order of 1e-06 on the maximum concentration in the single dose scenario and 1e-04 in the repeated administration scenario.

2.2.14 Ondansetron

Parameters Estimation Verification

Covariates: weight, age, sex
Base parameters encoded in the model are:

- Bioavailability F = 0.55
- Distribution volume V = 140
- Lag Tlag = 0.0
- Elimination half-time T12 = 3.0
- Time of maximum concentration Tmax = 1.9

Calibration step will infer Ke and Ka from numerical inversion of T12 and Tmax data. If we compute T12 and Tmax with calibrated parameters and compare with original values, we can measure the calibration error.

On subject 1, a standard patient (weight=70, sex=male, age=40), we have values in Table 47.

Table 47: Parameters calibration values for subject 1, ondansetron.

Parameter	Calibrated	Expected	Calib Error
Ke		/	/
Ka		/	/
T12	3.0	3.0	0.0
Tmax	1.900000	1.90	1e-13

For non-standard weight, age or for females, there is an additional calibration step. On subject 2, a female with weight = 140 and age= 62, we have values in Table 48.

Table 48: Parameters calibration values for subject 2, ondansetron.

Parameter	Calibrated	Expected	Calib Error
V (subject 2)	420.0	420.0	0.0
F (subject 2)	0.6050000	0.605	1e-16
Ke (subject 2)	0.169889	0.169889	0.0

Calibration matches expectations perfectly on these patients.

Maximum Concentration Verification

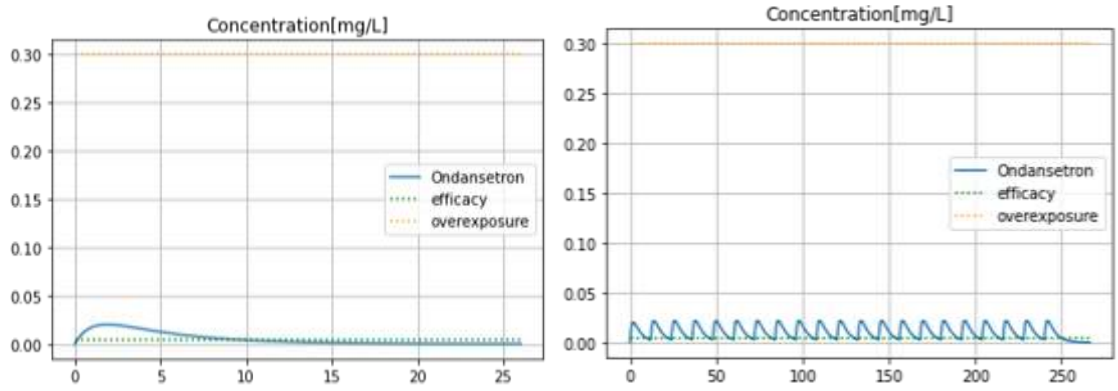

Figure 27: *Numerical simulation with a patient with weight=70 and GFR=100, Ondansetron is administered orally in immediate release form every 12 hours with a dose of 8.0mg, for a period of 10 days (where steady state is practically obtained).*

Results on maximal concentration are shown in Table 49.

Table 49: Results of numerical vs theoretical max concentrations comparison test for ondansetron.

Value \ Scenario	Single dose	Repeated admin
Numerical max concentration	0.020251	0.022020

Value \ Scenario	Single dose	Repeated admin
Theoretical max concentration	0.020261	0.022032
Numerical Error	1e-05	1e-05

We see a match at the order of 1e-05 on the maximum concentration in both scenarios.

2.2.15 Sotalol

2.2.15.1 Parameters Estimation Verification

Covariates: weight, glomerular filtration rate (GFR)
Base parameters encoded in the model are:

- Bioavailability F = 0.80
- Distribution volume V = 84.7
- Lag Tlag = 0.0
- Elimination half-time T12 = 7.18
- Time of maximum concentration Tmax = 3.1

Calibration step will infer Ke and Ka from numerical inversion of T12 and Tmax data. If we compute T12 and Tmax with calibrated parameters and compare with original values, we can measure the calibration error.

On subject 1, a standard patient (weight=70, GFR=90), we have values in Table 50.

Table 50: Parameters calibration values for subject 1, sotalol.

Parameter	Calibrated	Expected	Calib Error
Ke	0.096538	/	/
Ka	0.763717	/	/
T12	7.179999	7.18	2e-15
Tmax	3.099999	3.10	3e-13

For non-standard weight or GFR, there is an additional calibration step. On subject 2, with weight = 140 and GFR = 30, we have values in Table 51.

Table 51: Parameters calibration values for subject 2, sotalol.

Parameter	Calibrated	Expected	Calib Error
V (subject 2)	169.4	169.4	0.0
Ke (subject 2)	0.051487	0.051487	0.0

Calibration matches expectations perfectly on these patients.

2.2.15.2 Maximum Concentration Verification

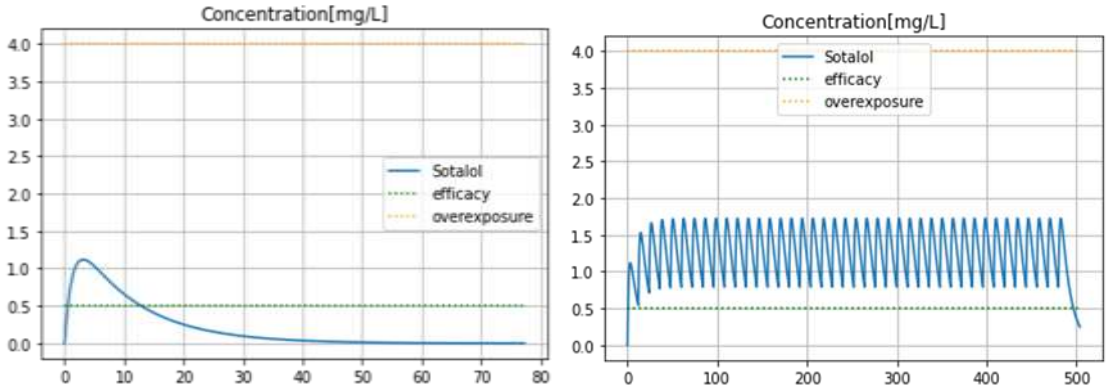

Figure 28: *Numerical simulation with a patient with weight=70 and GFR=90, Sotalol is administered orally every 12 hours with a dose of 160mg, for a period of 20 days (where steady state is practically obtained).*

Results on maximal concentration are shown in Table 52.

Table 52: Results of numerical vs theoretical max concentrations comparison test for sotalol.

Value \ Scenario	Single dose	Repeated admin
Numerical max concentration	1.120008	1.724555
Theoretical max concentration	1.120354	1.724586
Numerical Error	3e-04	3e-05

We see a match at the order of 1e-04 on the maximum concentration in the single dose scenario and 1e-05 in the repeated administration scenario.

2.2.16 Vandetanib

2.2.16.1 Parameters Estimation Verification

Covariates: weight, renal status
Base parameters encoded in the model are:

- Bioavailability F = 1.0
- Distribution volume V = 3876
- Lag Tlag = 0.0
- Elimination half-time T12 = 195.4
- Time of maximum concentration Tmax = 6.0

Calibration step will infer Ke and Ka from numerical inversion of T12 and Tmax data. If we compute T12 and Tmax with calibrated parameters and compare with original values, we can measure the calibration error.

On subject 1, a standard patient (weight=80.70, normal renal status), we have values in Table 53.

Table 53: Parameters calibration values for subject 1, vandetanib.

Parameter	Calibrated	Expected	Calib Error
Ke	0.003547	/	/
Ka	0.932085	/	/
T12	195.4	195.40	0.0
Tmax	5.9999999	6.0	4e-13

For non-standard weight and renal status, there is an additional calibration step. On subject 2, with weight = 100 and moderate renal impairment, we have values in Table 54.

Table 54: Parameters calibration values for subject 2, vandetanib.

Parameter	Calibrated	Expected	Calib Error
V (subject 2)	4802.973977	4802.973977	0.0
Ke (subject 2)	0.002217	0.002217	0.0

Calibration matches expectations perfectly on these patients.

2.2.16.2 Maximum Concentration Verification

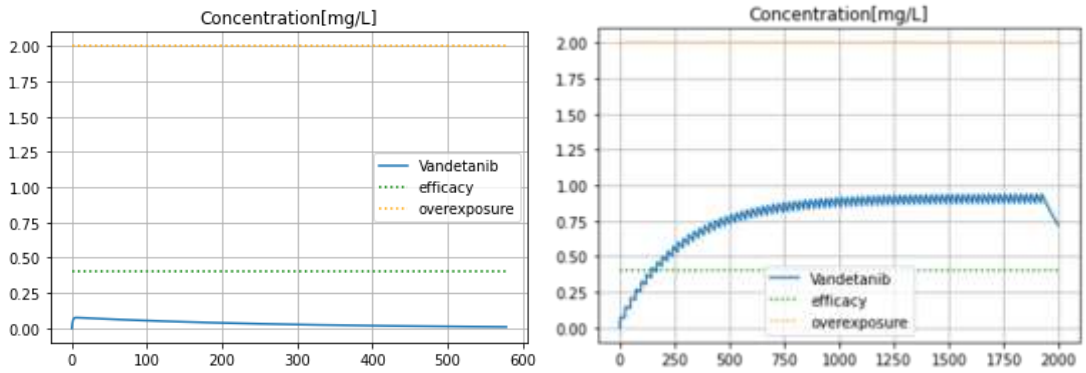

Figure 29: *Numerical simulation with a patient with weight=80.70 and normal renal status, Vandetanib is administered orally every 24 hours with a dose of 300mg, for a period of 80 days (where steady state is practically obtained).*

Results on maximal concentration are shown in Table 55.

Table 55: Results of numerical vs theoretical max concentrations comparison test for vandetanib.

Value \ Scenario	Single dose	Repeated admin
Numerical max concentration	0.075767	0.936377
Theoretical max concentration	0.075769	0.9373355
Numerical Error	2e-06	1e-03

We see a match at the order of 1e-06 on the maximum concentration in the single dose scenario and 1e-03 in the repeated administration scenario.

2.2.17 Summary

Maximum calibration error on model parameters is at most 1e-13, which is materially negligible.

Concerning maximum concentrations, we have the values summarized in Table 56.

Table 56: Summary of maximum concentration numerical error for verified drugs.

Numerical Error on Cmax	Single dose	Repeated admin
Clozapine	1e-06	3e-06
Chlorpromazine	1e-06	4e-06
Escitalopram	9e-07	5e-06
Risperidone	8e-07	6e-06
Carvedilol	5e-06	6e-06
Clarithromycine	2e-04	1e-04
Disopyramide	5e-04 | 3e-03	5e-04 | 5e-05
Domperidone	3e-06 | 4e-06	9e-06 | 6e-06
Droperidol	1e-05	4e-08
Flecainide	2e-05 | 1e-04	3e-07 | 1e-03
Metronidazole	6e-04 | 2e-03	2e-05 | 1e-03
Mexiletine	3e-06	1e-04
Nicorandil	6e-07	1e-04
Ondansetron	1e-05	1e-05
Sotalol	3e-04	3e-05
Vandetanib	2e-06	1e-03

On these molecules, no instability was observed and the numerical error on the quantity of interest is most of the time between 1e-03 and 1e-06. Numerical simulation of these models is accurate and robust with default error tolerances. In all cases, this numerical error is way smaller than the therapeutic range (toxicity or overexposure threshold minus the efficacy threshold). Hence, the simulation is suitable to solve drug concentration time courses and answer the Question of Interest.

2.3 Use Error

Use-Error in the PK part is managed at different levels to make sure meaningful drug concentration figures are obtained:

- Input control at the public interface simulation.
- Input control at the ExaTwin simulation request level.
- Peer-review of the Model file level and consistency checks in ExaTwin of the encoding.
- Finally, the verification itself has been reviewed guaranteeing results and conclusions.

3 Conclusion

This document is an annex of SimCardioTest deliverable D6.1, and reports technical details relative to the verification of the PK numerical model developed for Use Case 3. General conclusions relative to the verification of UC3 numerical model are reported in main deliverable D6.1.

4 Bibliography

[1] “SciPy Org.,” [Online]. Available: https://scipy.org/about/.

This project received funding from the European Union’s Horizon 2020 research and innovation program under grant agreement No 101016496

EU Horizon 2020 Research & Innovation Program
Digital transformation in Health and Care
SC1-DTH-06-2020
Grant Agreement No. 101016496

SimCardioTest - Simulation of Cardiac Devices & Drugs for in-silico Testing and Certification

SIM CARDIO TEST

Technical Report

D6.1-UC3-PK-IST: Use Case 3 PK Verification Annex - IST Integration

Work Package 6 (WP6)

Verification, validation, uncertainty quantification & certification

Annex Lead: UPV, Spain
Task Lead: UBx, France
WP Lead: MPC, France

PUBLIC

Document history			
Date	**Version**	**Author(s)**	**Comments**
15/06/2023	V1	A. BARETTA	Final Draft for Consolidation
29/06/2023	V2	R. SETZU	Format consolidation
29/06/2023	V3	H. AREVALO	Quality Review
30/06/2023	V4	R. SETZU	Final Version
01/07/2024	V5	R. SETZU M. BARBIER	Format editing

TABLE OF CONTENTS

EXECUTIVE SUMMARY

This document is an annex of SimCardioTest deliverable D6.1 and was elaborated for Use Case 3 in the context of drug safety assessment. It reports the tests aimed to ensure that the different features of ExactCure Pharmacokinetics (PK) model are correctly reproduced in the cloud-based platform provided by InSilicoTrials for the European Project H2020 – SimCardioTest.

Acronyms

Table 1: List of Acronyms.

Acronym	Meaning
IST	InSilicoTrials
SCT	SimCardioTest

1. Test Scenarios: PK Models Specifications

1.1 Objectives

The following tests aim to ensure that the different features of ExactCure Pharmacokinetics (PK) model are correctly reproduced in the cloud-based platform provided by InSilicoTrials for the European Project H2020 – SimCardioTest.

The ExactCure API called for PK simulations referred as PAPI, that is requesting EXC simulations engine ExaTwin.

1.2 Description

The person in charge of the tests must:

- Have access to an up-to-date version of the cloud-based platform allowing simulations for EXC PK models.

Those tests must be performed after each major update of the In-silico-trial simulation interface, EXC PAPI API and EXC ExaTwin simulation engine.

They allow to:

- Ensure coherence between information provided by the users of the web interface and the results displayed.
- Test different features of the PK models provided by EXC.

This document must be updated by an EXC referent if new PK models features would become available in the simulation interface.

1.3 Reference Material

This section lists all documents that describe or influence the test process.

There are no specific documents to be listed.

1.4 Traceability

Test traceability is shown in Table 2.

Table 2: Test Traceability.

Date (MM/DD/YYYY)	06/14/2023
Tester(s)	Fianne Sips, PhD (InSilicoTrials Technologies) Matteo Gazzin (InSilicoTrials Technologies)
Initials	FS MG
Computer System	Windows 10, 11th Gen Intel(R) Core(TM) i7-1185G7 @ 3.00GHz, x64 processor
Browser version	Google Chrome, Version 114.0.5735.111 (64 bit)

Interface version	V23.06.14
(EXC) PAPI version	V2.5.1
(EXC) ExaTwin version	V4.3
Other information	-

1.5 Test Scenarios

1.5.1 Scenario 1 - Flecainide

Tested functionalities are:

- Simulation of models with non-compartmental declaration
- Management of multiple galenic forms
- Fluctuation on continuous covariate (weight)
- Management of Tlag in timeseries

1.5.1.1 Standard Patient - Immediate Release

- Select molecule: flecainide
- Form: immediate_release (IR) (ex : Drug_id : 8918)
- Set patient weight to 70 kg.
- Posology: 100 mg (single intake)

As comparison material, EXC simulation is shown in Figure 1. Results are shown in Table 3.

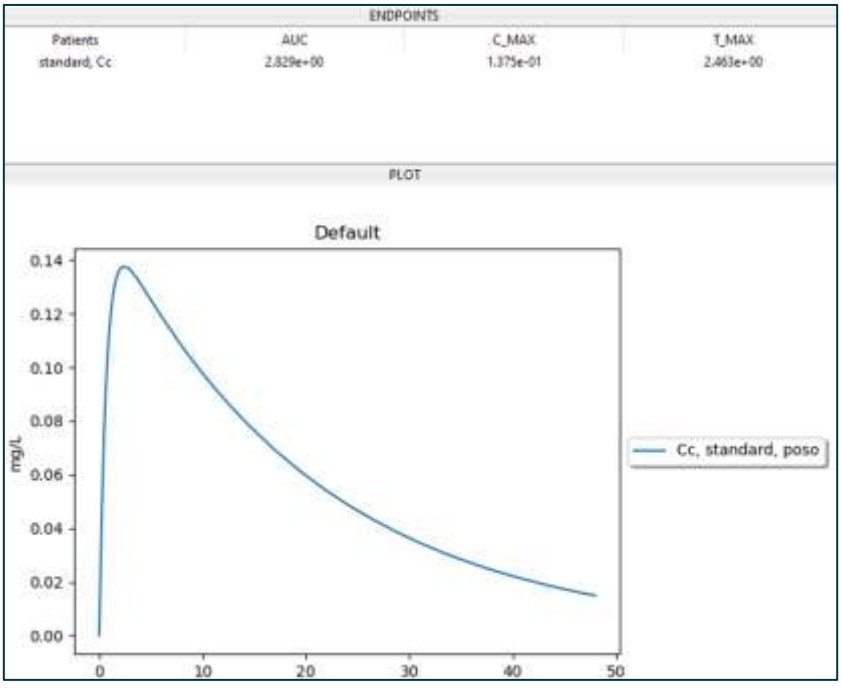

Figure 1: *Scenario 1 - Flecainide - Standard Patient - Immediate Release.*

Table 3: Scenario Results.

Q	The simulated curve displays a similar shape as the blue curve above.
R	**Yes** / ~~No~~
Q	The simulated curve reaches a maximal value of 0.1375mg/L at time 2.463 h.
R	**Yes** / ~~No~~

1.5.1.2 Standard Patient - Controlled Release

- Select molecule: flecainide
- Form: controlled_release (CR) (ex : Drug_id : 11217)
- Set patient weight to 70 kg.
- Posology: 100 mg (single intake)

As comparison material, EXC simulation is shown in Figure 2. Results are shown in Table 4.

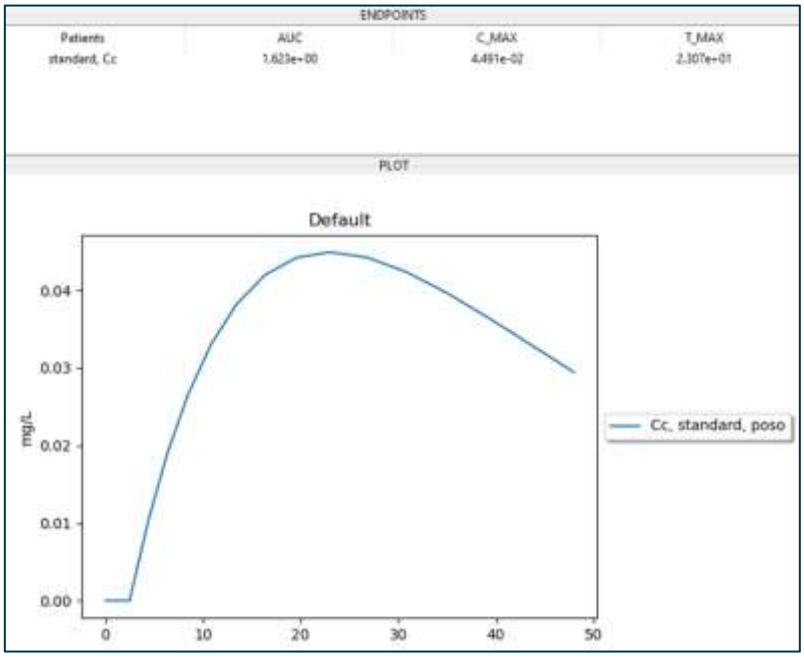

Figure 2: *Scenario 1 - Flecainide -Standard Patient - Controlled Release.*

Table 4: Scenario Results.

Q	The simulated curve displays a similar shape than the blue curve above.
R	**Yes** / ~~No~~
Q	The simulated curve reaches a maximal value of 0.04491 mg/L at time 23.07 h.
R	**Yes** / ~~No~~
Q	After intake, a Tlag (time before intake is effective) of 2.5h can be observed.
R	**Yes** / ~~No~~

1.5.1.3 Obese Patient - Controlled Release

- Select molecule: flecainide
- Form: controlled_release (CR) **(ex : Drug_id : 11217)**
- Set patient weight to 140 kg.
- Posology: 100 mg (single intake)

As comparison material, EXC simulation is shown in Figure 3. Results are shown in Table 5.

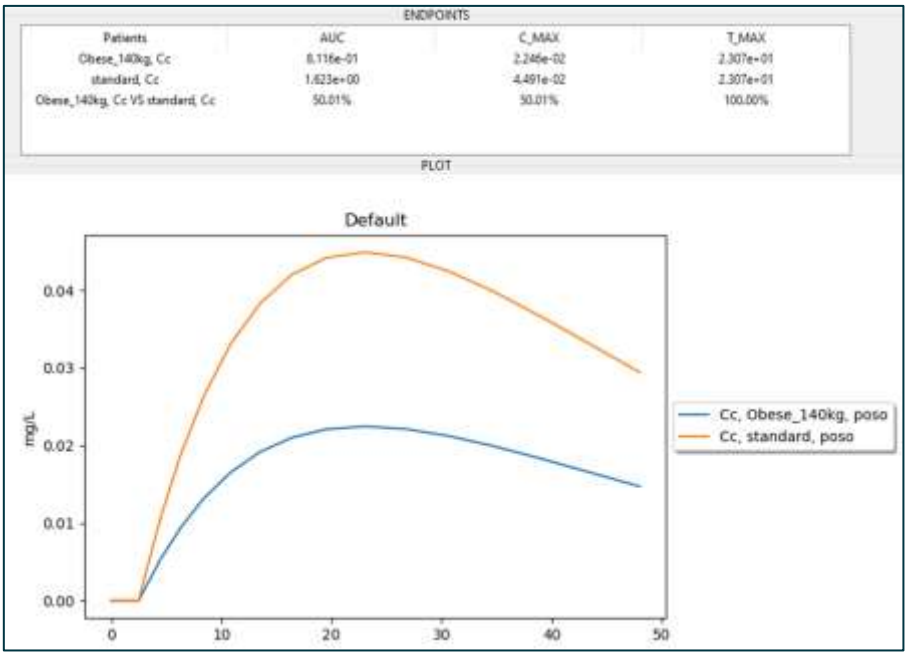

Figure 3: *Scenario 1 - Flecainide -Obese Patient - Controlled Release.*

Table 5: Scenario Results.

Q	The simulated curve displays a similar shape than the blue curve above.
R	**Yes** / ~~No~~
Q	The simulated curve reaches a maximal value of 0.0225 mg/L at time 23.07 h.
R	**Yes** / ~~No~~
Q	After intake, a Tlag (time before intake is effective) of 2.5h can be observed.
R	**Yes** / ~~No~~

1.5.1.4 Conclusion

Test evaluation is reported in Table 6.

Table 6: Test Section Evaluation.

Test Section Evaluation	
Status	**Signature**
Passed / ~~Not passed~~	FS

1.5.2 Scenario 2 - Escitalopram

Tested functionalities are:

- Simulation of models with compartmental declaration
- Fluctuation on continuous covariate (age)
- Fluctuation on indirect continuous covariate (BMI trough height modification) (Test of EXC Digital Twin component).
- Fluctuation of a categorial covariate (mutation_cyp2c19)

1.5.2.1 Standard Patient

- Select molecule: escitalopram
- Form: immediate_release **(ex : Drug_id : 832)**
- Set patient weight to 70 kg.
- Set patient height to 170 cm.
- Set patient age to 40 years.
- Set patient "mutation_cyp2c19": "extensive"
- Posology: 20 mg (single intake)

As comparison material, EXC simulation is shown in Figure 4. Results are shown in Table 7.

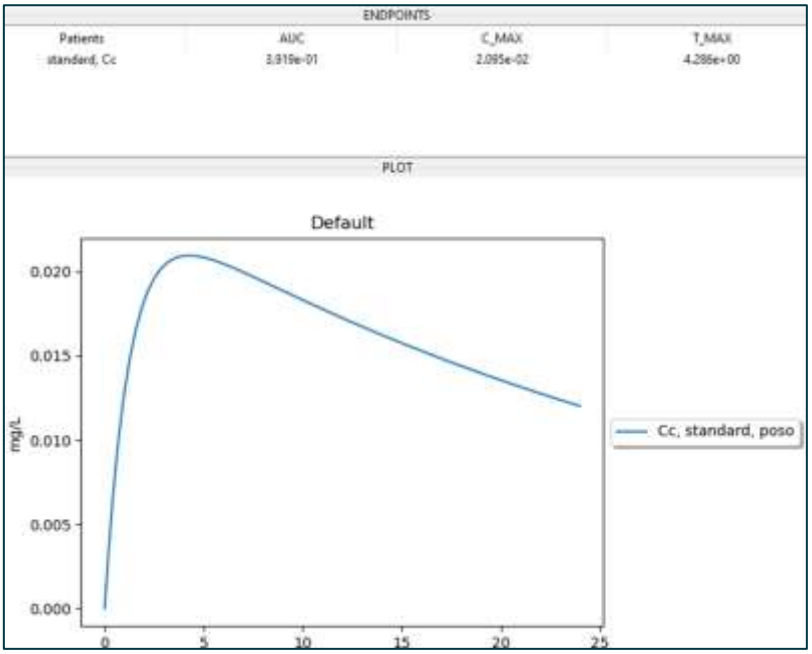

Figure 4: *Scenario 2 - Escitalopram -Standard Patient.*

Table 7: Scenario Results.

Q	The simulated curve displays a similar shape than the blue curve above.
R	**Yes** / ~~No~~
Q	The simulated curve reaches a maximal value of 0.02097mg/L at time 4.286 h.
R	**Yes** / ~~No~~

1.5.2.2 *Elderly Patient*

- Select molecule: escitalopram
- Form: immediate_release (ex : Drug_id : 832)
- Set patient weight to 70 kg.
- Set patient height to 170 cm.
- Set patient age to 70 years.
- Set patient "mutation_cyp2c19": "extensive".
- Posology: 20 mg (single intake)

As comparison material, EXC simulation is shown in Figure 5. Results are shown in Table 8.

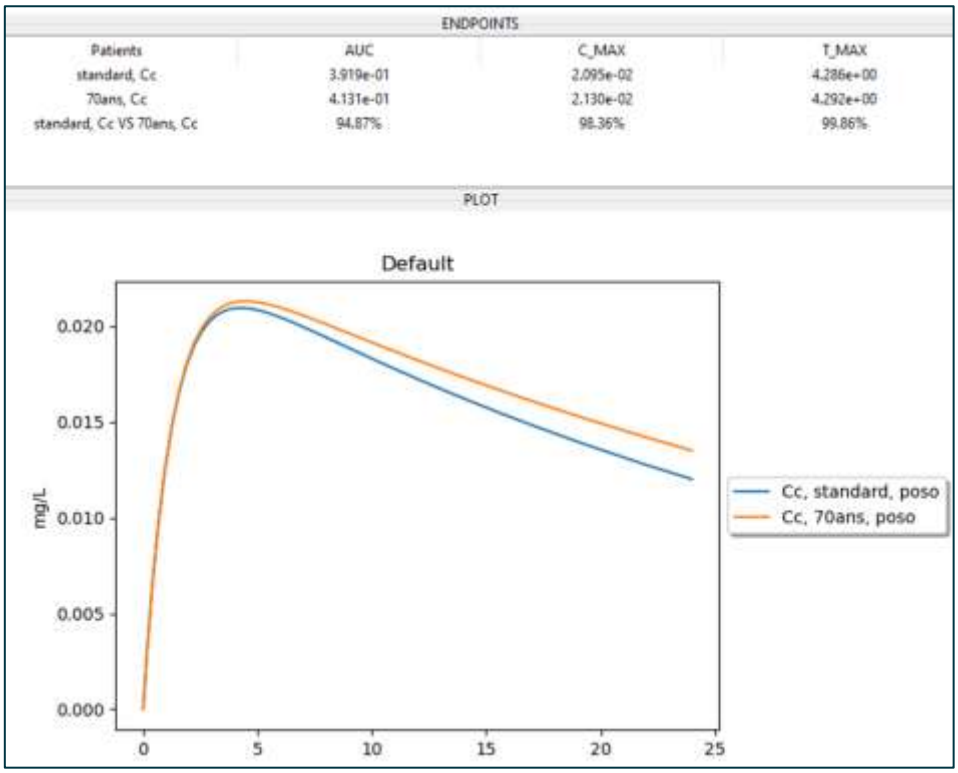

Figure 5: *Scenario 2 - Escitalopram - Elderly Patient.*

Table 8: Scenario Results.

Q	The simulated curve displays a similar shape than the orange curve above.
R	**Yes** / ~~No~~
Q	The simulated curve reaches a maximal value of 0.0213 mg/L at time 4.292 h.
R	**Yes** / ~~No~~

1.5.2.3 *Tall Elderly Patient*

- Select molecule: escitalopram
- Form: immediate_release (ex : Drug_id : 832)
- Set patient weight to 70 kg.
- Set patient height to 200 cm.
- Set patient age to 70 years.
- Set patient "mutation_cyp2c19": "extensive".
- Posology: 20 mg (single intake)

As comparison material, EXC simulation is shown in Figure 6. Results are shown in Table 9.

ENDPOINTS

Patients	AUC	C_MAX	T_MAX
70ans_2m, Cc	5.312e-01	2.954e-02	3.915e+00
standard, Cc	3.919e-01	2.095e-02	4.286e+00
70ans_2m, Cc VS standard, Cc	135.54%	141.00%	91.34%

PLOT

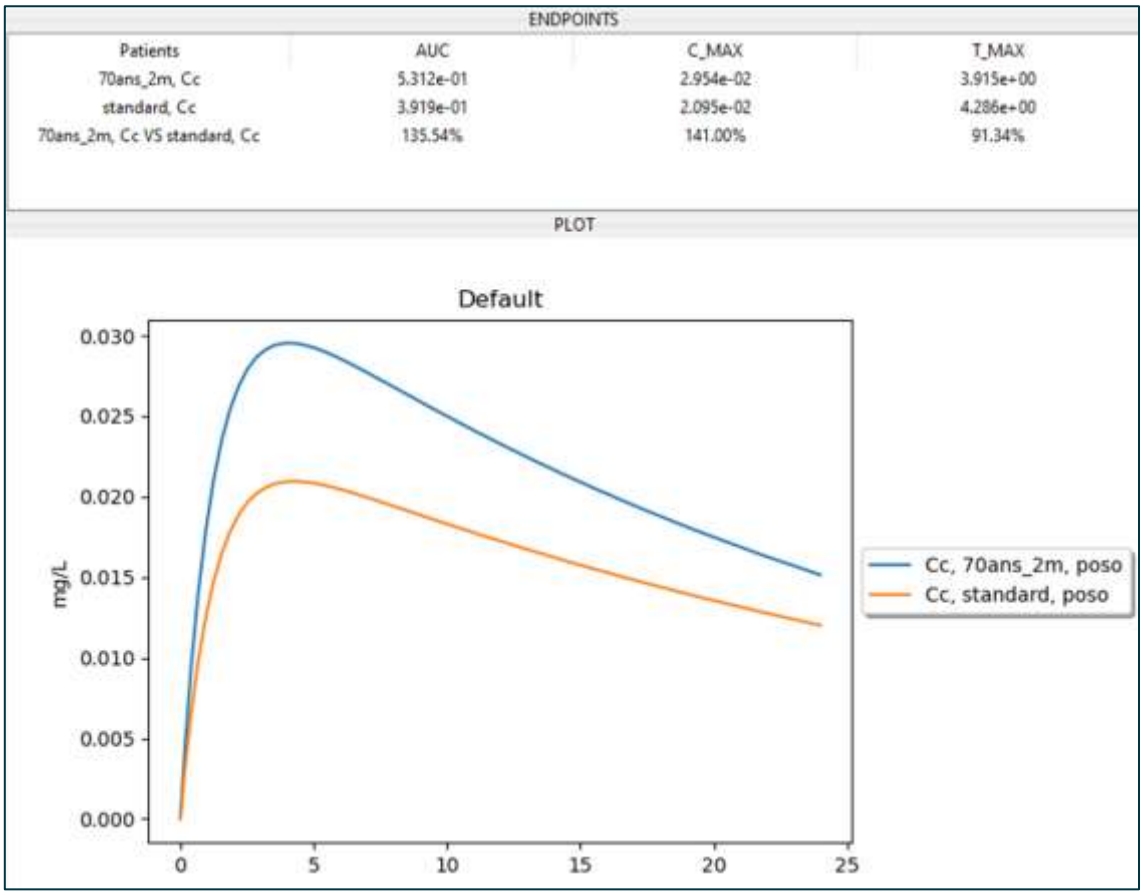

Figure 6: *Scenario 2 - Escitalopram - Tall Elderly Patient.*

Table 9: Scenario Results.

Q	The simulated curve displays a similar shape than the blue curve above.
R	**Yes** / ~~No~~
Q	The simulated curve reaches a maximal value of 0.02955 mg/L at time 3.916 h.
R	**Yes** / ~~No~~

1.5.2.4 Tall Elderly Patient Poor Metabolizer

- Select molecule: escitalopram
- Form: immediate_release **(ex : Drug_id : 832)**
- Set patient weight to 70 kg.
- Set patient height to 200 cm.
- Set patient age to 70 years.
- Set patient "mutation_cyp2c19": "poor".
- Posology: 20 mg (single intake)

As comparison material, EXC simulation is shown in Figure 7. Results are shown in Table 10.

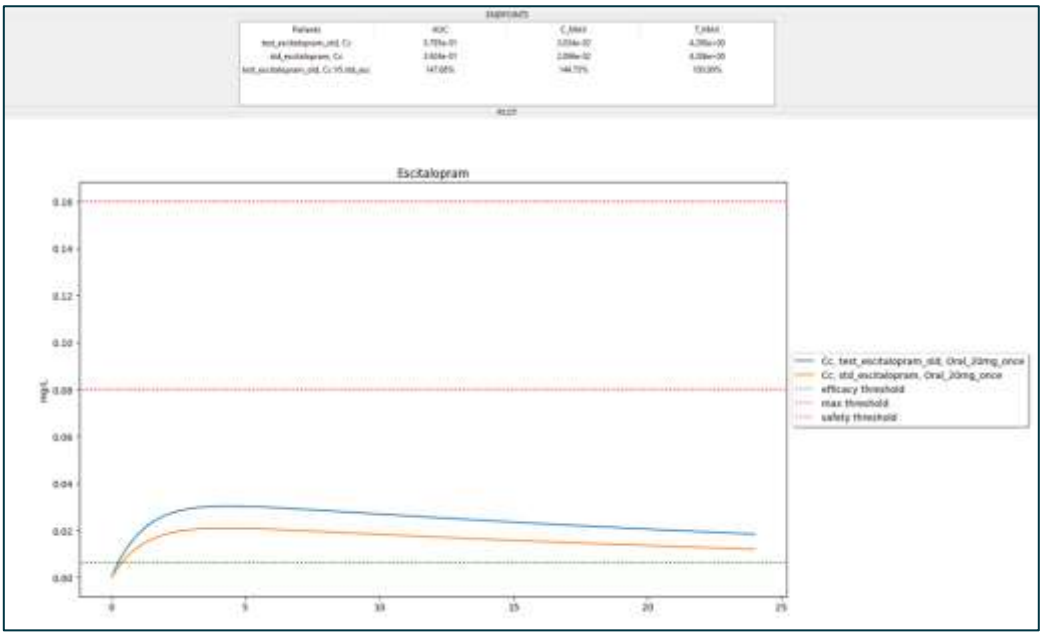

Figure 7: *Scenario 2 - Escitalopram - Tall Elderly Patient Poor Metabolizer.*

Table 10: Scenario Results.

Q	The simulated curve displays a similar shape than the blue curve above.
R	**Yes** / ~~No~~
Q	The simulated curve reaches a maximal value of 0.03034 mg/L at time 4.290h.
R	**Yes** / ~~No~~

1.5.2.5 Conclusion

Test evaluation is reported in Table 11.

Table 11: Test Section Evaluation.

Test Section Evaluation	
Status	**Signature**
Passed / ~~Not passed~~	FS

1.5.3 Scenario 3 - Clozapine

Tested functionalities are:

- Simulation of models with compartmental declaration
- Simulation of multiples intakes
- Fluctuation on indirect Boolean covariate (sex_m trough sex modification) (Test of EXC Digital Twin component)

1.5.3.1 Standard Male Patient

- Select molecule: clozapine
- Form: immediate_release (ex : Drug_id : 9120)
- Set patient sex to M (male)
- Set patient weight to 70 kg
- Set patient height to 200 cm
- Set patient age to 70 years
- Set patient "mutation_cyp2c19": "poor"
- Posology: 450 mg every 12h (multiples intakes)

As comparison material, EXC simulation is shown in Figure 8. Results are shown in Table 12.

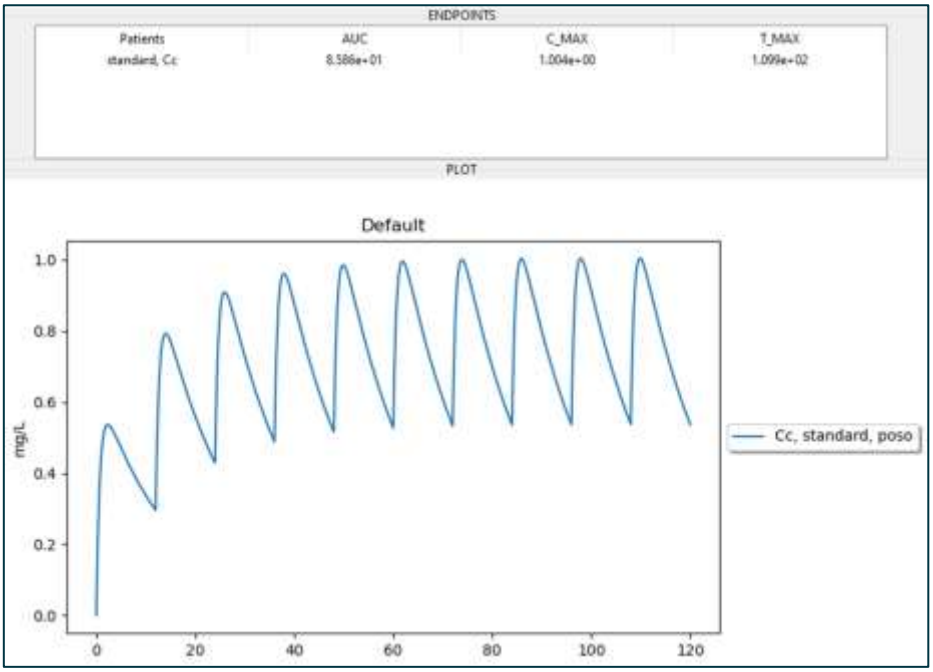

Figure 8: *Scenario 3 - Clozapine - Standard Male Patient.*

Table 12: Scenario Results.

Q	The simulated curve displays a similar shape than the blue curve above.
R	**Yes** / ~~No~~
Q	The simulated curve reaches a maximal value of 1 mg/L at time 109.9 h.
R	**Yes** / ~~No~~

1.5.3.2 *Standard Female Patient*

- Select molecule: clozapine
- Form: immediate_release **(ex : Drug_id : 9120)**
- Set patient sex to F (female)
- Set patient weight to 70 kg
- Set patient height to 200 cm
- Set patient age to 70 years
- Set patient "mutation_cyp2c19": "poor"
- Posology: 450 mg every 12h (multiples intakes)

As comparison material, EXC simulation is shown in Figure 9. Results are shown in Table 13.

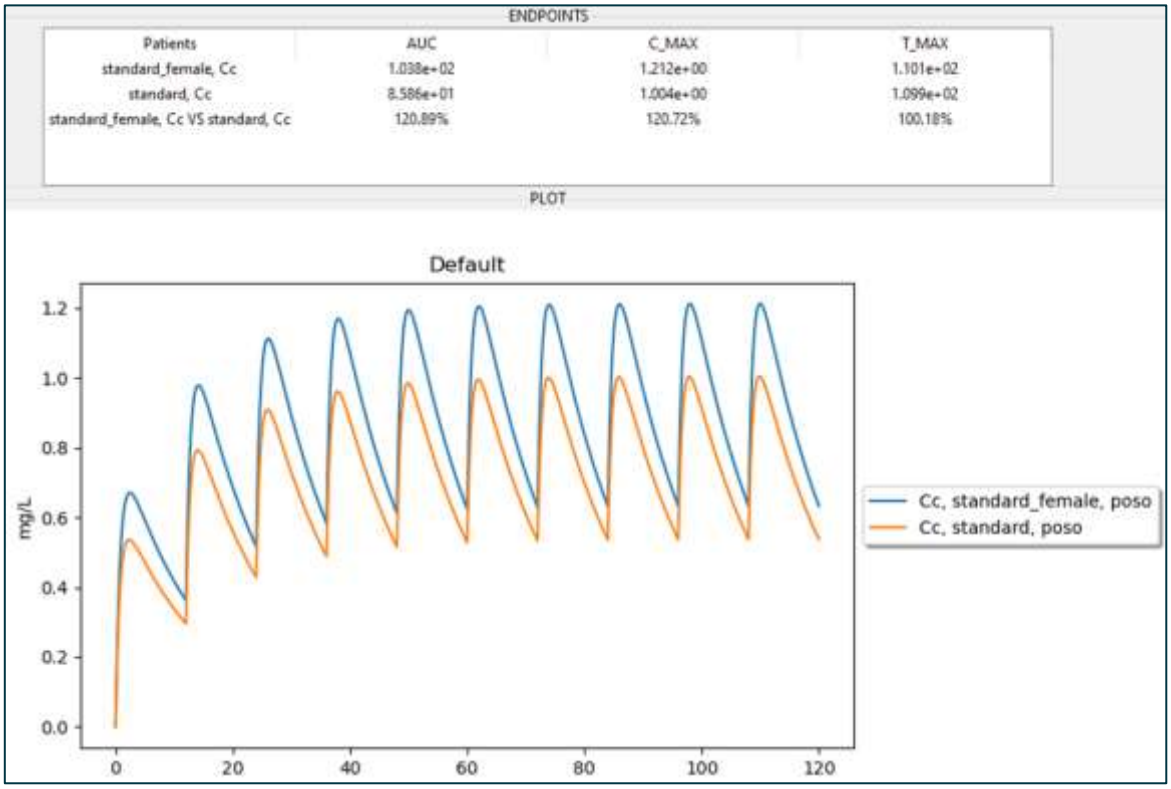

Figure 9: *Scenario 3 - Clozapine - Standard Female Patient.*

Table 13: Scenario Results.

Q	The simulated curve displays a similar shape than the blue curve above.
R	**Yes** / ~~No~~
Q	The simulated curve reaches a maximal value of 1.212 mg/L at time 110.1 h.
R	**Yes** / ~~No~~

1.5.3.3 Conclusion

Test evaluation is reported in Table 14.

Table 14: Test Section Evaluation.

Test Section Evaluation	
Status	**Signature**
Passed / ~~Not passed~~	FS

1.6 Conclusion

1.6.1 Bug Report

No bugs were reported (cf. Table 15).

Table 15: Bug Report.

Ref	Description
MM/DD/YYYY	-

1.6.2 Global Evaluation

Global evaluation is reported in Table 16.

Table 16: All Tests Evaluation.

All Tests Evaluation	
Status	**Signature**
Passed / ~~Not passed~~	FS

1.7 Annex

ExactCure standard patient covariates are by default set to :

- Weight: 70 kg
- Height: 170 cm
- Age: 40 years
- Sex: ”M”
- “mutation_cyp2c19” : “extensive”

Example of Drug_id to request is shown in Table 17.

Table 17: Example of Drug_id to request.

Drug	Drug_ID	CIS
Flecaidine IR	8918	61264178
Flecaidine CR	11217	64645960
Escitalopram IR	832	65988086
Clozapine IR	9120	68735825

2. Conclusion

This document is an annex of SimCardioTest deliverable D6.1, and reports technical details relative to the verification of the 3D numerical model developed for Use Case 3. General conclusions relative to the verification of UC3 numerical model are reported in main deliverable D6.1.

This project received funding from the European Union's Horizon 2020 research and innovation program under grant agreement No 101016496

EU Horizon 2020 Research & Innovation Program
Digital transformation in Health and Care
SC1-DTH-06-2020
Grant Agreement No. 101016496

SimCardioTest - Simulation of Cardiac Devices & Drugs for in-silico Testing and Certification

Technical Report

D6.1-UC3-0D: Use Case 3 0D Verification Annex

Work Package 6 (WP6)
Verification, validation, uncertainty quantification & certification

Annex Lead: UPV, Spain
Task Lead: UBx, France
WP Lead: MPC, France

PUBLIC

Document history			
Date	**Version**	**Author(s)**	**Comments**
26/05/2023	V1	M. T. MORA	First Draft of UPV
15/06/2023	V2	F. SIPS, A. BARETTA	Add IST contribution
19/06/2023	V3	B. TRENOR	Review
21/06/2023	V4	M. T. MORA	Final version prior consolidation
23/06/2023	V5	R. SETZU	Format consolidation
29/06/2023	V6	H. AREVALO	Quality Review
30/06/2023	V7	R. SETZU	Final Version
01/07/2024	V8	R. SETZU M. BARBIER	Format editing

TABLE OF CONTENTS

EXECUTIVE SUMMARY

This document is an annex of SimCardioTest deliverable D6.1 and was elaborated for Use Case 3 in the context of drug safety assessment. It contains the technical details for the verification of the electrophysiological models at the cellular level and the verification activities performed by InSilicoTrials during the integration of the aforementioned model in the cloud platform of SimCardioTest project.

Acronyms

Table 1: List of Acronyms.

Acronym	Meaning
AP	Action potential
IST	InSilicoTrials
ODE	Ordinary differential equation
SCT	SimCardioTest
TdP	Torsade de pointes

1. Code Verification

1.1 Software Quality Assurance

We selected a well-established human ventricular action potential (AP) model, known as ORd and published in 2011 by O'Hara and colleagues [1], to perform the electrophysiological simulations. The electrophysiological cellular model was originally implemented on MATLAB (by MathWorks), a commercial software that includes numerical computation methods to implement algorithms, develop models and analyse data, among others. This computing platform is widely used by engineers and scientists and is technically supported by MathWorks, which provides twice a year thoroughly tested new releases adding new features and performance improvements.

1.1.1 Installation Qualification Document

For the model development phase, software installation was performed following the official installation guide and licensing [2] in a local machine with the recommended system requirements to run 2021b Release (Windows 10, Intel® CORE™ i7-6700 @3.4 GHz, x64 processor with eight logical cores, 32 GB RAM). Bench function, which measures the execution time of six different benchmarking tasks on the computer and compares the results to other computers, was run to check MATLAB installation on this machine (Figure 1). One of the tasks was to solve a differential equation, so the performance of the ODE function, which will be used later, was evaluated and verified during this test, among others.

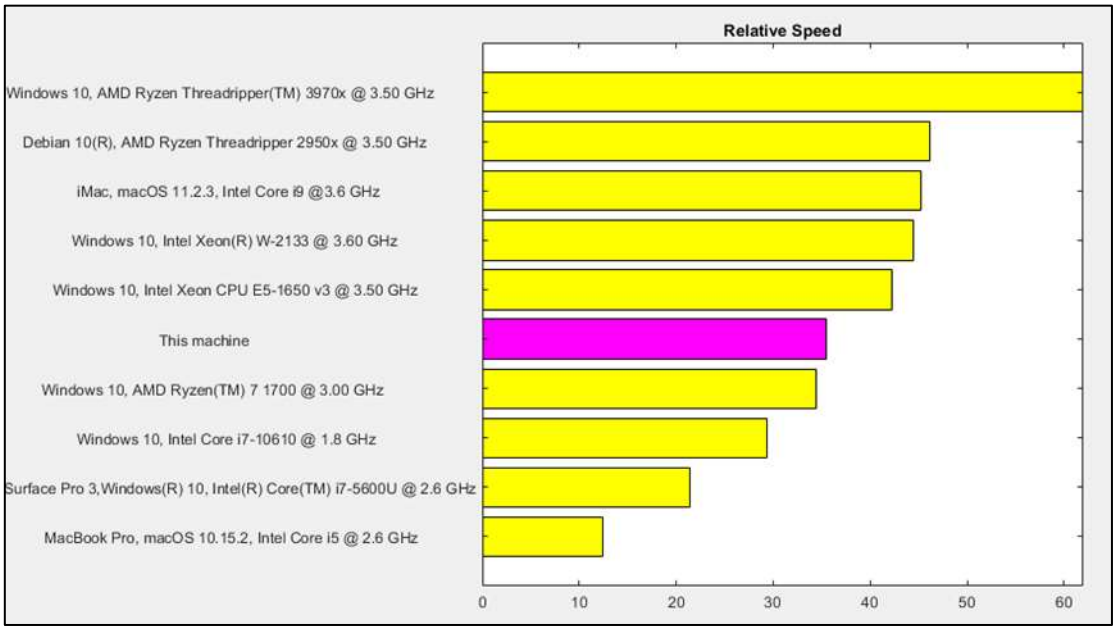

Figure 1: *Output of MATLAB bench function that compares the performance of benchmarking tasks on different machines.*

For integration onto the SimCardioTest platform, code integration and additional testing was performed on a machine with MATLAB 2021a release (Windows Server 2019 Datacenter, AMD EPYC 750P @2.5 GHz, x64 processor with 32 cores). On this machine, the bench testing was repeated (Figure 2). For integration into the web-interface, a Python® package was built from the MATLAB

code using MATLAB Compiler SDK™ (running in MATLAB 2021a Release) following the instructions provided by MathWorks®. The Python® package is run using MATLAB Runtime.

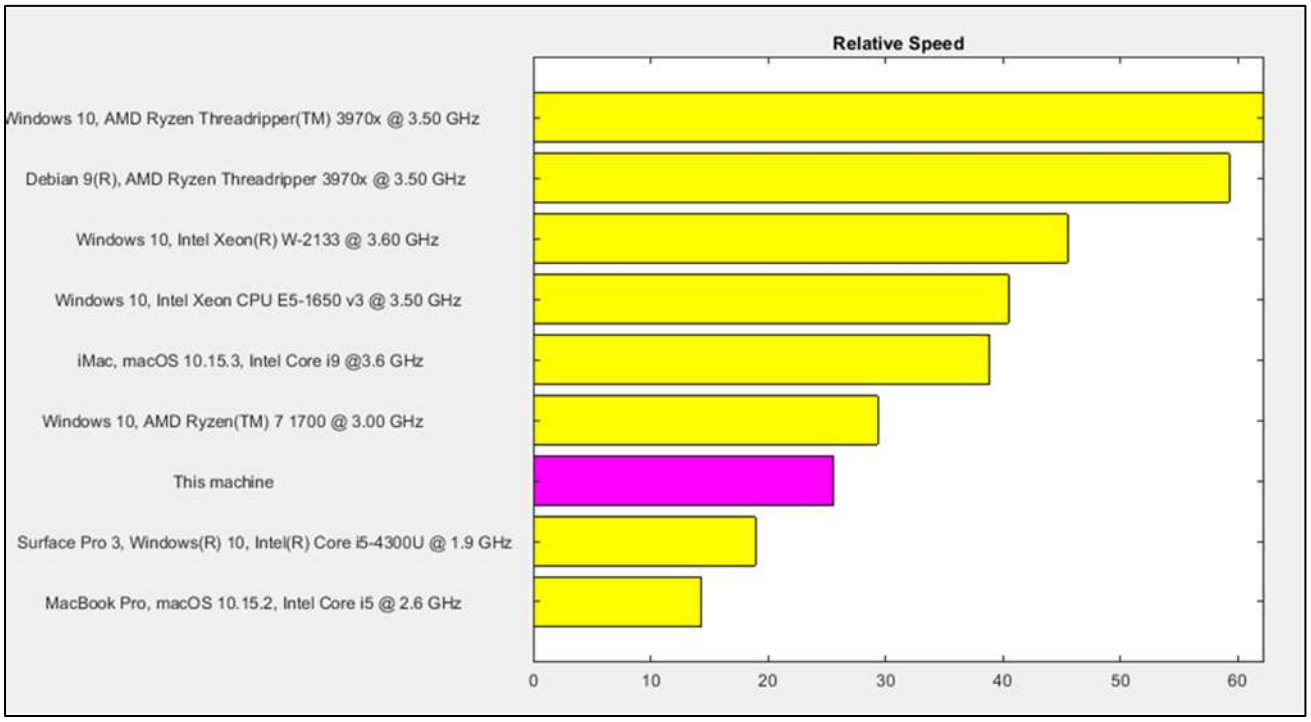

Figure 2: *Output of MATLAB bench function ion IST machine.*

1.2 Numerical Code Verification

The original electrophysiological cellular model and its derivative versions were checked to ensure that the equations were solved correctly. The cellular model includes algebraic expressions and systems of ordinary differential equations (ODEs), known as Hodgkin-Huxley equations. To solve the complex problem, an ODE solver is needed, and in this case, the MATLAB ode15s solver was selected. Verification was straightforward using a verified commercial ODE solver, and additional tests performed in section 2.1 complemented and confirmed the correct functioning of the numerical code.

In the absence of a gold-standard solution, our outputs were compared with the expected theoretical results (time course shapes and biomarkers measured on them) known from experimental observations. Solutions given by other codes that also recreate human cellular electrophysiology [3–5] with similar purposes also served as comparators.

Figure 3 shows the main electrophysiological outputs used to verify the correct implementation of equations. The depolarization and repolarization of membrane potential generate an expected shape of the AP, and intracellular Ca2+ concentration increases during positive potentials and then decreases to resting levels, reproducing the expected Ca2+ transient shape. The introduction of electromechanical coupling causes a tolerable variation in Ca2+ transient and allows simulation of the characteristic isometric twitch.

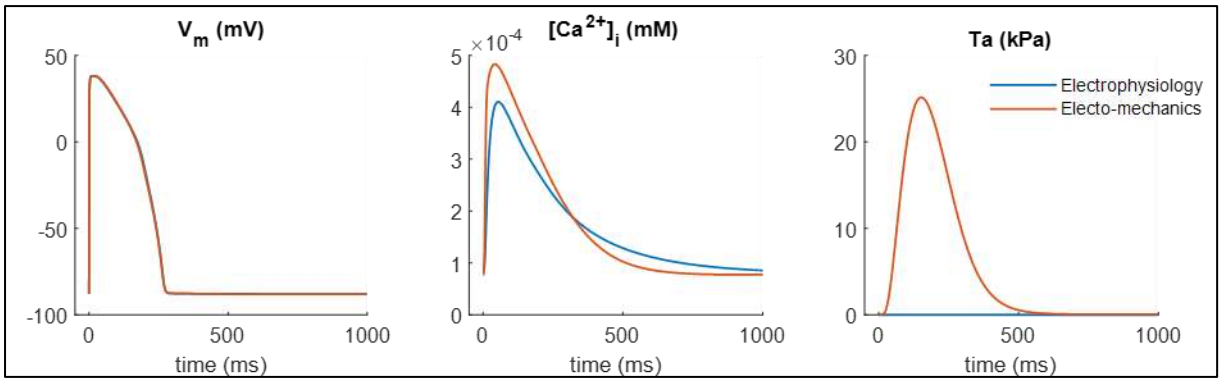

Figure 3: *Qualitative comparison of cellular outputs of two models.*

Table 2 shows critical in vitro biomarker ranges that set the bounds to assure physiological behaviour. These limits can be used for model verification, but they are indeed crucial for validation, the second part of credibility assessment. AP duration at 90% repolarization (APD90), one of the main quantities of interest for this particular question of interest, was quantified and analysed during calculation verification.

Table 2: Biomarker limits for physiological behavior.

Biomarker		Min Value	Max Value
APD_{40} (ms)	AP duration at 40% of repolarization	85	320
APD_{50} (ms)	AP duration at 50% of repolarization	110	350
APD_{90} (ms)	AP duration at 90% of repolarization	180	440
Tri_{90-40} (ms)	AP triangulation	50	150
dV/dt_{max} (mV/ms)	maximal upstroke velocity	150	1000
V_{peak} (mV)	peak voltage	10	55
RMP (mV)	Resting membrane potential	-95	-80
CTD_{50} (ms)	CaT duration at 50% of recovery	120	420
CTD_{90} (ms)	CaT duration at 90% of recovery	220	785
$[Ca^{2+}]_i$ systolic (μM)	maximal intracellular $[Ca^{2+}]$	0.26	2.23
$[Ca^{2+}]_i$ diastolic (μM)	minimal intracellular $[Ca^{2+}]$	--	0.40
$[Na^+]_i$ peak (mM)	maximal intracellular $[Na^+]$	--	39.27
ΔAPD_{90} (%) under 90% I_{Ks} block		-54.4	62
ΔAPD_{90} (%) under 70% I_{Kr} block		32.25	91.94
ΔAPD_{90} (%) under 50% I_{K1} block		-5.26	14.86

The compiled Python package running on the SimCardioTest platform runs the model using the same MATLAB ode15s solver. Following integration of the model on the SimCardioTest platform, generation of Figure 3 was repeated. The results (Figure 4) confirm the electrophysiological and electromechanical models are being simulated correctly.

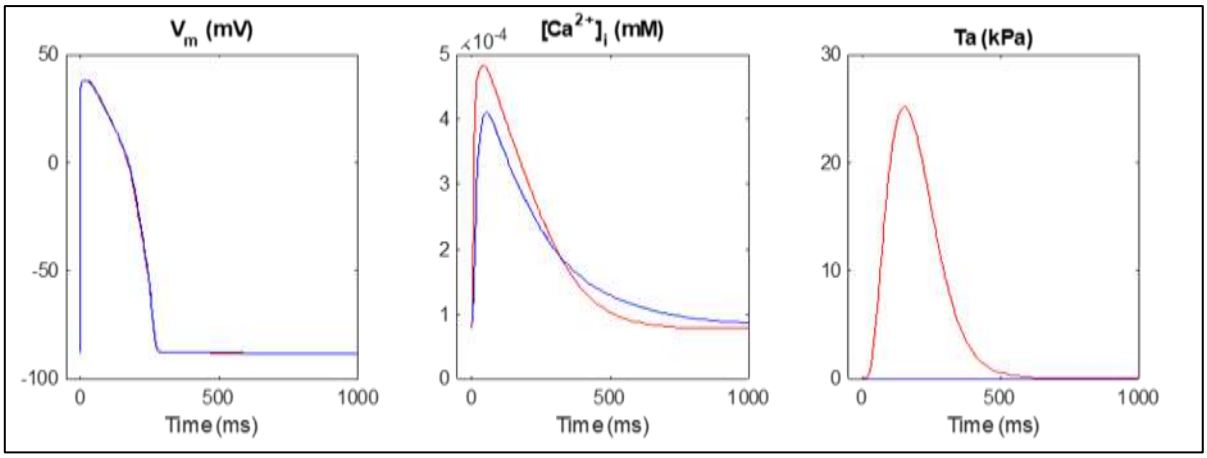

Figure 4: *IST verification of the qualitative comparison of cellular outputs of two models.*

In the implementation of drug models, using scaling factors calculated with Hill equations, it was verified that cellular ion currents were modulated. The effect on action potential was quantified and analysed later as part of the validation strategy. As an example, changes in currents modulated by the presence of Quinidine are depicted in Figure 5. The response increases with increasing doses, and variations in the correct direction are observed, which is consistent with the level of simulated blockade, i.e. drug effect.

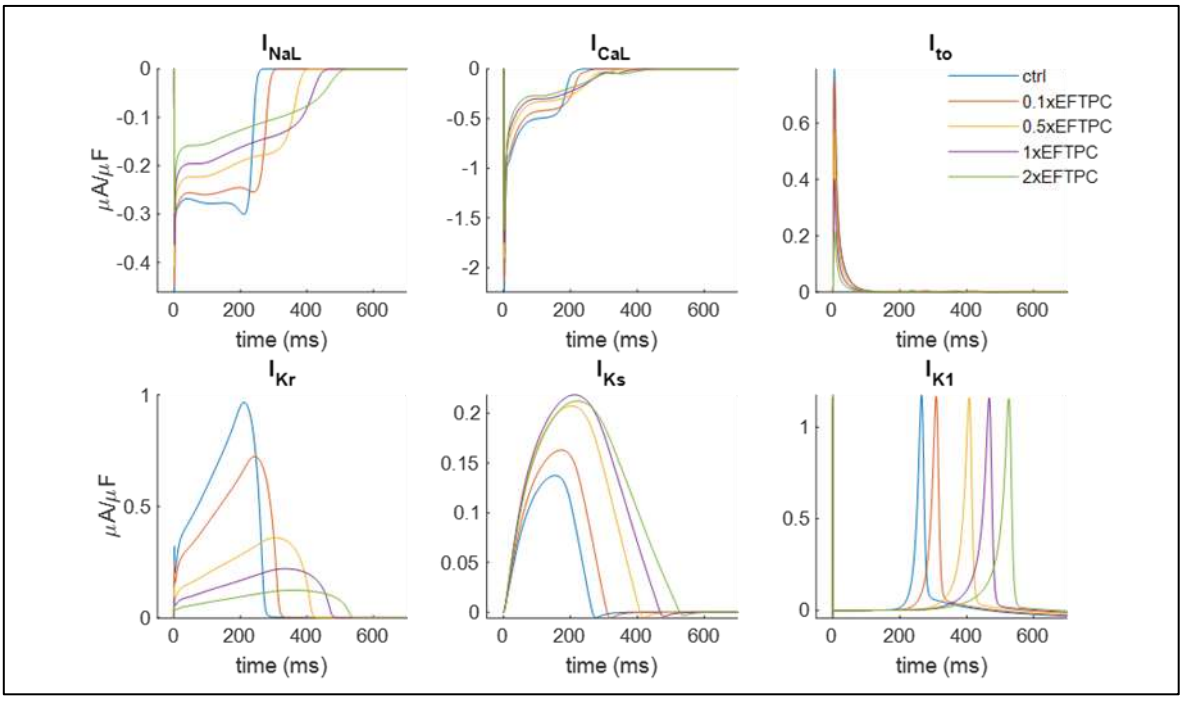

Figure 5: *Ion currents modulated by increasing doses of Quinidine.*

Again, to verify the behaviour of the model following integration onto the platform, generation of Figure 5 was repeated (Figure 6).

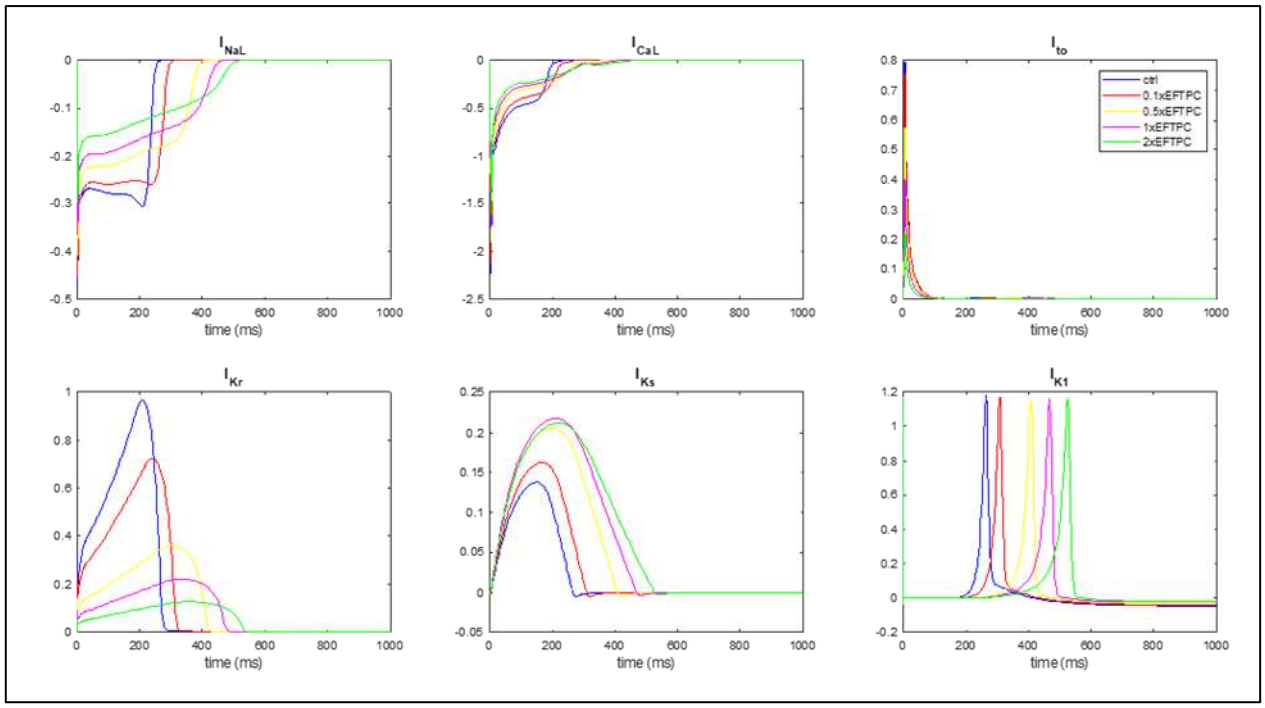

Figure 6: *IST verification of ion currents modulated by increasing doses of Quinidine.*

2. Calculation Verification

2.1 Discretisation and Numerical Solver Error

In electrophysiology, the temporal discretization required is on the order of milliseconds, whereas simulation time can achieve thousands of seconds, which prolongs computational time.

For the electrophysiological cellular model implemented in MATLAB, the ode15s solver was used as in the original numerical integration [1]. This variable order method was robust enough to solve the system of equations.

In these action potential models, convergence depends on the initialization of state variables. Stabilization tests, which run the code until variables do not change from beat to beat (steady state), are executed to assure solution convergence. As an example, a cellular 1000-beat simulation at a basic cycle length of 1000 ms shows that Na^+, Ca^{2+} and K^+ concentrations, which are main critical variables, achieve steady state after 500 seconds of simulation. In this case, a minimum of 700 simulation seconds starting at default initial conditions should be run before quantifying outputs. Therefore, running simulations to steady state was a requirement for each scenario.

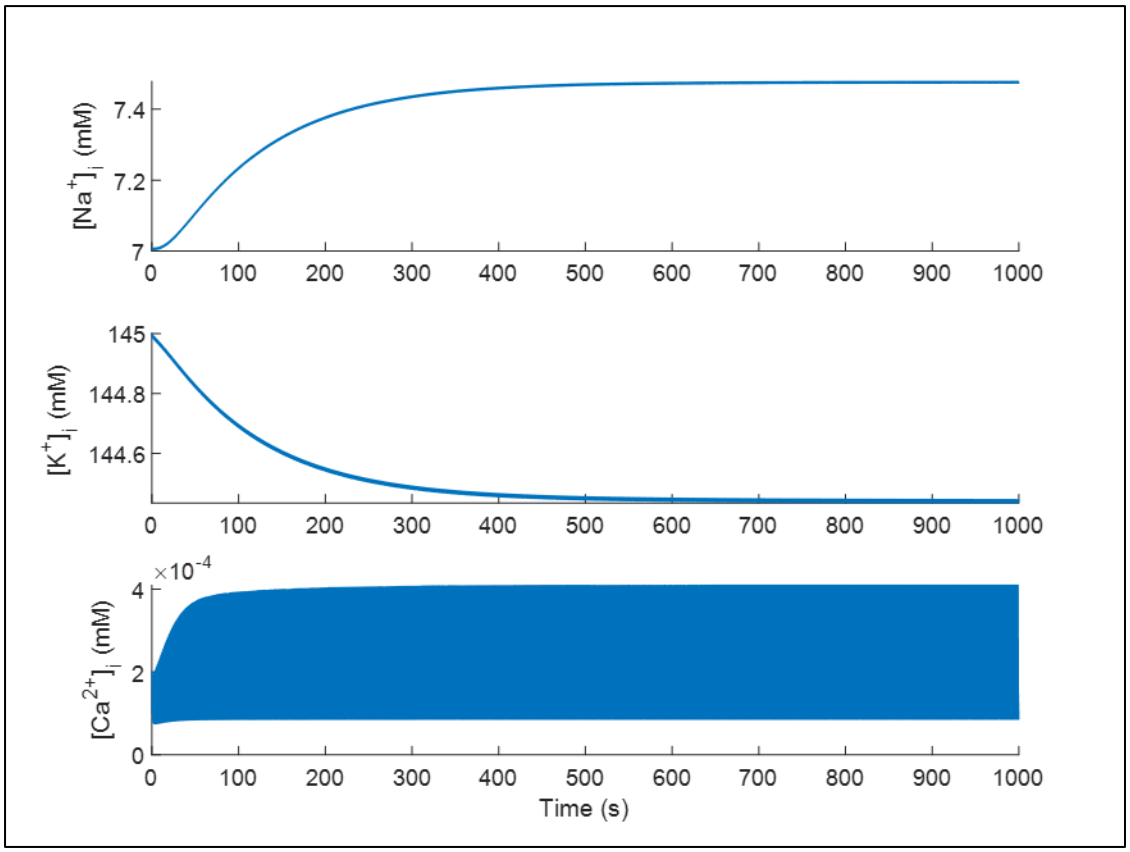

Figure 7: *Time courses of intracellular concentrations over the running time.*

Depending on the characteristics of the problem, MATLAB provides different solvers. Ode45 performs well with most ODE systems, and it is indicated as the first choice. However, despite being able to solve the electrophysiological equations, it was very slow compared to the stiff ode15s solver (Table 3).

Table 3: MATLAB ODE solvers performance in a 1000-second simulation.

ODE solver	Computation Time (s)
ode45	1200
ode15s	47
ode23s	549

The ode15s solver uses a variable time step, adapted to solve the integration problem in each step, which allows better control of numerical error. Other solver parameters were set to default values, from which error tolerances were analysed to verify the suitability of integration settings. Figure 8 and Figure 9 show that smaller tolerance values did not improve the accuracy, while larger tolerances could compromise the solution. Finally, the characteristics of the selected solver are specified in Table 4.

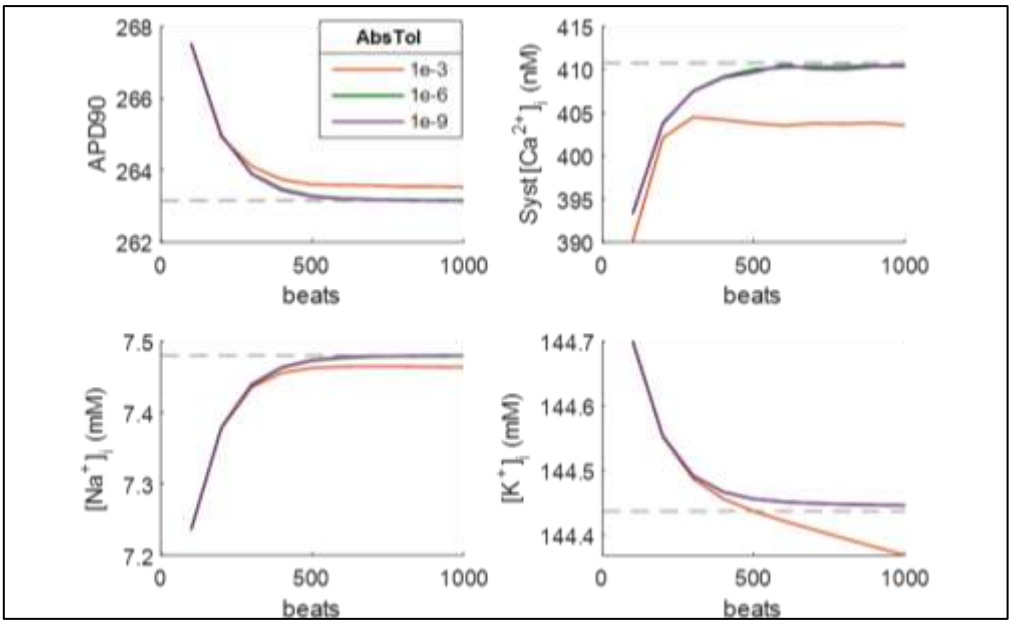

Figure 8: *Effect of absolute tolerance error on convergence.*

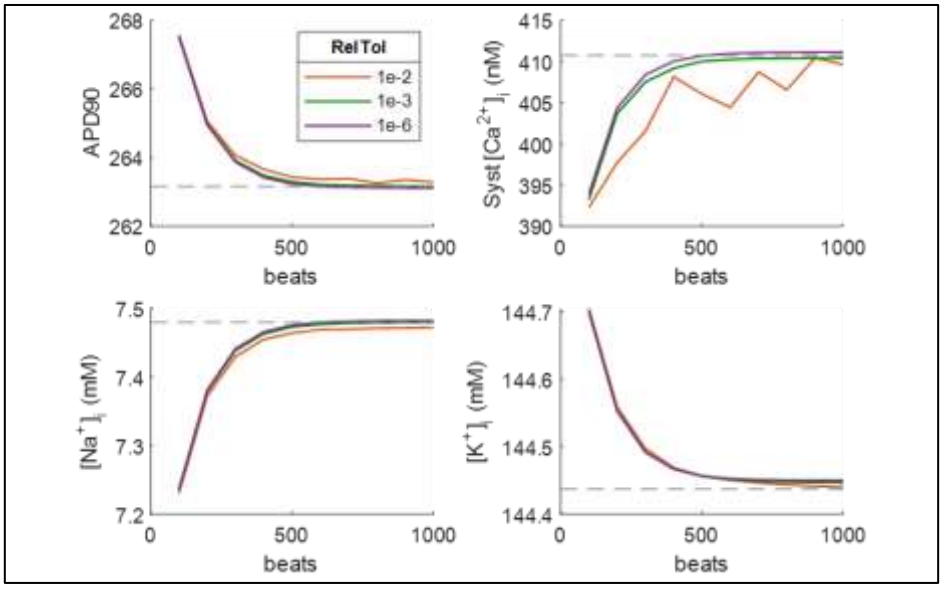

Figure 9: *Effect of relative tolerance error on convergence.*

Table 4: Solver parameters used to solve the cellular model.

Type	ode15s
Step size	variable
Absolute tolerance	1e-6
Relative tolerance	1e-3

Table 5 compares steady-state ADP90 values from different human AP models. All quantities are within the established physiological ranges (Table 2), and observed discrepancies between models align with biological variability. The same applies to the rest of the measured biomarkers.

Table 5: Comparison of Quantities of Interest at steady state.

Model	APD_{90}	APD_{50}	Tri_{90-40}	Syst $[Ca^{2+}]$	$CaTD_{50}$
Electrophysiological	263 ms	212 ms	68 ms	410 nM	218 ms
Electromechanical	262 ms	209 ms	71 ms	483 nM	218 ms
Other codes					
Bartolucci et al. 2020 [3]	239 ms	176 ms	79 ms	316 nM	105 ms
Tomek et al. 2019 [4]	271 ms	220 ms	74 ms	387 nM	207 ms

The analyses performed in Figure 7, Figure 8, and Figure 9 were again repeated and the results confirmed by IST. The verification of the full set of code verification and numerical verification tests provide further verification that the final implementation of the code is correct.

2.2 Use Error

During model development, use error is controlled by internal peer-review to avoid incorrect inputs that can compromise simulation execution (for instance, due to negative values) or results (ex. due to incorrect unit conversion). However, clients will interact with the graphical user interface implemented in the IST platform, in which typographical errors are controlled more automatically to warn the user in case of input error.

More details on the IST platform and its automatic control of user input can be found in section 2.3.

2.3 Use Error on InSilicoTrials Platform

The user interacts with the cloud-based platform through the Input Interface (by inserting input parameters) and through the Results Interface (by viewing and downloading simulation outputs).
Therefore, the error associated with potential human errors (e.g., errors that occur when entering model input parameters on the web interface) needs to be assessed.
In the following paragraphs, we describe the tests and actions taken to mitigate the risks of use error.

2.3.1 Input Interface

Input lower and upper limits are checked automatically by interface for every field. Warnings appear when the user types a number that is outside the boundaries. Examples are illustrated in the picture below.

Figure 10: *InSilicoTrials platform - example of input lower and upper limits automatic check.*

To demonstrate that the user inputs inserted in the webpage are correctly submitted to the simulation workflow, we performed a test for the cellular electromechanics workflow by inserting specific values in the fields on the web interface, and verified that the values collected by the system and passed to the calculation were the same.

The workflow guides the user along following web interfaces requiring inputs from the user as shown in the screenshots in Figure 11, Figure 12, Figure 13, Figure 16, and Figure 17.

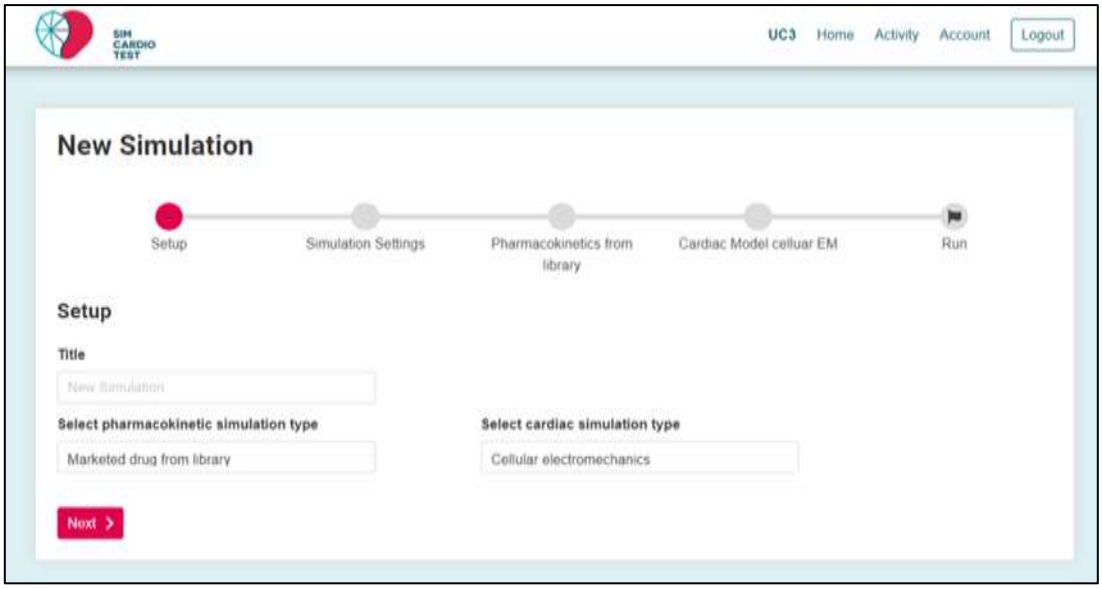

Figure 11: *InSilicoTrials - New Simulation - Setup.*

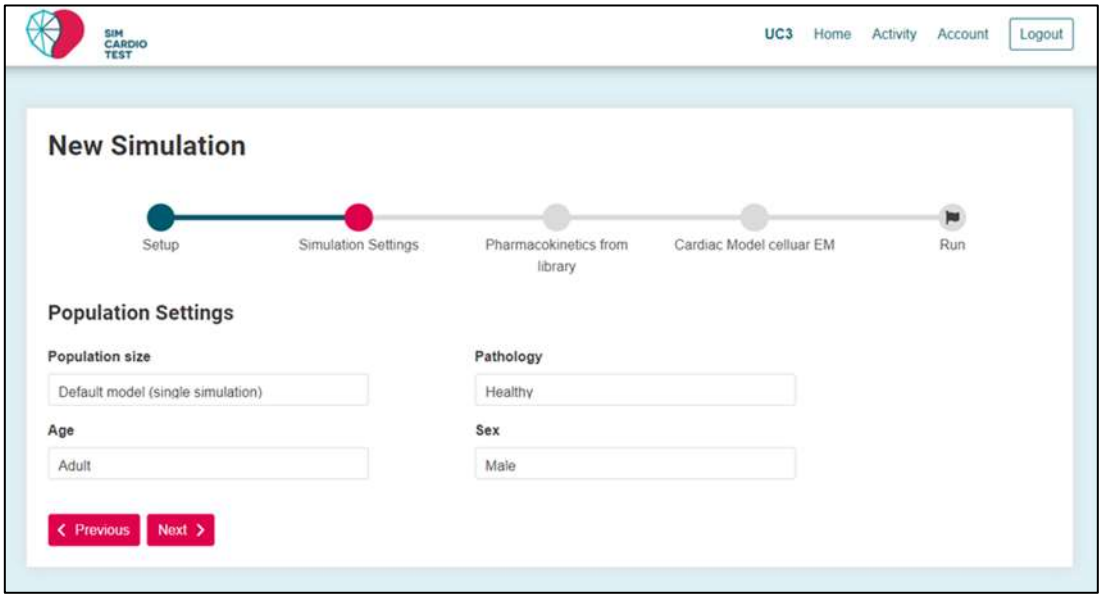

Figure 12: *InSilicoTrials - New Simulation - Simulation Settings.*

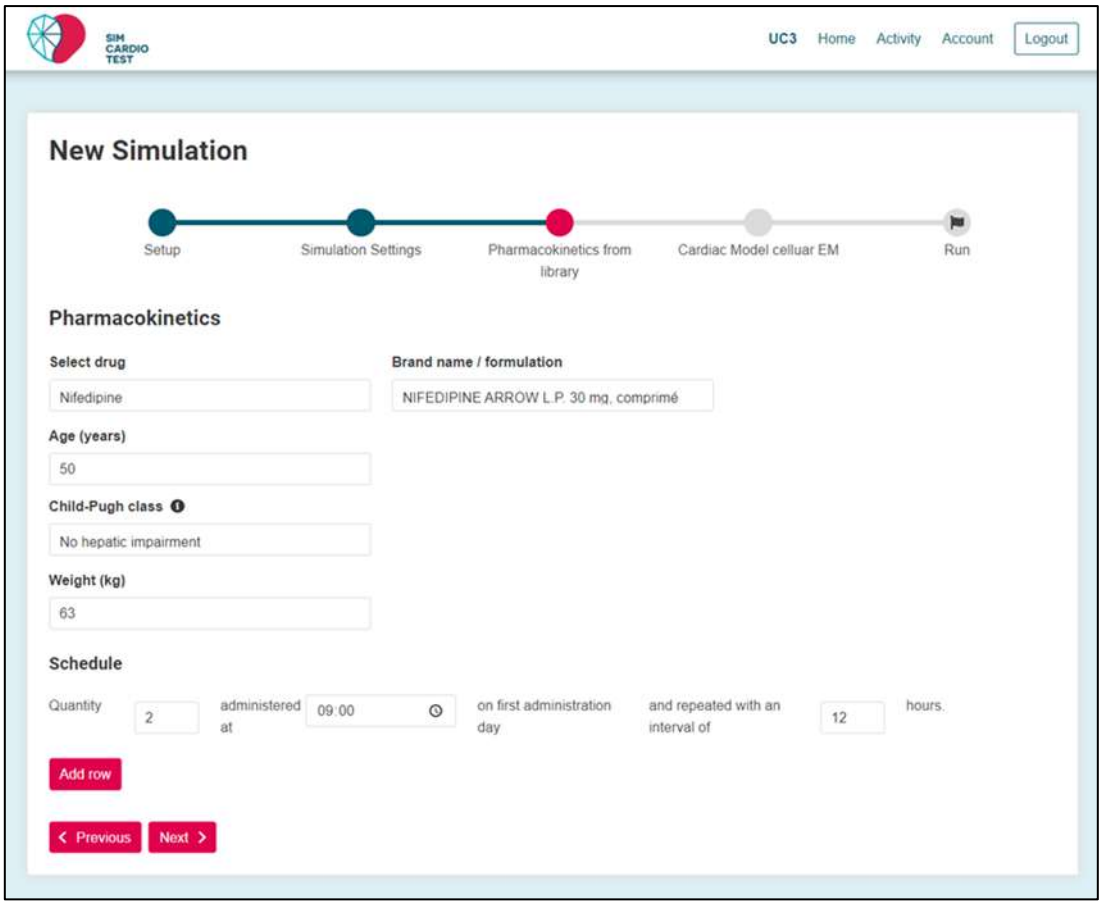

Figure 13: *InSilicoTrials - New Simulation - Pharmacokinetics from Library.*

The selection of the drug triggers EXC API and retrieves the list of the drug Brand name/formulation. The following screenshots from Google Chrome Developer Console demonstrates the HTTP Request (Figure 14) and Response corresponding to the Drug Selection (Figure 15).

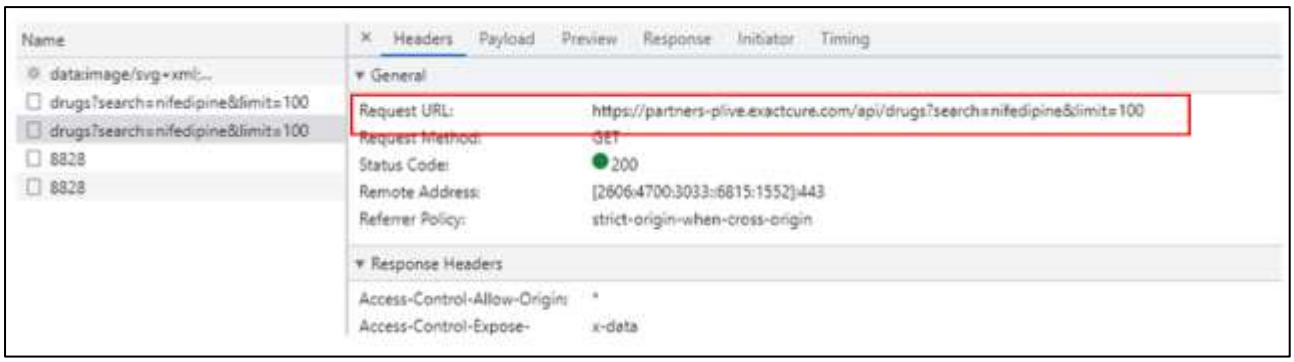

Figure 14: *InSilicoTrials - Interaction with EXC API - HTTP Request.*

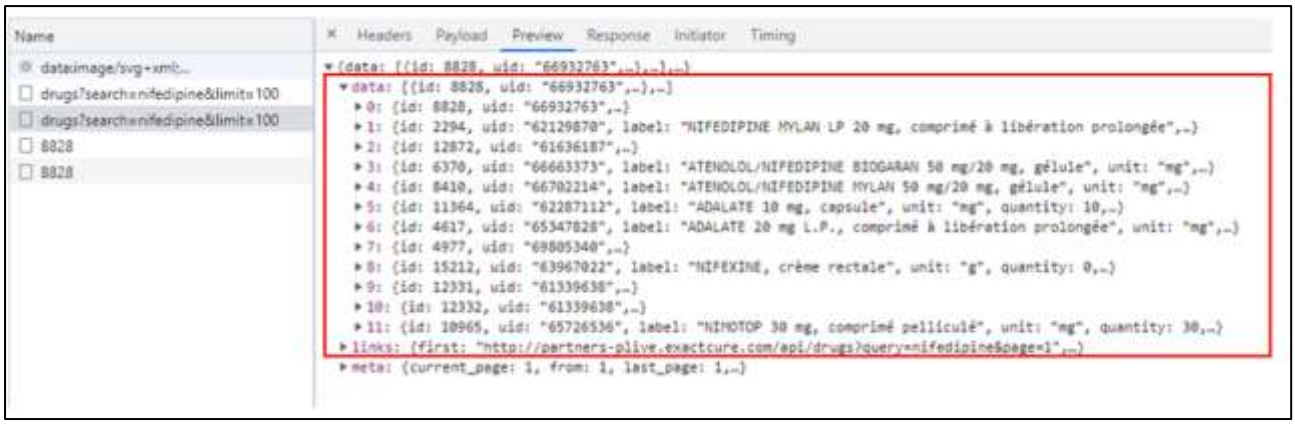

Figure 15: *InSilicoTrials - Interaction with EXC API - Response to HTTP Request.*

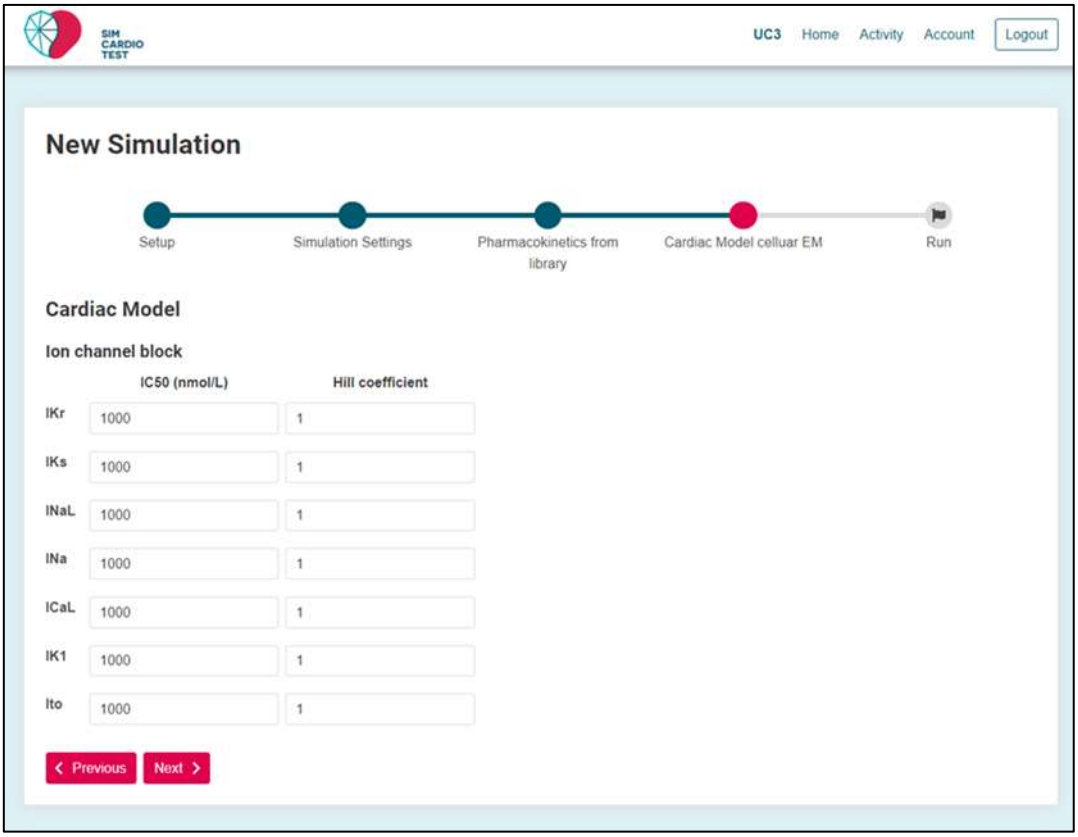

Figure 16: *InSilicoTrials - New Simulation - Cardiac Model Cellular EM.*

A webpage at the end of the input submission shows the summary of all data entered by the user and notifies the user in case any information is missing before allowing the user to run the model on the cloud.

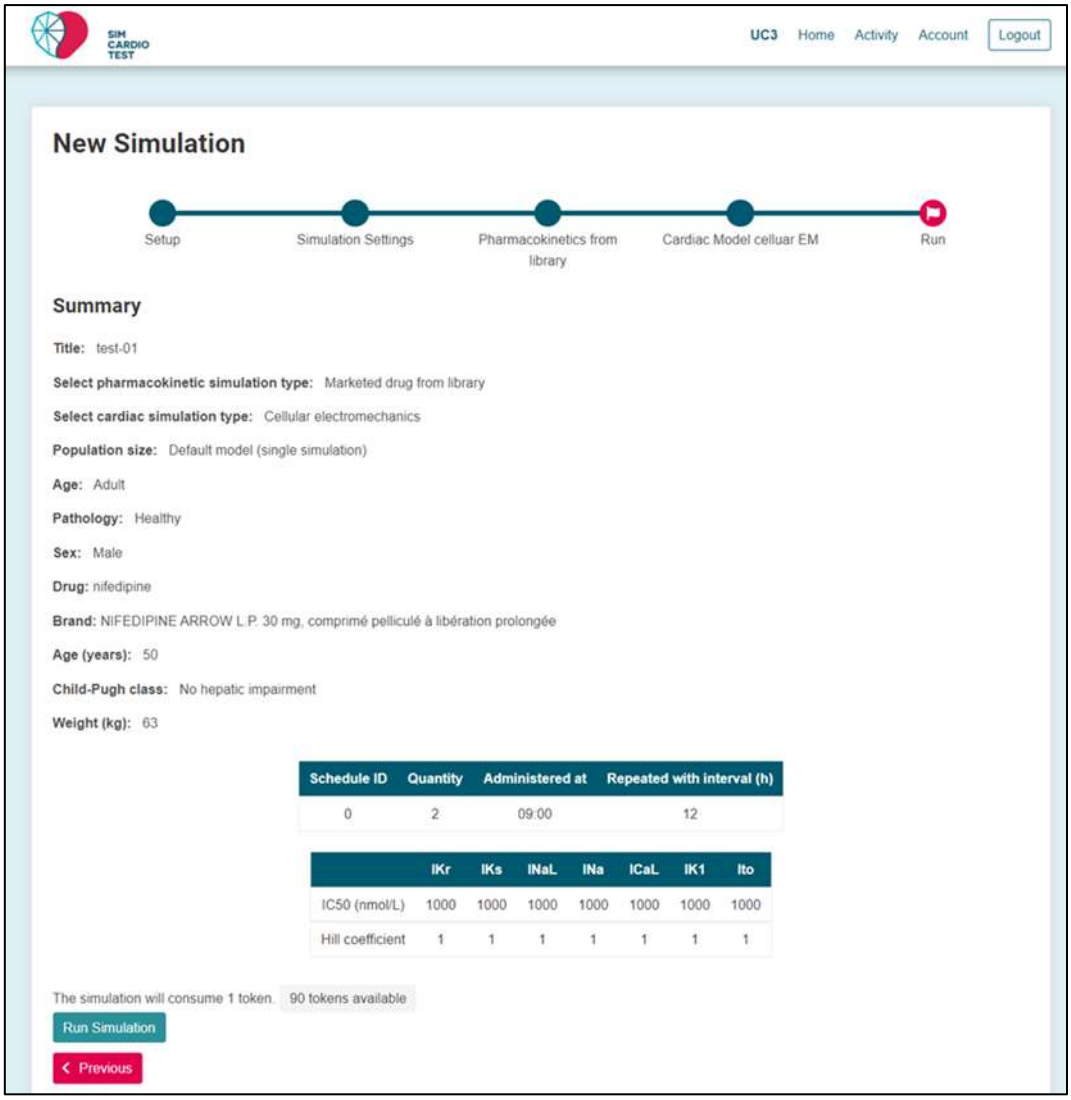

Figure 17: *InSilicoTrials - New Simulation - Run.*

After clicking on the "Run Simulation" button, an input.json file is created and stored in the corresponding repository in the dedicated environment (simcardiotestuc3) created on Microsoft Azure (Figure 18).

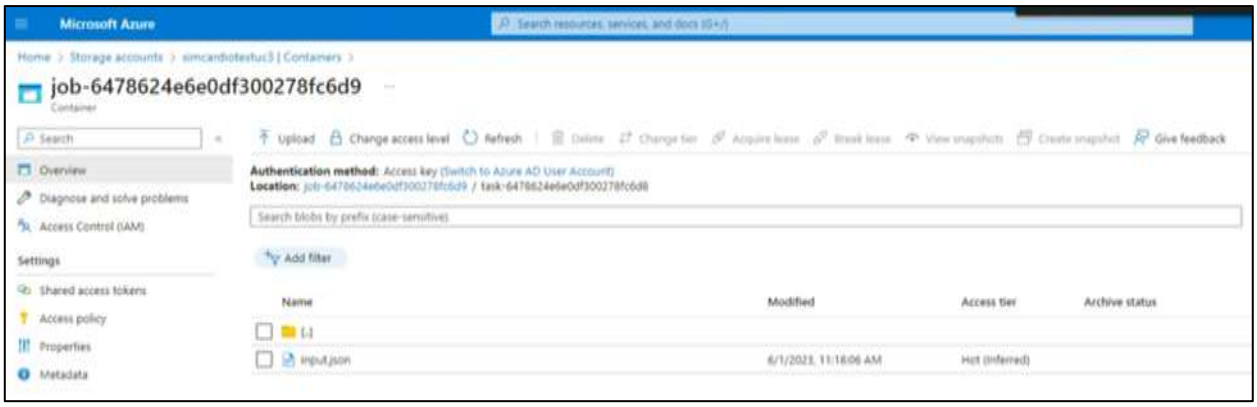

Figure 18: *InSilicoTrials - input.json file created and stored in the corresponding repository in the dedicated environment (simcardiotest-uc2) created on Microsoft Azure.*

The file contains the list of variables displayed on the web interface, and values correspond to the ones inserted by the user, meaning that the test has passed (Figure 19).

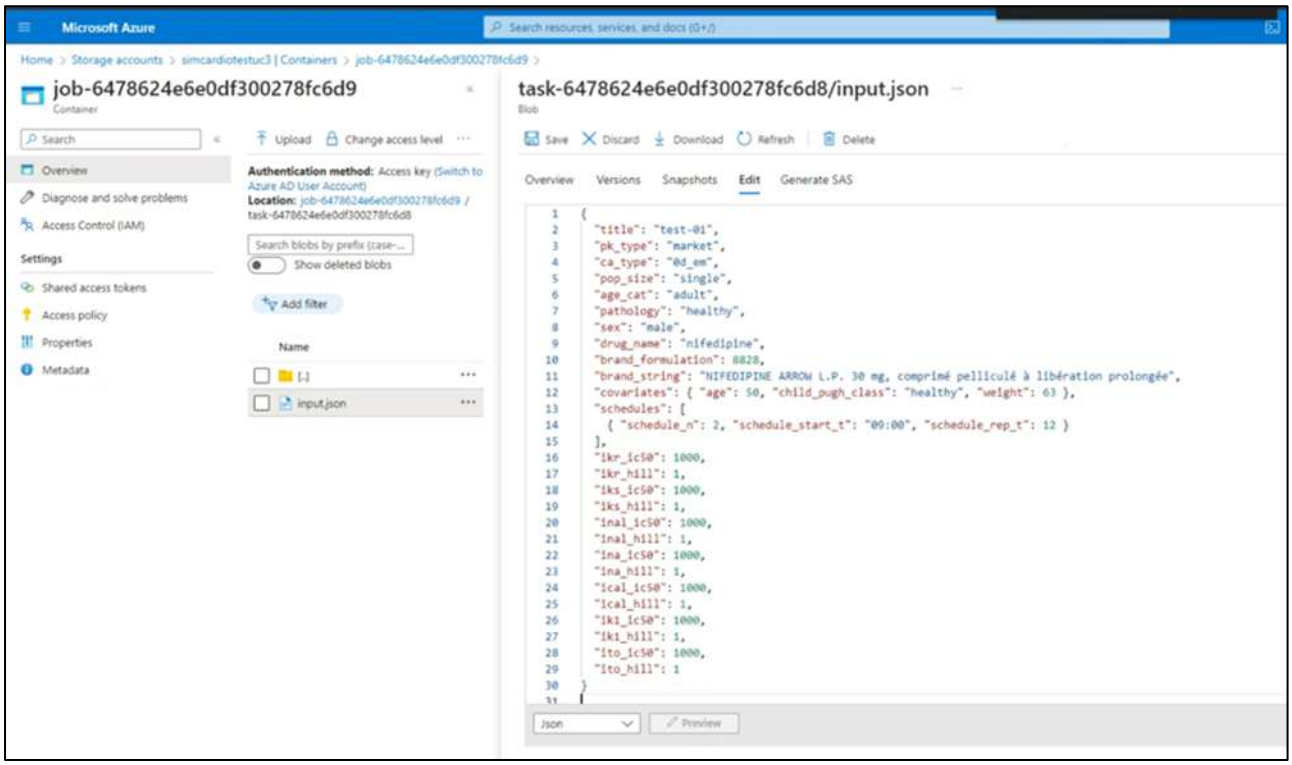

Figure 19: *InSilicoTrials - input.json file content displaying the list of input variables inserted by the user.*

The .json file is then forwarded to EXC ReST API.

2.3.2 Results Interface

Results are displayed in the Results Interface as shown in Figure 21.

At the top of the webpage, a summary of the input parameters is shown (Figure 20).

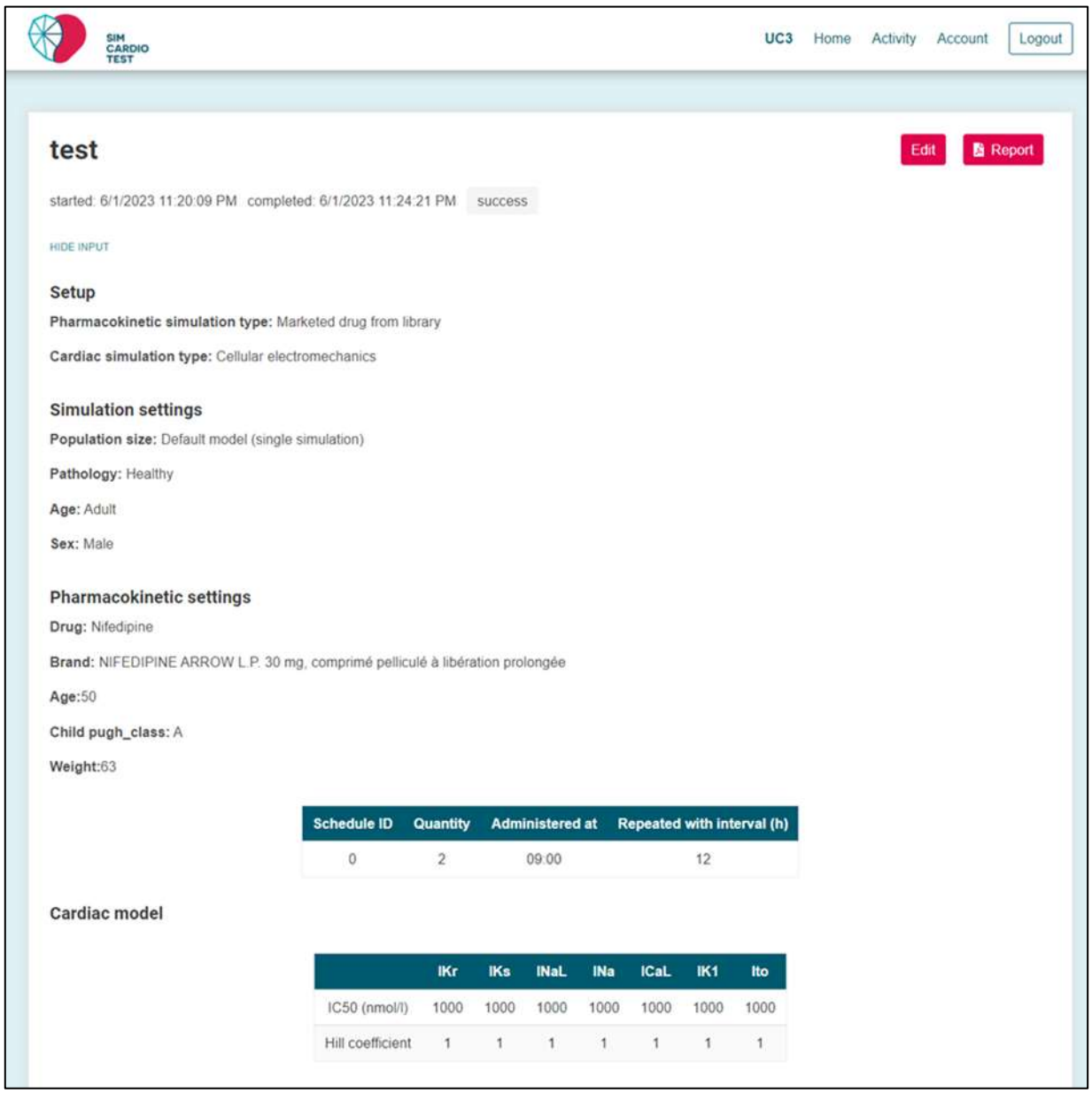

Figure 20: *InSilicoTrials - Results Interface - Summary of Input Parameters.*

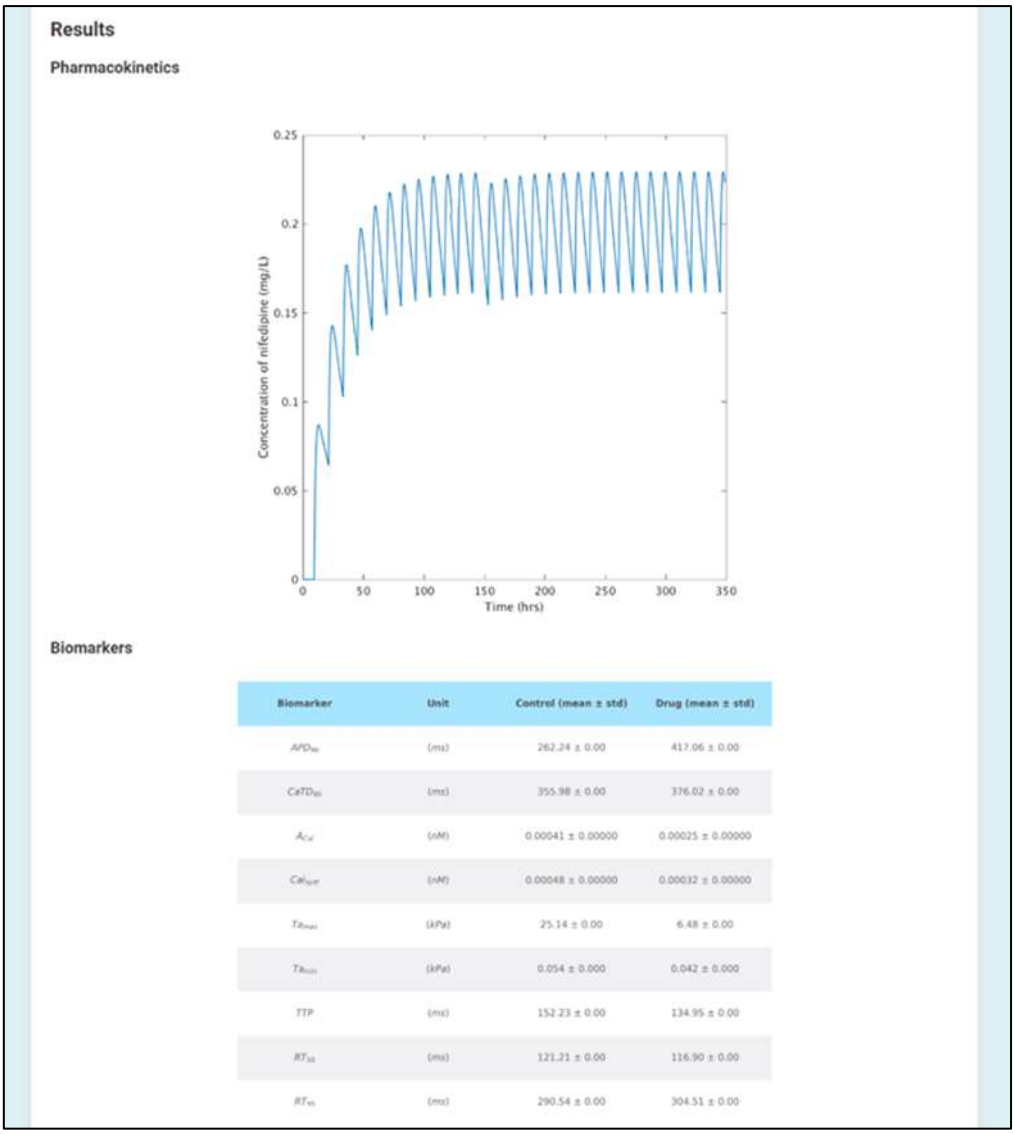

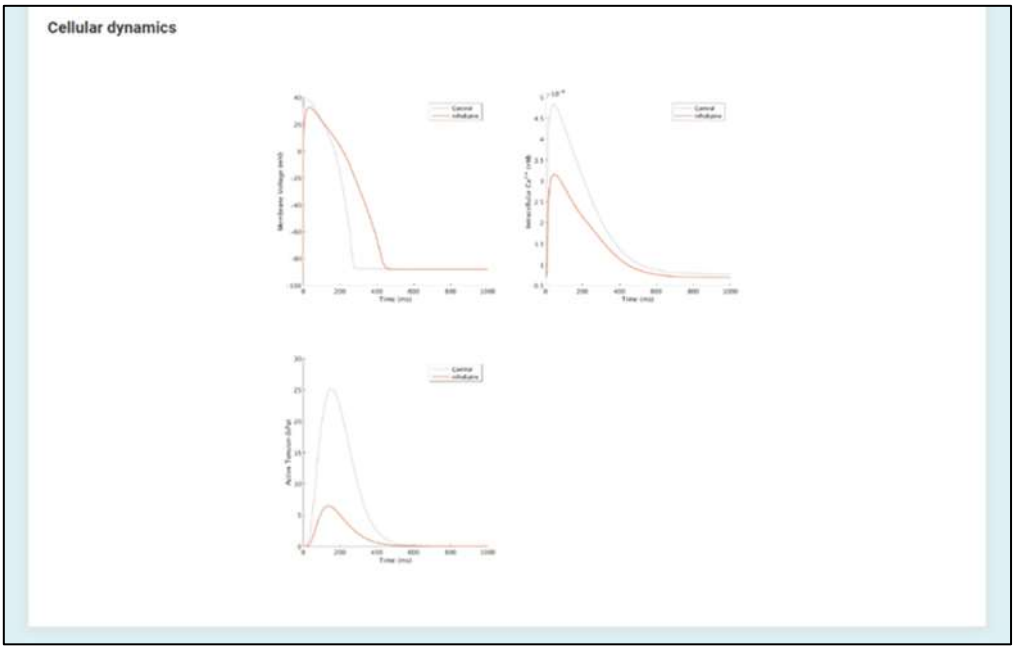

Figure 21: *InSilicoTrials - Results Interface.*

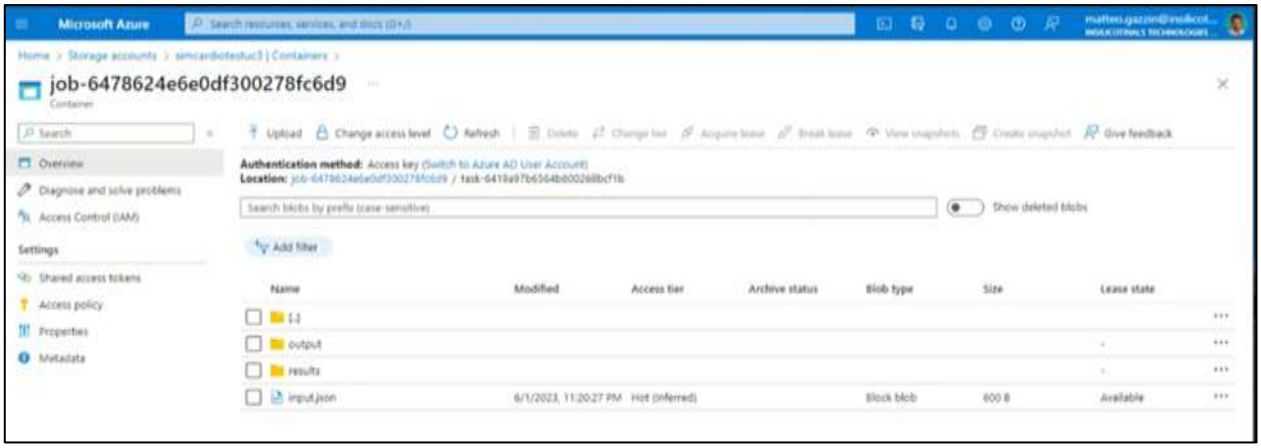

Figure 22: *InSilicoTrials - "output" and "results" folders created and stored in the corresponding repository in the dedicated environment (simcardiotest-uc3) created on Microsoft Azure.*

In the same repository created in the environment (simcardiotestuc3), a folder called "output" and a folder called "results" are created and stored (Figure 22 and Figure 23).

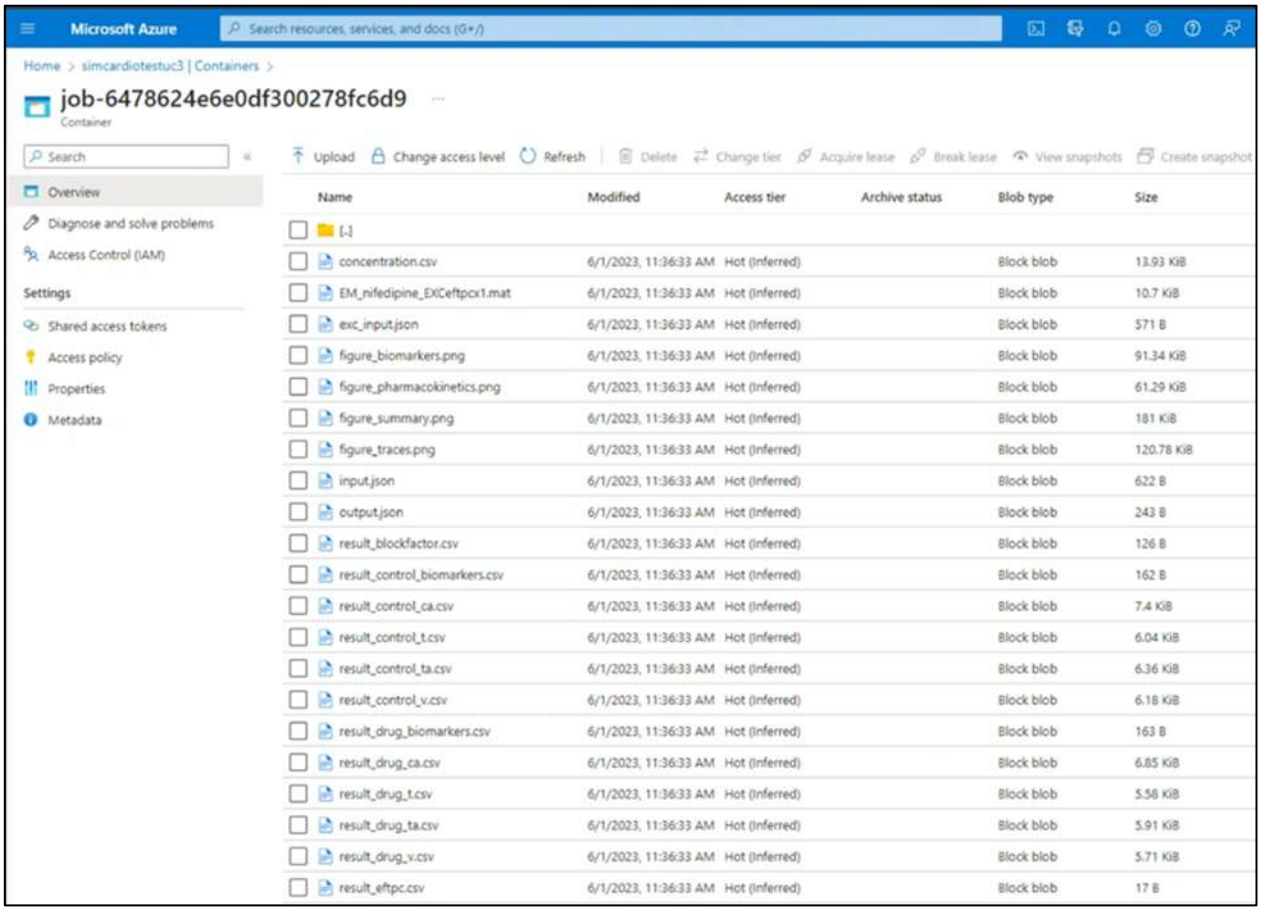

Figure 23: *InSilicoTrials - content of folders created and stored in the corresponding repository in the dedicated environment (simcardiotest-uc3) created on Microsoft Azure.*

Final user will be responsible that outputs are relayed and used correctly. IST will not be responsible for the use of the outputs.

3. Conclusion

This document is an annex of SimCardioTest deliverable D6.1, and reports technical details relative to the verification of the 0D numerical model developed for Use Case 3. General conclusions relative to the verification of UC3 numerical model are reported in main deliverable D6.1.

4. Bibliography

[1] T. O'Hara, L. Virág, A. Varró and Y. Rudy, "Simulation of the undiseased human cardiac ventricular action potential: model formulation and experimental validation," *PLoS Comput Biol.,* vol. 7, no. DOI: https://doi.org/10.1371/journal.pcbi.1002061, p. e1002061, 2011.

[2] "Installation and Licensing Installation Guide R2022b," 2022. [Online]. Available: www.mathworks.com.

[3] C. Bartolucci, E. Passini, J. Hyttinen and others, "Simulation of the Effects of Extracellular Calcium Changes Leads to a Novel Computational Model of Human Ventricular Action Potential With a Revised Calcium Handling," *Front Physiol.,* vol. 11, no. DOI: https://doi.org/10.3389/fphys.2020.00314, p. 314, 2020.

[4] J. Tomek, A. Bueno-Orovio, E. Passini and others, "Development, calibration, and validation of a novel human ventricular myocyte model in health, disease, and drug block," *Elife.,* vol. 8, no. DOI: https://doi.org/10.7554/eLife.48890, p. 1–47, 2019.

[5] V&V40, Assessing Credibility of Computational Modeling Through Verification and Validation: Application to Medical Devices, New York: ASME, 2018.

[6] E. Grandi, F. S. Pasqualini and D. M. Bers, "A novel computational model of the human ventricular action potential and Ca transient," *J Mol Cell Cardiol,* vol. 48, no. DOI: https://doi.org/10.1016/j.yjmcc.2009.09.019, p. 112–121, 2010.

This project received funding from the European Union's Horizon 2020 research and innovation program under grant agreement No 101016496

EU Horizon 2020 Research & Innovation Program
Digital transformation in Health and Care
SC1-DTH-06-2020
Grant Agreement No. 101016496

SimCardioTest - Simulation of Cardiac Devices & Drugs for in-silico Testing and Certification

Technical Report

A6.1-UC3-3D: Use Case 3 3D Verification Annex

Work Package 6 (WP6)

Verification, validation, uncertainty quantification & certification

Annex Lead: UPV, Spain

Task Lead: UBx, France

WP Lead: MPC, France

PUBLIC

Document history			
Date	**Version**	**Author(s)**	**Comments**
05/06/2023	V1	I. VAN HERCK	Draft
06/06/2023	V2	H. FINSBERG	Draft
21/06/2023	V3	M. T. MORA	Final version prior consolidation
23/06/2023	V4	R. SETZU	Format consolidation
29/06/2023	V5	H. AREVALO	Quality Review
30/06/2023	V6	R. SETZU	Final Version
01/07/2023	V7	R. SETZU M. BARBIER	Format Editing

TABLE OF CONTENTS

EXECUTIVE SUMMARY

This document is an annex of SimCardioTest deliverable D6.1 and was elaborated for Use Case 3 in the context of drug safety assessment. It contains the technical details for the verification of the electrophysiological models at the tissue level and the verification activities performed by InSilicoTrials during the integration of the aforementioned model in the cloud platform of SimCardioTest project.

Acronyms

Table 1: List of Acronyms.

Acronym	Meaning
AP	Action potential
IST	InSilicoTrials
SCT	SimCardioTest
TdP	Torsade de pointes
ODE	Ordinary differential equation
PDE	Partial differential equation
EP	electrophysiology
PyPI	Python packaging index

1. Code Verification

1.1 Software Quality Assurance

The Simula Cardiac Electro-Mechanics Solver (simcardems) is a FEniCS-based solver developed as part of the SimCardioTest project. Simcardems is a state of the art 3D cardiac electromechanical simulator that is released under the GNU LGPL (ver. 2.1) license. It can perform fully coupled electromechanical simulations as well as purely electrophysiological (EP) simulations.

Development of simcardems was performed exclusively by researchers at Simula Research Laboratory and followed good programming practices. Extensive documentation of the software is available at https://computationalphysiology.github.io/simcardems/ and is continuously updated when new features are incorporated in the software. The robustness of the documentation and installation of the software has been tested and peer reviewed recently [1].

1.2 Software Installation

During the model development phase, software and required packages were installed following the instructions on [2] (see Figure 1).

When implemented in the cloud service, the software and all required packages will be installed similarly (according to requirements of the system architecture).

A docker image containing all the required dependencies is available for both AMD and ARM architectures and can be downloaded from the GitHub repository. This is the recommended way to install and use the software.

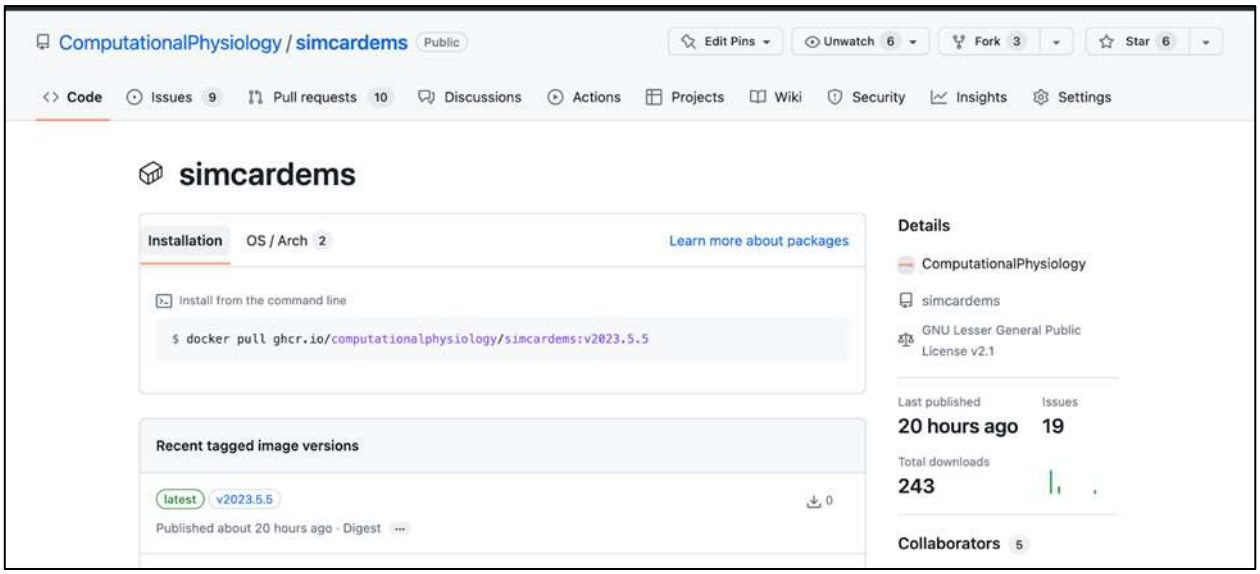

Figure 1: *GitHub installation page for software.*

A version of the software is also available on the python packaging index (PyPI) (see Figure 2), but this requires additional packages, such as FEniCS to be installed in advance. New docker images

and wheels (PyPI) is uploaded automatically whenever a new version is published to the GitHub repository.

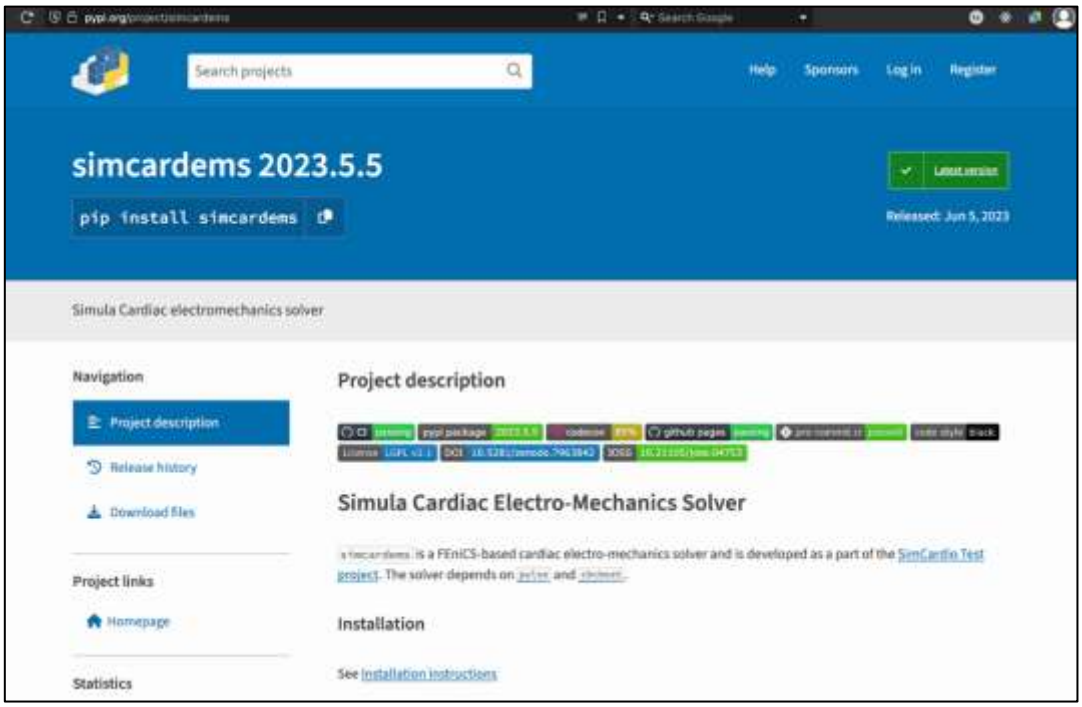

Figure 2: *PyPI page for simcardems package.*

1.3 Continous Integration

We use Git and GitHub to track changes in the software (Figure 3). All changes to the code will be implemented using a pull requests workflow and reviewed by another developer.

The software uses continuous integration which runs on every push to the repository using GitHub actions. The continuous integration consists of unit tests, integration tests, static type checking and linters.

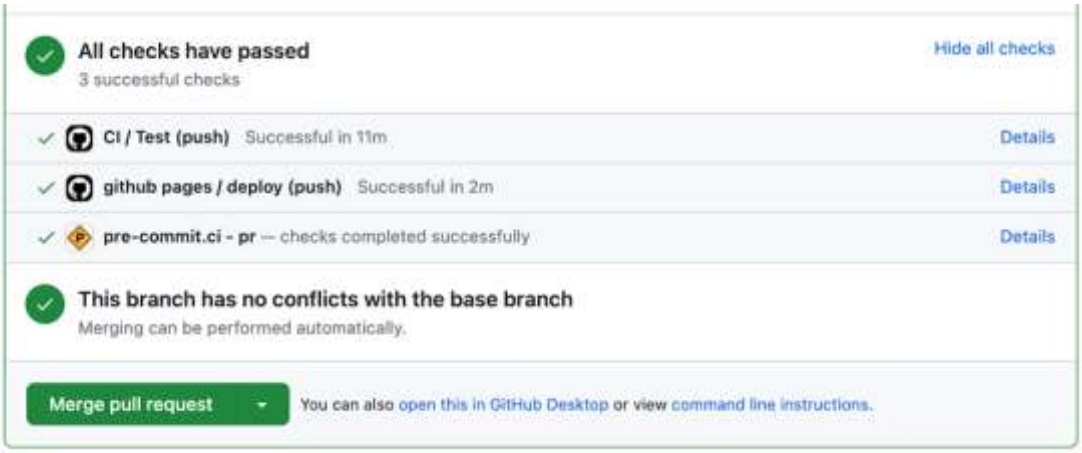

Figure 3: *GitHub actions for automated testing of simcardems code.*

The software has extensive documentation with tutorials and API documentation, see [3]. The documentation also contains a verification section that shows the resulting output of running a predefined benchmark for each commit. This section also contains a spatial convergence test where the output from different spatial discretizations are compared as well as a temporal convergence test which compares the output from different temporal discretizations. The convergence tests are run on every new release of the software and the output from the convergence tests are uploaded to a public gist on GitHub [4] (see Figure 4).

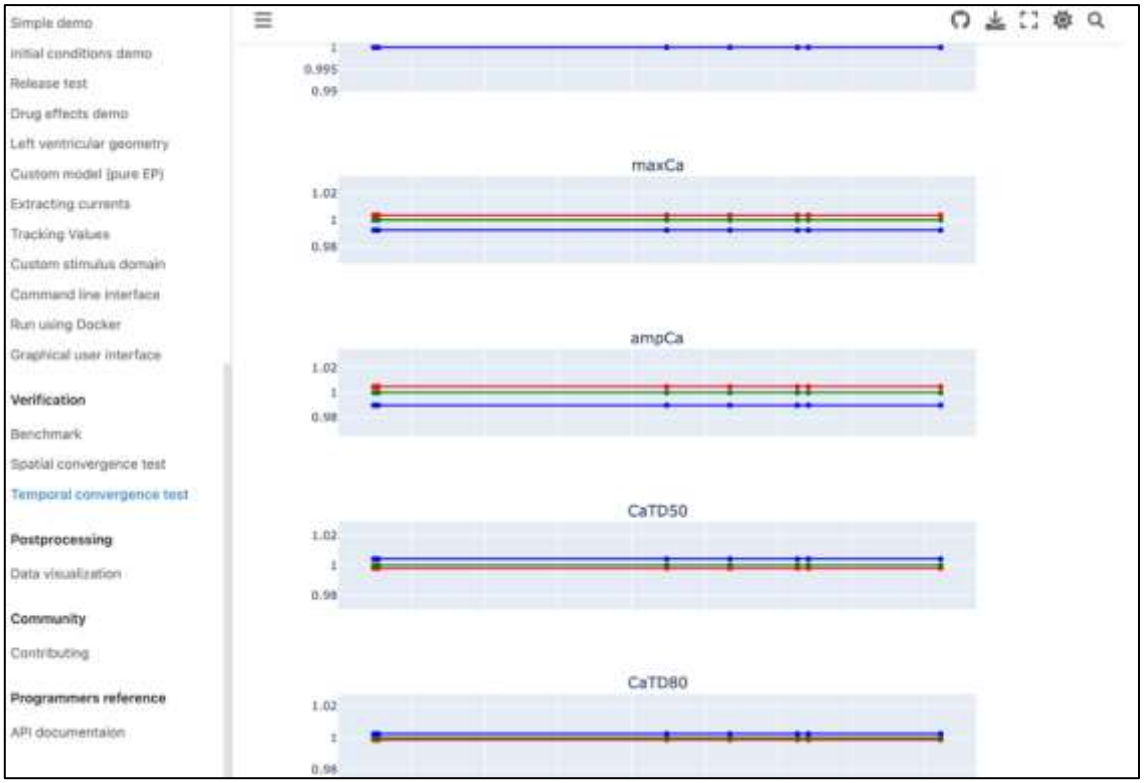

Figure 4: *Location and result of benchmark in public simcardems documentation.*

Simcardems also depends on several other libraries such as cbcbeat, pulse and FEniCS which all follow a similar quality assurance process.

Links/references:

- simcardems
  - Repository: https://github.com/ComputationalPhysiology/simcardems
  - Documentation: https://computationalphysiology.github.io/simcardems
- cbcbeat
  - Repository: https://github.com/ComputationalPhysiology/cbcbeat
  - Documentation: https://computationalphysiology.github.io/cbcbeat/
- pulse
  - Repository: https://github.com/finsberg/pulse
  - Documentation: https://finsberg.github.io/pulse/
- FEniCS
  - Repository: https://bitbucket.org/fenics-project/
  - Documentation: https://fenicsproject.org/olddocs/dolfin/latest/python/

1.4 Numerical Code Verification

Simcardems is based on FEniCS which uses PETSc (version 3.18.2) as the linear algebra backend. PETSc contains a suite of solvers that are already verified and well tested [5].
For solving the PDEs and ODEs we use FEniCS [6] which is a well-established framework for solving partial differential equations using the finite element method.
CBCbeat, which is the implementation of the solver for the electrophysiology, is verified against the Niederer benchmark [7], and the implementation of the benchmark can be found in the CBCbeat GitHub repository. Similarly, the mechanics solver is verified against the Land benchmark [8] and the implementation can be found in the pulse GitHub repository.

1.4.1 NCV of InSilicoTrials Platform

SimCardEms version 22.1.3 was installed on the platform via its docker image. Following installation, tests were performed to verify that the software was installed properly and all installation requirements has been met.

2. Calculation Verification

2.1 Discretisation Error

We have implemented both a temporal and spatial convergence test for the fully coupled electro-mechanics model. For the in-silico trials platform, only the pure electrophysiology model will be used and we have therefore also implemented a separate script for running the same convergence tests using only the EP model. In both cases we consider a slab of size 3x7x20 mm which is the same as the geometry used in [7] (see Figure 5). We fix one side with a Dirichlet boundary condition and let the opposite side move freely. We computed a range of different features such as APD40 and triangulation from the resulting voltage and calcium traces using the ap_features library [9].

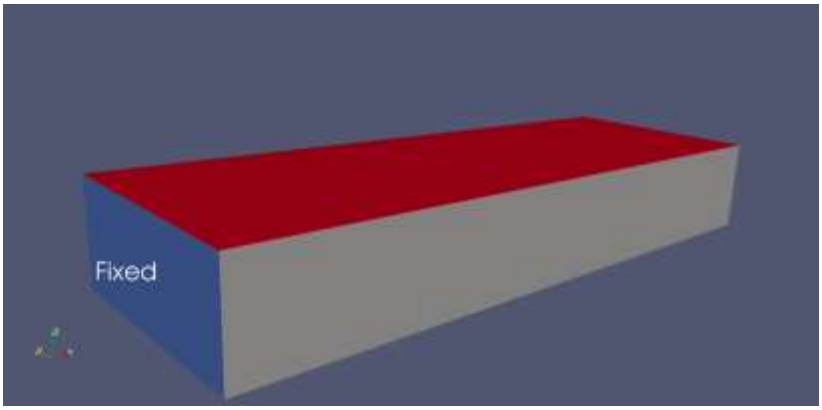

Figure 5: *Example of mesh outline with indication of fixed boundary condition in contracting direction*.

2.1.1 Spatial Convergence Test

We ran one beat of the benchmark using three different spatial discretizations corresponding to a dx of 0.1, 0.2 and 0.4 for the mechanics mesh. The EP mesh is then uniformly refined after the mechanics mesh is created. Also note that even this benchmark uses a pure EP model, but since simcardems is designed for electro-mechanics it also needs a mechanics mesh. The resulting values of the different features are displayed in Table 2 and Figure 6.

Table 2: Model details and biomarkers in spatial convergence test.

Feature	dx = 0.1 mm	dx = 0.2 mm	dx = 0.4 mm
import time	4.590256e-07	4.590256e-07	4.590256e-07
num cells mechanics	2520	180	60
num cells ep	20160	1440	480
num vertices mechanics	672	88	36
num vertices ep	4305	441	165
create runner time	7.042421	7.505218	6.100608
solve time	615.0033	79.85127	49.73124
APD40	240.4079	240.4079	240.4079
APD50	266.7946	266.7946	266.7946
APD90	333.8508	333.8508	333.8508
triangulation	92.78771	92.78771	92.78772
Vpeak	51.11934	51.11934	51.11934
Vmin	-88.02138	-88.02138	-88.02137
dvdt max	144.1165	144.1165	144.1165
maxCa	0.0002344468	0.0002344468	0.0002344468
ampCa	0.0001669904	0.0001669904	0.0001669904
CaTD50	306.8837	306.8837	306.8837
CaTD80	439.279	439.279	439.279

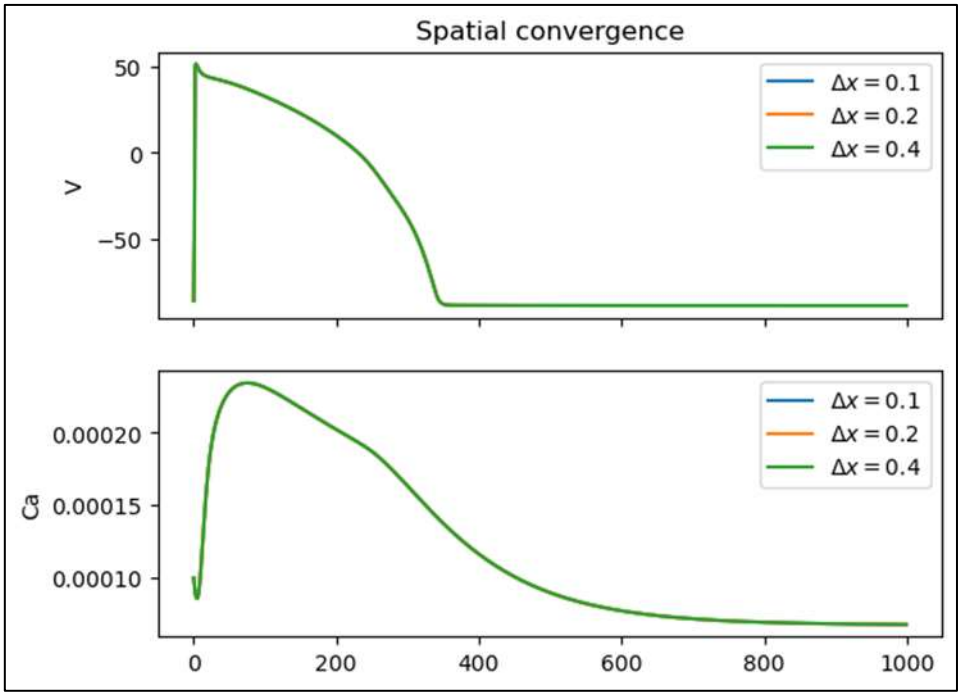

Figure 6: *Resulting traces of spatial convergence test.*

2.1.2 Temporal Convergence Test

We ran the same benchmark using three different time steps, namely 0.1 ms, 0.05 ms and 0.025 ms and used a spatial discretization of 0.2 mm. Results are shown inTable 3 and Figure 7.

Table 3: Model details and biomarkers in spatial convergence test.

Feature	dt = 0.025 ms	dt = 0.05 ms	dt = 0.1 ms
import time	4.590256e-07	4.590256e-07	4.590256e-07
create runner time	6.209884	7.505218	6.057917
solve time	142.5939	79.85127	46.45854
APD40	241.384	240.4079	238.2046
APD50	267.4623	266.7946	265.315
APD90	333.9916	333.8508	333.5371
triangulation	91.95933	92.78771	94.66245
Vpeak	50.48862	51.11934	52.51387
Vmin	-88.02136	-88.02138	-88.0214
dvdt max	144.29	144.1165	143.8713
maxCa	0.0002351415	0.0002344468	0.0002329743
ampCa	0.0001676838	0.0001669904	0.0001655207
CaTD50	306.5283	306.8837	307.62
CaTD80	438.9012	439.279	440.0477

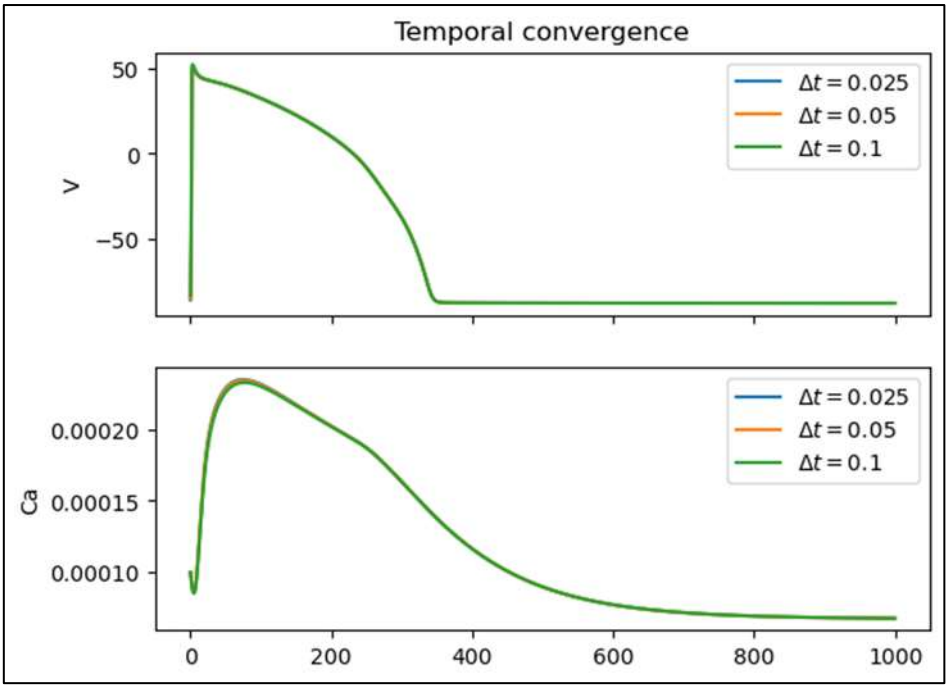

Figure 7: *Resulting traces of temporal convergence test.*

2.2 Numerical Solver Error

N.A. - Users in IST platform will not be able to change the settings for the solver and default values will be used.

2.3 Use Error

Simcardems performs checks to make sure that input parameters from the user are valid. If the input is not valid, the software will display an error. The IST platform will limit the input option even further. Clients will interact with the graphical user interface implemented in the IST platform, in which typographical errors are controlled more automatically to warn the user in case of input error.

3. Conclusion

This document is an annex of SimCardioTest deliverable D6.1, and reports technical details relative to the verification of the 3D numerical model developed for Use Case 3. General conclusions relative to the verification of UC3 numerical model are reported in main deliverable D6.1.

4. Bibliography

[1] Finsberg and others, "simcardems: A FEniCS-based cardiac electro-mechanics solver," *Journal of Open Source Software,* vol. 8(81), no. DOI: https://doi.org/10.21105/joss.04753, p. 4753.

[2] "simcardems," [Online]. Available: https://computationalphysiology.github.io/simcardems/install.html.

[3] "Computationalphysiology github - simcardems," [Online]. Available: https://computationalphysiology.github.io/simcardems.

[4] "GIST hosting convergence tests," [Online]. Available: https://gist.github.com/finsberg/73fa6531f28da2b3633a7ddaca38a7cd.

[5] Balay, Satish and others, "PETSc.," 2001. [Online]. Available: http://www.mcs.anl.gov/petsc.

[6] Logg, Anders, Mardal and others, Automated solution of differential equations by the finite element method: The FEniCS book. Vol. 84, Springer Science & Business Media, 2012.

[7] Niederer, Steven and others, "Verification of cardiac tissue electrophysiology simulators using an N-version benchmark," *Philosophical Transactions of the Royal Society A: Mathematical, Physical and Engineering Sciences,* vol. 369.1954, pp. 4331-4351, 2011.

[8] Land, Sander and others, "Verification of cardiac mechanics software: benchmark problems and solutions for testing active and passive material behaviour," *Proceedings of the Royal Society A: Mathematical, Physical and Engineering Sciences,* vol. 471.2184, no. 20150641, 2015.

[9] "Computational Physiology - ap_features," [Online]. Available: https://github.com/ComputationalPhysiology/ap_features.

This project received funding from the European Union's Horizon 2020 research and innovation program under grant agreement No 101016496

EU Horizon 2020 Research & Innovation Program
Digital transformation in Health and Care
SC1-DTH-06-2020
Grant Agreement No. 101016496

SimCardioTest - Simulation of Cardiac Devices & Drugs for in-silico Testing and Certification

SIM CARDIO TEST

Technical Annex

Annex A – WP6 complement of D6.1 and D6.2 Technical Reports on Verification, Validation and Uncertainty Quantification for the Use Cases of WP2-4

(Tasks 6.1 and 6.2 – covering M30-M54)

Work Package 6 (WP6)

Verification, validation, uncertainty quantification & certification

WP Lead: MPC, France

PUBLIC

ANNEX A INFORMATION

Annex title	**WP6 complement of D6.1 and D6.2 Technical Reports on Verification, Validation and Uncertainty Quantification for the Use Cases of WP2-4 (Tasks 6.1 and 6.2 – covering M30-M54)**
Description	Report of additional verification, validation and uncertainty quantification activities conducted during M30-M54 period for the different Use Cases (pacing leads, LAAO and drug safety and efficacy)
Lead authors	Romano SETZU (MPC)
Contributors	For UC1 (WP2): Yves COUDIERE, Michael LEGUEBE, Delphine DESHORS (UBx) For UC2 (WP3): Oscar CAMARA, Andy OLIVARES (UPF) For UC3 (WP4): Beatriz TRENOR, Maria Teresa MORA (UPV)
Due date	M54
Submission date	30/06/2025
Comments	-

Document history			
Date	**Version**	**Author(s)**	**Comments**
29/04/2025	V1	R. SETZU	First Draft
30/06/2025	V2	R. SETZU, M. LEGUEBE, A. OLIVARES, M. T. MORA	First consolidated draft including contributions from UC1/2/3
30/07/2025	V4	R. SETZU	Final Version

TABLE OF CONTENTS

EXECUTIVE SUMMARY

This annex summarizes all verification, validation, and uncertainty quantification (VVUQ) activities conducted in the frame of work-package WP6 after the consolidation of deliverables D6.1 and D6.2 in June 2023 (M30) till the end of the SimCardioTest Project in June 2025 (M54) for assessing the credibility of computational models developed within Use Cases 1 to 3 (cf. WP2, 3, and 4 respectively).

This annex is meant to be a self-contained stand-alone document, however, in order to fully comprehend the whole VVUQ activities conducted on the selected computational models since the beginning of the SimCardioTest project, it is recommended to review content of deliverable D6.1 and D6.2 first, as they are often referenced as propaedeutic to this document.

Acronyms

Table 1: List of Acronyms.

Acronym	Meaning
AF	Atrial Fibrillation
ASME	The American Society of Mechanical Engineers
Avg.	Average (abbreviation)
CEPS	Cardiac ElectroPhysiology Solver (cf. Use Case 1)
CFD	Computational Fluid Dynamic
CI	Continuous Integration
CiPA	Comprehensive in-vitro Proarrhythmia Assay (cf. Use Case 3)
COU	Context of Use
CT	Computer Tomography
DE	Discretization Error (in Verification)
DRT	Device-Related Thrombosis
EAB	Exponential Adams-Bashforth
ECG	Electrocardiogram
EP-0D	0D Electrophysiology Model (cf. Use Case 3)
EP-3D	3D Electrophysiology Model (cf. Use Case 3)
EXC	ExactCure
FBE	Forward-Backward Euler
FDA	US Food and Drug Administration
IST	INSILICOTRIALS TECHNOLOGIES SRL Also referring to the Cloud service hosting the models
LA	Left Atrium
LAAO	Left Atrial Appendage Occluder
MOTS	Modified Off-the-Shelf Software
MPC	MICROPORT CRM - SORIN CRM SAS
MV	Mitral Valve
N.A. / n.a.	Not Applicable
NCV	Numerical Code Verification

Acronym	Meaning
NSE	Numerical Solver Error (in Verification)
ODE	Ordinary Differential Equations
OTS	Off-the-Shelf Software
PIV	Particle Image Velocimeter
PK	Pharmacokinetics Model (cf. Use Case 3)
PR	Pulmonary Ridge
PSA	Pacing System Analyzer
PV	Pulmonary Vein
QI	**Question** of Interest
QoI	**Quantity** of Interest
RL	Rush Larsen
SCT	SimCardioTest
SQA	Software Quality Assurance (in Verification)
SRL	SIMULA RESEARCH LABORATORY AS
TAWSS	Time-Averaged Wall Shear Stress
TC	Test Condition (in Validation)
TdP	Torsade de Pointes
TS	Test Sample (in Validation)
UB / U.B.	Uncertainty Budget
UBx	Université de Bordeaux
UC	Use Case
UD	User Developed (Software)
UE	Use Error (in Verification)
UPF	UNIVERSIDAD POMPEU FABRA
UPV	UNIVERSITAT POLITECNICA DE VALENCIA
V&V, VV	Verification & Validation
VVUQ	Verification, Validation, and Uncertainty Quantification
WP	Work Package

Acronym	Meaning
WSS	Wall Shear Stress

Table 2: Table cell background colour-code used across the document to identify and differentiate VV40 items: Verification, Validation, Applicability.

Background Cell Colour-Code
"Light Green" for Verification Items
"Salmon" for Validation Items
"Light Blue" for Applicability Items

1. Introduction

This annex summarizes all verification, validation, and uncertainty quantification (VVUQ) activities conducted in the frame of work-package WP6 after the consolidation of deliverables D6.1 and D6.2 in June 2023 (M30) till the end of the SimCardioTest Project in June 2025 (M54) for assessing the credibility of computational models developed within Use Cases 1 to 3 (cf. WP2, 3, and 4 respectively).
This annex is meant to be a self-contained stand-alone document, however, in order to fully comprehend the whole VVUQ activities conducted on the selected computational models since the beginning of the SimCardioTest project, it is recommended to review content of deliverable D6.1 and D6.2 first, as they are often referenced as propaedeutic to this document.

1.1 Normative Background

Credibility assessment of computational models through VVUQ is paramount for gaining confidence on the models' ability to address the intended Question of Interest in the relevant Context of Use [1]. VVUQ activities on the selected computational models are conducted according to ASME VV40 standard [2]. ASME VV40 organizes the V&V activities in three distinct phases:

- Model Verification
- Model Validation
- Model Applicability

Model Verification comprises those activities meant to demonstrate that the numerical model accurately represents the underlying mathematical model. Model Validation comprises those activities meant to show how well the numerical model represents reality. Finally Model Applicability comprises those activities meant to show the relevance of validation activities to support the use of the numerical model in the selected context of use.
Each V&V activity listed in ASME VV40 addresses a specific credibility factor. All credibility factors contribute to the overall credibility of the numerical model. How well a credibility factor must be investigated depends on the model risk, intended as the result on the importance that the numerical model supposedly has in taking clinical decisions and the severity of clinical consequences in case the model leads to wrong decisions.

1.2 Global V&V Strategy

The selected models will address these specific aspects:

- For Use Case 1 (WP2): Pacing leads electrical performance
- For Use Case 2 (WP3): Left Atrial Appendage Occluders (LAAO) safety
- For Use Case 3 (WP4): Drugs safety

The following sub-sections present the V&V activities undertaken by each Use Case on the selected models.

1.2.1 Model Description

According to ASME VV40 guidelines, for each Use Case and for the selected numerical model the following key concepts are clarified:

- **Device/Drug Description**: the device or drug for which the numerical model is developed
- **Question of Interest**: the question concerning the device/drug safety/efficacy addressed by the selected numerical model

- **Context of Use**: the context in which the numerical model is used in the device/drug life cycle (e.g. device/drug design, validation, clinical use)
- **Model Risk**: the risk related to using the numerical model in the defined context of use

1.2.2 Model Verification

The purpose of Model Verification as intended by ASME VV40 is to demonstrate that the computational model numerical implementation is a robust and accurate representation of the mathematical model describing the phenomenon that the model aims to replicate.
Verification Credibility factors are grouped in two main areas:

- Code Verification
- Calculation Verification

Code Verification credibility factors are intended to demonstrate that the numerical model is developed and runs using robust software and hardware, and correctly implements the underlying mathematical equations which describe the model.
Calculation Verification credibility factors are intended to assess the numerical error associated with the numerical discretization of the mathematical problem, as well as with the implemented numerical solver strategy. In addition, this phase addresses how user errors are handled and possibly mitigated in both model inputs and outputs management.
Table 3 summarizes the Credibility Factors to be addressed in the frame of the computational model validation activities according to ASME VV40.

Table 3: Verification Credibility Factors (cf. ASME VV40).

Activity	Credibility Factor	VV40§
Code Verification	Software Quality Assurance Software functions correctly and gives repeatable results in a specified Hardware/Software environment. (OTS / MOTS / UD)	5.1.1.1
Code Verification	Numerical Code Verification - NCV Demonstrate correct implementation and functioning of algorithms. Compare to analytical solutions.	5.1.1.2
Calculation Verification	Discretization Error Run spatial/temporal grid sensitivity analysis	5.1.2.1
Calculation Verification	Numerical Solver Error Run solver parameters sensitivity analysis	5.1.2.2
Calculation Verification	Use Error [Verify I/O controls in place]	5.1.2.3

1.2.3 Model Validation

The purpose of Model Validation as intended by ASME VV40 is to demonstrate that the computational model provides reliable information about the real-life phenomena it wants to represent.
Validation Credibility factors are grouped in three main areas:

- Computational Model
- Comparator
- Assessment

Computational Model credibility factors are intended to fully describe and quantify the model ability to address its question of interest. Its form, properties and conditions are addressed, as well as its inputs. The investigation includes both sensitivity analysis and uncertainty analysis of these quantities (when applicable) meant to assess the model accuracy.
Comparator credibility factors are intended to fully describe and quantify the comparator(s) used for validating the computational model. Comparators may be of different nature depending on the nature of the numerical model: pre-existing clinical literature data, in-vitro comparators, pre-clinical (animal) or clinical data. There may be one or more comparators addressing different aspects of the numerical model under investigation. Comparator uncertainties are also investigated.
Assessment credibility factors are relative to the actual comparison of the numerical model with the selected comparator. Both inputs and outputs to the comparison are taken into account in this analysis.
Table 4 summarizes the Credibility Factors to be addressed in the frame of the computational model validation activities according to ASME VV40.

NOTE: when multiple items are given for a specific credibility factor, not all of them may be applicable to the numerical model under consideration. Each Use Case will select and justify the credibility factor items to be addressed.

Table 4: Validation Credibility Factors (cf. ASME VV40).

Activity	Credibility Factor	VV40§
Computational Model	Model Form: • Conceptual Formulation of Numerical Model • Mathematical formulation of Numerical Model Address 4 items: • Governing Equations (governing modeled phenomena) • System Configuration (Geometry of device/environment) • System proprieties (Bio. Chem. Phys. Properties) • System conditions (boundary & initial cond.)	5.2.1.1
Computational Model	Model Inputs Address 4 items: • Governing Equations Parameters (governing modeled phenomena) • System Configuration (Geometry of device/environment) • System proprieties (Bio. Chem. Phys. Properties) • System conditions (boundary & initial cond.) Quantification of Sensitivities Quantification of Uncertainties	5.2.1.2

Activity	Credibility Factor	VV40§
Comparator	Test Samples (TS) Address 4 items: • Quantity of TS • Range of Characteristics of TS • Measurements of TS • Uncertainty of TS measurements	5.2.2.1
Comparator	Test Conditions (TC) Address 4 items: • Quantity of TC • Range of TC • Measurements of TC • Uncertainty of TC measurements	5.2.2.2
Assessment	Equivalency of Input Parameters between Numerical Model and Comparator	5.2.3.1
Assessment	Output Comparison Address 4 items: • Quantity • Equivalency of Output Parameters • Rigor of Output Comparison • Agreement of Output Comparison	5.2.3.2

1.2.4 Model Applicability

The ultimate purpose of verifying and validating the numerical model is to gain confidence that the model outputs can be used to make predictions on the represented medical device/drug. However, the validation space (*in primis* the comparator selected for model validation) is a limited representation of the reality which the model aims to replicate.
ASME VV40 predicates an additional analysis, referred to as applicability, meant to assess the relevance of the engaged validation activities to support the use of the numerical model for the selected context of use.
Table 5 summarizes the Credibility Factors to be addressed in the frame of the computational model applicability assessment according to ASME VV40.

Table 5: Model Applicability (cf. ASME VV40).

Activity	Credibility Factor	VV40§
Applicability	Relevance of the Quantities of Interest QoI of Validation may be surrogate to the QoIs of COU	5.3.1
Applicability	Relevance of the Validation Activities to the COU Proximity of Validation Points to COU	5.3.2

1.2.5 Credibility Factors Coverage Level

According to ASME VV40, the model risk is the result of the combination of two factors:

- The ***Decision Consequence***: the clinical consequence of making a wrong decision based on a false prediction of the model

- The ***Model Influence***: the importance of the contribution of the model outcome in making clinical decisions, weighted amongst all other available inputs, such as available literature, design, in-vitro, pre-clinical and clinical information

Decision Consequence can be weighted as:

- **low**: an incorrect decision would not adversely affect patient safety or health, but might result in a nuisance to the physician or have other minor impacts
- **medium**: an incorrect decision could result in minor patient injury or the need for physician intervention, or have other moderate impacts
- **high**: an incorrect decision could result in severe patient injury or death, or have other significant impacts

Model Influence can be weighted as:

- **low**: simulation outputs from the computational model are a minor factor in the decision
- **medium**: simulation outputs from the computational model are a moderate factor in the decision
- **high**: simulation outputs from the computational model are a significant factor in the decision

Figure 1 gives a graphical representation of the Model Risk resulting from the combination of Decision Consequence and Model Influence.

Model influence	**high**	**3**	**4**	**5**
	medium	**2**	**3**	**4**
	low	**1**	**2**	**3**
		low	**medium**	**high**
		Decision consequence		

Figure 1: Model Risk Matrix (cf. ASME VV40).

Each of the credibility factors previously described may be investigated in several ways, each with a different level of investigation. The selected way of investigating each credibility factor may depend on several variables, such as complexity, available knowledge, or available means in the timeframe of this project.

ASME VV40 gives guidance on how to evaluate whether the credibility factors have been sufficiently investigated. For each credibility factor, a score varying from 1 to 5 is given to indicate how deeply the item has been investigated, where 1 means none or little investigation, and 5 means a thorough investigation. The scores are then compared to the model risk level as defined. Whenever a credibility factor coverage level does not match the risk level, a justification is given. This evaluation is summarized in a matrix as shown in Table 6.

Table 6: Credibility Factors Coverage Level (cf. ASME VV40). The model risk level is set to Medium (3) in this table for illustration purposes. The coverage level of the credibility factors is given an arbitrary score on a 1-to-5 scale for illustration purposes.

Model Risk					x		
Credibility Factor Coverage Level		1	2	3	4	5	
Code Verification: Software Quality Assurance	I			x			
Code Verification: Numerical Code Verification - NCV	I			x			
Calculation Verification - Discretization Error	II			x			
Calculation Verification - Numerical Solver Error	II			x			
Calculation Verification - Use Error	III			x			
Validation - Model [Form]	III			x			
Validation - Model [Inputs]	III			x			
Validation - Comparator [Test Samples]	IV			x			
Validation - Comparator [Test Conditions]	IV			x			
Validation - Assessment [Input Parameters]	IV			x			
Validation - Assessment [Output Comparison]	V			x			
Applicability: Relevance of the Quantities of Interest	V			x			
Applicability: Relevance of the Validation Activities to the COU	V			x			

2. Use Case 1

2.1 UC1 Model Summary

2.1.1 Background

The role of a cardiac pacing lead is to effectively stimulate the heart when it is deficient. Current pacemakers offer a wide range of stimulation pulse amplitudes and pulse durations to ensure that the therapy is effectively delivered. However, the higher the stimulation amplitude (and duration), the more energy is drained from the pacemaker battery, which can have an impact on the device longevity. When developing new leads, it is therefore important that the stimulation threshold remains in normal range.

2.1.2 Device Description

Medical devices addressed by the model are cardiac pacing leads. More precisely, their electrical behaviour, and interaction with the cardiac tissue is addressed.

2.1.3 Question of Interest

The Question of Interest addressed by the model is the following:

- What are the stimulation pulse characteristics (voltage amplitude in V and pulse duration in ms) required for a bradycardia lead in bipolar (tip/ring) mode to capture (stimulate) healthy cardiac tissue?

2.1.4 Context of Use

The computational model can be used to help pacing lead manufacturers when developing new products, providing information on the energy levels (pulse amplitudes and durations) required to successfully trigger action potentials and stimulate cardiac tissue.

2.1.5 Model Risk

The following considerations support the assessment of the risk associated with the numerical model.

- Decision Consequence: Low

An error in the model prediction may result in either an underestimation or an overestimation of the energy required to stimulate the cardiac tissue for a given pacing lead design. The clinician will adjust the energy in order to stimulate correctly. An overestimation of the energy by the model has no negative clinical influence on the delivered therapy, as it would result in an increase of the device battery life, which would actually be an unexpected benefit. An underestimation of the energy would have a minor clinical influence, as it would require the physician to increase the programmed therapy energy in order to achieve cardiac stimulation, resulting in a decrease of the expected battery life.

- Model Influence: Medium

Results of simulations with a new design will be systematically compared to those of previous well-established designs. In addition, pre-clinical and clinical data collected during the validation of the new lead design would contribute to corroborate the data provided by the models.

- Model Risk: 2/5 (Low-Medium)

Model Risk is based on Decision Consequence and Model Influence stated above, according to Risk Matrix in Figure 2 (cf. section 1.2.5).

Model influence	**high**	**3**	**4**	**5**
	medium	**2 COU**	**3**	**4**
	low	**1**	**2**	**3**
		low	**medium**	**high**
		Decision consequence		

Figure 2: *Model Risk Matrix (cf. ASME VV40) evaluating the COU included in UC1.*

2.1.6 Model Description

The model aims to reproduce capture threshold detection measurements that are performed ex vivo on a healthy ventricular wedge.

The model includes the tissue and the surrounding electrolyte, the pacing circuit of the device, and a contact model between the device and the tissue. Given a pulse duration and amplitude, it

computes the transmembrane voltage in the cardiac tissue, the electric potential in the tissue and electrolyte, as well as the voltage drops at the tip and ring electrodes.

Simulations are parametrized by:

- Contact properties between the leads and the tissue/electrolyte (modelled by parallel RC-circuits)
- The geometry of both the lead and computational domain
- Micro-structural description of the tissue and its electrical properties
- A model that describes ionic exchanges at the cell membranes

The contact properties are characterized by bench experiments. The geometry and microstructure of the tissue are obtained from 9.4T MR imaging. The shape of the lead is chosen among a family of designs, with the possibility of modifying several parameters (such as inter electrode distance, or radius). The ionic model is chosen from the standardized "cellML" database [3], with parameters adjusted from optical mapping data.
To compute an approximate solution of the model, we need a geometrical mesh of the domain, a spatial discretization scheme (e.g. P1 Lagrange Finite Elements), a time stepping method and an algorithm to solve large linear systems.

In Figure 3 we show the computation of the electric field created by the pacemaker in a slab of passive tissue, which will be the shape of the excitation of the cardiac tissue at the beginning of pacing.

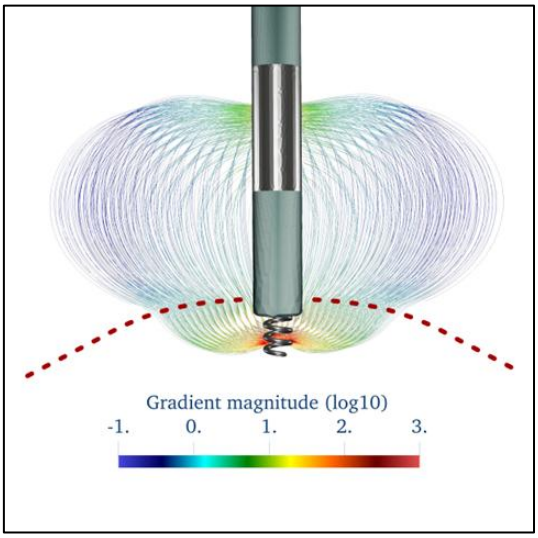

Figure 3: Electric field generated by a pacemaker lead, computed in a computational domain representing blood and a passive tissue, above and below the dotted line, respectively.

Computing the solution for various amplitudes and durations of stimulation allows to locate the so-called Lapicque curve, which is the threshold between capturing and non-capturing stimulations in the amplitude/duration plane (see Figure 4).

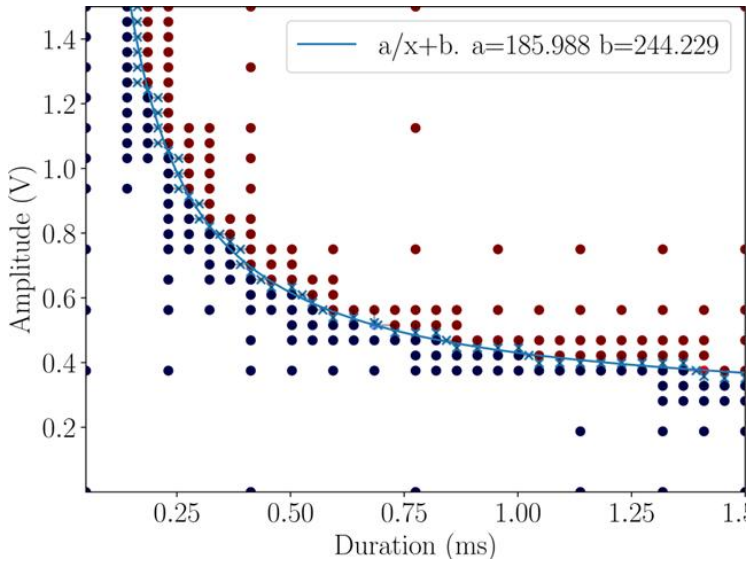

Figure 4: Lapicque Curve obtained from the solutions of an exploratory 0D model. For each blue/red point of the diagram, ie for each pair of amplitude and duration of stimulation, the model computes the response to 5 stimulations, and evaluates whether or not an action potential was triggered after each stimulation. Blue dots are for 0 out of 5 captures, red dots are for 5 out 5 captures.

2.2 UC1 Model Verification – M30-M54 Activities

This section only contains additional Verification activities conducted on UC1 selected computational model during the M30-M54 period. Verification activities conducted during the M1-M30 period are already reported in the UC1 section of deliverable D6.1. Results reported in this section are meant to complete or (in some cases) supersede results of deliverable D6.1. The latter case will be explicitly mentioned, when applicable.

The results presented in this section are focused on the accuracy of our in-house software CEPS, which is used to determine if a piece of cardiac tissue is stimulated by a pacemaker. In particular, we investigate the influence of the discretization of the mesh that represents the pacemaker lead and its surroundings, as well as the chosen time step. Then, we show the influence of the numerical parameters of the linear solver that is used in CEPS.

2.2.1 Discretization Error

2.2.1.1 CEPS Model

The problem which describes the stimulation of cardiac tissue in a bath by a pacemaker has discontinuity properties which prevent from applying standard numerical analysis theorems. In consequence, we present accuracy results on each of the constitutive elements of the problem. Namely, we report the convergence of the results for our implementation of the following items:

- ODE solvers for cardiac ionic models,
- Solvers for the monodomain, bidomain and bidomain-with-bath models which were proposed by Pathmanathan and Gray [4] and approved by the FDA for validation of cardiac electro-physiology software,

- Bidomain model with the Beeler-Reuter ionic model [5], which is used in our pipelines.

Discretization error for ionic models

Before coupling a reaction/diffusion equation to ionic models, we study the convergence of numerical solvers suited for such models. This is performed by suppressing any spatial component from the code. A dedicated executable can be compiled to this aim. CEPS includes several ionic models, which were imported from the CellML repository [3]. They consist of ODE systems for which there exists no fully determined analytic expression. In consequence, we compute a reference solution with a very small time-step and high-order numerical scheme. This reference is used to evaluate the difference with solutions computed with larger time steps and lower order numerical schemes. We report in **Figure 5** the convergence rates of the Forward-Backward Euler (FBE), Rush Larsen (RL) and Exponential Adams-Bashforth (EAB) time schemes, applied to some implemented ionic models (cf CEPS online documentation [1]and references therein). The error is measured in L2([0,100]) norm in time.

[1] CEPS Online Documentation: https://carmen.gitlabpages.inria.fr/ceps/

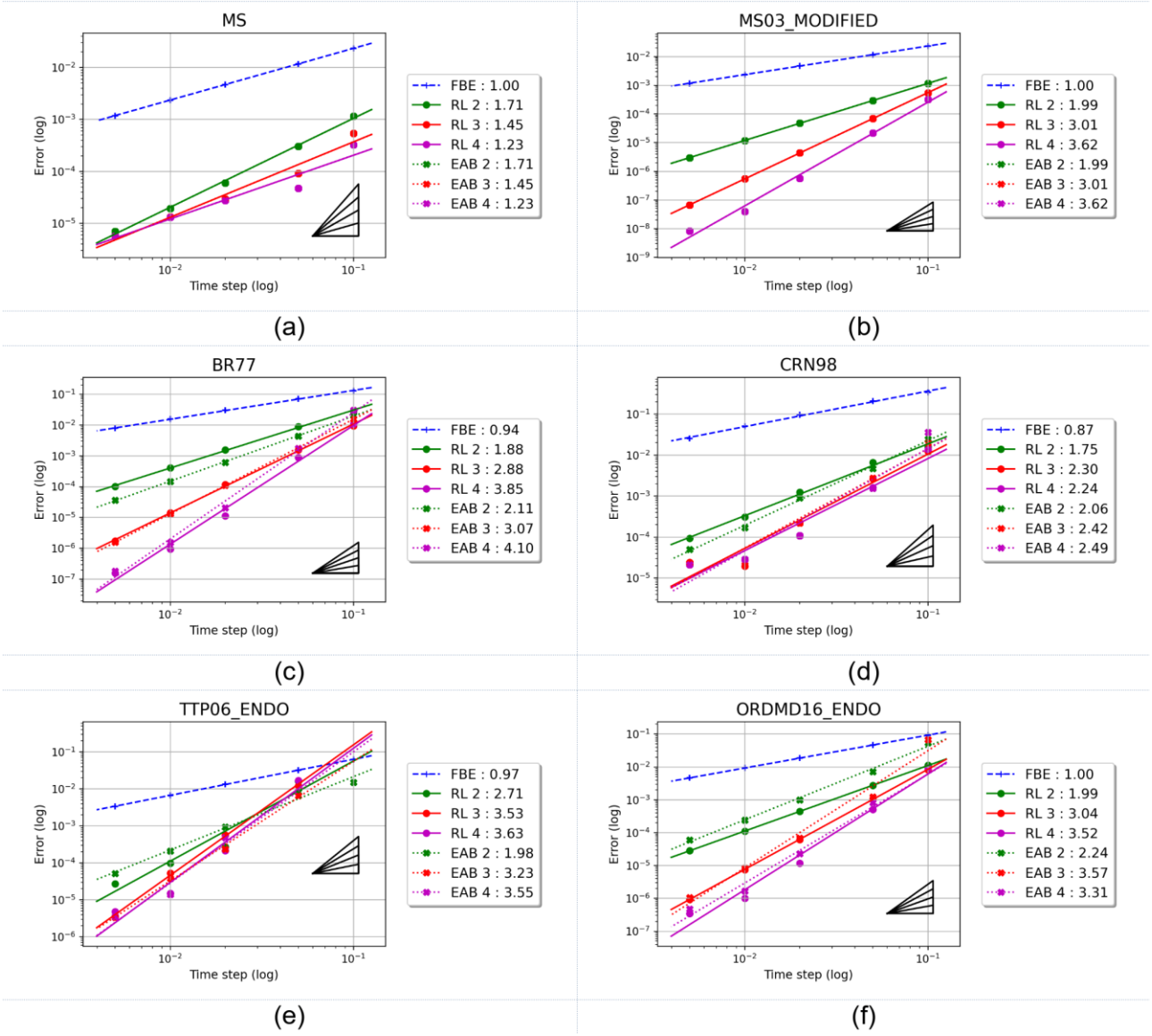

Figure 5: Convergence rates of Forward-Backward-Euler (FBE), Rush-Larsen(RL) and Exponential Adams-Bashforth (EAB) numerical solvers for different ionic models: Mitchell-Scheffer (a), regularized Mitchell-Scheffer (b), Beeler-Reuter (c), Courtemanche-Ramirez-Nattel (d), ten Tuscher-Panvilov (e) and modified O'Hara (f). Numbers in boxes indicate the slope of linear regressions for each set of points, i.e. the measured order of convergence.

Discretization error for the monodomain, bidomain and bidomain-with-bath models

Pathmanathan and Gray [4] introduced a collection of nine manufactured functions which are solutions to the monodomain, bidomain and bidomain-with-bath equations, in computational domains which are 1, 2 and 3 dimensional. The part of the solution that replaces the ionic model follows the same standard as the usual cardiac models. In consequence, the implementation in CEPS was relatively easy. In this document, we report the convergence results of CEPS for the 2D version of the three cardiac problems.

Numerical error is measured relatively to the analytic solution, with all combinations of the following norms:

- In time: value at final time t=1, $L^1([0,1])$ and $L^\infty([0,1])$,
- In space: $L^1(\Omega)$, $L^2(\Omega)$ and $L^\infty(\Omega)$.

Linear solver parameters are set to 10^{-12} for relative and absolute tolerances (cf section 2.2.2.1 for the definition of these parameters). The physical parameters of the model, namely conductivities, membrane capacitance and surface, are set following the instructions given in the FDA verification instructions. Unfortunately, the "ionic" part of this model does not allow to use the ODE solvers that take advantage of the specific form of evolution equations for ionic gate variables. The tests can only be performed with the usual "semi-implicit backward differentiation formula" (SBDF) time schemes for the ionic part.

Given a collection of meshes and time steps, the errors are computed for all combinations of mesh size and time steps. For multi-steps methods, such as SBDF, we replace the result of the first iterations by the analytic solution in order to measure the actual accuracy of the methods, and not that of lower order methods that are used for those first steps. When the fit the errors as the maximum of two linear functions (in log), in both space and time directions. We illustrate this fitting process in **Figure 6**, for the bidomain problem, solved with first order polynomial Lagrange finite elements combined with the SBDF time scheme of order 2. The fitted convergence rates are reported in Table 7, Table 8 and Table 9 for the 2D-monodomain, 2D-bidomain and 2D-bidomain-with-bath problems, respectively.

The convergence rates are in agreement with the numerical methods that were selected. However, order 4 in time is not reached for the SBDF 4 + P2 solver. We identified two reasons. Firstly, our selection of meshes and time steps resulted in errors that were dominated by the error in space for all but three data points. Therefore, the automatic fit leads to loose estimates of the convergence rate. Secondly, our solver is not completely written as a SBDF scheme. At each time step, the ionic current is evaluated explicitly instead of implicitly, to reduce significantly computation time. This adaptation of the numerical scheme comes with a slight loss of accuracy.

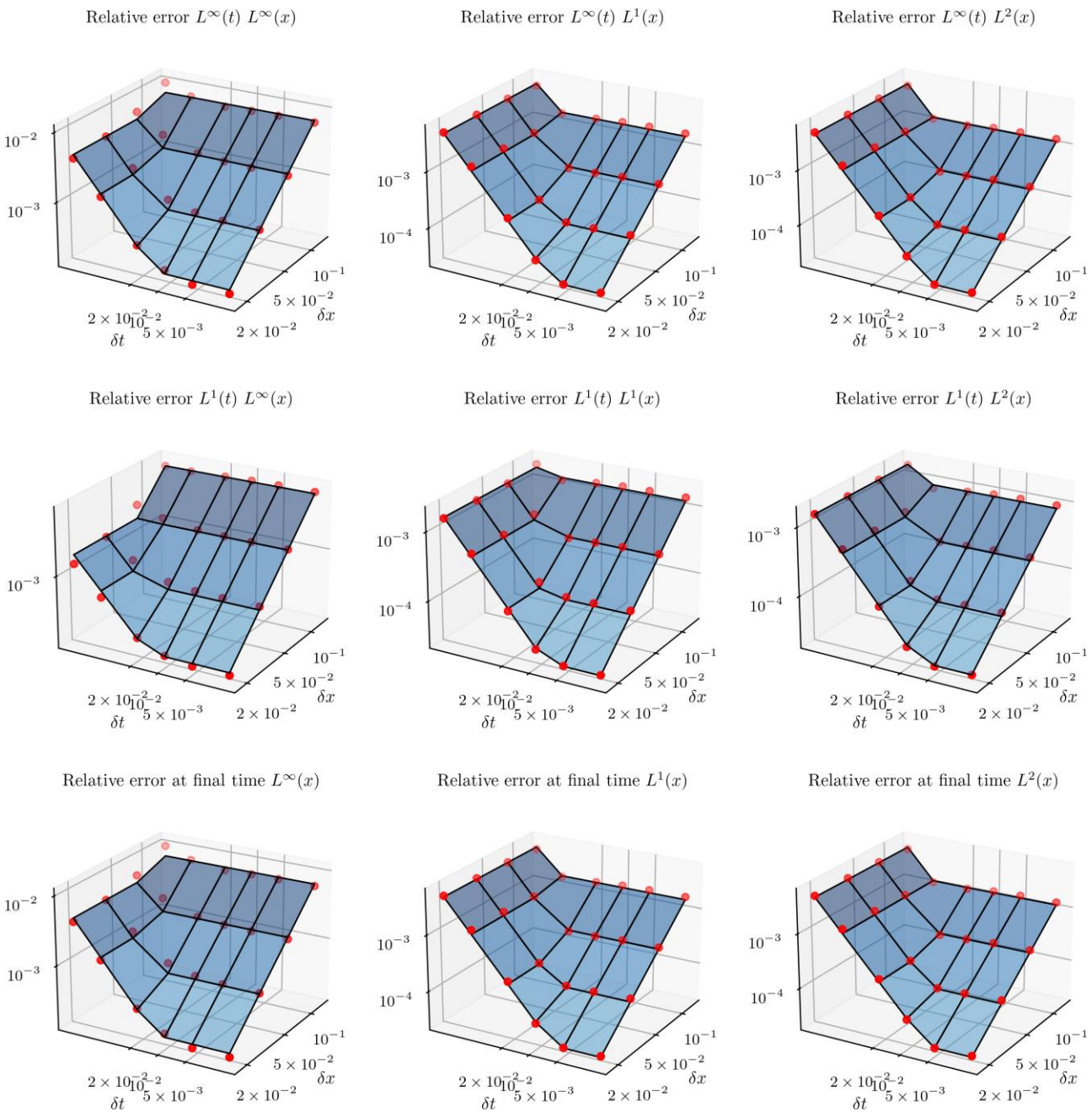

Figure 6: Numerical errors (red dots) with respect to the analytic solution of the manufactured bidomain with bath problem from Pathmanathan and Gray [4], solved with P1 finite elements and SBDF 2 time scheme. The blue surface is the fitted intersection of two planes in δx and δt directions, whose slopes determine the convergence order of the implementation of CEPS.

Table 7: Convergence rates of the 2D monodomain benchmark. Coefficients with stars indicate that no or too few points were generated to accurately measure the convergence rate.

	P1 – SBDF2	P1 – SBDF2	P2 - SBDF4	P2 - SBDF4
Norm	**Spatial cv. rate**	**Time cv. rate**	**Spatial cv. rate**	**Time cv. rate**
$L^\infty([0,1]), L^\infty(\Omega)$	1.86	1.40	2.82	2.16*
$L^\infty([0,1]), L^1(\Omega)$	1.95	1.67	3.22	3.45*
$L^\infty([0,1]), L^2(\Omega)$	1.96	1.67	3.27	3.56*
$L^1([0,1]), L^\infty(\Omega)$	1.78	1.18	2.83	1.07*
$L^1([0,1]), L^1(\Omega)$	1.90	1.35	3.10	2.91*
$L^1([0,1]), L^2(\Omega)$	1.91	1.35	3.11	3.07*
at t=1, $L^\infty(\Omega)$	1.86	1.40	2.82	2.16*
at t=1, $L^1(\Omega)$	1.95	1.67	3.22	3.45*
at t=1, $L^2(\Omega)$	1.96	1.67	3.27	3.56*
Target rate	**2**	**2**	**3**	**4**

Table 8: Convergence rates of the 2D bidomain benchmark. Coefficients with stars indicate that no or too few points were generated to accurately measure the convergence rate.

	P1 – SBDF2	P1 – SBDF2	P2 - SBDF4	P2 - SBDF4
Norm	**Spatial cv. rate**	**Time cv. rate**	**Spatial cv. rate**	**Time cv. rate**
$L^\infty([0,1]), L^\infty(\Omega)$	1.85	1.72	2.88	2.15*
$L^\infty([0,1]), L^1(\Omega)$	2.03	1.62	3.08	3.42*
$L^\infty([0,1]), L^2(\Omega)$	2.01	1.67	3.09	3.52*
$L^1([0,1]), L^\infty(\Omega)$	1.79	1.39	2.86	1.03*
$L^1([0,1]), L^1(\Omega)$	1.94	1.46	3.02	2.87*
$L^1([0,1]), L^2(\Omega)$	1.95	1.47	3.00	3.03*
at t=1, $L^\infty(\Omega)$	1.85	1.72	2.88	2.15*
at t=1, $L^1(\Omega)$	2.03	1.62	3.08	3.42*
at t=1, $L^2(\Omega)$	2.01	1.67	3.09	3.52*
Target rate	**2**	**2**	**3**	**4**

Table 9: Convergence rates of the 2D bidomain with bath benchmark.

	P1 – SBDF2	P1 – SBDF2	P2 - SBDF4	P2 - SBDF4
Norm	**Spatial cv. rate**	**Time cv. rate**	**Spatial cv. rate**	**Time cv. rate**
L∞([0,1]), L∞(Ω)	1.79	1.60	2.88	2.98
L∞([0,1]), L1(Ω)	1.87	1.83	3.08	3.20
L∞([0,1]), L2(Ω)	1.81	1.82	3.09	3.24
$L^1([0,1]), L^\infty(\Omega)$	1.77	1.32	2.86	2.42

	P1 – SBDF2	P1 – SBDF2	P2 - SBDF4	P2 - SBDF4
Norm	**Spatial cv. rate**	**Time cv. rate**	**Spatial cv. rate**	**Time cv. rate**
$L^1([0,1]), L^1(\Omega)$	1.81	1.58	3.02	2.74
$L^1([0,1]), L^2(\Omega)$	1.68	1.56	3.00	2.78
at t=1, $L^\infty(\Omega)$	1.79	1.60	2.88	2.98
at t=1, $L^1(\Omega)$	1.87	1.83	3.08	3.20
at t=1, $L^2(\Omega)$	1.81	1.82	3.09	3.24
Target rate	**2**	**2**	**3**	**4**

Convergence of bidomain model with cardiac ionic model

In this section, we report the accuracy of CEPS when solving the bidomain equations, with a Beeler-Reuter ionic model, which is a usual computation of electrophysiology. Since there is no analytic solution for this problem, we compute numerical errors with respect to a reference solution. This reference is computed with a very fine time step and a high-order numerical scheme. We report in **Figure 7** the convergence towards this solution, for the $L^\infty([0,1]), L^2(\Omega)$ norm. Other norms yield similar results. The convergence rates are in accordance with the selected numerical method, with the exception of order 4 methods, for which we see a deterioration of the convergence rate, between 3 and 4.

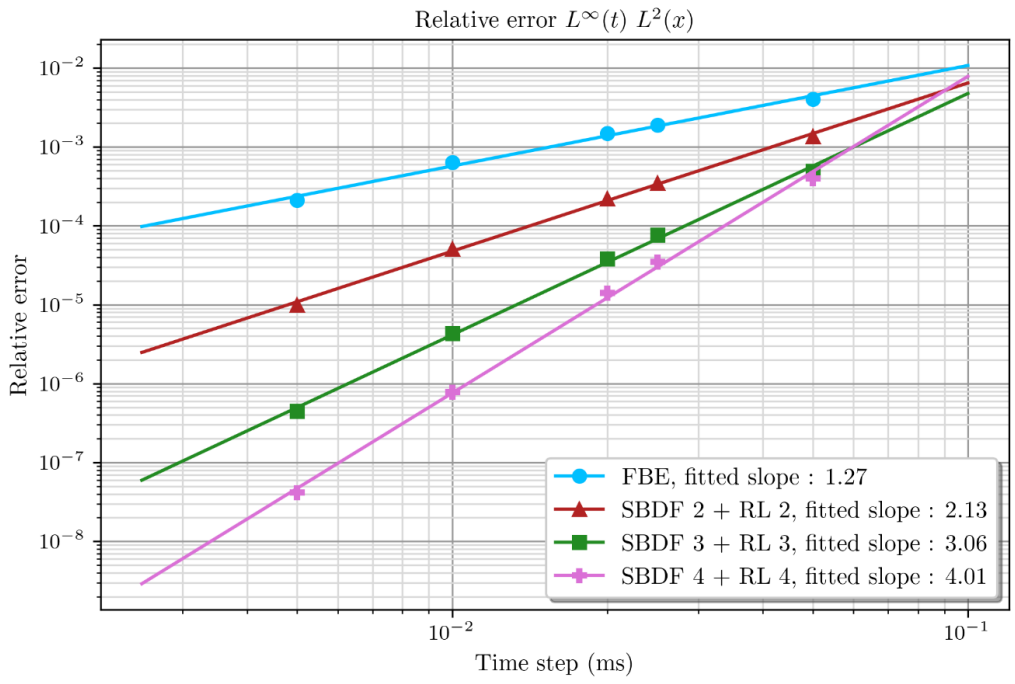

Figure 7: Numerical errors with respect to a reference solution, for the bidomain problem with Beeler-Reuter ionic model.

From each computation, be it the reference or the coarser ones, CEPS extracts the activation map, i.e. for each point of the computational domain, the time when the action potential is detected. On

Figure 8, we show that convergence of activation maps towards the reference map is at best of order 1. This is explained by the simplistic method that is used to detect when a point in tissue is activated.

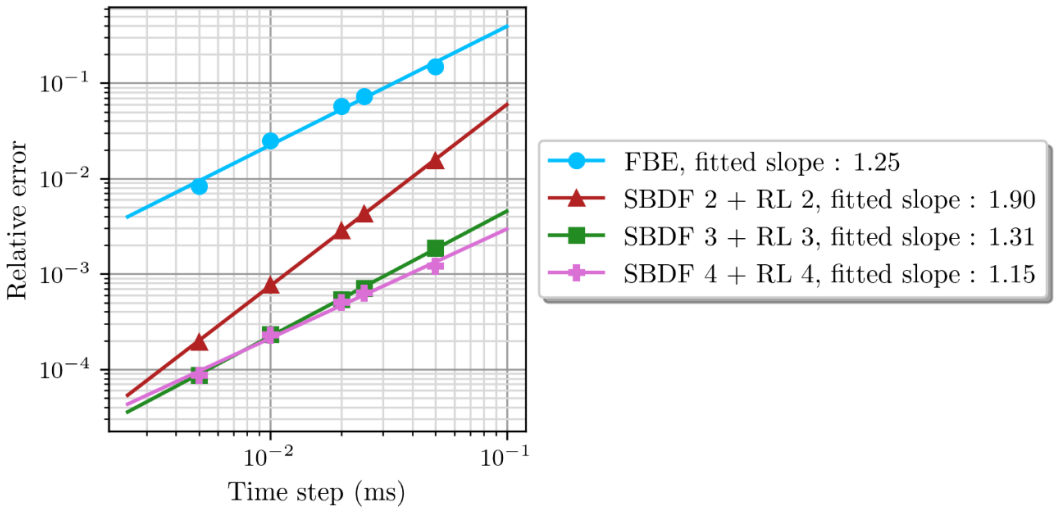

Figure 8: Convergence of activation maps for the bidomain problem with Beeler-Reuter ionic model. Error is measured with respect to the activation map extracted from a reference solution.

2.2.2 Numerical Solver Error

2.2.2.1 CEPS Model

In this section, we modify the few available parameters which tune the linear solver from the library PETSc [2], used by CEPS. We generally use either the Conjugate Gradient (CG), Stabilized Conjugate Gradient (BICGSTAB) or GMRES iterative solvers, as they allow computations in parallel. The stopping criterion used by PETSc is the following: $|r| < \max(\varepsilon_r|r_0|,\varepsilon_a)$, where r is the current residual of the linear system, r_0 is the residual at start, ε_r and ε_a are the relative and absolute tolerances that can be set from the CEPS input file, respectively. Additionally, a maximum number of linear solver iterations can be set. Reaching the maximum of iterations before convergence stops the program.

In this section, we check the influence of the linear solver parameters on the result of the bidomain with bath benchmark problem from section 2.2. Computations are run on a mesh of characteristic size 0.0125, using a SBDF 4 numerical scheme with a time step of 0.01.

[2] PETSc: https://petsc.org/

Error with respect to relative tolerance

ε_a is set to 10^{-20}, and the maximum number of iterations to 5 000. Errors are reported on **Figure 9**.

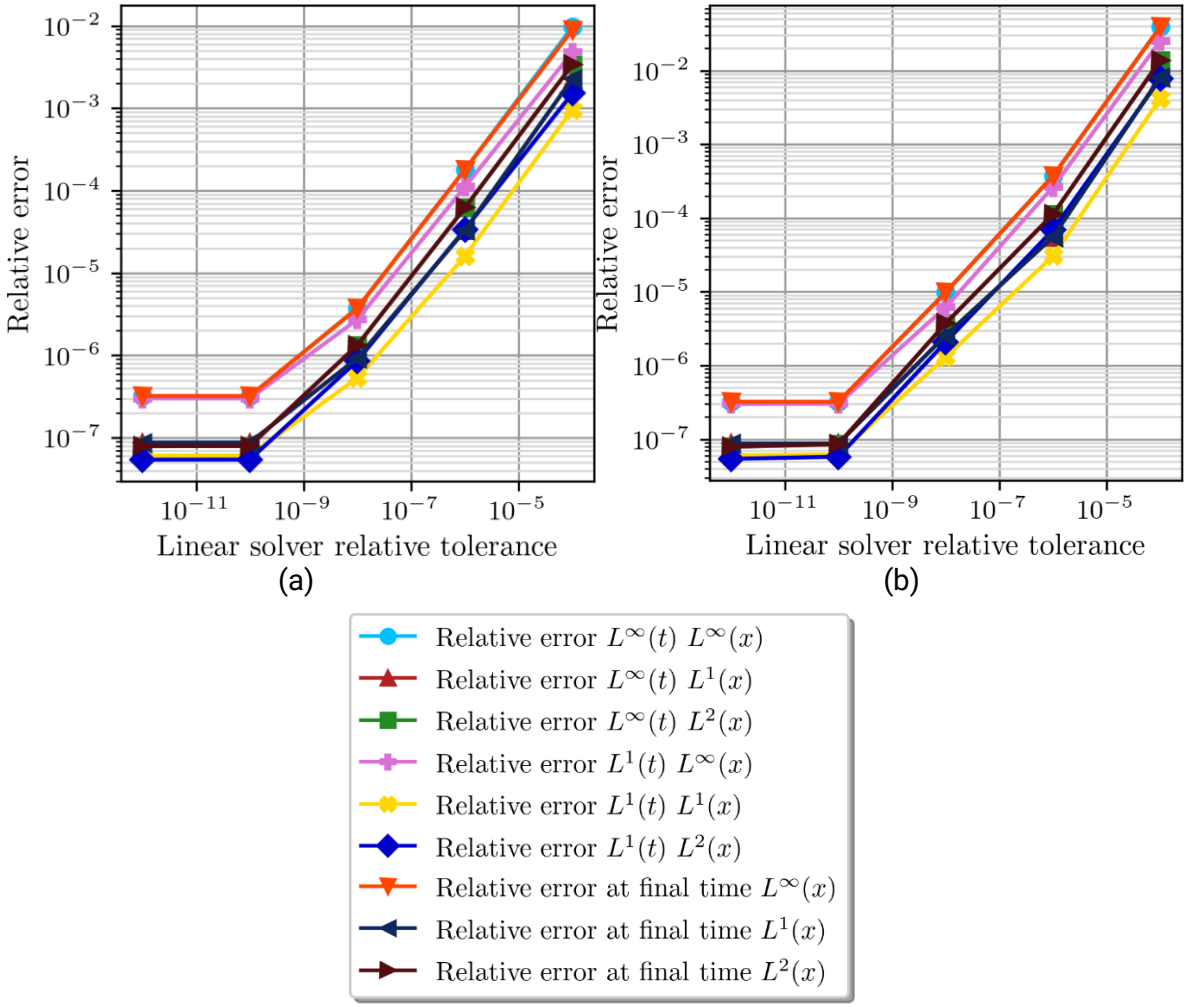

Figure 9: Errors with respect to relative tolerance of linear solver. Bidomain with bath problem, for the BICGSTAB (a) and GMRES (b) linear solver.

Error with respect to absolute tolerance

ε_r is set to 10^{-20}, and the maximum number of iterations to 5 000. Errors are reported on **Figure 10**.

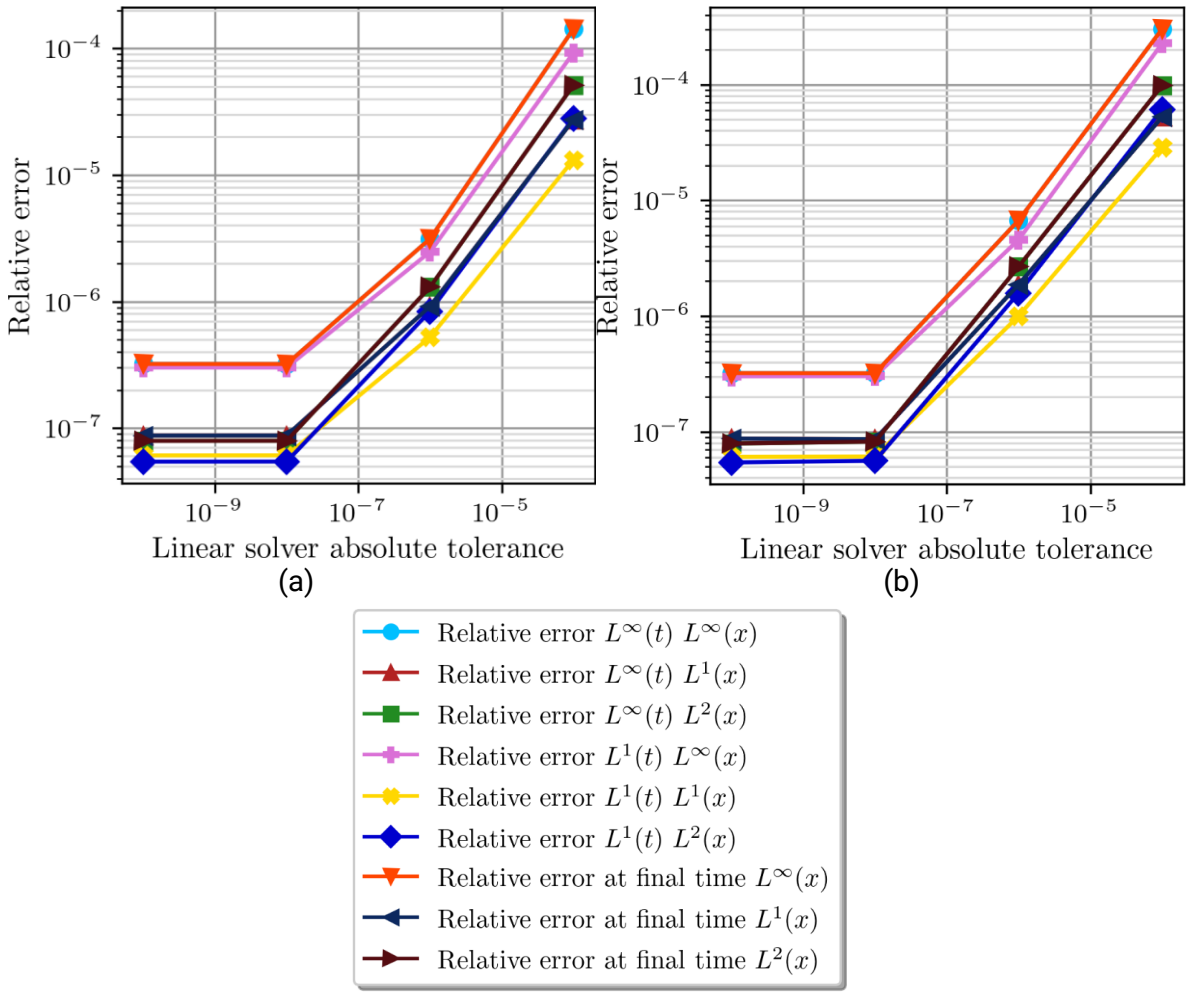

Figure 10: Errors with respect to absolute tolerance of linear solver. Bidomain with bath problem, for the BICGSTAB (a) and GMRES (b) linear solvers.

2.3 UC1 Model Validation – M30-M54 Activities

This section only contains additional Validation activities conducted on UC1 selected computational model during the M30-M54 period. Validation activities conducted during the M1-M30 period are already reported in the UC1 section of deliverable D6.2. Results reported in this section are meant to complete or (in some cases) supersede results of deliverable D6.2. The latter case will be explicitly mentioned, when applicable.

2.3.1 Computational Model Form

The 3D mathematical model that we derived to answer our QI consists of a partial differential equation which is well-known in the electrophysiology community (bidomain with bath), and an ordinary differential equation system that models the circuitry of the pacemaker. The two compartments are coupled via a boundary condition that depends on time, which is not standard for electrophysiology models. To validate our choice of model, we proved mathematically the existence and uniqueness of solutions to our problem, using a generic formalism for pacing devices. This proof is already given in V. Pannetier's PhD thesis [6], and will be submitted as a journal paper.

2.3.2 Computational Model Inputs

The computational model inputs were described in D6.2, UC1 section. The simulation run for model validation used the following additional specifications:

- Geometry of the VEGA lead provided by MPC, and a generic cylindrical domain encompassing the cardiac tissue and bath.
- The contact parameters have values obtained after experimental calibration (see deliverable D2.3), Table 10.
- The conductivity coefficients are taken from the literature, Table 10.
- Parameters from the literature are considered for the ionic model (Beeler-Reuter [5]).
- The initial conditions are set to the equilibrium state of the ionic model.

Table 10: Simulation parameters for the 3D computational model.

Parameter	Symbol	Value	Unit
PSA and contact parameters			
Pulse equivalent capacitance	C	4.97	µF
Opposite discharge equivalent capacitance	C	10.63	µF
Equivalent resistance	R	0.13	kΩ
Tip equivalent capacitance	C_0	18.74	µF
Tip equivalent conductance	G_0	0.5	mS
Ring equivalent capacitance	C_1	5.55	µF
Ring equivalent conductance	G_1	33.33	mS
3D model parameters			
Membrane surface per unit volume	X	2 500	cm
Extracellular conductivity, fiber direction	$\sigma_{e,l}$	3.91	mS cm^{-1}
Extracellular conductivity, transverse direction	$\sigma_{e,t}$	1.97	mS cm^{-1}
Intracellular conductivity, fiber direction	$\sigma_{i,l}$	1.74	mS cm^{-1}
Intracellular conductivity, transverse direction	$\sigma_{i,t}$	0.19	mS cm^{-1}
OD model parameters			
Membrane surface	S_m	15	cm^2
Surface extracellular conductance	g_e	$1.33\,10^{-3}$	mS cm^{-2}
Surface intracellular conductance	g_i	$3.33\,10^{-3}$	mS cm^{-2}

Complete sensitivity analysis was carried out for these contact parameters, and equivalent parameters in a surrogate 0D model (explained in deliverable D2.3), given also in Table 10. Computations with these parameters have been published [7], sensitivity analysis and statistical properties have been documented in deliverable D5.5 (cf. [6] and [8]).

2.3.3 Comparator Description

2.3.3.1 Comparator 1 – Lapicque Curve

We realized computational capture tests with the goal of reproducing experimental Lapicque curves [9].
Since 3D simulations are very expensive computationally, it is impossible to reproduce exactly the experiments that generated Lapicque curves. It is in particular impossible to use the same criterion to determine whether cardiac tissue is captured or not by the pacemaker. During the experiments,

capture is assessed with both an ECG and the expertise of our collaborator in electrophysiology. For 3D simulations, we consider a slab of tissue to be captured when we see an increase of the volume of "activated" tissue (i.e. for which the transmembrane voltage passes an activation threshold), during the first milliseconds after pulse delivery. We also ran simulations with a surrogate 0D model which is significantly less expensive. With this model, we can simulate all the consecutive experimental stimulations. Capture is then determined from the whole time-series of the transmembrane voltage of the in silico experiment.

2.3.4 Comparator – Test Samples

2.3.4.1 Comparator 1 – Lapicque Curve

Experimental Setup and Main Recordings

Cardiac ventricular wedges from sheep aged 1-2 years old were prepared as described in [10] and stretched on a frame to immobilize the tissue in a bath of saline solution **Figure 11** (left). The MICROPORT CRM VEGA bipolar pacing lead was implanted (fully deploying its screw fixture) at a maximum of three locations in the right ventricle (RV), among apex, septum and base, depending on the animal. It is implanted in the RV septum, as shown in **Figure 11**. A total of seven animals were used, including two with an induced infarct scar, Table 11. A pseudo ECG from distant electrodes, and the voltage between the ring to the tip electrodes of the lead were recorded simultaneously by an external device (PowerLab, ADInstruments). The measured voltage has a large deflection during pulses, which last 0.25 ms to 2 ms, as can be seen on **Figure 11** (top-right). We could record these fast events with a sufficient resolution of 100 kHz only for the last five animals.

Table 11: **Summary of animal experiments. The given number of stimulations is an estimate and does not exclude data that could not be used.**

N.	Date	Type	Implantation sites	Generator	Lead(s)	Camera Pixel count	Stim. freq. (BPM)	#stims
1	07/060/2022	healthy	apex	Borea	Vega	100	90	~100
	Pilot experiment. Noise from power outlets in measurements. The tissue slab was placed in the MR scanner in a folded position.							
2	08/11/2022	healthy	apex, base, septum	Borea	Vega	256	90	~320
	No MR scan.							
3	18/10/2023	healthy	apex, septum	Borea	Vega	256	90	~1500
	Ectopic beats with >90bpm frequency.							
4	04/06/2024	infarct	apex, mid	PSA	Vega	256	120	~1500
	Small scar, large moderator band.							
5	05/06/2024	healthy	apex, mid	PSA	Vega, Solia	192	120	~2000
	RAM issues (too much data), optical window was scaled down. Solia lead could not be tested at mid location due to tissue fatigue.							
6	06/06/2024	healthy	mid	PSA	Vega, Solia	192	120	~1000
	Two papillary muscles.							
7	07/06/2024	infarct	apex, mid	PSA	Vega	256	120	~1500
	Recurring ventricular tachycardia, lower signal to noise ratio in ECG. Lots of fat.							

Experimental Capture Test

Capture is detected by applying pulse trains of fixed duration D, and decreasing the voltage V from train pulse to train pulse, starting by capturing values until capture is lost. The actual threshold is located in the interval between the last value that captures V^c (D), and the first value that loses capture V_c (D). Capture occurs when an action potential has been triggered by the pulse, as observed on the pseudo ECG. **Figure 11** (top-right), shows such a transition from capturing (V^c = 0.5 V) to non capturing (V_c = 0.4 V), using trains of eight pulses of duration D = 1 ms at 1.5 Hz. As a consequence, the accuracy of the localization of the curve depends on the time and voltage resolution of the pulse generator. We report here capture data recorded with a Pacing System Analyzer (PSA) instead of a traditional pacemaker, because of its higher voltage and time resolution. Example experimental Lapicque curves obtained by this process with trains of eight pulses at 1 or 1.5 Hz are reported on **Figure 13**, where the coloured region are between the upper and lower bounds V^c and V_c. Data shows curves for several healthy implantation sites stimulated by the PSA, with recorded voltages at 100 kHz. For instance, for each of the 24 durations allowed by the PSA, searching for the threshold requires to pace the tissue 56 times on average (i.e. to test 7 amplitudes with trains of 8 pulses each). The total duration to obtain the Lapicque curve at a single site is around 30 min.

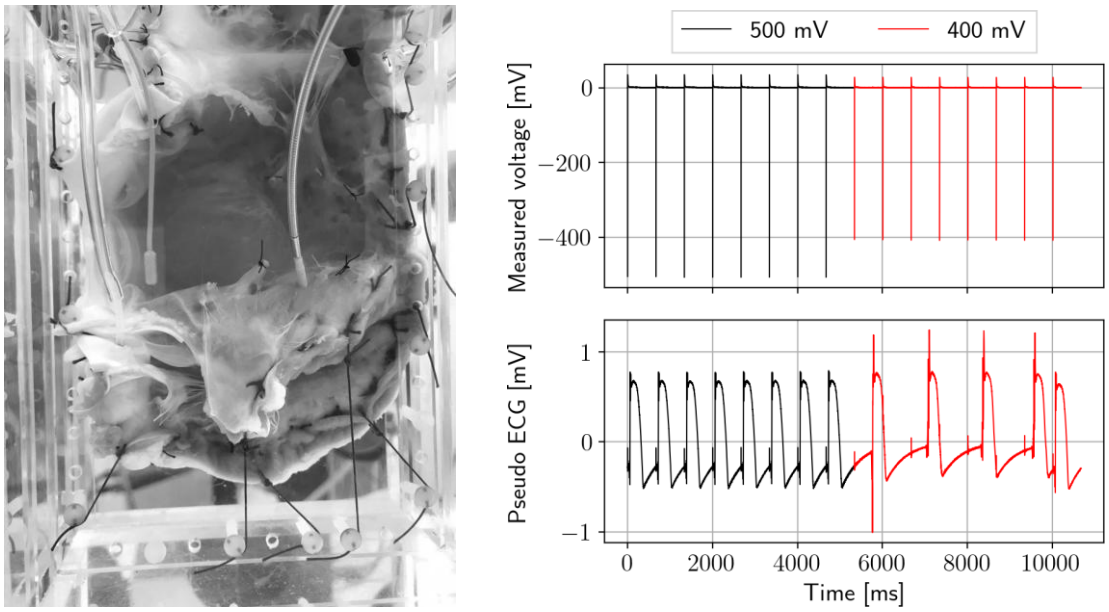

Figure 11: Photography of the tissue preparation in sheep heart #3 experiment (left), measured voltage at device pins (top-right), and the corresponding pseudo ECG recorded (bottom-right) during a threshold search, with a pulse duration of 1 ms. The pulses with amplitude of 0.4 V (in red) resulted in non-capturing stimulations. The action potentials in red are those of ectopic beats. This is deduced from their asynchronicity with the pacemaker stimulations, and corroborated with optical maps (not shown here).

2.3.4.2 Comparator 2 – Optical Map

In parallel of the capture tests described in the previous section, propagation of the action potential on the surface of the endocardium and epicardium were recorded for each sheep, using standard optical mapping techniques [10], as shown on **Figure 12** (left). Additionally, we imaged the structure of the tissue at high resolution using 9.4T MR, for the sheep #4 to 7. We do not have the images of sheep #1 to 3 as they were used to alleviate the technical difficulties of the procedure. An example of the segmentation of the ventricle of sheep #4 is given on **Figure 12** (right). As shown, the ventricle was put back into its resting state in order to fit into the small bore of the MR machine. Unfortunately, this prevents us from comparing directly experimental activation maps with simulated ones, which can only be computed on the folded ventricle mesh. The deformation is too large to project activation data onto the mesh.

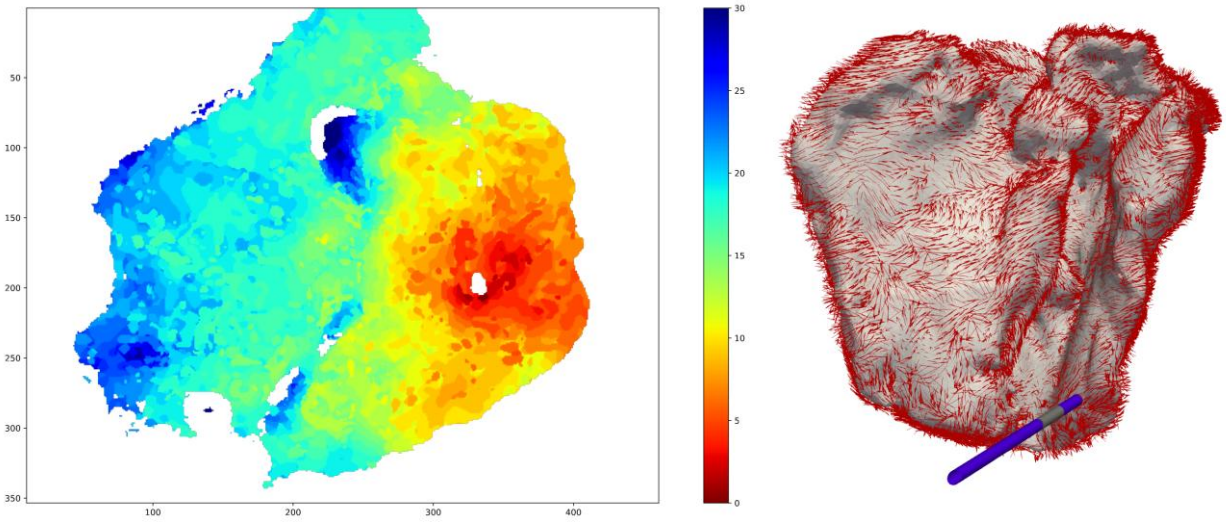

Figure 12: Left: endocardial activation map obtained from sheep #1 experiments. Right: segmented mesh from sheep #4, with fibre direction imported from the MR sequences. The pacemaker lead has been added to the mesh.

2.3.5 Output Comparison

2.3.5.1 Comparator 1 – Lapicque Curve

The Lapicque curves obtained with both models are reported in **Figure 13**, as well as some curves from the sheep experiments. The threshold curves vary significantly, even for the same animal. This variability can be explained by the variability between animals, the tissue structure at the implantation sites, by uncertainty on the insertion depth, and by the degradation of the myocardium during an experiment that lasts several hours. Our model has not been calibrated yet, and hence cannot explain these variations. However, simulations provide curves with a profile similar to the experimental ones, and with the correct order of magnitude, even with standard parameters. This semi-quantitative agreement is encouraging for the forthcoming work of calibrating the models to this data.

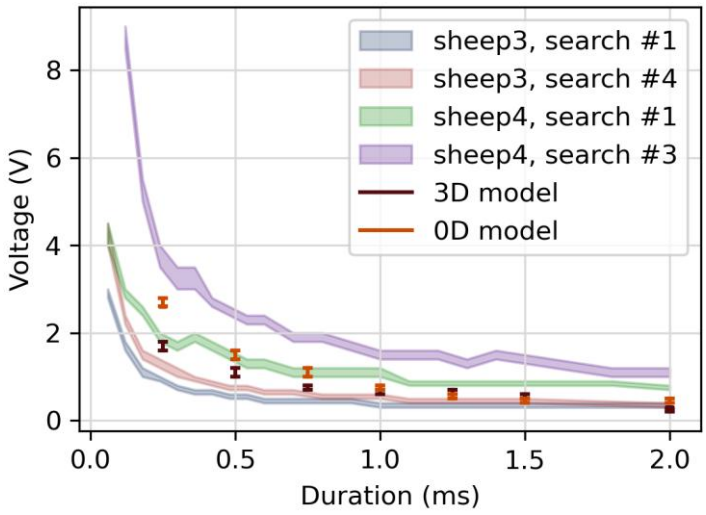

Figure 13: Experimental stimulation threshold detection intervals (filled), for two out of seven sheep ventricles. Search numbers indicate different implantation sites. Intervals marked with brackets are from the computational models.

2.4 UC1 Uncertainty Quantification – M30-M54 Activities

No additional specific Uncertainty Quantification (UQ) activities were conducted during M30-M54 in the frame of UC1 model credibility assessment. Uncertainty Quantification results and discussion in deliverable D6.2 apply. Moreover, sensitivity analysis results and statistical studies detailed in deliverable D5.5 provide a first analysis of the effect of some sources of uncertainty, notably the device parameters and conductivity coefficients.

2.5 UC1 Model Applicability – M30-M54 Activities

No additional specific Model Applicability activities were conducted during M30-M54 in the frame of UC1 model credibility assessment. Applicability discussion in deliverable D6.2 apply.

2.6 UC1 Discussion

We have been able to entirely execute the verification activities initiated in deliverable D6.1, and even add additional verification activities, e.g. running the FDA tests on manufactured solutions. The validation activities have been carried out, and we obtained satisfactory results for comparator 1 (Lapicques curves) with biological parameters (ionic ones, and tissue conductivity) from the literature.

Comparator 2 (optical maps) could not be setup for technical reasons: the deformation of the tissue sample between optical ex-vivo experiments and final post-mortem structure imaging is too large for standard registration tools to apply, so that the comparison was not possible. The computational software code has been delivered to IST for integration on the web-based platform, where verification tests will be also executed to ensure that the integrated model performs ad intended, and that the integration process did not affect the numerical outcome and the credibility level of the model.

A complementary statistical analysis has been carried out and has been explained in deliverable D5.5. It tends to show that a deterministic comparator, like comparator 1, badly accounts for the high variability across biological samples. This is especially true for capture, because it is a threshold, so that it probably follows a Bernoulli law, with a bimodal distribution of the output. In the context of threshold detection, a goal-oriented statistical comparator would be more relevant. For instance, comparing the probability of capture at one (or a few) relevant points of the Lapicque plane would be of interest. Finally, this issue concerning the comparison methodology is a known bias of ASME V&V40 approach, as also discussed in deliverable D6.4.

Table 12: Credibility Factors Coverage Level for Use Case 1 (cf. ASME VV40).

Model Risk				x			
Credibility Factor Coverage Level		1	2	3	4	5	
Code Verification: Software Quality Assurance	V		x				
Code Verification: Numerical Code Verification - NCV	V		x				
Calculation Verification - Discretization Error	V		x				
Calculation Verification - Numerical Solver Error	V		x				
Calculation Verification - Use Error	IV		x				
Validation - Model [Form]	III		x				
Validation - Model [Inputs]	III		x				
Validation - Comparator [Test Samples] [3]	II		x				
Validation - Comparator [Test Conditions]	II		x				
Validation - Assessment [Input Parameters]	III		x				
Validation - Assessment [Output Comparison]	II		x				
Applicability: Relevance of the Quantities of Interest	V		x				
Applicability: Relevance of the Validation Activities to the COU	V		x				

2.7 UC1 – VVUQ Publications

This section lists all scientific publications relating to the UC1 VVUQ activities conducted within the frame of the SimCardioTest project.

Table 13: UC1 – List of publications related to VVUQ activities.

Reference	VVUQ Topic
Pannetier et al. (FIMH 2025) [7]	Validation
Pannetier et al. (FIMH 2023) [9]	Validation
Pannetier et al. (CANUM 2024) [11]	Validation

[3] Initially set to "Level IV", the coverage level for the Validation - Comparator [Test Samples] credibility factor has been decreased to "Level II" to account for all the technical difficulties encountered during the real experiments and the fact that one animal intended for the validation died before testing (thus diminishing the initial sample size). The new coverage level is still sufficient to cover the assessed model risk.

Reference	VVUQ Topic
Pannetier (PhD) [6]	Validation, Verification, Uncertainty Quantification
Pannetier et al. (CINC 2024) [8]	Uncertainty Quantification
Pannetier et al. (VPH 2024) [12]	Validation
Leguèbe (draft) [13]	Verification

3. Use Case 2

3.1 UC2 Model Summary

3.1.1 Background

Atrial fibrillation (AF) is considered the most common of human arrhythmias. AF is currently seen as a marker of an increased risk of stroke since it favours thrombus formation inside the left atrium (LA). Around 99% of thrombi in non-valvular AF are formed in the left atrial appendage (LAA) [14]. LAA shapes are complex and have a high degree of anatomical variability among the population [15]. Percutaneous left atrial appendage occlusion (LAAO) can be an efficient strategy to prevent cardioembolic events in selected non-valvular AF patients, as an alternative to life-long oral anticoagulation (OAC) [16], as shown in large clinical trials (ACP Multicentre [17], EWOLUTION [18]), where LAAO procedures demonstrated non-inferiority. However, a successful implantation of LAAO devices remains a challenge in some cases, due to the complexity of LA geometry. Sub-optimal LAAO settings can lead to device-related thrombosis (DRT), i.e., a thrombus formed at the device, becoming a major concern [19] since it can lead to stroke. Based on the Virchow's triad, three factors are thought to contribute to thrombus formation: hypercoagulability, endothelial injury (replaced by a nitinol surface after LAAO) and blood stasis [20]. Related to the latter, key hemodynamic factors with demonstrated influence in thrombus formation in LAAO include (see Figure 14):

1. Occluder design and position: The geometry and characteristics of the occluder device can impact the flow patterns in the left atrium. Different occluder designs, such as shape, size, and surface properties, can influence the likelihood of thrombus formation. The position and alignment of the occluder within the left atrium can affect the flow patterns and the likelihood of thrombus formation. For instance, covering the pulmonary ridge (see Figure 15) may have a protective effect regarding DRT. Studying different occluder positions can help determining the optimal placement to minimize the DRT risk.

2. Blood flow velocity: Areas with low flow velocity or regions of recirculation may be prone to stasis and clot formation.

3. Blood viscosity: Altering the viscosity can provide insights into how changes in blood composition or conditions, such as hematocrit or temperature, affect thrombus formation. Parameters related to blood coagulation, such as platelet activation or coagulation cascade dynamics, can be simulated to understand their impact on thrombus formation.

4. Wall shear stress: Wall shear stress is the frictional force exerted by the flowing blood on the atrial wall. Low wall shear stress regions can be associated to thrombus formation. Evaluating different wall shear stress levels can help identify critical areas. Wall injuries due to abnormal stresses can also be caused by the device deployment.

To avoid blood stasis, it is crucial to properly choose the type of device and the position where the device is going to be deployed. Thus, different planning tools has emerged to find the optimal device configuration for each patient such as the commercial products from FEOPS [21] and Pie Medical [22], or the VIDAA platform [23], developed by UPF. However, none of these solutions include functional information on blood stasis, which is key for assessing the risk of DRT. In-silico computational fluid dynamic (CFD) can help to describe and relate patient-specific LA/LAA morphology and complex hemodynamics to understand the mechanism behind thrombus formation. Moreover, computational models of the blood flow can be used to predict the effectiveness of LAAO devices, to evaluate new device designs, and to better understand clinical outcomes such as DRT.

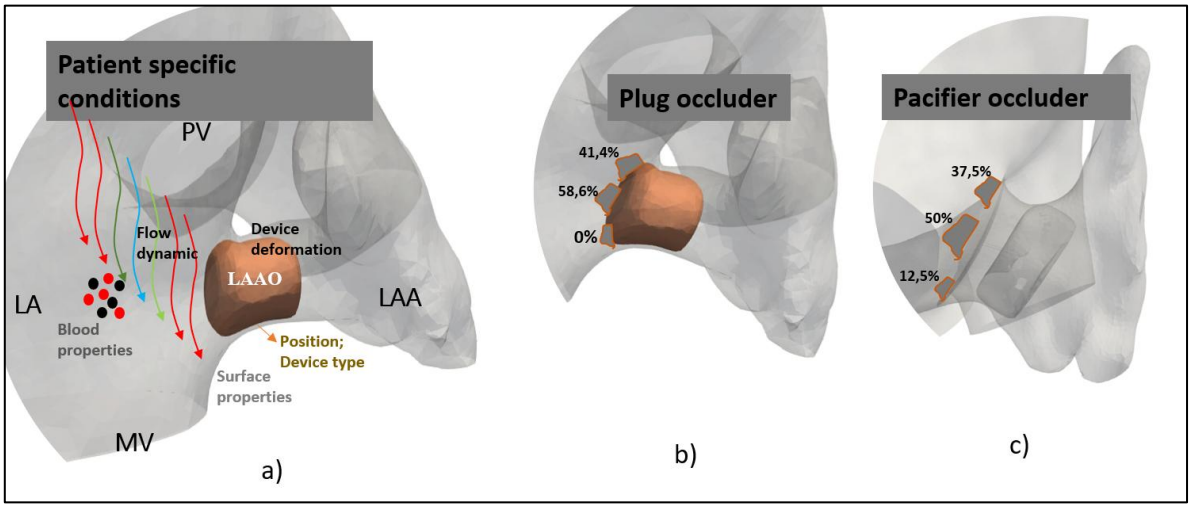

Figure 14: a) Principal factors associated to thrombus formation, including blood properties, device type and positioning. b,c) Percentages of device-related thrombus (DRT) in different parts of the device, reported in Sedaghat et al. [19] for the plug- and pacifier-type of occluder devices (b and c, respectively). LAAO: left atrial appendage occluder. MV: mitral valve. PV: pulmonary veins.

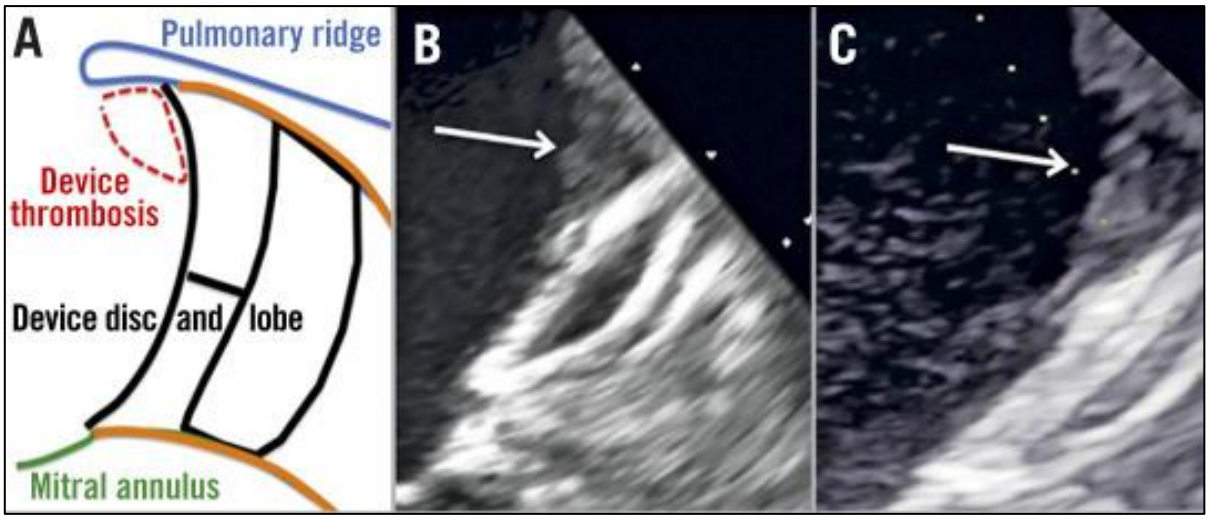

Figure 15: Influence of covering the pulmonary ridge (PR) for avoiding device-related thrombosis, from Freixa et al. ***[24].*** *The arrows point to uncovered PR where thrombus is found after left atrial appendage occluder implantation.*

3.1.2 Device Description

Left atrial appendage closure devices (see Figure 16) are used to reduce the risk of stroke in patients with atrial fibrillation by occluding or sealing off the left atrial appendage, which is a small pouch-like structure in the heart where blood clots can form. Here are two commonly used device types:

1. Plug-Type Devices
   - Plug-type left atrial appendage occluders are designed to completely seal off the left atrial appendage (LAA). These devices typically consist of a self-expanding frame or mesh structure that fills and completely occludes the LAA, preventing blood flow into the appendage. The frame or mesh is often covered with a fabric or membrane material to enhance closure.
   - The Watchman device is an example of a plug-type occluder. It is developed by Boston Scientific, and it is a fabric-covered, self-expanding nitinol frame with fixation barbs. It is delivered through a minimally invasive procedure and placed in the left atrial appendage to block blood flow, thereby preventing blood clots from forming and potentially causing a stroke.

2. Pacifier-Type Devices
   - Pacifier-type left atrial appendage occluders, as the name suggests, partially occlude the LAA while allowing some blood flow to continue. These devices have a central channel or opening that allows limited blood flow through the LAA while reducing the risk of blood clot formation. This design is intended to maintain some physiological flow patterns and potentially reduce the risk of complications associated with complete occlusion.
   - The Amplatzer Amulet device is an example of a pacifier-type occluder. It is manufactured by Abbott and it consists of a self-expanding nitinol frame covered with a permeable polyester fabric. Similar to the Watchman, it is implanted in the left atrial appendage to close it off and reduce the risk of stroke.

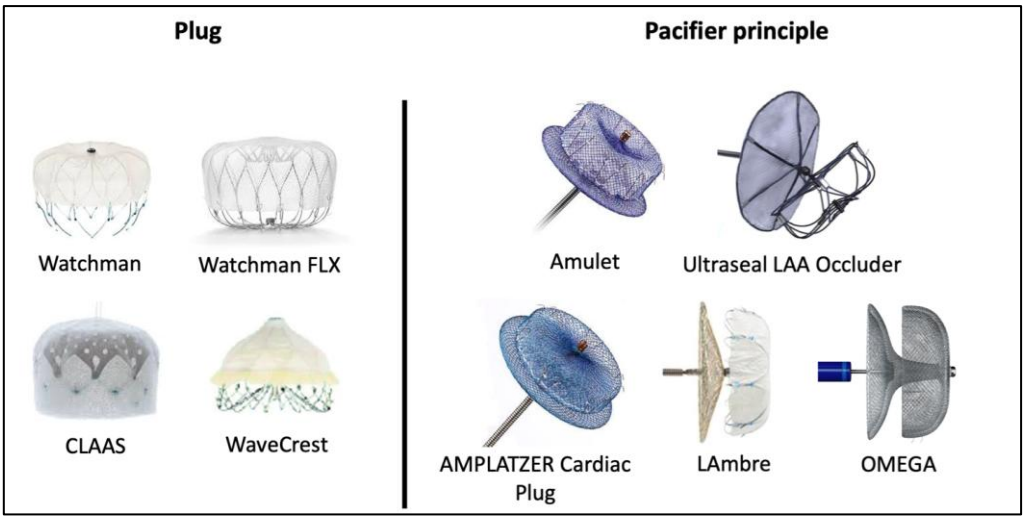

Figure 16: Types of left atrial appendage devices, classified as plug or pacifier types. The most used devices are the Watchman and Watchman FLX (plug-type), developed by Boston Scientific (left), and the Amplatzer Amulet device (pacifier-type), manufactured by Abbott (right).

3.1.3 Question of Interest

Several relevant questions of interest (QI) can be answered by computational fluid simulations applied to left atrial appendage occluder devices, encompassing different aspects of the device design and applicability. The different stakeholders involved in SimCardioTest, including device manufacturers, clinicians and academic partners defined multiple QIs during the project, which were ranked based on the most critical aspects to study in relation to possible adverse events during the implantation, especially regarding DRT. The QI that had the maximum level of priority and feasibility, being selected to guide the V&V exercise of Use Case 2 according to ASME VV40 guidelines, is the following:

- Does covering of the pulmonary ridge with a LAAO device (plug or pacifier) relate with the likelihood of low blood flow velocities around the device and induce the device-related thrombus (DRT)?

The QI above follows the formulation found in pioneering V&V works on cardiac devices [25] and studies the influence of device settings (type and position) in relation to DRT by measuring low blood flow velocities.

3.1.4 Context of Use

From the selected QI, two different Contexts of Use (COU), assessing the device performance, were defined. These COUs have different level of influence on the decision of whether the covering of the pulmonary ridge (PR) with the LAAO device is equivalent to or better than placing it deeper into the LAA (i.e., with an uncovered PR). In both cases, the computational model is used to assess blood flow velocities near the device. The performed evaluations are based on two different cohorts, depending on the COU. In the first COU, pre-operative and follow-up imaging data from twenty patients who underwent LAAO has been used, half of them suffering DRT. The second COU is based on a set of two patient-specific geometries obtained from clinical cases: one suffer from AF, and the other acts as a control case.

- **COU1** - Performance evaluation with computational fluid simulations only. Computational modelling is used to identify low blood flow velocities near the device, placed in a proximal or distal position (e.g., covering or not the PR) with both device types (i.e., plug and pacifier). There is no supporting data from in-vitro testing available for assessing the performance of the occluder devices.

- **COU2** - Performance evaluation with computational fluid simulations and in-vitro data. In addition to in-silico experiments, in-vitro testing is conducted to create additional evidence on whether the covering of the PR is critical for DRT with both types of device.

3.1.5 Model Risk

The following considerations support the assessment of the risk associated with the numerical model.

- Decision Consequence: Medium

Based on VV40 guidelines, both COUs have a Medium consequence since the intended users are engineers from manufacturers, using computational fluid simulations and in-vitro testing experiments to optimize the design of next-generation occluder devices and provide better implantation guidelines to prevent DRT. If simulations and experiments are incorrect (i.e., under- or over-estimating the risk of DRT), they could lead to sub-optimal design of new devices and recommendations, potentially increasing abnormal events after implantation such as device embolization, DRT or peri-device leaks.

- Model Influence for COU 1: High
- Model Influence for COU 2: Medium

Based on VV40 guidelines, COU1 has a High influence because the computational model results are the only ones informing the decision. COU2 has a Medium influence because supporting data from in-vitro testing complement the computational modelling studies.

- Model Risk for COU 1: 4/5 (Medium-High)
- Model Risk for COU 2: 3/5 (Medium-Medium)

Model Risk is based on Decision Consequence and Model Influence stated above, according to Risk Matrix in Figure 17 (cf. section 1.2.5).

Model influence	**high**	**3**	**4 COU1**	**5**
	medium	**2**	**3 COU2**	**4**
	low	**1**	**2**	**3**
		low	**medium**	**high**
		Decision consequence		

Figure 17: Model Risk Matrix (cf. ASME VV40) evaluating the COU1 and COU2 included in UC2.

3.1.6 Model Description

Simulating blood flow in the left atrium with an implanted occluder device can indeed facilitate the identification of the parameters that may contribute to thrombus formation. By conducting blood flow simulations with the occluder device in place, researchers can explore the impact of various factors, such as the shape or position of the device, on flow characteristics and the potential for thrombus formation. The initial step involves processing patient-specific medical images to extract a three-dimensional model, followed by the building of an appropriate 3D volumetric mesh. In COU1, for each left atrial geometry, the two studied device positions (covering and uncovering the pulmonary ridge) have been previously defined. In COU2, fluid simulations from two patients are compared with an in-vitro setup. The blood flow magnitude and directions will serve as the primary parameters evaluated in the current V&V study, for detecting blood stagnation zones around the LAAO device.

As a previously required step for VV40 analysis of flow simulations with LAAO devices, verification and validation experiments to assess the credibility of blood flow simulations in the left atria without a device are also required. In SimCardioTest, we performed the largest VV40 study available in literature for such type of simulations, testing several numerical parameters in mesh and time-step convergence analysis, as reported in SCT deliverable D3.2, and recently published [26]. This study contributed to identify most of the numerical parameters to be used in fluid simulations of the left atria. The rest of the document will mainly focus on the complementary VV40 experiments performed on simulations including LAAO devices.

3.2 UC2 Model Verification – M30-M54 Activities

No additional specific Verification activities were conducted during M30-M54 in the frame of UC2 model credibility assessment. Verification results and discussion in deliverable D6.2 apply.

3.3 UC2 Model Validation – M30-M54 Activities

This section only contains additional Validation activities conducted on UC2 selected computational model during the M30-M54 period. Validation activities conducted during the M1-M30 period are already reported in the UC2 section of deliverable D6.2. Results reported in this section are meant to complete or (in some cases) supersede results of deliverable D6.2. The latter case will be explicitly mentioned, when applicable.

3.3.1 Comparator – Test Conditions and Validation Results from the In-Vitro Set-Up developed in MIT

As we mentioned in deliverable D6.2, one of the most important advantages of the in vitro experimental set-up developed by MIT is the ability to include left atrial movement, thereby differentiating between movements for patients with atrial fibrillation and healthy atrial movements. The motion generated from the placement of actuators along these key regions, guided by fibre orientation, was validated through M-mode ultrasound imaging (**Figure 18**a). The input pressure for these actuators was systematically varied from 0 to 40 psi to assess the range of wall displacement. Ultrasound imaging (**Figure 18**b) confirmed the effectiveness of individual actuators in producing tunable wall motion. These results demonstrated that the actuators could reliably replicate both

healthy and AF contractile behaviour. This biomimetic contractile motion can support the ejection of blood from the LA and LAA and prevent stagnation, critical for reducing thrombus formation in healthy physiology.

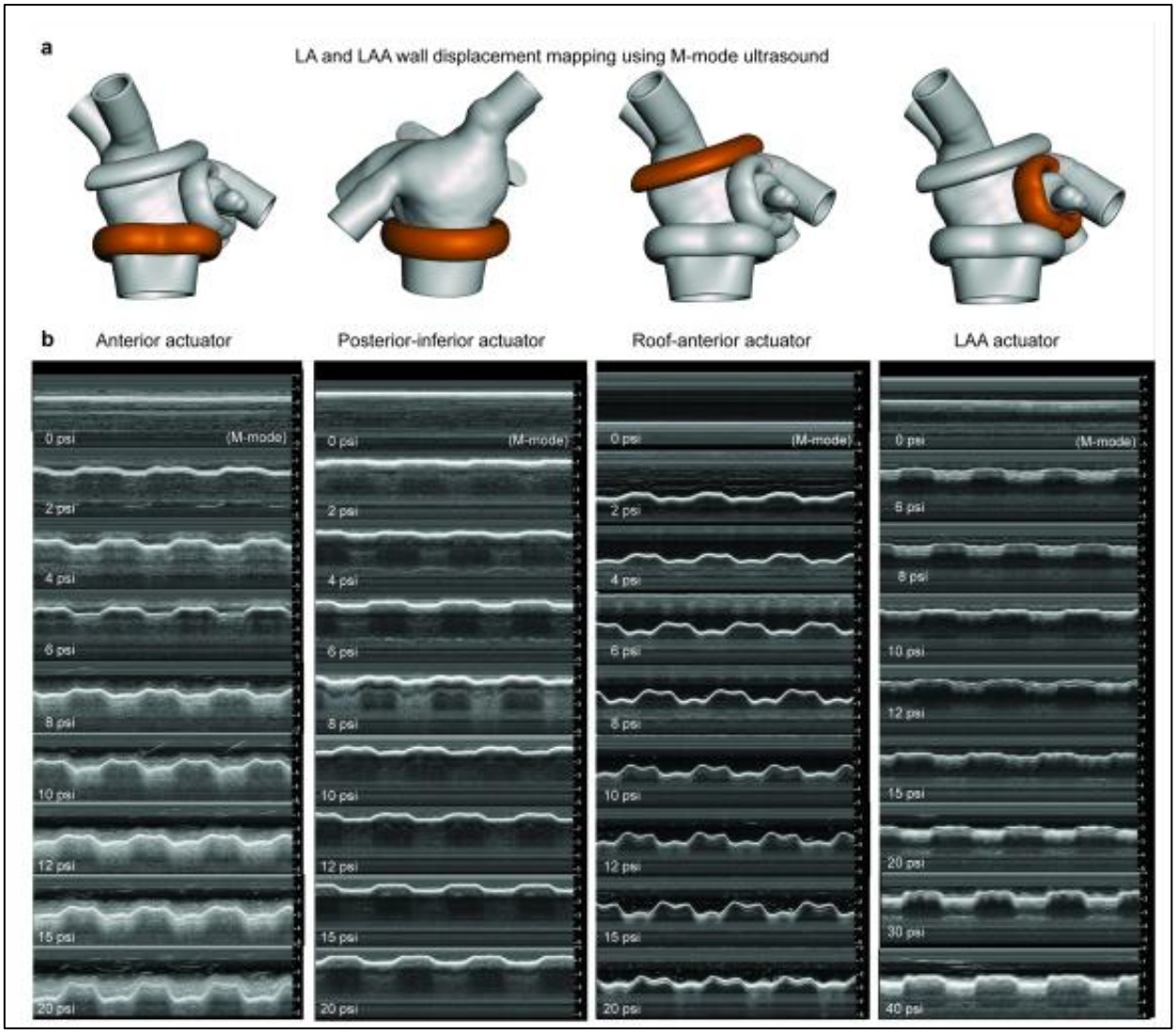

Figure 18: Soft robotic actuator positioning influences left atrium (LA) and left atrial appendage (LAA) wall motion and displacement under varying pressures. (a) Different configurations of soft robotic actuators wrapped around the LA and LAA structures at distinct anatomical orientations (highlighted in orange), impacting the extent of wall motion and direction of simulated atrial contraction. (b) M-mode ultrasound images capturing wall displacement at increasing actuator pressures ***[27]****.*

The circulatory flow loop developed by MIT was specifically designed to simulate systemic circulation, incorporating adjustable parameters such as preload, afterload, vascular compliance, and resistance (**Figure 19**). The system utilized two clinically standard mechanical valves (mitral and aortic) to ensure unidirectional flow through the circuit, with the soft robotic LV functioning as the primary pump to drive fluid flow. The actuation of soft robotic elements on the LA and LAA successfully replicates the atrial kick, a dynamic contraction crucial for active ventricular filling, which cannot be achieved with passive 3D-printed models. The soft robotic LV generated biphasic

ventricular pressures (120/6 mmHg) and drove systemic circulation, producing phasic aortic systemic pressures of 115/60 mmHg at a sinus rhythm of 60 bpm. When combined with the soft robotic LA, the system reproduced physiologically accurate flow waveforms for left-sided circulation. The system demonstrates alternating mitral and aortic flow, with a cardiac outflow of over 5 L/min. The mitral valve flow waveform exhibited distinct E and A wave regions, representing passive ventricular filling during early diastole and active filling driven by atrial contraction, respectively. These findings confirm the capability of the soft robotic LA to contribute to active ventricular filling, mimicking the functional role of atrial contraction in the cardiac cycle. Pulsed wave Doppler imaging was used to measure fluid flow velocities in the soft robotic LA, visualizing E and A wave patterns associated with mitral flow.

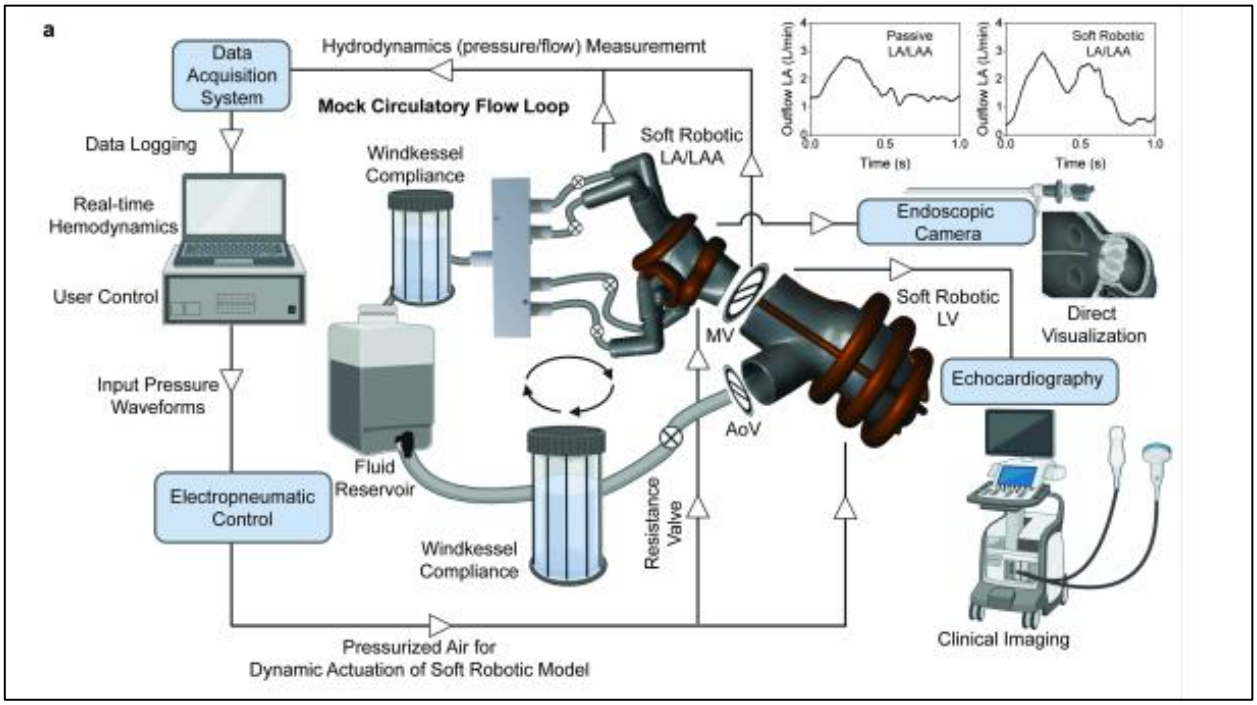

Figure 19: A mock circulatory flow loop enables hemodynamic measurements in the soft robotic left heart simulator. (a) Schematic of the mock circulatory flow loop with components to replicate cardiac and vascular hemodynamics, including the soft robotic left atrium (LA) left atrial appendage (LAA), and left ventricle (LV) models. The circuit includes mechanical mitral valve (MV) and aortic valve (AoV) components, which are essential for simulating unidirectional flow [27].

Figure 20 shows the patient model used in the experiments, where an initial planning was performed using VIDAA software and then a mesh cut. The resulting geometry was 3D printed with the materials and technology described in previous deliverables. The locations where the measurements were acquired are marked in the figure; this proved to be relevant for comparison purposes. Therefore, results are shown with pulmonary vein lengths with normal dimensions and others with elongated dimensions that represent the area where the measurements were actually taken. The experimental and simulation results show better fits in the models with elongated veins, as shown in **Figure 21**.

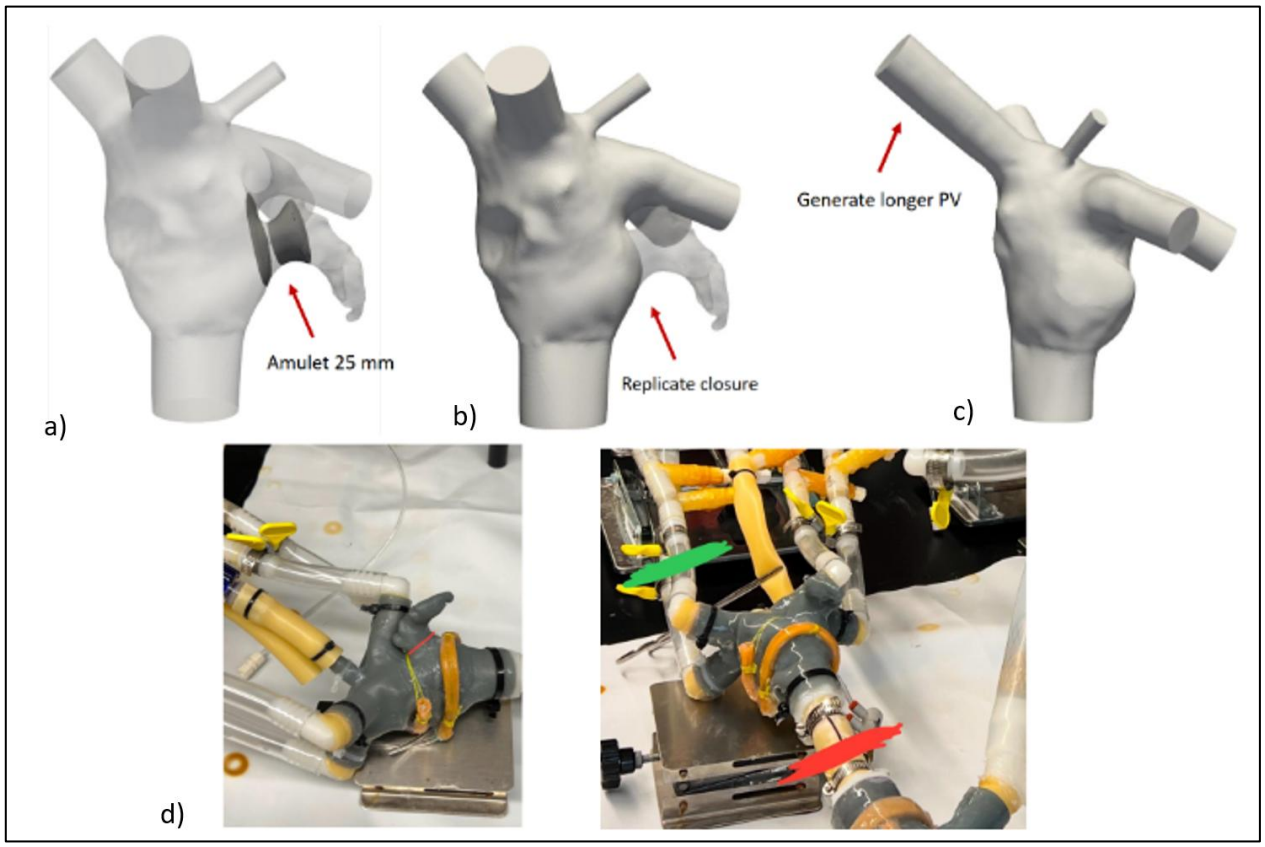

Figure 20: a) Left atrial model with occluder. b) Approximation of the 3D atrium with the occluder, printed for in vitro testing. c) Subsequent adaptation of the CFD model with the generation of longer PV to obtain parameters in areas similar to those measured in the (d) in vitro test (marked in green and red).

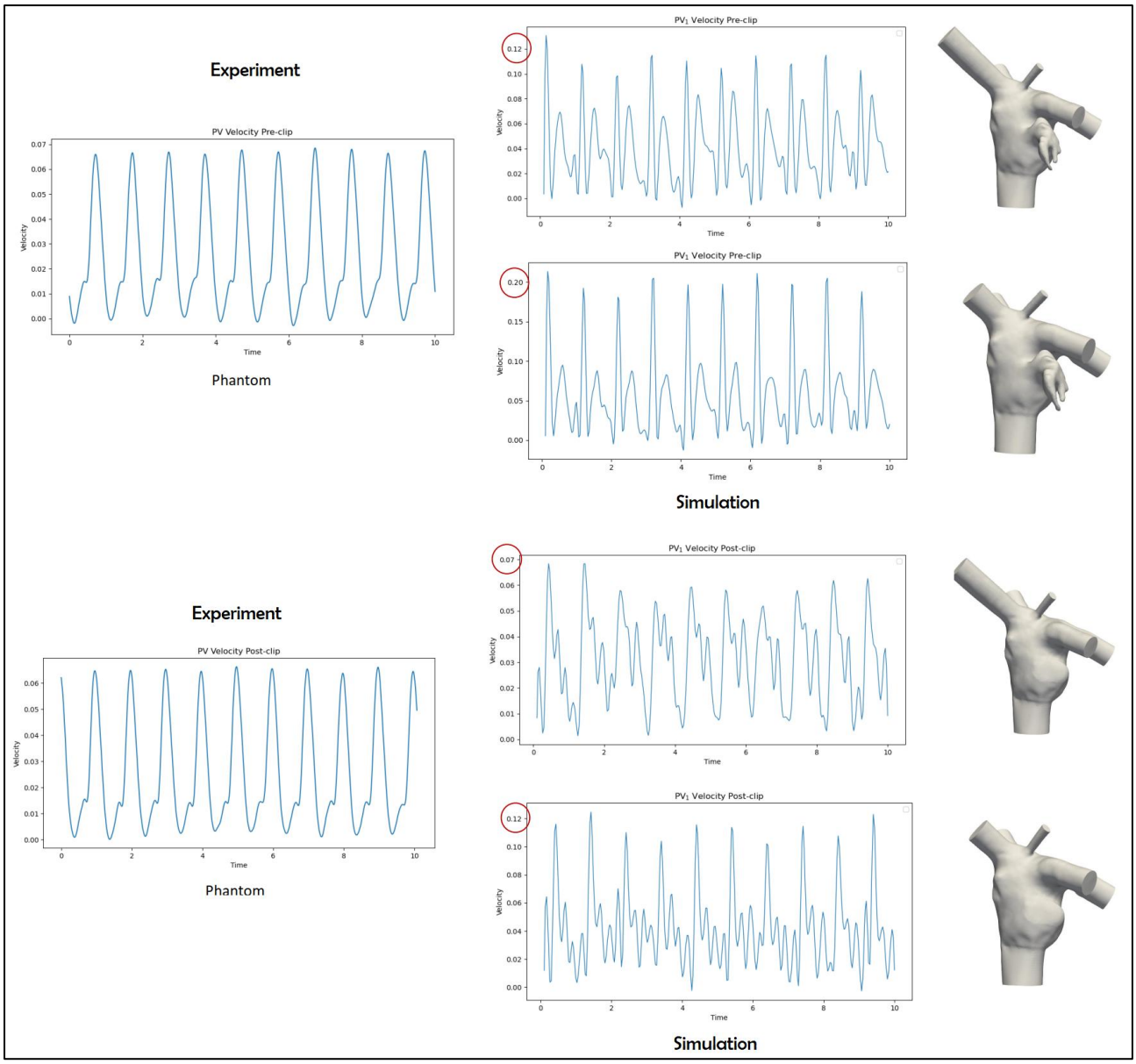

Figure 21: Comparative results of pulmonary vein velocities before and after LAAO implantation measurements in experiments and simulations. The elongated veins and their original configuration were compared in order to obtain a better calibration of the results in relation to where the sensors were placed.

3.3.2 Comparator – Test Conditions and Validation Results from the In-Vitro Set-Up developed in BioCardioLab

In collaboration with BioCardioLab (Massa, Italy) a new left atria simulator for the fluid dynamic was created. Using computed tomography (CT) images, a three-dimensional LA with LAA model was generated and then properly fabricated. The model was integrated into a mock circulatory loop, and fluid dynamic under physiological conditions was evaluated using particle image velocimeter (PIV) technique.

The model of the LA phantom was obtained by segmenting the CT dataset, the same patient using in the others experiments with MIT. The phantom was realized in Sylgard 184 silicone (Dow, Wiesbaden, Germany), given its optical properties and its compliance (Young's modulus of 2 MPa and Poisson modulus of 0.495) with the PIV technique. Two molds were designed and realized to manufacture the silicone phantom, the inner core and the external mold (**Figure 22** b-c). The inner core consists of the inner surfaces of the phantom. It was made of ABS using Fused Deposition Modeling (**Figure 22**d) and then underwent acetone vapours treatment to obtain smooth surfaces suitable for PIV investigation. The external mold was designed by outwarding the external surfaces of the model, to obtain a mold thickness of 5 mm. Given the phantom undercuts, to allow an easy molds assembly and the silicone phantom demolding, the outer mold was subdivided in six subcomponents. The outer mold subcomponents were manufactured using stereolithography techniques with Clear v4 resin (**Figure 22**e)

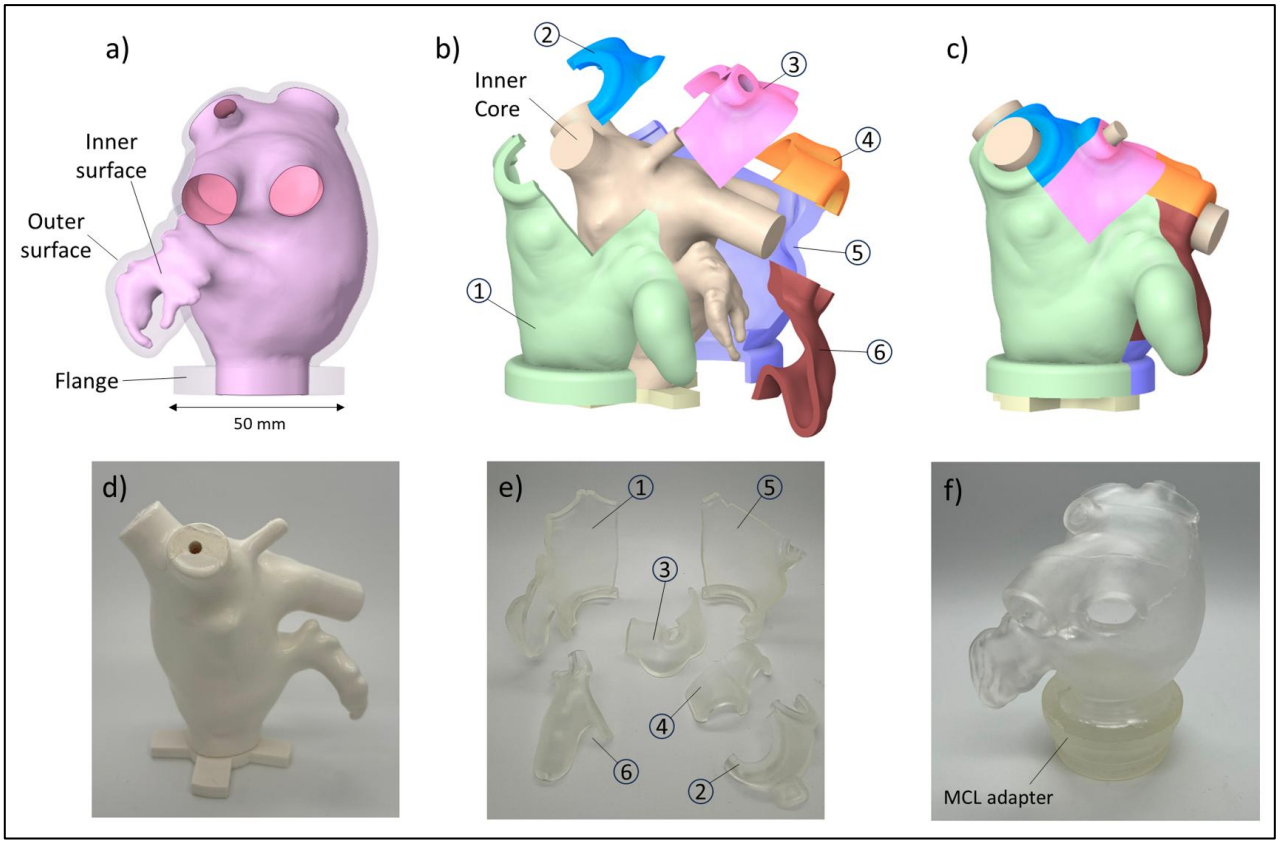

Figure 22: a) Phantom of left atrium (LA) and molds design and fabrication: b) LA phantom model , exploded view of the inner core and the outer mold subcomponents (1-6) , c) molds assembly, d) realized inner core , e) outer molds subcomponents (1-6) and f) silicone LA phantom.

The phantom required 65 g of material obtained by mixing the silicone and the curing agent with a ratio of 10:1. The material was then poured into the molds in three steps to prevent air bubbles from being trapped in thick layers. The silicone was then cured at 65°C for 24 hours. After curing, the phantom was demolded from the outer mold and the inner core was dissolved by an acetone bath (**Figure 22**f). An adapter was designed and realized in Clear resin to allow the connection of the phantom to the mock circulatory loop.

Mock Circulatory Loop and PIV Setup

The fluid dynamic experiments on the phantom were conducted using a mock circulatory loop integrated with a PIV system. An overview of the experimental setup is shown in **Figure 23**. Regarding the boundary conditions imposed on the phantom, a constant pressure of 0 mmHg was applied at the pulmonary veins using an atmospheric reservoir in which the phantom was positioned and secured. A time-varying mitral flow profile was imposed at the phantom's mitral outlet using a pulsatile piston pump. This setup replicated the healthy physiological mitral waveform from and imposed a cardiac output of 5.92 L/min, which was estimated from CT-derived left ventricular volumes and heart rate. A flow sensor (CO.55/190 V2.0, Sonotec) was installed to measure the flow rate at the mitral inlet accurately. The PIV system captured the velocity field within the phantom, enabling detailed analysis of fluid dynamics.
The PIV system featured a pulsed high-power LED system as the illumination source. A fibre optic line light with a cylindrical lens was used to form the light sheet required for experiments. Images were acquired using a high-speed camera. Both the camera and the light-generating components were mounted on an optical cage system (Thorlabs, USA), which was attached to a 2D motorized XY translation stage (PLSXY, Thorlabs, USA). This setup enabled control over the system's height, depth, and alignment relative to the phantom. A working fluid composed of water (44%), glycerine (34%), and urea (22%) was adopted to match the refractive index of Sylgard silicone. This mixture simultaneously maintained the density ρ (1060 kg/m3) and the dynamic viscosity μ (0.0035 Pa-s) of the blood. The flow was seeded with hollow spherical particles with 10 μm in diameter and density of 1100 kg/m3, to perform the PIV.

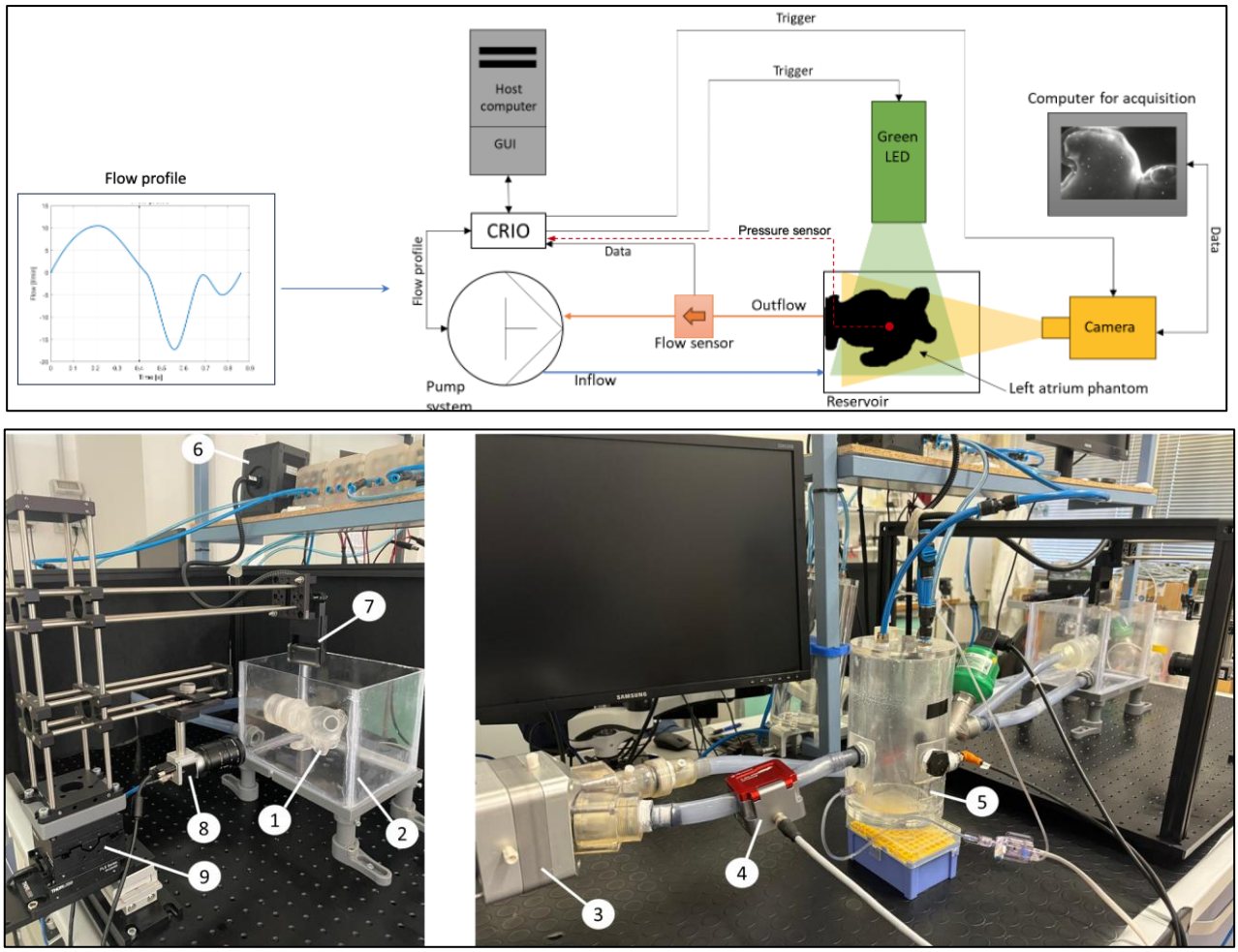

Figure 23: Mock circulatory loop: (1) left atrium phantom model, (2) reservoir, (3) piston pump, (4) flow sensor, (5) hybrid chamber, (6) LED illuminator, (7) Cylindrical lens, (8) camera and (9) translational stage.

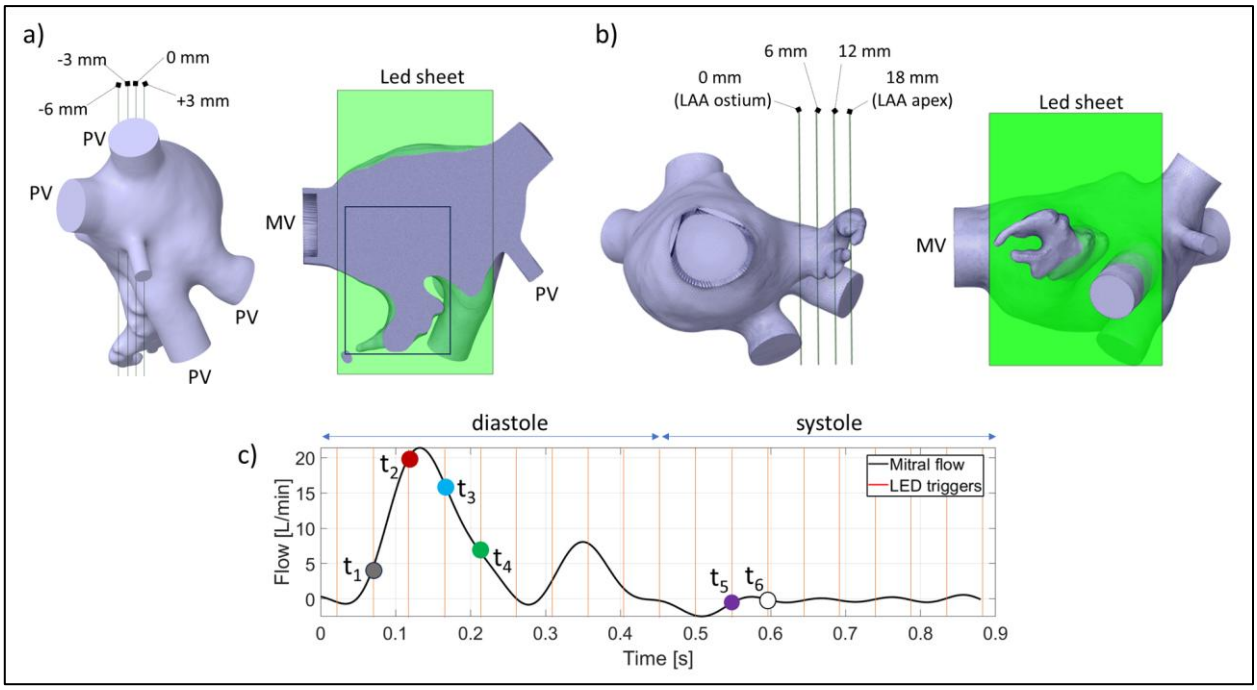

Figure 24: PIV acquisition planes of the left atrial appendage region: longitudinal plane a) with depths reference (-6 mm, -3 mm, 0 mm, +3 mm) and transversal plane b) with depths reference (0 mm, 6 mm, 12 mm, 18 mm). Mitral valve outlet (MV) and pulmonary veins (PV) inlets are reported. Imposed transient mitral flow in a cardiac cycle c) with led triggers and evaluated instants (t1 = 75 ms, t2 = 118 ms, t3 = 160 ms, t4 = 204 ms, t5 = 506 ms, t6 = 549 ms).

Fluid Model Simulate the In Vitro Condition

To further complement the experimental observations, a proof-of-concept CFD model was developed to simulate the flow dynamics under analogous conditions. The CFD simulation was performed using Ansys Fluent 2022 solver (ANSYS Inc, USA). Blood rheology was modelled as an incompressible Newtonian fluid with a density of ρ = 1060 kg m−3 and a viscosity of μ = 0.0035 kg/m·s, assuming a laminar flow regime. The outlet boundary condition was defined by the mitral flow profile of the PIV setup, while zero pressure was set to the pulmonary vein inlets, ensuring alignment with the experimental mock circulatory loop.

Preliminary Results

The phase averaged magnitude of the velocity at the 0 mm longitudinal location in different instants of the cardiac cycle is reported in **Figure 25**. The velocity is synchronous with the mitral flow throughout the cardiac cycle. During the acceleration phase (t1, t2) the fluid velocity increases reaching its maximum velocity (equal to 0.44 m/s), coinciding with the mitral E peak instant. During this phase, a parabolic velocity profile is observed near the mitral valve outlet, and a high-velocity channel appears at the pulmonary vein inlet; conversely, the velocity in the LAA remains near zero. As the cardiac cycle progresses (t3, t4), the deceleration of the PV channel combined with the low velocity in the LAA contributes to the formation of a vortex at the ostium, followed by a gradual slowing of the flow. At the systole phase (t5), the flow velocity becomes negligible in all regions of LA. Regarding the spatial distribution of the velocity field, the magnitude decreases from the atrium centre to the ostium and the LAA (**Figure 25**). Within the LAA, flow velocities remain near zero

throughout the cardiac cycle creating a zone of stagnation. **Figure 25** depicts the phase averaged velocity magnitude at the different transversal depths, over the cardiac cycle. The transversal velocities reach the maximum value (0.06 m/s) at the ostium (0 mm) and decrease to the LAA apex location. This trend is confirmed by the bulk velocity, computed in the transverse region of interest in the LAA, which decreases from 0.021 m/s at the ostium to 0.001 m/s at the LAA apex. The maximum LA displacement measured from the PIV images was 0.25 mm.

The velocity ranges are in agreement with the in-vivo measurements from MRI echocardiography. During the acceleration phase, the velocity peak corresponds with the peak of mitral inflow. The subsequent formation of vortices at the ostium demonstrates the relationship between morphological and spatial gradient of the velocity. The transversal plane analysis complements these findings by illustrating the directional dependency of flow velocities. Lower maximum velocities observed in transversal planes (**Figure 25**) indicate predominant flow along the longitudinal axis, driven by pulmonary vein inflow and mitral valve outflow. The reduction in transversal velocity magnitude and the increasing temporal delay of velocity peaks relative to mitral flow in distal regions highlight kinetic energy dissipation.

The PIV system captured the velocity field within the phantom, enabling a detailed analysis of the fluid dynamics. In addition, a preliminary proof-of-concept CFD simulation with the same boundary conditions was performed as a parallel analysis. The initial results from the computational simulation, presented in **Figure 25** and in **Figure 26**, were compared to the experimental results to demonstrate the potential of the experimental dataset to serve as a benchmark for the future validation for LAAO intervention and detecting DRT.

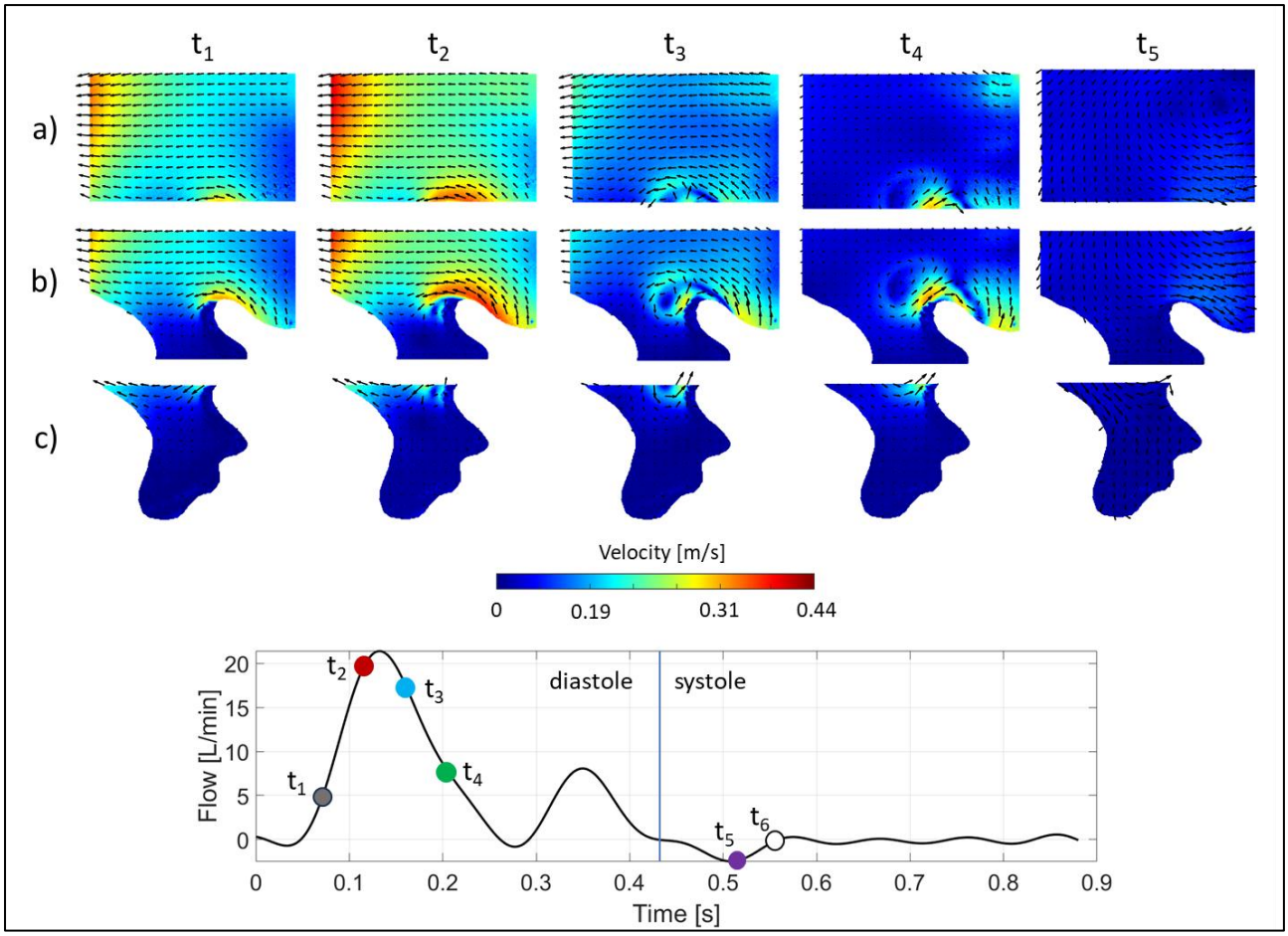

Figure 25: a) Phase average velocity field at the 0 mm longitudinal plane in left atrium (LA) a), Ostium b) and left atrial appendage (LAA) c) views, during the cardiac cycle (t1 = 75ms, t2 = 118ms, t3 = 160ms, t4 = 204ms, t5 = 506ms).

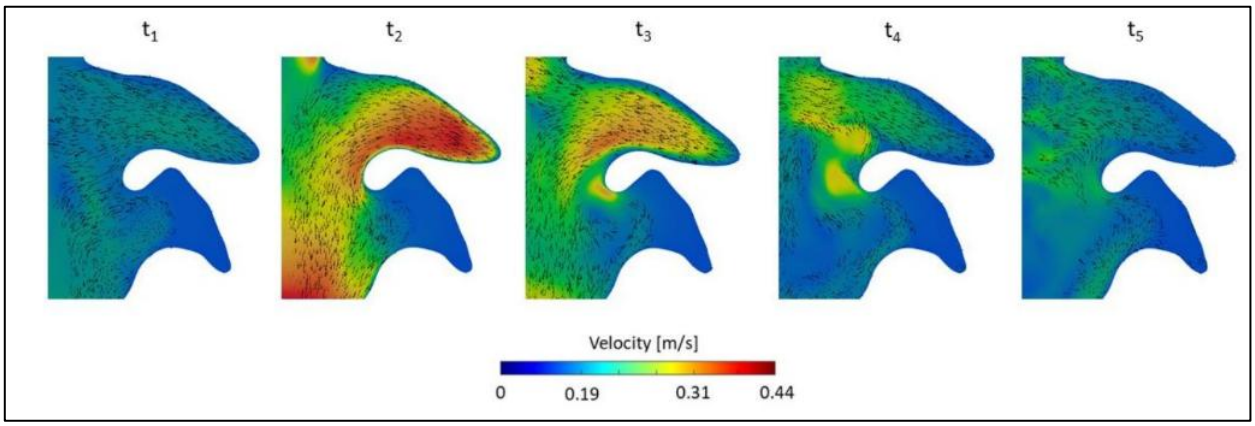

Figure 26: Velocity Magnitude field from CFD in a) longitudinal plane during the cardiac cycle (t1 = 75ms, t3 = 160ms, t4 = 204ms, t5 = 506ms).

In accordance with the guidelines (V&V40), the obtained data potentially represent the benchmark required to fully validate numerical methods, ensuring their accuracy and reliability in replicating the complex fluid dynamics within LAA models, as already demonstrated in different cardiovascular districts. The presented setup can potentially represent the basis for the development of new numerical methods to provide insights in the clinical context. Additionally, the experimental setup could be used to explore different clinical scenarios, such as the LAA closure procedures and their efficacy (estimation of device related thrombus and peri device leak risks), in a controlled environment. Velocity fields-derived metrics, such as kinetic energies and shear stresses, could be processed from the experimental datasets to serve as a reference for verifications. By offering a validated dataset with metrics, this study would potentially establish the basis for collaborative challenges within the scientific community, to increase realism and predictive power of computational modelling techniques. Future developments will overcome limitations related to wall movement neglection and constant pressure conditions at the pulmonary veins. Further improvements will include a complete left heart phantom, with both atrium and ventricle, the study of the fluid dynamic behaviour of the left atrial appendage occluder devices and the analysis of additional patient specific LA and LAA morphologies.

3.4 UC2 Validation Uncertainty – M30-M54 Activities

This section only contains additional Uncertainty Quantification (UQ) activities conducted on UC2 selected computational model during the M30-M54 period. UQ activities conducted during the M1-M30 period are already reported in the UC2 section of deliverable D6.2. Results reported in this section are meant to complete or (in some cases) supersede results of deliverable D6.2. The latter case will be explicitly mentioned, when applicable.

Large-Scale Sensitivity Analysis of Modelling Settings Influencing Hemodynamics after Left Atrial Appendage Occlusion

During the SimCardioTest project the numbers of fluid simulations reached around 2,100. The last study developed in the scope of the virtual population to increase the number of cases was conducted resulting in a total of 1,000 CFD simulations. For that, a selected dataset of 50 atrial fibrillation (AF) patients from CHU Bordeaux (France) was analysed. For each patient-specific left atrium (LA), two occluders, Amplatzer Amulet and Watchman FLX, were implanted in two positions: either covering or uncovering the pulmonary ridge (PR), a key factor in device related thrombus formation. Computational fluid dynamics (CFD) simulations were conducted in Ansys Fluent 2021R2 (ANSYS Inc, US) under five modelling conditions: (1) blood modelled as a Newtonian fluid (AF Newtonian); (2) blood modelled as a non-Newtonian fluid (AF non-Newtonian); (3) inclusion of the A-wave in the mitral velocity profile (No-AF Newtonian); (4) scaling the outlet velocity profile by 1.25 (high-velocity AF Newtonian); and (5) scaling the outlet velocity profile by 0.75 (low-velocity AF Newtonian). **Figure 27** shows that AF conditions resulted in lower velocities near the device, while No-AF increased both flow velocity and complexity near the device. The non-Newtonian model caused slight velocity variations, but its overall impact was minimal in comparison with the Newtonian model under same physiological conditions. In contrast, higher velocity enhanced both flow activity and complexity, reducing flow recirculations around the LAAO device and increasing the washout from the device region.

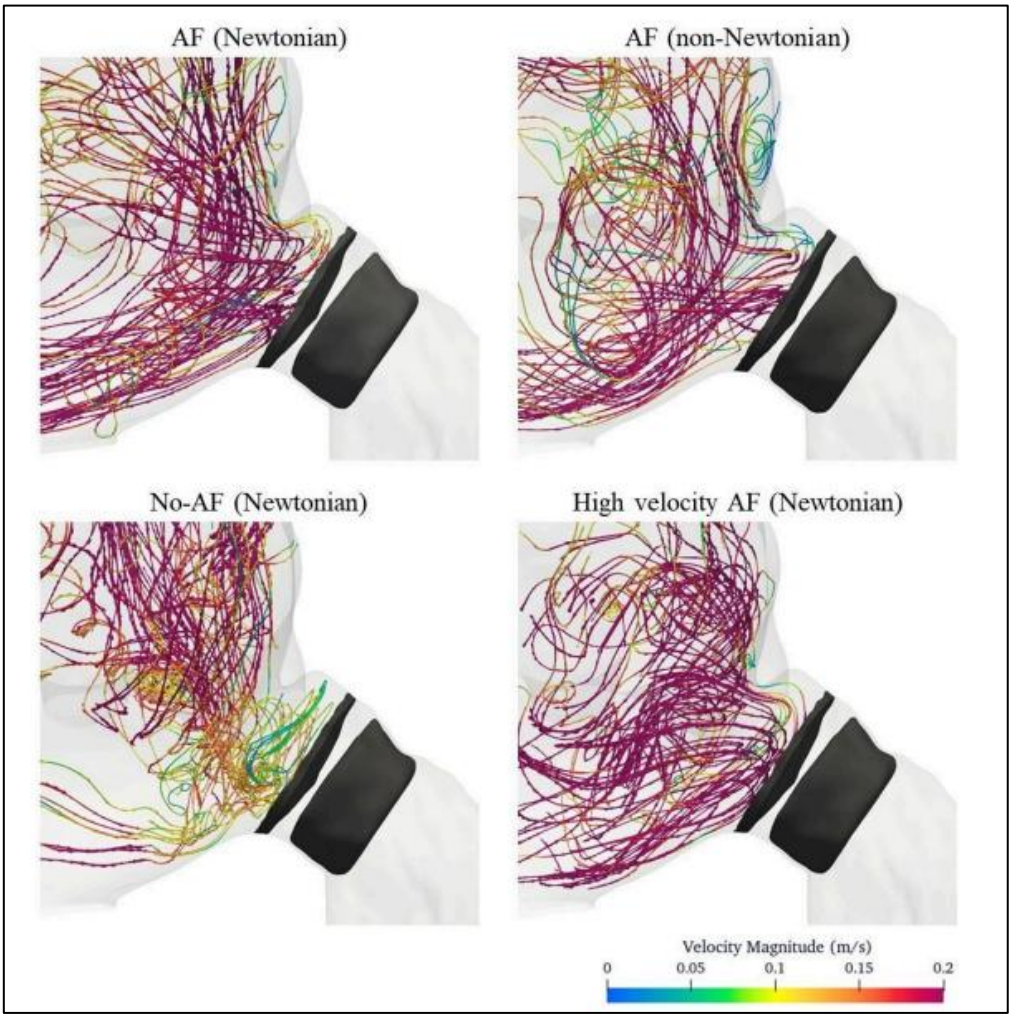

Figure 27: Simulated flow patterns at late diastole for four modelling conditions (case 44, Amplatzer Amulet with the PR uncovered).

Initiative: FLAMES Workshop – Fluid Simulations of the Left Atrium with Multi-Source Experimental Data

As part of ongoing efforts to advance cardiovascular hemodynamic modelling, the FLAMES Workshop (Fluid Simulations of the Left Atrium with Multi-source Experimental Data) has been launched. This initiative aims to establish best practices for fluid simulations of the left atrium through collaborative efforts based on a shared dataset.
The organizers have compiled a comprehensive validation dataset that integrates multiple imaging modalities. This dataset will enable the scientific community to conduct verification and benchmarking studies, identify the most promising modelling strategies, and address current challenges in the field. The available data include:

- In vitro data from particle image velocimetry (PIV) experiments, collected and curated by BioCardioLab, Fondazione Toscana G. Monasterio (Massa, Italy),
- 4D flow magnetic resonance imaging (MRI) data, collected by Hospital Clínic de Barcelona and curated by Universitat Pompeu Fabra (Barcelona, Spain),

- Dynamic opacity computed tomography (CT) data, collected by the University of California San Diego (La Jolla, USA) and curated by the University of Washington (Seattle, USA).

Beyond technical benchmarking, the workshop also addresses a critical but often overlooked source of variability in simulation: **the role of the user** in the modelling process. One of the main challenges in verification and validation lies in evaluating how user expertise—or lack thereof—can introduce modelling errors that become intertwined with numerical uncertainties. To explore this aspect, the FLAMES Workshop is designed as an open platform, encouraging participation from research groups with varying levels of experience in atrial flow simulation and experimentation. This collaborative setting allows us to assess how user-dependent factors impact simulation results and to better understand the cumulative uncertainties arising simply from differences in model construction approaches.

Workshop outcomes and methodologies will be presented in a dedicated session at the FIMH25 conference (June 1–5, Texas, USA), with hybrid participation options available. A second in-person meeting will take place during the CMBBE25 conference (September 3–5, Barcelona, Spain).

The primary output of the workshop will be a co-authored scientific publication summarizing key lessons learned. All methodologies will be anonymized to emphasize collective insights and foster community-driven progress rather than individual performance metrics.

3.5 UC2 Model Applicability – M30-M54 Activities

The IDEAL-LAAC (Impact of Flow Dynamics according to Device Implant Depth after Left Atrial Appendage Occlusion) study, led by UPF, included a cohort of 285 patients who underwent LAAC across 10 centres in Europe and North America between January 2019 and October 2023. Eligible patients received either Watchman or Amulet devices, had follow-up cardiac CT imaging, and pulsed-wave Doppler assessment of the mitral valve within six months of the CT scan. A final core dataset of over 250 patients was compiled, maintaining an approximately 1:10 ratio between cases with device-related thrombus (DRT) and those without, to ensure sufficient statistical power given the low incidence of DRT. All patients provided informed consent, and the study adhered to local ethics requirements and the Declaration of Helsinki.

To evaluate the impact of device positioning on flow dynamics, patients were stratified into proximal and distal implant groups based on the depth of the device relative to the pulmonary ridge (PR). Definitions of proximal implantation varied by device type: for lobe/disc devices, the disc had to be positioned at the level of the PR; for single-lobe devices, a proximal implant was defined as a position within <10 mm from the PR. Any device placement outside these criteria was considered distal. Device success was defined as complete deployment within the LAA, while DRT was identified via CT as thrombus adherent to the atrial surface of the device. Other procedural outcomes were classified using established consensus definitions.

The primary objective of the study was to analyse flow dynamic differences between proximal and distal device implants using computational simulations. These simulations provide valuable insights into how implantation depth affects intra-atrial blood flow, particularly in relation to thrombus formation. Secondary analyses included a more granular evaluation of flow dynamics across incremental depth categories and a comparison of flow patterns in patients with and without DRT. The results from these simulations can inform optimal implantation strategies, improve device positioning protocols, and potentially reduce the incidence of post-procedural thrombus formation.

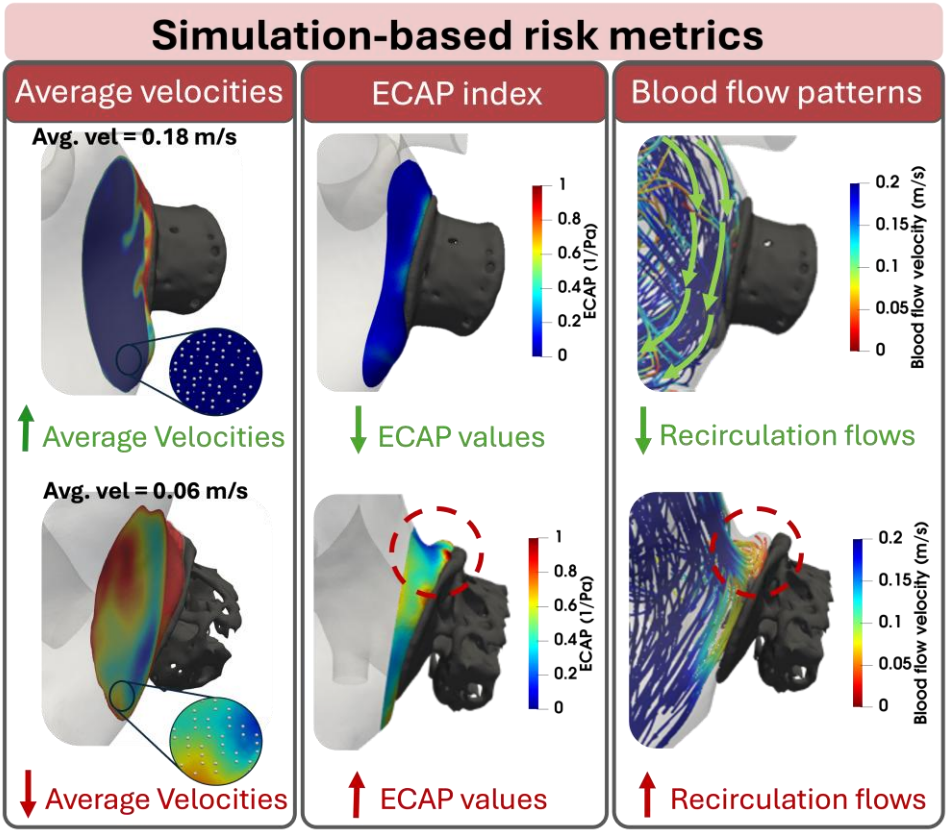

Figure 28: Main risk metrics used for thrombus detection in the IDEAL study. The example shown in the upper part illustrates an LAAO safety scenario with high blood velocity, low ECAP, and laminar flow patterns. The lower part shows a poorly positioned device, indicated by a poor index and a high probability of DRT.

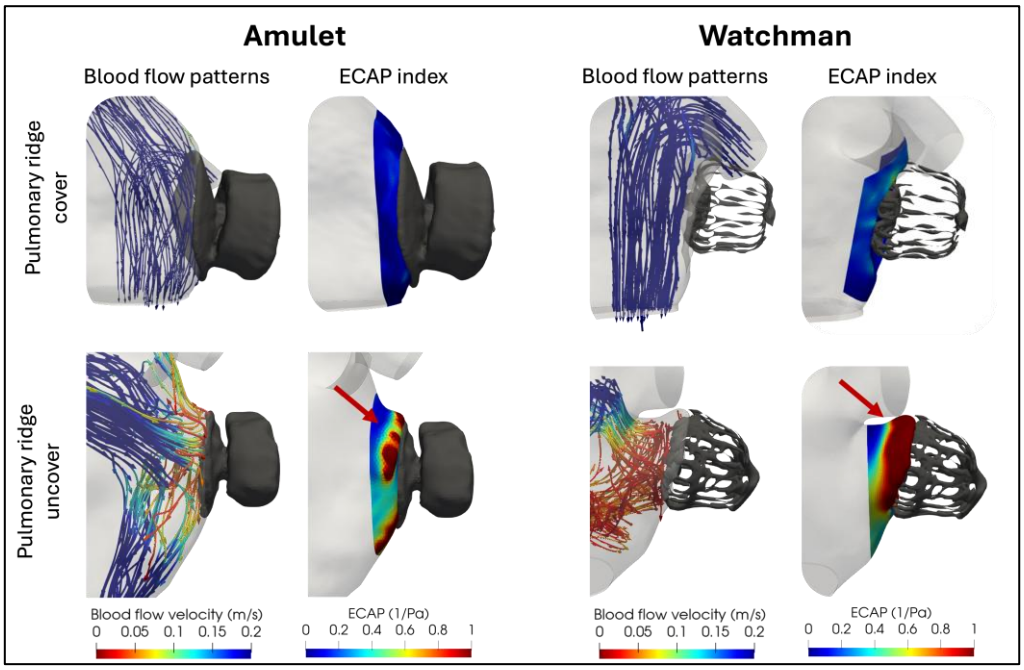

Figure 29: Patients with uncovers and covers pulmonary veins. Results show the importance to take in account the position and type of the device.

In addition, we have participated in several live cases where doctors have used our simulations to support their decisions, examples in CSI congress Frankfurt 2025, LAAO Summit 2025, CSCEstructural, CSI Focus LAA Congress, etc. (**Figure 30**).

Figure 30: Live CSI congress Frankfurt 2025. A successful live case was performed from the University Hospital of Salamanca, where our simulations was used for the preprocedural planning of a left atrial appendage closure with an Amulet device from Abbott, achieving an excellent result.

3.6 UC2 Discussion

During this period, the primary focus has been on consolidating previously obtained results. First, the number of simulations has been increased to approximately 2100, using the parameters established in the verification study. This extensive set of simulations forms a comprehensive virtual database, which will be subjected to statistical analysis in the near future. Regarding validation, significant progress has been made with the initial setup developed by MIT, yielding high-quality fluid dynamics results, including atrial motion and physiological flow conditions. Additionally, a comparative analysis has been initiated with a second experimental setup at BioCardioLab. Preliminary findings from this comparison are promising and will enable a more detailed investigation of local velocity behaviours, with the ultimate goal of improving our understanding of the left atrial appendage occlusion (LAAO) procedure. Progress has also been made in enhancing the credibility and applicability of the models, which are now employed in retrospective analyses to determine device-related thrombosis (DRT), as well as to identify the optimal device positioning in cases involving real-time clinical interventions.

Table 14: Credibility Factors Coverage Level for Use Case 2 – COU1 (cf. ASME VV40).

Model Risk					x	
Credibility Factor Coverage Level		1	2	3	4	5
Code Verification: Software Quality Assurance	V				x	
Code Verification: Numerical Code Verification - NCV	V				x	
Calculation Verification - Discretization Error	V				x	
Calculation Verification - Numerical Solver Error	V				x	
Calculation Verification - Use Error *	III				x	

Validation - Model [Form]	III					x	
Validation - Model [Inputs]	III					x	
Validation - Comparator [Test Samples]	III					x	
Validation - Comparator [Test Conditions]	I					x	
Validation - Assessment [Input Parameters]	III					x	
Validation - Assessment [Output Comparison]	IV					x	
Applicability: Relevance of the Quantities of Interest	V					x	
Applicability: Relevance of the Validation Activities to the COU	IV					x	

Table 15: Credibility Factors Coverage Level for Use Case 2 – COU2 (cf. ASME VV40).

Model Risk					x		
Credibility Factor Coverage Level			1	2	3	4	5
Code Verification: Software Quality Assurance	V				x		
Code Verification: Numerical Code Verification - NCV	V				x		
Calculation Verification - Discretization Error	V				x		
Calculation Verification - Numerical Solver Error	V				x		
Calculation Verification - Use Error	III				x		
Validation - Model [Form]	III				x		
Validation - Model [Inputs]	III				x		
Validation - Comparator [Test Samples]	I				x		
Validation - Comparator [Test Conditions]	III				x		
Validation - Assessment [Input Parameters]	V				x		
Validation - Assessment [Output Comparison]	V				x		
Applicability: Relevance of the Quantities of Interest	V				x		
Applicability: Relevance of the Validation Activities to the COU	IV				x		

3.7 UC2 – VVUQ Publications

This section lists all scientific publications relating to the UC2 VVUQ activities conducted within the frame of the SimCardioTest project.

Table 16: UC2 – List of publications related to VVUQ activities.

Reference	VVUQ Topic
Albors et al. 2022 [28]	Verification
Albors et al. 2023 [29]	Verification
Mill et al. 2024 [30]	Verification, Uncertainty quantification
Khalili et al. 2024 [31]	Verification
Albors et al. 2024 [32]	Validation, Applicability

Reference	VVUQ Topic
Olivares et al. (draft) [33]	Verification, Validation, Uncertainty Quantification
Gasparotti et al. 2025 [34]	Validation
Roche et al. 2025 (preprint) [27]	Validation
Albors et al. (draft) [35]	Clinical Validation
Casademunt et al. 2025 [36]	Clinical Validation, Uncertainty Quantification
Barrouhou et al. 2025 [37]	Verification, Uncertainty Quantification
Albors et al. 2025 [38]	Verification, Applicability
Kjeldsberg et al. 2024 [39]	Verification

4. Use Case 3

4.1 UC3 Model Summary

4.1.1 Background

Safety pharmacology studies evaluate cardiac risks induced by drugs. Since Torsade de Pointes (TdP), a well-known malignant arrhythmia, was related to pharmacological effects, regulatory guidelines have looked for biomarkers able to identify arrhythmogenic effects of drugs in order to withdraw them from the development process. Consequently, research efforts to ensure the safety of new molecules have become time-consuming and expensive for drug developers, delaying the release of new medicines into the market. Besides, initial tests focused on hERG (human ether-à-go-go related gene) activity and in vitro repolarization assays limited the development of potentially beneficial compounds, and the increasing attrition rate urged the design of new strategies.

The first initiative to include in-silico models was the Comprehensive in-vitro Proarrhythmia Assay (CiPA), which proposed integrating drug effects obtained in-vitro into a cardiomyocyte model to predict TdP risk. Furthermore, the continuous development of new models opens the possibility to personalize computer simulations to optimize drug therapy.

4.1.2 Drug Description

Drugs are chemical compounds that exert a therapeutic action by modulating physiology. Besides the therapeutic effects, undesirable secondary effects can alter the normal functioning of different organs, including the heart.

Some molecules can modulate cardiac function by interacting with cellular mechanisms. Specifically, molecules that induce critical changes in ion channel permeability alter myocyte electrical activity, causing changes in heart rhythm with potentially fatal consequences. For this reason, drug developers need to perform safety pharmacology tests to evaluate drug candidates.

Before reaching cardiac tissue, drugs undergo a series of processes inside the body from its administration, including a distribution phase. Pharmacokinetics describes all these steps inside a

living organism until the complete elimination of the substance, but interactions between each chemical compound and each organism differ. Pharmacokinetic processes are influenced by many external variables such as gender, age, weight, and previous pathologies, and the analysis of all the contributors is needed to determine the better therapeutic dose and route of administration.

Integrating pharmacokinetics and electrophysiology studies in drug assessment allows a more complete and personalized evaluation of the proarrhythmic risk by including the dosage and specific characteristics of the patient.

4.1.3 Question of Interest

The Question of Interest addressed by the model is the following:

- What is the maximum concentration/dose regimen of a drug to assure TdP-related safety in a population of healthy subjects?

4.1.4 Context of Use

A human electrophysiological (EP) model with pharmacokinetics (PK) can be used at early phases of drug development to obtain biomarkers that guide in selecting drugs and doses without TdP-risk for each subpopulation (male/ female/ age). This computational model is not intended to replace in vitro or animal experiments but to enrich and complement them by predicting additional outcomes. The goal of the in-silico trials is to help in designing clinical trials, to reduce the number of participants and protect them from suffering malignant arrhythmogenic events.

TdP-risk index is a metric obtained from a single or a set of electrophysiological biomarkers. By using appropriate threshold values, it performs a binary classification (safe/unsafe).

Quantities of Interest (QoI)

To obtain TdP-risk index, we considered action potential duration (APD90) and QT interval as the main indicators. Secondary biomarkers were calculated to improve predictions.

4.1.5 Model Risk

The following considerations support the assessment of the risk associated with the numerical model.

- Decision Consequence: Medium

An incorrect prediction with the computational model can have a risk on the development of the clinical trial if torsadogenic concentrations were administered. Low concentrations, on the other hand, do not have negative electrophysiological consequences.

- Model Influence: Medium

The model will complement preclinical and non-clinical (animal) experimental data and will help to design and refine the inclusion criteria and dosage in posterior clinical trials. In vitro and in vivo tests will still be required, but the number of participants in clinical trials as well as malignant

arrhythmogenic events can be reduced. Therefore, the model will act as a complementary approach in determining safe drug concentrations.

- Model Risk: 3/5 (Medium-Medium)

Model Risk is based on Decision Consequence and Model Influence stated above, according to Risk Matrix in Figure 31 (cf. section 1.2.5).

Model influence	**high**	**3**	**4**	**5**
	medium	**2**	**3 COU**	**4**
	low	**1**	**2**	**3**
		low	**medium**	**high**
		Decision consequence		

Figure 31: Model Risk Matrix (cf. ASME VV40) evaluating the COU included in UC3.

4.1.6 Model Description

The computational model for proarrhythmia risk prediction integrates the following steps:

- Pharmacokinetics
- Heart electrophysiology
- Cardiac mechanics

One particular aspect of this in-silico strategy we propose for drug assessment is the inclusion of patient characteristics to optimize predictions.

The model pipeline initiates with drug pharmacokinetics, which consists of obtaining the plasmatic concentration following a specific compound dosage. This concentration is used as the input of the cellular model to simulate the drug effect on myocyte electrophysiology based on the interaction of the pharmacological molecule with ion channels. The last step of the computational model is to simulate and predict the electrophysiological activity in the whole heart.

Verification activities were evaluated separately in each computational model because the tools were developed independently.

4.1.7 UC3 Stakeholder Update

ExactCure terminated its participation before the end of the SimCardioTest project and related V&V activities on pharmacokinetics finished 10 months beforehand. Although UC3 had pharmacokinetics as the first step in the workflow, electrophysiological simulations can be conducted with input data collected from literature and the independent validation approach allowed to complete EP activities despite the departure of ExactCure.

4.2 UC3 Model Verification – M30-M54 Activities

This section only contains additional Verification activities conducted on UC3 selected computational model during the M30-M54 period. Verification activities conducted during the M1-M30 period are already reported in the UC3 section of deliverable D6.1. Results reported in this section are meant to complete or (in some cases) supersede results of deliverable D6.1. The latter case will be explicitly mentioned, when applicable.

4.2.1 PK Model

4.2.1.1 Numerical Solver Error

Quantities of interest (concentrations) sensitivities to tolerances level have been expanded for the following molecules/models in the COU: Cisapride, Quinidine, Pimozide, Azimilide and Dofetilide. The complete report can be found in Annex B.

4.3 UC1 Model Validation – M30-M54 Activities

This section only contains additional Validation activities conducted on UC3 selected computational model during the M30-M54 period. Validation activities conducted during the M1-M30 period are already reported in the UC3 section of deliverable D6.2. Results reported in this section are meant to complete or (in some cases) supersede results of deliverable D6.2. The latter case will be explicitly mentioned, when applicable.

4.3.1 PK Model Validation

Model form and input sources, test samples and conditions, equivalency of input parameters and output comparisons were expanded and detailed for the following molecules: Azimilide, Chlorpromazine, Cisapride, Clarythromycin, Sotalol, Disopyramide, Dofetilide, Domperidone, Droperidol, Flecainide, Metronidazole, Mexiletine, Nicorandil, Ondansetron, Pimozide, Quinidine and Vandetanib. New quantification of sensitivities and uncertainties was included for the 21 drugs included in the report. All the details can be found in Annex C.

4.3.2 EP (0D and 3D) Model Validation

4.3.2.1 Comparators description, samples and conditions

The initial list of 22 drugs was updated with the cellular comparators for the remaining 6 drugs to complete the 28 compounds included in the CiPA initiative [40], including the clinical TdP-risk category assigned by a committee of experts.

Table 17: Experimental comparators from the literature that provide 0D electrophysiological data for the molecules under study. TdP-risk categories according to the criterion stablished for CiPA drugs [40].

Drug Comparator		Samples			
Molecule	**Ref.**	**Type**	**Concentrations**	**Conditions**	**Quantity**
High Risk					
Bepridil	[41]	guinea pig ventricular papillary muscles	1 μM, 4 μM, 10 μM, 20 μM	0.1 – 5 Hz	4
Ibutilide	[42]	dog left ventricle muscle	1 μM	0.25 Hz, 0.67 Hz, 2 Hz	5
Intermediate Risk					
Astemizole	[43]	isolated guinea pig ventricular myocytes	$0.3 \cdot 10^{-3}$ μM, 10^{-3} μM	1 Hz, 3Hz	4
Terfenadine	[44]	hiPSC-CM	3 μM, 10 μM, 30 μM, 100 μM	1 Hz	6
Low Risk					
Nitrendipine	[45]	hiPSC-CM	0.01 μM - 0.3 μM	1 Hz	3-5
Verapamil	[44]	hiPSC-CM	0.03 μM - 3 μM	1 Hz	7

The characteristics of the new comparators used to assess APD variation, which correspond to the experimental settings of several preclinical in-vitro studies found in the literature, are summarized in Table 17. Molecules are categorized according to their clinical TdP-risk label.

A new set of comparators was introduced to make use of the electrophysiological model in a ventricular geometry (3D model) and provide new outputs based on the simulation of the electrocardiogram (ECG), which are more comparable to the clinics. Data were obtained from sources different to the cellular ones, since the experimental settings to obtain the ECG differ. After thorough search to find clinical human data in the literature, Table 18 summarizes the selected comparators. The main criterion for their selection was that published information provided quantitative details about the critical input and output parameters needed to replicate during the simulations, as detailed below. This explains that some comparators were preclinical and with animal models.

Due to the computational cost of 3D simulations, a single dose and a single condition was compared for each molecule, those closer to the therapeutic scenarios when possible. Drugs without available comparators were nevertheless simulated, because we can qualitatively validate the outputs according to their TdP-risk category.

Table 18: Experimental comparators from the literature that provide 3D electrophysiological data for the molecules under study. TdP-risk categories according to the criterion stablished for CiPA drugs [40].

Drug Comparator		Samples			
Molecule	**Ref.**	**Type**	**Quantity**	**Settings**	**Effective C_{max}**
High Risk					
Bepridil	[46]	males	12	12-lead ECG QT interval on lead II 71 beats/min	23.5 nM
Disopyramide	[47]	beagle dogs of either sex	6	Lead II ECG Bazett-corrected QT interval (QTcB)	11782.9 nM
Dofetilide	[48]	males	10	Leads V2, V5, and V6 Fridericia-corrected QT interval (QTcF)	4.76 nM
Ibutilide	[49]	patients with AF or flutter	266	12-lead ECG corrected QT interval (QTc)	92.8 nM
Quinidine	[50]	beagle dogs of either sex	5-6	Lead II ECG Van de Water-corrected QT interval (QTcV)	1020 nM
Sotalol	[50]	beagle dogs of either sex	5-6	Lead II ECG Van de Water-corrected QT interval (QTcV)	11280 nM
Vandetanib	[51]	males and females	18 (11:7)	12-lead ECG QTc interval	269.7 nM
Azimilide	-				122.0 nM
Intermediate Risk					
Astemizole	[52]	guinea pig hearts	5-10	pseudoECG constant RR	100 nM
Cisapride	[53]	males and females	12	12-lead ECG automatic QTcB interval	2.75 nM
Clarithromycin	[54]	males	23	12-lead ECG automatic QTcB interval	874.4 nM
Clozapine	[55]	males and females	82 (58:24)	12-lead ECG QTcB interval on leads II, V2, and V3	28.0 nM
Domperidone	[56]	isolated rabbit hearts	8	BCL = 900 ms	500 nM
Droperidol	[57]	males and females	16 (8:8)	12-lead ECG QTcF interval	37.7 nM
Ondansetron	[56]	isolated rabbit hearts	10	BCL = 900 ms	1000 nM
Pimozide	[58]	males and females	12 (7:5)	ECG machine QTcF, with tangent defining the end of the T-wave	0.095 nM

Drug Comparator		Samples			
Molecule	**Ref.**	**Type**	**Quantity**	**Settings**	**Effective C_{max}**
Risperidone	[59]	males and females	28 (22:6)	12-lead ECG QTc interval	17.2 nM
Terfenadine	[52]	guinea pig hearts	5-10	pseudoECG constant RR	100 nM
Chlorpromazine	-				78.4 nM
Low Risk					
Loratadine	[54]	males	24	12-lead ECG automatic QTcB interval	0.215 nM
Ranolazine	[60]	humans	22	12-lead ECG QTcF interval on lead II, with tangent defining the end of the T-wave	3288.6 nM
Verapamil	[60]	humans	22	12-lead ECG QTcF interval on lead II, with tangent defining the end of the T-wave	25.8 nM
Diltiazem	-				188.0 nM
Metoprolol	-				493.3 nM
Mexiletine	-				3359.8 nM
Nifedipine	-				100 nM
Nitrendipine	-				3.03 nM
Tamoxifen	-				7.04 nM

For TdP-risk assessment, the measurement of QT prolongation on the ECG is critical, because it is a main biomarker altered with drugs, as proposed by the pharmaceutical guidelines ICH S7B and E14 [61]. Our model is able to reproduce pseudo-ECGs, which is the electrical potential on the leads located on a torso but without computing the conductivity of the organs (**Figure 32**). Although different in amplitude, the pseudo-ECG and ECG have equivalent durations and main complexes match in time, which allowed us to compute the QT interval with less computational cost. As mentioned above, heterogeneous experimental settings and calculation methods may cause a wide variability in QT intervals among studies. To solve this issue, we considered the percentage of change instead of absolute variation values, as performed at the cellular level with APD comparisons.

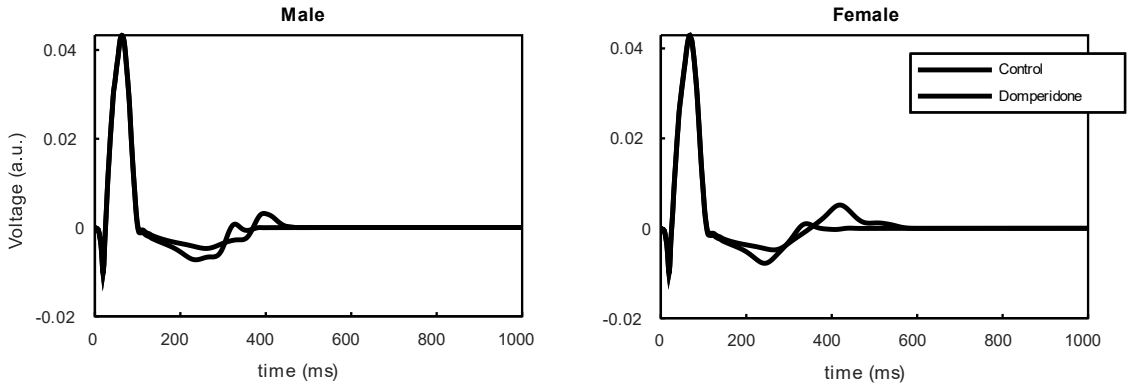

Figure 32: In silico pseudo-ECGs illustrating QT prolongation under the effect of Domperidone. One male and one female cellular models simulated in the biventricular geometry.

After validating drug effects, through 0D and 3D simulations, we applied a machine learning classifier based on Support Vector Machine for safety assessment. The main objective of this supervised learning approach is quantifying the predictive capacity of the validated mathematical model to classify the CiPA drugs according their TdP-risk category. As well as the risk labels (ground truth of reference), the training and validation sets were designated by a team of experts in the original work where the 28 known drugs were chosen [40], and we followed the same criterion. The features we used for classification were in-silico cellular biomarkers from populations as described in our previous work [62], with the difference that we generated two specific subpopulations, one for males and one for females [63]. This classifier has not been performed with experimental data, which means that does not exist an equivalent comparator per se, but we know the TdP-risk labels for the 28 CiPA drugs to evaluate the accuracy of predictions.

4.3.2.2 Equivalence of Input Parameters

Input parameters of the 0D model did not change. The unique update was applying different genotypic profiles in cell parameters to create populations of males and females for all the comparators, based on observed experimental data that differentiate control cellular properties between both sexes.

Regarding the 3D model, as it is an extension of the cellular model, it depends on the same input parameters: electrophysiological genotype and drug parameters. Three-dimensional new inputs are the ventricular mesh and all its properties to compute the electrical potential propagation. However, we used a generic geometry, parameterized in a previous study [63], for all the comparisons because experimental studies do not provide anatomical details about the hearts. Similarly, a single representative male and female electrophysiological profile from the cellular population were selected, given that this specific information is unknown.

The main drug-related input in the electrophysiological model is the effective plasmatic concentration, while IC50 and h parameters are inherited from the cellular model and they are specific for each molecule and ion channel. The comparators that quantify drug effects on the ECG usually provide the administered dose. Although PK models could predict plasmatic concentration from dose data, we used as input the maximal plasmatic concentration reported in the studies. It is

typically provided in ng/mL, and a minor direct transformation was necessary to convert it in effective concentration (nM), by means of molecular weight and binding fraction values, accessible data in drug databases [64].

4.3.2.3 Output Comparison

0D Model

Simulated drug-induced APD90 variation was directly compared to experimental APD variation for the new set of drug comparators (**Figure 33**), as previously done with 22 drugs. This time, we included the uncertainty linked to the experimental variability as horizontal error bars. There is at least one point for each drug whose interval reaches the diagonal, indicating the accuracy of predictions.

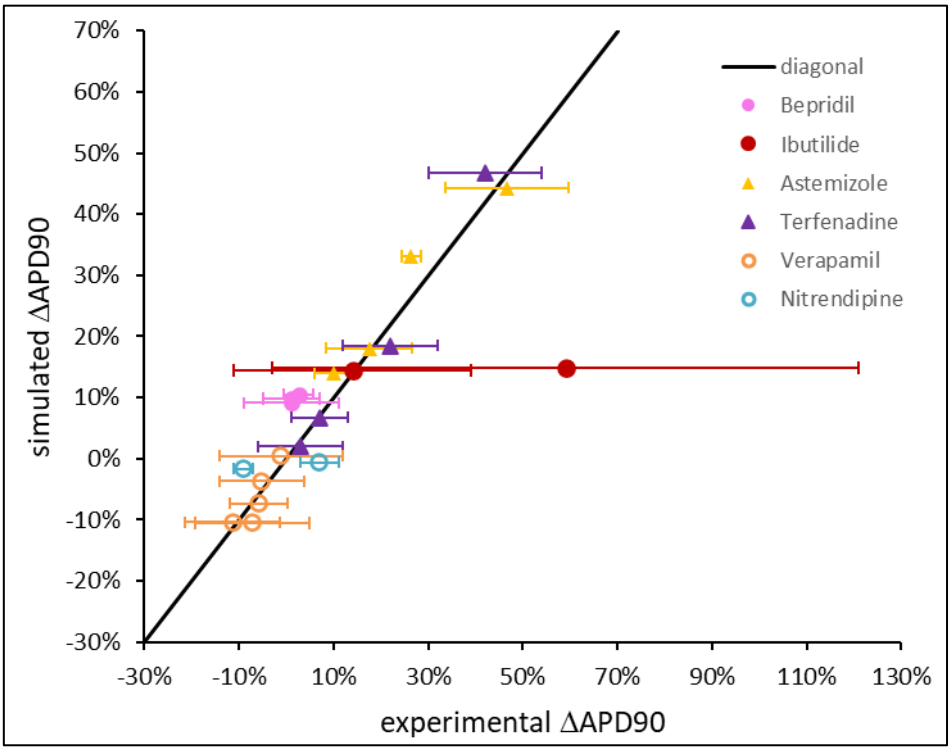

Figure 33: Output comparison: variation of action potential duration (% ΔAPD90) for high (filled circle), intermediate (triangle) and low (empty circle) TdP-risk drugs. Diagonal represents complete agreement between experimental and simulated results. Horizontal error bars denote experimental uncertainty.

Simulations can also reproduce output variability through input variability. It is the case of population of cell models, and we particularly created specific subpopulations, one for males and one for females. They were used to compare all drug effects also on APD. Although experimental data provided by the comparators was not specific for any of these subpopulations, this variability allows to examine how uncertainty due to patient characteristics (genomics) is propagated to the results.

Unlike **Figure 33**, in which drug effect is a single point, histograms of **Figure 34** show the variability in ΔAPD caused by drugs, divided in two subgroups. For these comparisons, a single concentration

per drug was evaluated; we selected the closest to the therapeutic value. The accuracy of predictions is dictated by the degree of overlap between histograms (model results) and the experimental range represented shaded areas. After applying variability is more probable that simulated results reach observed experimental bounds.

Depending on the drug comparator, output agreement quality differs. For molecules such as dofetilide, astemizole or nifedipine, despite the differences in means between experimental comparators, both populations are inside limits. Others are partially inside range, such as cisapride and diltiazem. When discrepancies are present, the causes have to be analysed one by one. For instance, the reduction in APD with metoprolol was not reproduced by the model, but as it is a low-risk drug, the lack of ΔAPD computed may be sufficient for safety prediction. In the case of chlorpromazine, instead, the in silico APD increase versus the experimental reduction needs further elucidation.

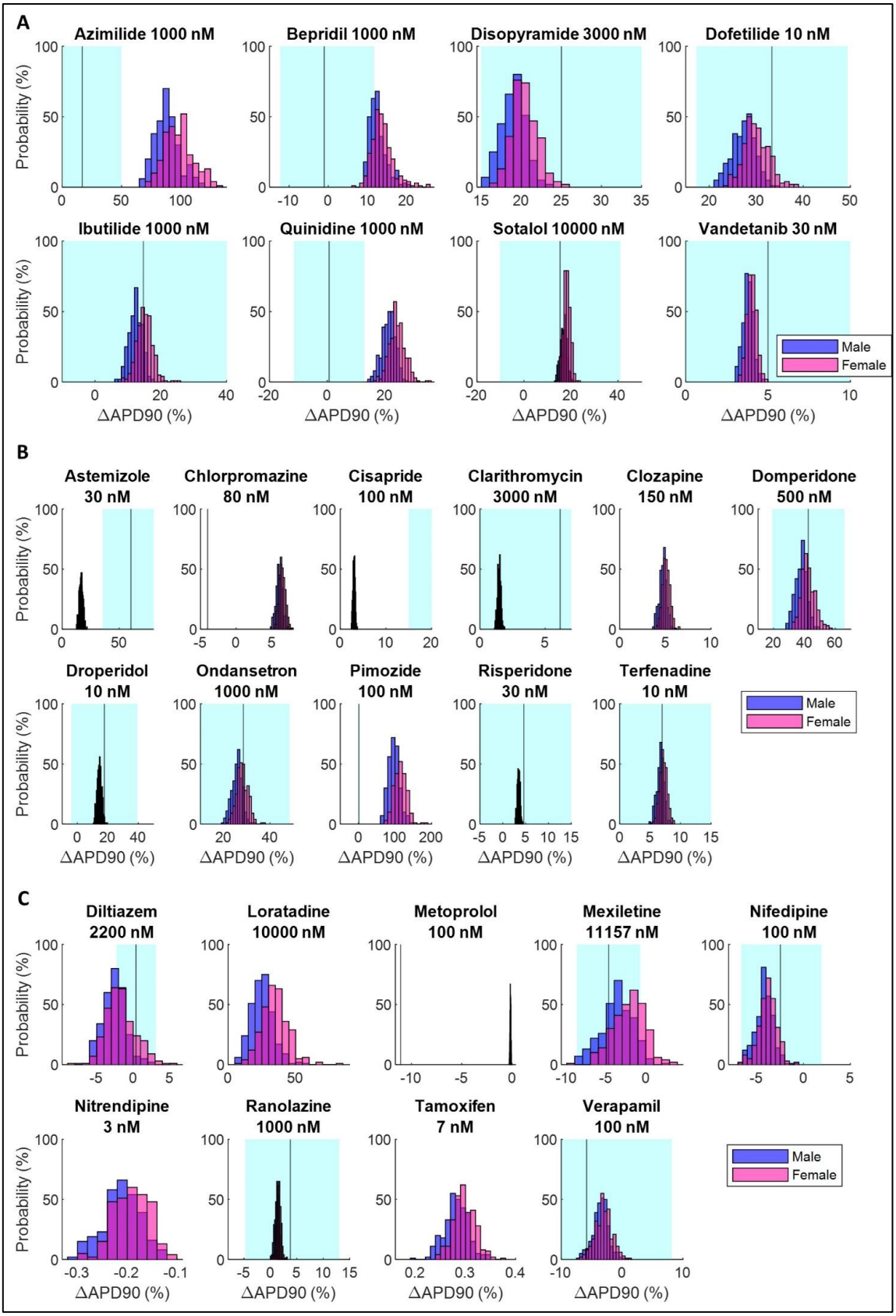

Figure 34: Output comparison in populations of cellular models divided in two subgroups by sex. A) High TdP-Risk drugs, B) Intermediate TdP-Risk drugs, C) Low TdP-Risk drugs. Shaded areas represent the experimental range, where the vertical line stands for the mean. ΔAPD90: variation of action potential duration.

3D Model

The numerical model is able to simulate an electrical signal equivalent to the ECG obtained in clinics, which allows the direct comparison between outputs. Changes on the QT interval quantified from the ECG was the only biomarker considered at the organ level to assess drug effects. Depending on the study, QT quantification varies, but the most common is an automatic value provided by the electrocardiograph based on 12-lead ECG and with heart rate correction. In our simulations, we used a constant heart rate of 1 Hz and quantified the QT on lead I.

Comparisons between in-vivo and in-silico data were evaluated molecule by molecule, similarly to the 0D comparisons, and the level of agreement obtained with the computational models can be observed in **Figure 35**. Although experimental comparators provide a mean value, we also considered the variability reported by the studies and we included it as an uncertainty interval. In-silico QT variation was considered valid if it fell within the clinical range or the distance to the limits was less than 5%. Drugs without a comparator can also be evaluated, and they perform well because ΔQT is larger in molecules from the high-risk group than in compounds with low risk, while a moderate effect is more common in the intermediate group.

Simulations were run with a single male model and a single female model selected from the population of cells, which led to two in-silico ΔQT values, although the real comparator does not distinguish sex-related effects. In fact, depending on the comparator, women may be included or not in the study, but they are usually underrepresented in clinical trials. This means that the validation should be flexible with subgroup results. Differences between male and female were considered part of the uncertainty propagated to outputs when the ionic profile differs between individuals.

Output comparisons displayed in **Figure 35** were inside the acceptable range.

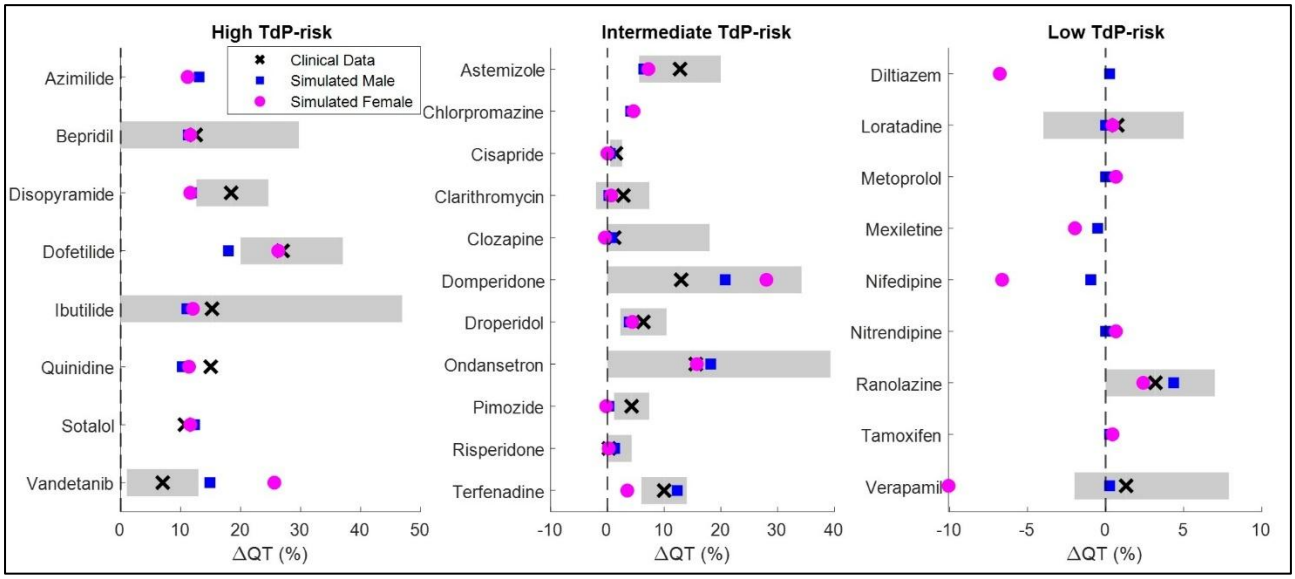

Figure 35: Comparison of in silico QT variation (ΔQT) with clinical data for 28 CiPA drugs. Simulated QT computed for one representative male and one representative female model from the population. Shaded areas represent the experimental range.

Machine Learning Classification

The quality of the classifier is evaluated with performance metrics (**Figure 36**). An accuracy of 87.5 % is obtained with the validation dataset of 16 molecules because there were two low TdP-risk drugs, loratadine and tamoxifen, misclassified as intermediate risk. The same performance metrics are obtained for the male and female populations, although TdP-scores were slightly larger in females. However, such differences were not enough to alter the classification results of any drug after using the same TdP thresholds to separate categories.

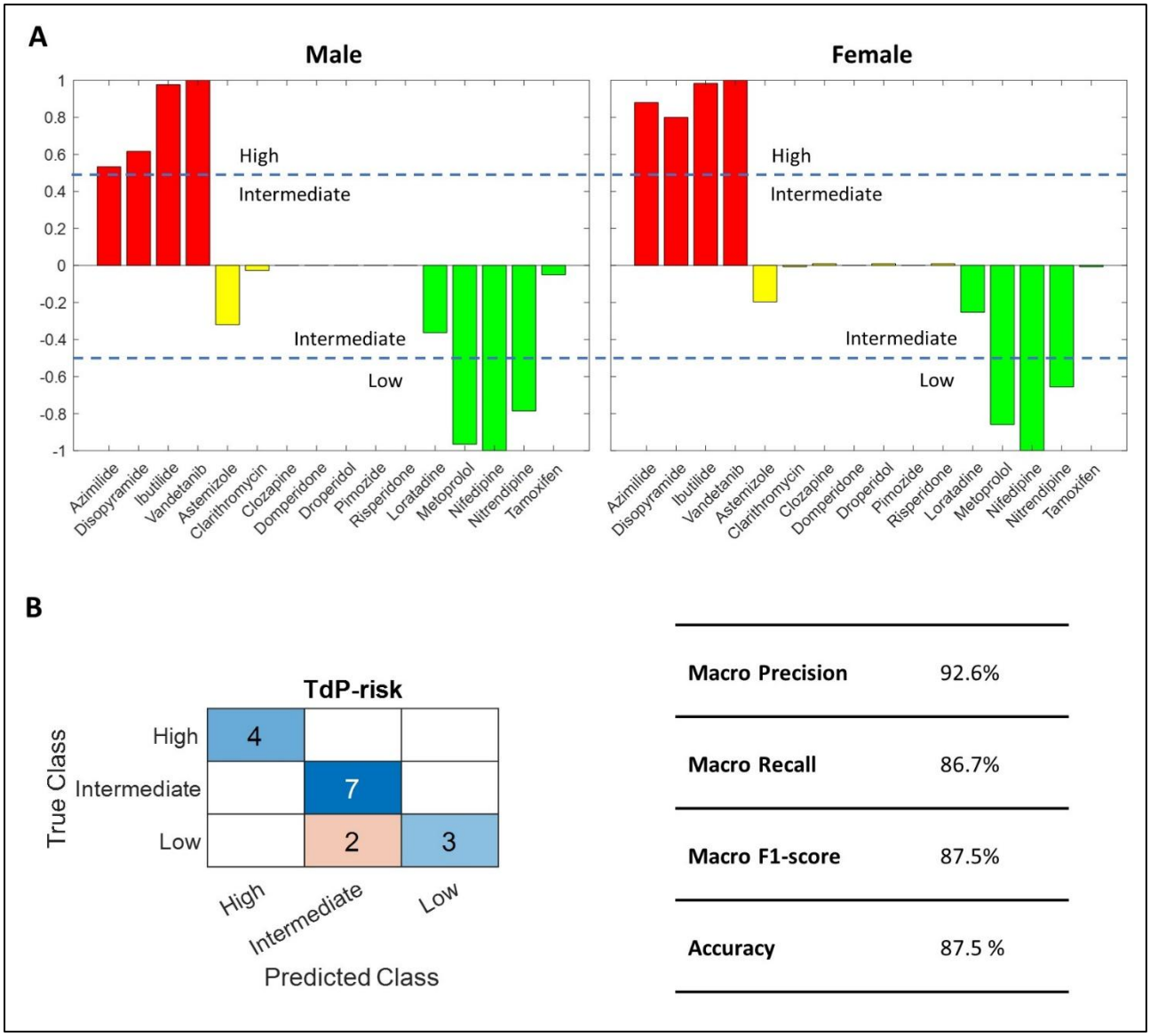

Figure 36: Classification results for the validation dataset of 16 drugs in male and female populations. A) TdP-score graphs and B) performance metrics (same results for males and females).

The predictive power of this machine learning model depends, in part, on the in-silico data provided. In this case, the electrophysiological features used for classification were obtained after validating drug-induced QT prolongations. If only APD prolongation was validated, the classifier performed

with a smaller accuracy (75%). This finding suggests that QT comparators are more reliable to validate drug parameters than cellular comparators.

4.4 UC1 Validation Uncertainty – M30-M54 Activities

This section only contains additional Uncertainty Quantification (UQ) activities conducted on UC3 selected computational model during the M30-M54 period. UQ activities conducted during the M1-M30 period are already reported in the UC3 section of deliverable D6.2. Results reported in this section are meant to complete or (in some cases) supersede results of deliverable D6.2. The latter case will be explicitly mentioned, when applicable.

4.4.1 Comparator Uncertainty

4.4.1.1 PK Model

New data about the uncertainty in PK comparators can be found in Annex C.

4.4.1.2 EP (0D and 3D) Model

Experimental uncertainty in published studies is usually presented in the form of standard deviation or standard error of the mean. We used this data to estimate the intervals for APD and QT variation that help inform about the accuracy of simulation outputs. The expected ranges are specific for each drug scenario and are illustrated in **Figure 34** and **Figure 35** as shaded areas.

4.4.2 Sources of Uncertainty

The populations of cellular models were designed to account for biological uncertainty with the purpose to study how this input variability is propagated to in silico outputs and how these biomarkers match with the uncertainty reported experimentally. The computational cost required to conduct population of models was only feasible at the cellular level, and **Figure 34** illustrates variability effects on APD for the 28 CiPA drugs.

Another uncertainty source is related to drug parameters. There are different studies that have evaluated dose-current blockage effects in their laboratories, leading to multiple possible IC50 values, whose range can span even up to two orders of magnitude (**Figure 37**). The comparators were useful to set the most appropriate parameters, contrasting first with reported cellular APD prolongation and validating later with the QT interval at the organ level. However, moving from 0D to 3D simulations with the same parameters was challenging because outputs did not always align with the expected results. In these cases, 3D comparators prevail because we found that safety assessment performed better after having validating with ECG data.

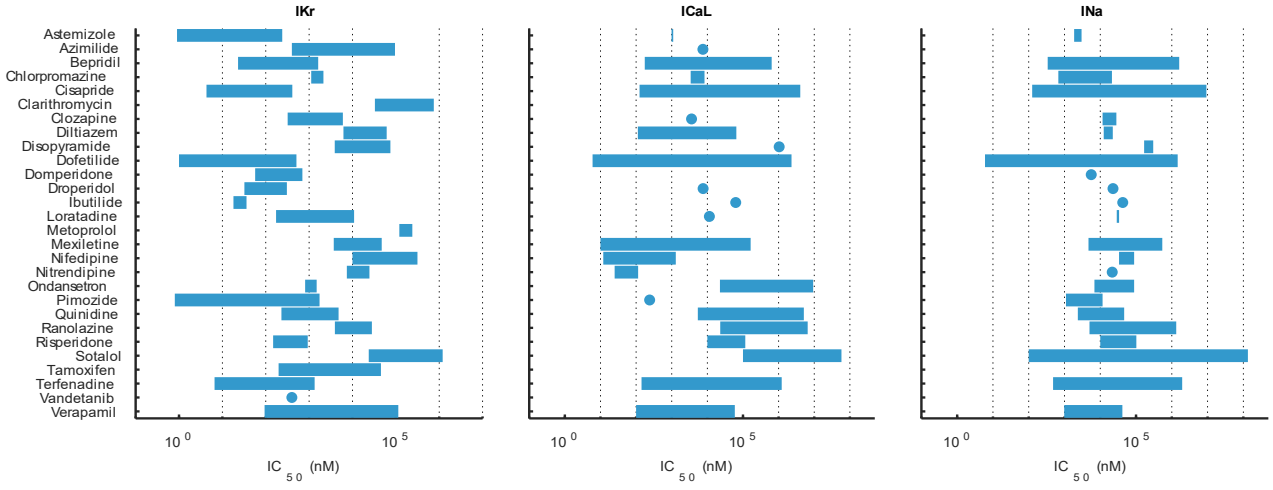

Figure 37: Variability range of IC50 for IKr, ICaL, and INa, based on values reported across multiple studies.

4.5 UC3 Model Applicability – M30-M54 Activities

Our models are part of an in-silico tool for drug safety assessment, which allows to calculate APD90 and QT interval, and provides a classification of drugs considering their torsadogenic risk. Therefore, the computational model was properly conceived to obtain relevant quantities of interest and to answer the Question of Interest.

The only concern is that in-silico predictions are not directly related with real patients, but they provide an estimation on how drugs could perform on a population, and particularly in two subgroups differentiated by sex. Cellular models were virtually generated based on reported data and validation was performed against general metrics gathered from the literature. This implies that, despite the suitability of the validation activities to the context of use, the model domain is large and uncertainty plays an important role. For instance, the experimental comparators did not provide sex differences in biomarkers or TdP risk, so the individual outputs from the numerical models had to be evaluated with the same reference data. In fact, the ground truth for each of the 28 drugs under study is a single TdP-risk label, based on clinical evidence and expert consensus on the effects of the molecule on patients.

To guarantee greater applicability, we attempted to apply two specific comparators per drug, one cellular and other at the organ level, with concentrations close to the therapeutic values. Currently, the relevance of validation points to the COU is limited by the available experimental data, but the methodology here proposed ensures minimal differences between the validation activities and the context of use, and it can be extended to other pharmacological molecules.

4.6 UC3 Discussion

The credibility on the predictive capability of the computational model for proarrhythmic assessment required V&V actions of at least intermediate rigor because the tool was considered to have a medium risk level for the defined COU. Table 9 shows that the score planned to be achieved by validation activities is equal to 3 for all factors except for test conditions. Each credibility factor is the combination of the different actions taken for each of the three individual models that comprise the computational application for drug evaluation, and the final score represents the most

restrictive level. The scarcity of comparator conditions for the electrophysiological model caused a low credibility level in this factor, but for the present COU, electrophysiological conditions were less relevant than sample type (drug) to assess TdP risk. Therefore, despite this particular low coverage level, we think that computational model predictions may still be sufficiently credible for decision-making.

4.6.1 PK Model

Many pharmacokinetic models can be validated thanks to the availability of therapeutic thresholds, which provide a good understanding of drug efficacy and toxicity levels. However, this validation only reflects the a priori accuracy of the models, and is not satisfactory in the case of drugs with narrow therapeutic margins. For this reason, it is important to carry out higher-level validations for certain drugs requiring a higher level of precision.

Validation datasets are difficult to obtain, however, after a thorough search, we found the external comparators needed to complete the list of molecules.

Another additional step incorporated to the validation pipeline was to include inter-individual variability in the predictions. This makes it possible to predict the most likely concentration ranges where an individual would be at a given dose, taking into account the variability of the models implemented. In the context of SimCardioTest, we conducted the entire PK validation of the molecules included for EP assessment.

4.6.2 EP (0D and 3D) Model

With the aim to gain credibility in assessing the TdP risk in drugs, several validation activities have been conducted with the EP model, some of them expanded in this last term with more elaborated outputs regarding the computational cost. Multiple parameters integrate the cellular model but only channel conductance and ion-transport proteins have been analysed as part of the genetic variability determined by protein quantity and function, and because most of the electrophysiological effects induced by pharmacological compounds are linked to the alteration of ion currents. Drug effects were evaluated at the cellular an organ level to obtain in silico biomarkers that can be directly compared with in-vitro and in vivo metrics. Available experimental data from previous published studies were the base for the validation process. We sought in-vitro drug tests to compare APD prolongation and clinical studies reporting changes in QT for each compound. Populations of cellular models show the output variability and two representative sex-differentiated models illustrate differences in the ECG between males and females.
After validating the drug models with key electrophysiological features, a classification tool is implemented to predict the torsadogenic risk of each molecule. This last step strengthens the validation process by directly targeting the question of interest and providing a risk label to each molecule, which allows to identify safe compounds and suggests those that should be discarded because of their TdP risk.

Table 19: Verification Credibility Factors Coverage Level for Use Case 3 (cf. ASME VV40).

Model Risk					x		
Credibility Factor Coverage Level		1	2	3	4	5	
Code Verification: Software Quality Assurance	III			x			
Code Verification: Numerical Code Verification - NCV	IV			x			
Calculation Verification - Discretization Error	III			x			
Calculation Verification - Numerical Solver Error	III			x			
Calculation Verification - Use Error	IV			x			
Validation - Model [Form]	III			x			
Validation - Model [Inputs]	III			x			
Validation - Comparator [Test Samples]	III			x			
Validation - Comparator [Test Conditions]	II			x			
Validation - Assessment [Input Parameters]	III			x			
Validation - Assessment [Output Comparison]	III			x			
Applicability: Relevance of the Quantities of Interest	III			x			
Applicability: Relevance of the Validation Activities to the COU	II			x			

4.7 UC3 – VVUQ Publications

This section lists all scientific publications relating to the UC3 VVUQ activities conducted within the frame of the SimCardioTest project.

Table 20: UC3 – **List of publications related to VVUQ activities**.

Title	VVUQ Topic
Mora MT. (draft) [65]	Validation, Uncertainty Quantification

5. Conclusion

This annex describes all validation, verification, and uncertainty quantification (VVUQ) activities engaged within the SimCardioTest project between M30 (June 2023) and M54 (June 2025) for assessing the credibility of computational models developed in the frame of Use Cases 1 to 3 (cf. WP2, 3, and 4 respectively). This annex follows and completes project deliverables D6.1 and D6.2 issued in June 2023 (M30).

VVUQ activities were conducted on the same computational models introduced in deliverables D6.1 and D6.2, one specific model per each Use Case, corresponding to a pre-selected Question of Interest (QI). All VVUQ activities were conducted according to ASME VV40 standard guidelines.

For what concerns Use Case 1, the activities were completed satisfactorily, ensuring credibility of the model in the sense of the ASME VVUQ framework. Some technical limitations were encountered, which do not endanger the credibility of this work. Verification activities made our software code

more visible and robust, and its continuous development process extremely healthy. Limitations were identified in the formulation of the comparators, which can be considered as induced by the ASME guideline itself. It prompts, for a threshold detection test, to consider goal-oriented criteria, such as the probability of capture at a given point as a more relevant indication for validation activities.

For what concerns Use Case 2, all planned activities related to Verification, Validation, and Uncertainty Quantification (VVUQ) have been successfully completed. Nonetheless, we recognize that clinical validation requires a significantly broader scope of experimentation and verification efforts. Based on the work conducted throughout the duration of the project, we draw the following key conclusions:

- A numerically stable configuration was established with respect to both discretization schemes and numerical methods, specifically within the Ansys Fluent software environment.
- Atrial motion dynamics were incorporated into the simulations, supported by experimental validation. This advancement enabled the application of motion profiles from patients with atrial fibrillation and facilitated comparative analyses with those from healthy individuals.
- Hemodynamic indices related to thrombus formation in the vicinity of left atrial appendage occlusion (LAAO) devices were analysed, providing insights into the influence of device type, positioning, and patient-specific conditions.
- Initial validation of both global and localized flow parameters was undertaken using diverse experimental setups.
- The developed simulation framework was applied to real-world clinical cases, including both retrospective analyses and preliminary prospective (live) studies.

For what concerns Use Case 3, we implemented validation activities following VV40 standard guidelines in a model used to assess the torsadogenic risk of drugs. An independent analysis of the three computational models integrating the drug assessment tool (pharmacokinetics, cellular, and tissue electrophysiology) allowed to focus on the different parameters, inputs, outputs, existing comparators, and uncertainty sources. Executed activities varied depending on the complexity of the model, and we planned all validation steps according to available resources. An intermediate credibility level was achieved after conducting all the tasks in pharmacokinetics and electrophysiological models. This methodology provides robustness to the study results and, although TdP-risk predictions were based on known and validated drugs, the approach can be extended to new molecules.

For each Use Case, a list of scientific publications related to VVUQ activities engaged during the SimCardioTest project is also given.

6. Bibliography

[1] R. Setzu, A. Olivares, J. Mill and others, “Building credibility of computational models in cardiovascular medicine through verification and validation,” *EDMA,* vol. 19, pp. 86-90, 2024.

[2] V&V40, “Assessing Credibility of Computational Modeling Through Verification and Validation: Application to Medical Devices,” ASME, New York, 2018.

[3] "cellML database," [Online]. Available: https://models.cellml.org/electrophysiology.

[4] P. Pathmanathan and R. A. Gray, "Verification of computational models of cardiac electrophysiology," *International Journal for Numerical Methods in Biomedical Engineering,* vol. 30 (5), no. DOI: 10.1002/cnm.2615, p. 525–544, 2014.

[5] G. W. Beeler and H. Reuter, "Reconstruction of the action potential of ventricular myocardial fibres," *The Journal of Physiology,* vol. 268 (1), no. https://pubmed.ncbi.nlm.nih.gov/874889/, p. 177–210, 1977.

[6] V. Pannetier, Simulations numériques standardisées de dispositifs de stimulation électrique cardiaque, PhD Thesis (in French), Université de Bordeaux, 2024.

[7] V. Pannetier, M. Leguèbe, Y. Coudière and others, "Towards validation of two computational models of artificial pacemakers," *Accepted at Functional Imaging and Modeling of the Heart (FIMH),* 2025.

[8] V. Pannetier, M. Leguèbe, Y. Coudière and others, "Sensitivity Analysis in a Rescaled 0D Pacemaker-Bimembrane Model," *Computing in Cardiology (CINC) Conference,* no. doi: 10.22489/CinC.2024.317, 2024.

[9] V. Pannetier, M. Leguèbe, Y. Coudière and others, "Modeling Cardiac Stimulation by a Pacemaker, with Accurate Tissue-Electrode Interface," *Functional Imaging and Modeling of the Heart,* no. doi:10.1007/978-3-031-35302-4_20, p. 194203, 2023.

[10] R. D. Walton, A. Pashaei, M. E. Martinez and others, "Compartmentalized Structure of the Moderator Band Provides a Unique Substrate for Macroreentrant Ventricular Tachycardia," *Circulation: Arrhythmia and Electrophysiology,* vol. 11 (8), no. https://doi.org/10.1161/circep.117.005913, p. e005913, 2018.

[11] V. Pannetier, Y. Coudière and M. Leguèbe, "Bidomain Model Coupled To A Realistic Multi-Electrode Device In Cardiac Electrophysiology," *Congrès National d'Analyse Numérique (CANUM),* no. https://inria.hal.science/hal-04610592v1, 2024.

[12] V. Pannetier, M. Leguèbe, Y. Coudière and others, "Determination of stimulation threshold in a 3D model of a pacemaker," *Virtual Physiological Human (VPH) conference,* 2024.

[13] M. Leguèbe and others, "CEPS : Cardiac Electrophysiology Solver," *Draft submitted to Journal of Open Source Software,* 2025.

[14] A. Cresti, M. García-Fernández, H. Sievert and others, "Prevalence of extra-appendage thrombosis in non-valvular atrial fibrillation and atrial flutter in patients undergoing cardioversion: a large transoesophageal echo study," *EuroIntervention,* vol. 15(3), p. e225–e230, 2019.

[15] M. Pons, J. Mill, A. Fernandez-Quilez and others, "Joint Analysis of Morphological Parameters and In Silico Haemodynamics of the Left Atrial Appendage for Thrombogenic Risk Assessment," *Journal of interventional cardiology,* 2022.

[16] A. Sedaghat and G. Nickenig, "Letter by Sedaghat and Nickenig Regarding Article, "device-Related Thrombus after Left Atrial Appendage Closure: Incidence, Predictors, and Outcomes," *doi:10.1161/CIRCULATIONAHA.118.036179,* 2019.

[17] J. Saw, A. Tzikas, S. Shakir and others, "Incidence and clinical impact of device-associated thrombus and peri-device leak following left atrial appendage closure with the amplatzer cardiac plug," *JACC: Cardiovascular Interventions,* vol. 10, p. 391–399, 2017.

[18] L. V. Boersma, B. Schmidt, T. R. Betts and others, "Implant success and safety of left atrial appendage closure with the watchman device: peri-procedural outcomes from the ewolution registry," *European heart journa,* vol. 37, p. 2465–2474, 2016.

[19] A. Sedaghat and others, "Device-Related Thrombus After Left Atrial Appendage Closure: Data on Thrombus Characteristics, Treatment Strategies, and Clinical Outcomes From the EUROC-DRT-Registry," *Circulation. Cardiovascular interventions,* Vols. 14,5, no. e010195, 2021.

[20] I. Chung and G. Y. Lip, "Virchow's triad revisited: Blood constituents," *Pathophysiology of Haemostasis and Thrombosis,* vol. 33, no. doi:10.1159/00008384, p. 449–454, 2003.

[21] O. D. Backer, X. Iriart, J. Kefer and others, "Impact of computational modeling on transcatheter left atrial appendage closure efficiency and outcomes," *JACC: Cardiovascular Interventions,* vol. 16, no. doi:10.1016/j.jcin.2023.01.008, p. 655–666, 2023.

[22] J. Saw, J. P. Lopes, M. Reisman and H. G. Bezerra, "CT Imaging for Percutaneous LAA Closure," *Cham: Springer International Publishing,* no. doi:10.1007/978-3-319-16280-5, p. 117–132, 2016.

[23] A. M. Aguado, A. L. Olivares, E. Silva and others, "In silico optimization of left atrial appendage occluder implantation using interactive and modeling tools," *Frontiers in physiology,* vol. 10, p. 237, 2019.

[24] X. Freixa and others, "Pulmonary ridge coverage and device-related thrombosis after left atrial appendage occlusion," *EuroIntervention : journal of EuroPCR in collaboration with the Working Group on Interventional Cardiology of the European Society of Cardiology,* vol. 16(15), no. doi:10.4244/EIJ-D-20-00886, pp. e1288-e1294, 2021.

[25] A. Santiago, C. Butakoff, B. Eguzkitza and others, "Design and execution of a verification, validation, and uncertainty quantification plan for a numerical model of left ventricular flow after lvad implantation," *PLoS computational biology,* vol. 18, no. e1010141, 2022.

[26] E. Khalili, C. Daversin-Catty, A. Olivares and others, "On the importance of fundamental computational fluid dynamics towards a robust and reliable model of left atrial flows: Is there more than meets the eye?," *arXiv:2302.01716 [physics.flu-dyn],* 2023.

[27] E. Roche, M. Singh, K. Mendez and others, "Integrating soft robotics and computational models to study left atrial hemodynamics and device testing in sinus rhythm and atrial fibrillation," *Research Square,* vol. PREPRINT (Version 1), no. DOI: 10.21203/rs.3.rs-6283242/v1.

[28] C. Albors, J. Mill, H. A. Kjeldsberg and others, "Sensitivity Analysis of Left Atrial Wall Modeling Approaches and Inlet/Outlet Boundary Conditions in Fluid Simulations to Predict Thrombus Formation," in *Statistical Atlases and Computational Models of the Heart. Regular and CMRxMotion Challenge Papers (STACOM 2022)*, 2022.

[29] C. Albors, A. L. Olivares, X. Iriart and others, "Impact of Blood Rheological Strategies on the Optimization of Patient-Specific LAAO Configurations for Thrombus Assessment," in *Functional Imaging and Modeling of the Heart (FIMH 2023)*, 2023.

[30] J. Mill, J. Harrison, M. Saiz-Vivo and others, "The role of the pulmonary veins on left atrial flow patterns and thrombus formation," *Sci Rep,* vol. 14, no. https://doi.org/10.1038/s41598-024-56658-2, p. 5860, 2024.

[31] E. Khalili, C. Daversin-Catty, A. L. Olivares and others, "On the importance of fundamental computational fluid dynamics toward a robust and reliable model of left atrial flows,"

Internatioanl Journal for Numerical Methods in Biomedical Engineering, vol. 40 (4), no. https://doi.org/10.1002/cnm.3804, p. e3804, 2024.

[32] C. Albors, J. Mill, A. L. Olivares and others, "Impact of occluder device configurations in in-silico left atrial hemodynamics for the analysis of device-related thrombus," *PLoS Comput Biol,* vol. 20 (9), no. doi: 10.1371/journal.pcbi.1011546, p. e1011546, 2024.

[33] A. Olivares and others, "Verification and validation pipeline of fluid simulations for optimising left atrial appendage occluder implantations: design and initial experiments," *draft*.

[34] E. Gasparotti, E. Vignali, R. Marangoni and others, "An Experimental Setup for the Analysis of Patient-Specific Left Atrial Appendage with Particle Image Velocimetry Investigation," *Functional Imaging and Modeling of the Heart* , no. DOI:10.1007/978-3-031-94559-5_17, pp. 186-196, 2025.

[35] C. Albors and others, "Impact of Flow Dynamics according to Device Implant Depth after Left Atrial Appendage Occlusion," *draft*.

[36] P. Casademunt and others, "Flow component analysis to study haemodynamic," in *CMBEE2025*, 2025.

[37] M. Barrouhou and others, "Large-scale sensitivity analysis of modeling settings influencing Hemodynamics after left atrial appendage occlusion," in *CMBEE2025*, 2025.

[38] C. Albors, N. Arrarte Terreros, M. Saiz and others, "In silico estimation of thrombogenic risk after left atrial appendage excision: Towards digital twins in atrial fibrillation," *Computers in biology and medicine,* vol. 194, no. DOI:10.1016/j.compbiomed.2025.110483, p. 110483, 2025.

[39] H. Kjeldsberg, C. Albors, J. Mill and others, "Impact of left atrial wall motion assumptions in fluid simulations on proposed predictors of thrombus formation," *International Journal for Numerical Methods in Biomedical Engineering,* vol. 40 (6), no. DOI:10.1002/cnm.3825, 2024.

[40] Z. Li, B. J. Ridder, X. Han and others, "Assessment of an In Silico Mechanistic Model for Proarrhythmia Risk Prediction Under the CiPA Initiative," *Clinical Pharmacology & Therapeutics,* vol. 105, no. 2, pp. 466-475, 2 2019.

[41] S. Nobe, M. Aomine and M. Arita, "Bepridil prolongs the action potential duration of guinea pig ventricular muscle only at rapid rates of stimulation," *General Pharmacology: The Vascular System,* vol. 24, no. 5, pp. 1187-1196, 9 1993.

[42] S. C. Verduyn, J. G. M. Jungschleger, M. Stengl and others, "Electrophysiological and proarrhythmic parameters in transmural canine left-ventricular needle biopsies.," *Pflugers Archiv : European journal of physiology,* vol. 449, no. 1, pp. 115-22, 10 2004.

[43] J. J. Salata, N. K. Jurkiewicz, A. A. Wallace, R. F. Stupienski, P. J. Guinosso and J. J. Lynch, "Cardiac Electrophysiological Actions of the Histamine H r Receptor Antagonists Astemizole and Terfenadine Compared With Chlorpheniramine and Pyrilamine," 1995.

[44] J. K. Gibson, Y. Yue, J. Bronson and others, "Human stem cell-derived cardiomyocytes detect drug-mediated changes in action potentials and ion currents," *Journal of Pharmacological and Toxicological Methods,* vol. 70, no. 3, pp. 255-267, 11 2014.

[45] Y. Yu, M. Zhang, R. Chen and others, "Action potential response of human induced-pluripotent stem cell derived cardiomyocytes to the 28 CiPA compounds: A non-core site data report of the CiPA study," *Journal of Pharmacological and Toxicological Methods,* vol. 98, 7 2019.

[46] B. Lecocq, V. Lecocq, P.-L. Prost and others, "Effects of bepridil and CERM 4205 (ORG 30701) on the relation between cardiac cycle length and QT duration in healthy volunteers," *The American Journal of Cardiology,* vol. 66, no. 5, pp. 636-641, 5 1990.

[47] S. Miyamoto, B. M. Zhu, T. Teramatsu and others, "QT-prolonging class I drug, disopyramide, does not aggravate but suppresses adrenaline-induced arrhythmias. Comparison with cibenzoline and pilsicainide," *European Journal of Pharmacology,* vol. 400, no. 2-3, pp. 263-269, 5 2000.

[48] F. L. Coz, C. Funck-Brentano, T. Morell and others, "Pharmacokinetic and pharmacodynamic modeling of the effects of oral and intravenous administrations of dofetilide on ventricular repolarization," *Clinical pharmacology and therapeutics,* vol. 57, no. 5, pp. 533-542, 1995.

[49] B. S. Stambler, M. A. Wood, K. A. Ellenbogen and others, "Efficacy and safety of repeated intravenous doses of ibutilide for rapid conversion of atrial flutter or fibrillation," *Circulation,* vol. 94, no. 7, pp. 1613-1621, 5 1996.

[50] H. M. Himmel, A. Bussek, M. Hoffmann and others, "Field and action potential recordings in heart slices: correlation with established in vitro and in vivo models," *British journal of pharmacology,* vol. 166, no. 1, pp. 276-296, 5 2012.

[51] K. Kiura, K. Nakagawa, T. Shinkai and others, "A Randomized, Double-Blind, Phase IIa Dose-Finding Study of Vandetanib (ZD6474) in Japanese Patients With Non-Small Cell Lung Cancer," *Journal of Thoracic Oncology,* vol. 3, no. 4, pp. 386-393, 5 2008.

[52] L. Testai, M. C. Breschi, E. Martinotti and V. Calderone, "QT prolongation in guinea pigs for preliminary screening of torsadogenicity of drugs and drug-candidates. II," *Journal of applied toxicology : JAT,* vol. 27, no. 3, pp. 270-275, 5 2007.

[53] A. D. V. Haarst, G. A. E. V. '. Klooster, J. M. A. V. Gerven and others, "The influence of cisapride and clarithromycin on QT intervals in healthy volunteers," *Clinical pharmacology and therapeutics,* vol. 64, no. 5, pp. 542-546, 1998.

[54] R. A. Carr, A. Edmonds, H. Shi and others, "Steady-state pharmacokinetics and electrocardiographic pharmacodynamics of clarithromycin and loratadine after individual or concomitant administration," *Antimicrobial agents and chemotherapy,* vol. 42, no. 5, pp. 1176-1180, 1998.

[55] I. Grande, A. Pons, I. Baeza and others, "QTc prolongation: is clozapine safe? Study of 82 cases before and after clozapine treatment," *Human psychopharmacology,* vol. 26, no. 6, pp. 397-403, 5 2011.

[56] G. Frommeyer, C. Fischer, C. Ellermann and others, "Severe Proarrhythmic Potential of the Antiemetic Agents Ondansetron and Domperidone," *Cardiovascular toxicology,* vol. 17, no. 4, pp. 451-457, 5 2017.

[57] B. Charbit, J. C. Alvarez, E. Dasque and others, "Droperidol and ondansetron-induced QT interval prolongation: a clinical drug interaction study," *Anesthesiology,* vol. 109, no. 2, pp. 206-212, 2008.

[58] Z. Desta, T. Kerbusch and D. A. Flockhart, "Effect of clarithromycin on the pharmacokinetics and pharmacodynamics of pimozide in healthy poor and extensive metabolizers of cytochrome P450 2D6 (CYP2D6)," *Clinical pharmacology and therapeutics,* vol. 65, no. 1, pp. 10-20, 1999.

[59] E. P. Harrigan, J. J. Miceli, R. Anziano and others, "A randomized evaluation of the effects of six antipsychotic agents on QTc, in the absence and presence of metabolic inhibition," *Journal of clinical psychopharmacology,* vol. 24, no. 1, pp. 62-69, 5 2004.

[60] L. Johannesen, J. Vicente, J. W. Mason and others, "Differentiating Drug-Induced Multichannel Block on the Electrocardiogram: Randomized Study of Dofetilide, Quinidine, Ranolazine, and Verapamil," *Clinical Pharmacology & Therapeutics,* vol. 96, no. 5, pp. 549-558, 5 2014.

[61] B. Darpo, "The thorough QT/QTc study 4 years after the implementation of the ICH E14 guidance," *British Journal of Pharmacology,* vol. 159, no. 1, pp. 49-57, 1 2010.

[62] J. Llopis-Lorente, B. Trenor and J. Saiz, "Considering population variability of electrophysiological models improves the in silico assessment of drug-induced torsadogenic risk," *Computer Methods and Programs in Biomedicine,* vol. 221, p. 106934, 6 2022.

[63] J. Llopis-Lorente, S. Baroudi, K. Koloskoff and others, "Combining pharmacokinetic and electrophysiological models for early prediction of drug-induced arrhythmogenicity," *Computer Methods and Programs in Biomedicine,* vol. 242, p. 107860, 12 2023.

[64] C. Knox, M. Wilson, C. M. Klinger and others, "DrugBank 6.0: the DrugBank Knowledgebase for 2024," *Nucleic Acids Research,* vol. 52, no. D1, pp. D1265-D1275, 1 2024.

[65] M. Mora, C. Ortigosa, H. Finsberg and others, "Refinement of electrophysiological drug safety assessment through validation-readjustment strategies," *draft*.

This project received funding from the European Union's Horizon 2020 research and innovation program under grant agreement No 101016496

EU Horizon 2020 Research & Innovation Program
Digital transformation in Health and Care
SC1-DTH-06-2020
Grant Agreement No. 101016496

SimCardioTest - Simulation of Cardiac Devices & Drugs for in-silico Testing and Certification

Technical Annex

Annex B – WP6 UC3 PK Verification
(complement to WP6 Task 6.1 – including M30-M54 activities)

Work Package 6 (WP6)
Verification, validation, uncertainty quantification & certification

WP Lead: MPC, France

PUBLIC

Document history			
Date	**Version**	**Author(s)**	**Comments**
07/06/2023	V1	J. WELZEL	Final version prior consolidation
23/06/2023	V2	R. SETZU	Format consolidation
29/06/2023	V3	H. AREVALO	Quality Review
30/06/2023	V4	R. SETZU	Final version
08/06/2024	V5	R. LESTREZ, J. WELZEL	Content editing
30/06/2024	V6	R. SETZU	Format editing Highlighted M36-M54 new content

Table Of Contents

Executive Summary

This technical annex expands on Annex A6.1-UC3-PK which was initially included in the SimCardioTest WP6 deliverable D6.1 and elaborated for Use Case 3 in the context of drug safety assessment. It completes the original annex with the work performed after M30 till the completion of the UC3 verification activities of the PK models in scope.

Acronyms

Table 1: List of Acronyms

Acronym	Meaning
PK	Pharmacokinetic
IST	InSilicoTrials
SCT	SimCardioTest
TdP	Torsade de pointes

1 Code Verification

1.1 Software Quality Assurance

ExactCure simulation service is composed of ExaTwin, the computation-dedicated component, and PAPI, the public interface. The simulation service is part of a Software Medical Device, ExaMed. As such, its life cycle follows all software quality activities to guarantee conformity with ISO/IEC 62304 norm on Software Medical Devices.
In particular, this means the following:

- Complete life cycle management: definition, analysis, development, release, maintenance, end-of-life.
- Risk management
- Quality Management system
- Process-driven development and release, with traceability and including change management, using:
    - JIRA, Agile Project Management Issue tracking
    - Git, version control system
    - Bitbucket, a CI/CD platform to automate testing and deployment
- Multi-environment management, for development, testing and production.
- Software Verification, following the declared architecture and functionalities:
    - Unit testing of software units
    - Integration testing of software elements
    - End-to-end testing of the system
    - Code reviews, use of software quality tools performing static code analysis (coding style, test coverage, code complexity)
- Documentation (in-code of external) about interfaces, usages, methodologies

This SQA is detailed in the Technical Folder of the Medical Device.

Current depth level is 4/5 (where the maximum level is compliance wrt MDR)

About installation & environments
ExaTwin is a software medical device that is accessible only with an API and is not distributed.
ExactCure has installed PAPI/ExaTwin on the following machines:

- Production environment
    - Intel(R) Xeon(R) CPU E5-2673 v4 @ 2.30GHz
    - 16Go RAM
    - 32 GB temporary storage
    - Max IOPS 6400
- Pre-production (Plive) environment
    - Intel(R) Xeon(R) Platinum 8171M CPU @ 2.60GHz
    - 8Go RAM
    - 16 GB temporary storage
    - Max IOPS 3200

Both are on Ubuntu 18.04 Operating System.

1.2 Numerical Code Verification

1.2.1 Verification Plan

PK models are systems of ordinary differential equations (ODEs) with a calibration layer relating model parameters to patient covariates and other data. These model features are described in a proprietary user-friendly language that ExactCure system (ExaTwin) parses and solves when simulating a drug intake scenario.
ODEs are solved numerically, and calibration may involve numerical inversions to infer parameters. The numerical algorithms are based on SciPy's library.

A *simulation request* is a drug intake scenario applied to the drug model and given patient, requested to an API (ExactCure public API or internal ExaTwin API).

Depth-levels considered for NCV are:
No NCV.
Visual inspection or graphical comparison of predictions to known benchmarks or to a reference software.
Numerical (discretization) error quantified between numerical and reference solutions (exact if possible), for the default accuracy setting.
"Black-box" convergence analysis w.r.t appropriate numerical parameter(s) (eg. timestep, number of iterations…), including the observed order of accuracy if accessible.
"White-box" verification of numerical algorithms (ie their internal behaviour).

We perform verification for each PK model and expected drug intake scenarios. We target a depth level between 3/5 and 4/5: Omiting White-box verification of numerical algorithms seems reasonable considering they come from Scipy [1] which is one of the most used and tested numerical package. A level of 3/5 for the drug simulation pipeline (ie request at API level) is also reasonable given that PK/PD models are ordinary differential systems with contextualization, and their numerical solving is well covered by the NCV on algorithms. Verification of the pipeline is mainly an integration test, checking the flow from model parsing to calibration to simulation to quantities of interest computation, which is included in SQA.

1.2.2 ODE Solver Algorithm

One of the key algorithms of ExaTwin simulation functionality is the ODE solver. SciPy, the widely used and sound numerical package for Python language, is integrated in the simulation algorithm, which uses the *solve_ivp* routine. SciPy has strong support from the scientific computing community, institutional partners and leading companies [1].

The explicit method "RK45" is a method of order O(h4) with an error estimator of order O(h5) and is the recommended default solver for non-stiff problems. PK models are most of the time non-stiff. Quoting Wikipedia: "*Runge-Kutta-Fehlberg Method 45 performs well with most ODE systems, and it is indicated as the first choice of solver. By performing one extra calculation, the error in the solution can be estimated and controlled by using the higher-order embedded method that allows for an adaptive stepsize to be determined automatically.*"

The discretization (stepsize) is controlled through the user-input tolerances “atol” and “rtol”, combined into Tol = atol + rtol * abs(y), where rtol controls a relative accuracy (number of correct digits), while atol controls absolute accuracy (number of correct decimal places). Default values are 1e-3 for rtol and 1e-6 for atol.

The RK45 solver implementation has been verified on several use-cases, for example (see *Figure **1***):

- Oral drug PK model: a linear, constant coefficient and scalar differential equation
- Riccati equation: a non-linear, constant coefficient and scalar differential equation

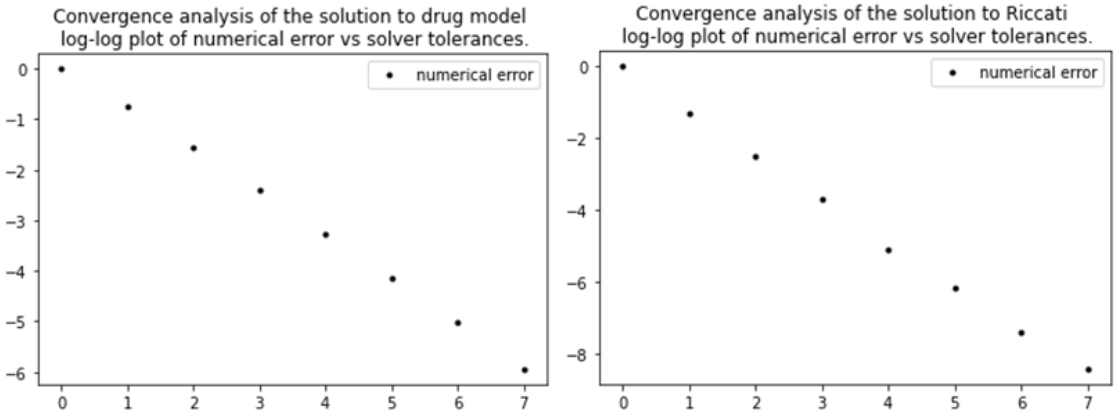

Figure 1: Convergence analysis shows that, as solver tolerances decrease, the numerical error converges to zero (thus, the numerical solution converges to the analytical solution).

Same convergence has been observed on other differential problems. This provides strong evidence about the capacity of the routine to solve (non-stiff) initial value problems, as required for PK model simulation.

1.2.3 Inversion Algorithm

Model parameters may be known through drug concentration curve features (“non-compartmental data”), for example AUC (Area Under the Curve), Cmax (max concentration) etc. ExaTwin is able to solve a combination of such data to infer model parameters. It proceeds by numerically inverting the relationship “parameters → NC data”, using classical root-solving algorithms provided by SciPy in the routine *root_scalar()*.

We have verified Bisection and Brent. Both conformed to expectations with respect to their documentation and are suitable for use in ExaTwin and parameter estimation.

1.2.3.1 Bisection

Bisection is the most classic root-finding algorithm. It is a robust iterative algorithm that halves the bracketing of the root each step. Using 3 simple benchmarks, we studied the convergence properties (see *Figure **2***).

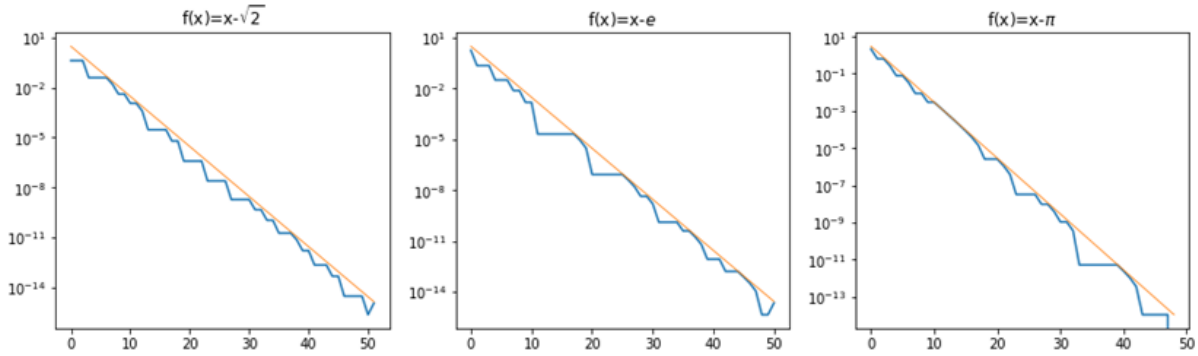

Figure 2: Bisection convergence properties with 3 simple benchmarks functions.

As expected, Bisection obeys a linear convergence scheme to the theoretical solution. Moreover, we checked that the implementation was robust enough against limit cases.

1.2.3.2 Brent

Brent's method combines root bracketing, interval bisection, and inverse quadratic interpolation. We studied the convergence properties on two benchmark functions that are differentiable with root zero but a different slope around it (see *Figure **3***).

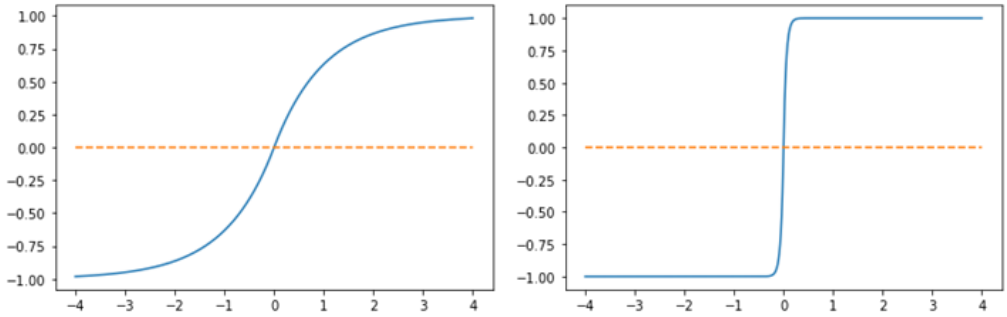

Figure 3: Brent convergence properties with 2 simple benchmarks functions.

Convergence to the root is displayed in *Figure **4***:

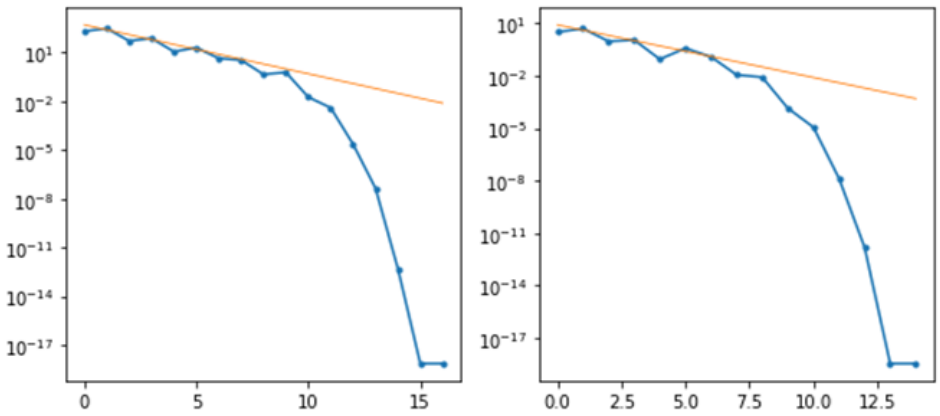

Figure 4: Brent converges to the root with 2 simple benchmarks functions.

As expected, Brent follows a super-linear convergence scheme for such well-behaved function and the terminal accuracy corresponds to the expected accuracy (1e-16).

1.2.4 Simulation from ExaTwin

We show here, on two relevant examples, that the ODE solving, the parameters calibration, and the drug intake scenario are all properly combined in ExaTwin simulation endpoint. These examples are PK models for which analytical solutions are known, and we compare the simulated concentration curve with the theoretical one.

To perform the simulation at ExaTwin level, we simply create an API request directly from a Python Notebook to a version of ExaTwin installed locally, and we store results. Computations from analytical formulae and plotting are done in the same Notebook.

First example is single-compartment model with linear absorption and elimination processes and respective rates ka and ke. Drug concentration is the drug quantity x1 in the central compartment divided by the so-called distribution volume V. The solution after a single drug intake D at t=0 is well-known in pharmacokinetics. In particular, the time at which the concentration is maximum is given by:

$$T_{max} = (\ln(ka)-\ln(ke)) / (ka-ke)$$

The elimination half-time is given by:

$$T_{1/2}=\ln(2)/ke$$

Now, we run the numerical simulation with the following input data:

- Scenario data: dose is 100 at t=0, meaning x0(t=0) = D
- Model parameters: ka and ke are inferred from the following observation data: concentration maximum should occur 1 hour after the drug intake, and the elimination half-time is 4 hours. Distribution volume is 50.0, bioavailability is 1.0.
- Ordinary differential system of the model, encoded in the request “model” section:
  - x0_dot = -ka*x0
  - x1_dot = +ka*x0 – ke*x1
- output is x1/V

Plotting the analytical solution on the same graph, we see that this numerical simulation conforms to expectations (see *Figure **5***).

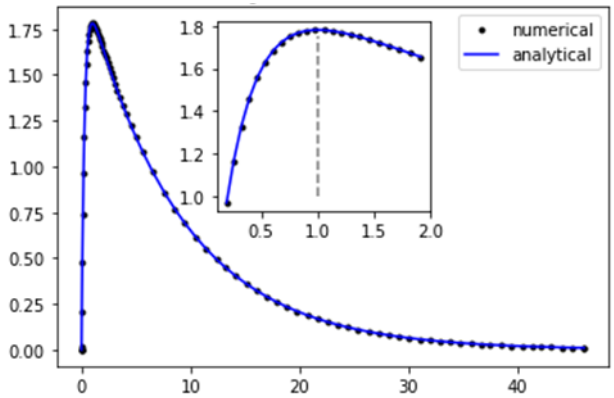

Figure 5: Simulation output against analytical solution. 1 compartment, linear model. Concentration in mg/L, vs time in hours.

We reproduce this verification with a slightly more complicated model. Kinematically, the model has two compartments and is fully linear. Calibration will be trivial. We run the numerical simulation with the following input data:

- Scenario data: dose is 100 at t=0
- Model parameters: ka=1.0, ke=0.25, and intercompartmental rates are k12=k21=0.2. Distribution volume is 50.0, bioavailability is 1.0
- Ordinary differential system of the model:
  - x0_dot = -ka*x0
  - x1_dot = +ka*x0 – ke*x1 + k21*x2 – k12*x1
  - x2_dot = - k21*x2 + k12*x1

We have again a match with the analytical solution (see *Figure **6***).

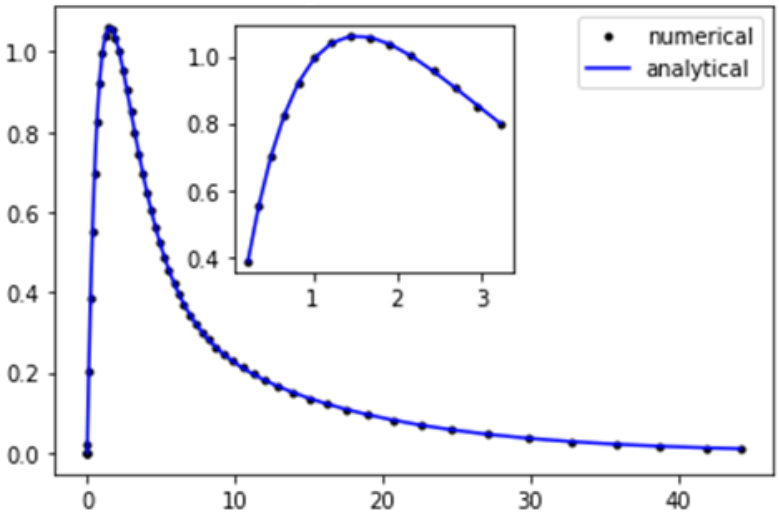

Figure 6: Simulation output against analytical solution. 2 compartments, linear model. Concentration in mg/L, vs time in hours.

This concludes the verification that a simulation request, at the level of ExaTwin, correctly integrates model parsing and numerical algorithms to solve a drug intake simulation. As said in the verification plan, exhaustive testing is scheduled for a later stage.

1.2.5 Simulation from the Public Interface

To verify the simulation functionality at the system level, in conditions reflecting its use for Use-Case 3, we need to perform simulations from PAPI, the public interface. We have requested the Plive environment, with the same access rights as IST.

We display the simulation of Clozapine (CIS= 67513540) on two patient profiles in *Figure **7*** and *Figure **8*** respectively, and simulation of Escitalopram (CIS=67219535) in *Figure **9***.

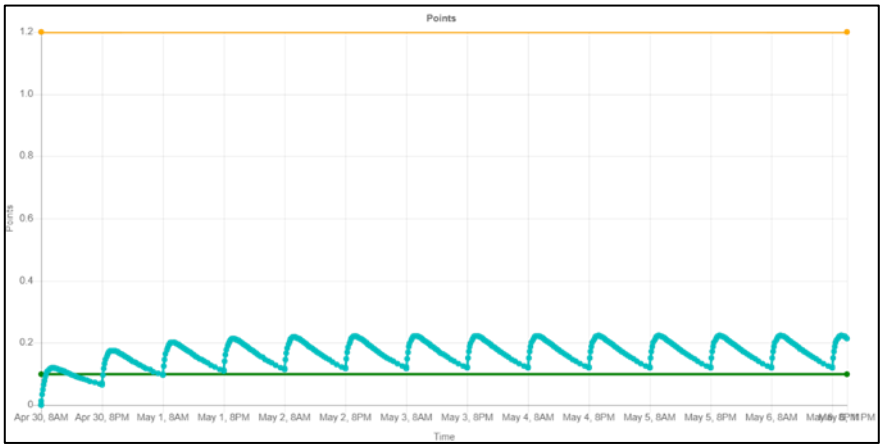

Figure 7: PAPI simulation: clozapine, male patient, 100mg twice daily.

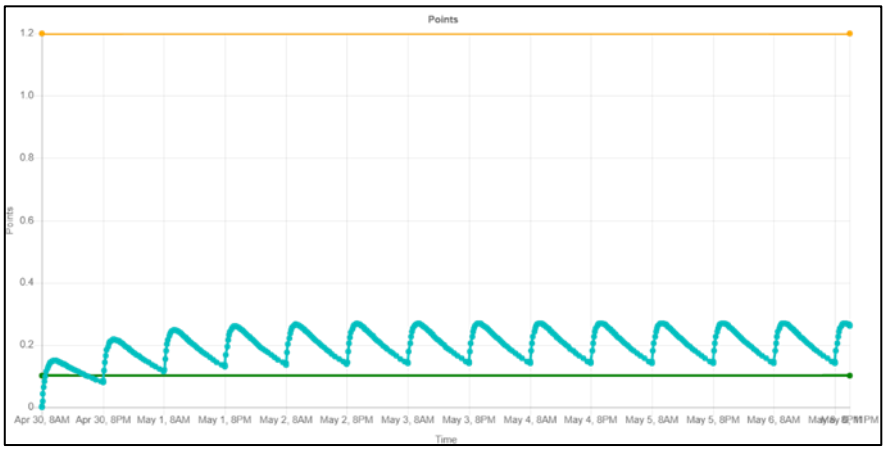

Figure 8: PAPI simulation: clozapine, female patient, 100mg twice daily.

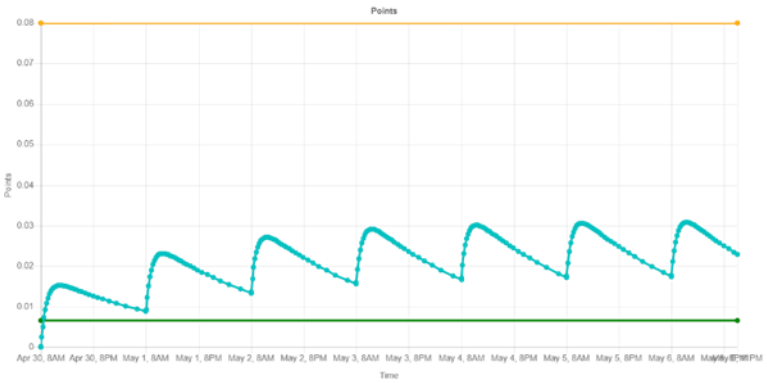

Figure 9: PAPI Simulation: Escitalopram, standard patient, 15mg daily.

This shows that PAPI correctly integrates ExaTwin simulation on the expected drug scope and that the interface responds to user inputs (drug, patient, administration). Note that those simulations match exactly what is obtained by requesting ExaTwin directly, as one can see from graphs in the Calculation Verification step.

Next sections will show simulation results of actual PK models for molecules in scope of Use-Case 3, making sure that for those models, the software and numerical code is accurate.

2 Calculation Verification

Calculation verificaiton contains the following steps:
Discretization error (DE): estimation of the discretization error on the quantities of interest (concentrations) for molecules/models in the COU, given a grid of tolerances on the system solver.
Numerical solver error (NSE): QOI (concentrations) sensitivies to tolerances level for molecules/models in the COU.
Use error (UE): The API has a partial validation of the input (completeness, types). Key inputs and outputs were verified by the practitioner.

2.1 Discretization Error

There is no spatial discretization in the numerical model, only temporal discretization to simulate the time-course of drug concentrations. Analysis of the associated numerical error is reported in the next section.

2.2 Numerical Solver Error

Recalling characteristics of the ODE solver, ExaTwin uses by default an adaptive solver based on RKF45 method. Accuracy in the numerical solving is controlled by user-input tolerances that loosely speaking, bounds the difference between the numerical solution and the exact solution on any time interval. However, the public interface as well as the model definition do not allow to change these tolerances, which are fixed to their default values (1e-06 and 1e-06 for relative and absolute tolerances). The same is true for the inversion algorithms.

NSE depth-levels:
No SV.
Visual (graphical) inspection of QOI predictions to known benchmarks or to a reference software, where defaut solver tolerances are used. Basic/manual input-output validation.
Error quantification on QOI/COU versus reference solutions, showing a stable behaviour around the chosen solver tolerance. Full/automatic input/output validation.
QOI convergence analysis w.r.t appropriate numerical parameter(s) (eg. timestep, number of iterations…) and numerical stability analysis showing negligible impacts of changes relative to the model accuracy goal. Full/automatic input/output validation.
DE: “White-box” verification of QOI computations, numerical stability analysis, peer-review of inputs/outputs.

We target a depth level of 3/5. Quantities of interest for the COU barely differ from the system solutions themselves (they only include a rescaling), and models are very close to benchmark problems considered in NCV. The convergence analysis would therefore be redundant with the NCV study. Hence, we consider that level 3 is enough.

The differential equations system solver at the heart of the simulation engine has no tweakable parameter beyond the tolerances on local error for adaptative time-steping.

Convergence analysis will not be performed but we will report the numerical accuracy on the simulation output compared to known solutions.

We perform a Parameters estimation verification and a Maximum concentration verification for each molecule available from the public interface and in scope of H2020/SimCardioTest.
Note that administration scenarios may not be therapeutically correct on the treatment duration. They are chosen so that the concentration curve attains a steady state in order to compare with theoretical concentrations accurately.

2.2.1 Clozapine

2.2.1.1 Parameters Estimation Verification

Covariates: sex_m is used, which is derived from the higher-level sex covariates. If the subject gender is male, then sex_m is True and valued to 1, else sex_m is False and valued to 0.
Parameters encoded in the model are:

- Bioavailability F = 1.0
- Lag Tlag = 0.0
- Absorption rate Ka = 1.24+(0.13*sex_m)
- Clearance Cl = 39.9+(8*sex_m)
- Distribution volume V = 564+(155*sex_m)
- Elimination rate Ke is Cl/V

Subjects:

- Subject 1: Male
- Subject 2: Female

Results are presented in Table 2 and Table 3.

Table 2: Parameters calibration values for subject 1, clozapine.

Parameter	Calibrated	Expected	Calib. Error
F	1.0	1.0	0.0
Tlag	0.0	0.0	0.0
Ka (subject 1)	1.37	1.37	0.0
Cl (subject 1)	47.9	47.9	0.0
V (subject 1)	719.0	719.0	0.0
Ke (subject 1)	0.066620	0.066620	0.0

Table 3: Parameters calibration values for subject 2, clozapine.

Parameter	Calibrated	Expected	Calib. Error
Ka (subject 2)	1.24	1.24	0.00
Cl (subject 2)	39.9	39.9	0.
V (subject 2)	564.0	564.0	0.0
Ke (subject 2)	0.070744	0.070744	0.0

Calibration matches expectations perfectly on these patients.

2.2.1.2 Maximum Concentration Verification

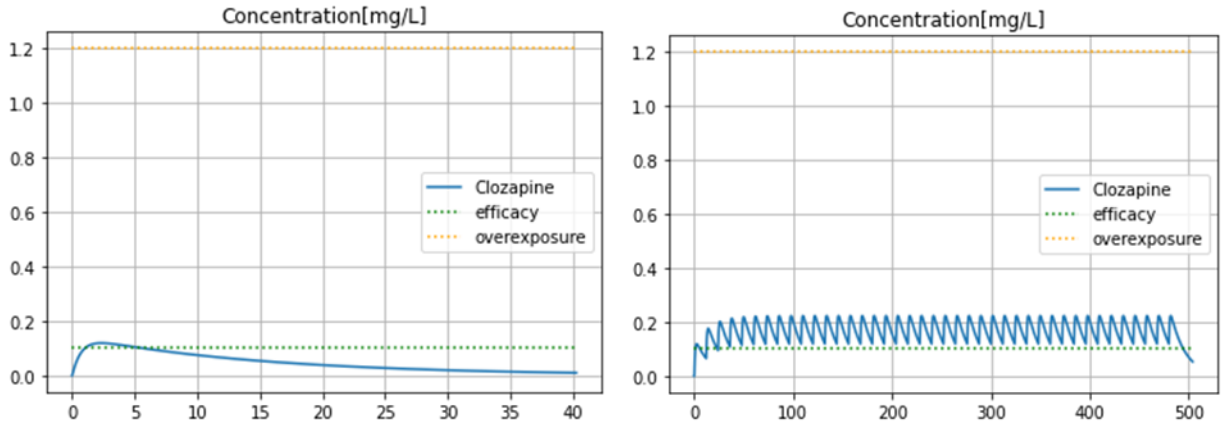

Figure 10: Numerical simulation with a male patient, clozapine is administered orally every 12 hours with a dose of 100mg, for a period of 20 days (where steady state is practically obtained).

We extract numerically the maximum concentration after one drug intake and at steady state. Similarly, we use the model parameters to compute the theoretical maximum concentration after one drug intake and at steady state. Table 4 displays results.

Table 4: Results of numerical vs theoretical max concentrations comparison test for clozapine.

Value \ Scenario	Single dose	Repeated admin
Numerical max concentration	0.119165	0.223206
Theoretical max concentration	0.119166	0.223209
Numerical Error	1e-06	3e-06

We see a match at the order of 10^{-6} on the maximum concentration in both scenarios.

2.2.2 Chlorpromazine

2.2.2.1 Parameters Estimation Verification

Covariates: weight, glomerular filtration rate (GFR)
Base parameters encoded in the model are:

- Bioavailability F = 0.32
- Distribution volume V = 1470
- Lag Tlag = 0.0
- Elimination half-time T12 = 30
- Time of maximum concentration Tmax = 2.5

Calibration step will infer Ke and Ka from numerical inversion of T12 and Tmax data. If we compute T12 and Tmax with calibrated parameters and compare with original values, we can measure the calibration error.

On subject 1, a standard patient (weight=70, GFR=100), we have values in Table 5.

Table 5: Parameters calibration values for subject 1, chlorpromazine.

Parameter-Data	Calibration	Expected	Calib Error
Ke	**0.0231049**	/	/
Ka	1.75522	/	/
T12	30.0	30	0.0
Tmax	2.49999	2.5	1e-14

For non-standard weight ($\neq$70) or GFR ($\neq$100), there is an additional calibration step. On subject 2, with weight = 140 and GFR = 50, we have values in Table 6.

Table 6: Parameters calibration values for subject 2, chlorpromazine.

	Calibrated	Expected	Calib Error
V (subject 2)	2940.0	2940.0	0.0
Ke (subject 2)	0.023047	0.023047	0.0

Calibration matches expectations perfectly on these patients.

2.2.2.2 *Maximum Concentration Verification*

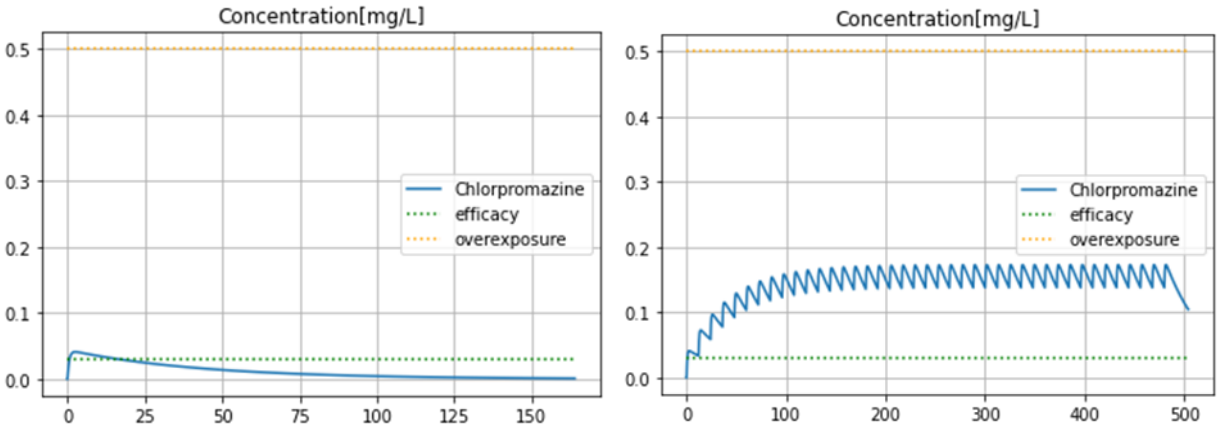

Figure 11: Numerical simulation with a patient with GFR=100 and weight=70, chlorpromazine is administered orally every 12 hours with a dose of 200mg, for a period of 20 days (where steady state is practically obtained).

Results on maximal concentration are reported in Table 7.

Table 7: Results of numerical vs theoretical max concentrations comparison test for chlorpromazine.

Value \ Scenario	Single dose	Repeated admin
Numerical max concentration	0.041092	0.172946
Theoretical max concentration	0.041093	0.172951
Numerical error	1e-06	4e-06

We see a match at the order of 10^{-6} on the maximum concentration in both scenarios.

2.2.3 Escitalopram

2.2.3.1 *Parameters Estimation Verification*

Covariates: weight, age, body mass index (BMI), CYP2C19 mutation status.
Parameters encoded in the model are:

- Bioavailability F = 1.0
- Lag Tlag = 0.0
- Absorption rate Ka = 0.80
- Clearance CL = 26.0 * power(age/40,-0.336)*power(weight/76,0.333)
- Distribution volume V = 947.0 * power(BMI/27,1.11)
- Elimination rate Ke is Cl/V

For non-standard CYP2C19 mutation status, there is an additional calibration step: The clearance Cl must be adjusted by a factor of 0.762.

Subjects:

- Subject 1: Standard (weight = 70, age = 40, BMI = 25, default CYP2C19 mutation status)
- Subject 2: Subject 1 with "poor" CYP2C19 mutation status

Results are reported in Table 8 and Table 9.

Table 8: Parameters calibration values for subject 1, escitalopram.

Parameter	Calibrated	Expected	Calib Error
F	1.0	1.0	0.0
Tlag	0.0	0.0	0.0
Ka	0.80	0.80	0.0
Cl	25.297643	25.297643	0.0
V	869.460007	869.4600075	2e-13
Ke (subject 1)	0.0290958	0.0290958	1e-17

Table 9: Parameters calibration values for subject 2, escitalopram.

Parameter	Calibrated	Expected	Calib Error
Ke (subject 2)	0.022171	0.022171	1e-17

Calibration matches expectations perfectly on these patients.

2.2.3.2 Maximum Concentration Verification

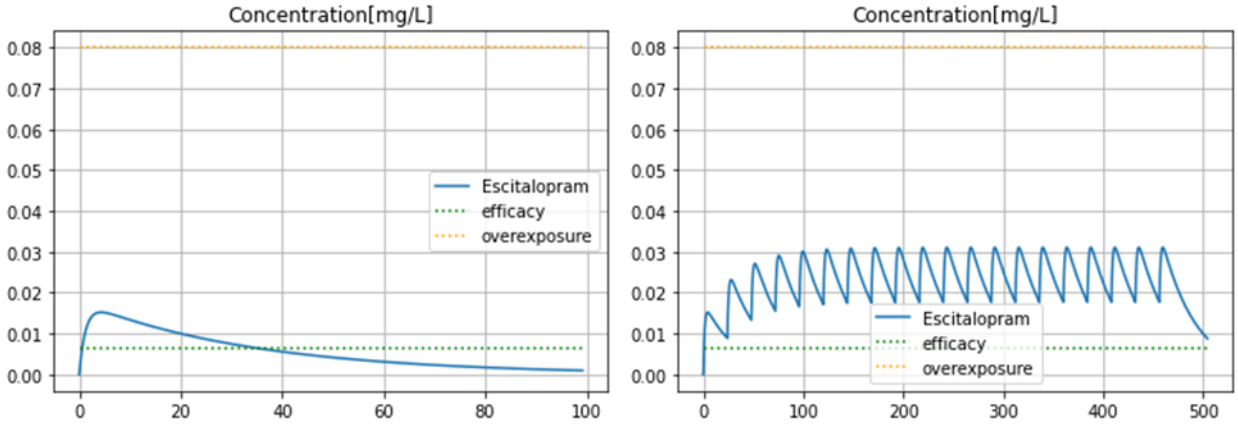

Figure 12: Numerical simulation with a patient with age = 40, weight = 70, BMI = 25 and CYP2C19 at "extensive", Escitalopram is administered orally every 24 hours with a dose of 15mg, for a period of 20 days (where steady state is practically obtained).

Results on maximal concentration are reported in Table 10.

Table 10: Results of numerical vs theoretical max concentrations comparison test for escitalopram.

Value \ Scenario	Single dose	Repeated admin
Numerical max concentration	0.015222	0.031083
Theoretical max concentration	0.015223	0.031088
Numerical error	9e-07	5e-06

We see a match at the order of 10^{-6} on the maximum concentration in both scenarios.

2.2.4 Risperidone

2.2.4.1 Parameters Estimation Verification

Covariates: weight, age and glomerular filtration rate (GFR)
Parameters encoded in the model are:

- Bioavailability F = 1.0
- Lag Tlag = 0.235
- Absorption rate Ka = 0.239
- Clearance CL = (4.66 * power(weight/70,0.75) + 0.00831*GFR) * power(age/18.1,-0.172)
- Distribution volume V1 = 137*weight/70
- Distribution volume V1 = 86.8*weight/70
- Intercompartmental clearance Q = 1.35
- Elimination rate Ke is Cl/V
- Intercompartmental transfer rates are K12=Q/V1 and K21=Q/V2

Subjects:

- Subject 1: standard patient (weight=70, age=40, GFR=90)
- Subject 2: non-standard patient (weight=100, age=60, GFR=50.0)

Results are shown in Table 11 and Table 12.

Table 11: Parameters calibration values for subject 1, risperidone.

Parameter	Calibrated	Expected	Calib Error
F	1.0	1.0	0.00
Tlag	0.235	0.235	0.
Ka	0.239	0.239	0.0
Q	1.35	1.35	0.0
Cl (subject 1)	4.718403	4.7184030	2e-14
V1 (subject 1)	137.0	137.0	0.0
V2 (subject 1)	86.8	86.8	0.0
Ke (subject 1)	0.034440	0.034440	2e-16

Parameter	Calibrated	Expected	Calib Error
K12 (subject 1)	0.009854	0.009854	0.0
K21(subject 1)	0.015552	0.015552	0.0

Table 12: Parameters calibration values for subject 2, risperidone.

Parameter	Calibrated	Expected	Calib Error
Cl (subject 2)	5.293074	5.293074	3e-14
V1 (subject 2)	195.714285	195.714285	2e-14
V2 (subject 2)	124.0	124.0	0.0
Ke (subject 2)	0.027044	0.02704490	1e-16
K12 (subject 2)	0.006897	0.00689781	1e-18
K21 (subject 2)	0.010887	0.01088709	0.0

Calibration matches expectations perfectly on these patients.

2.2.4.2 Maximum Concentration Verification

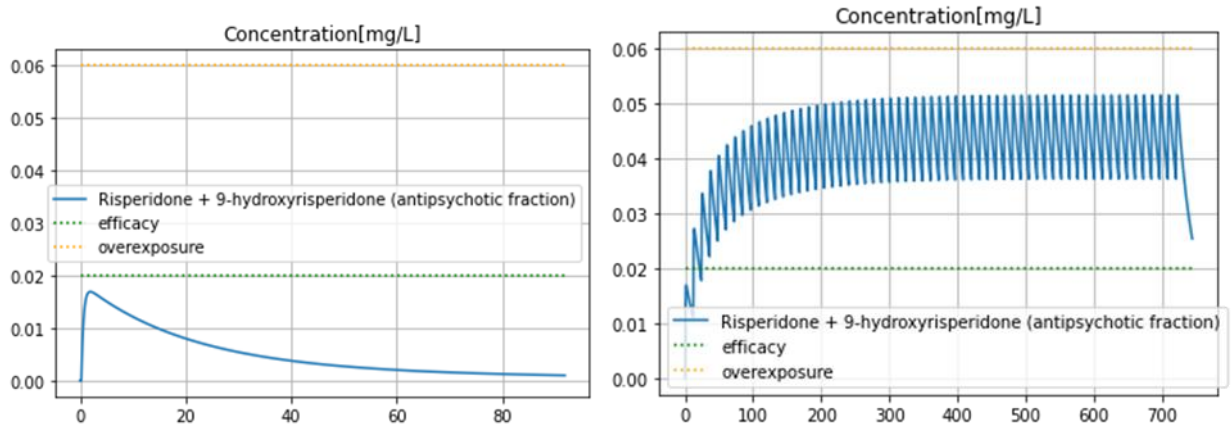

Figure 13: Numerical simulation with a patient with weight=70, age=40 and GFR=90, Risperidone is administered orally every 12 hours with a dose of 2.5mg, for a period of 30 days (where steady state is practically obtained).

Results on maximal concentration are shown in Table 13.

Table 13: Results of numerical vs theoretical max concentrations comparison test for risperidone.

Value \ Scenario	Single dose	Repeated admin
Numerical max concentration	0.0169259	0.051555
Theoretical max concentration	0.016926	0.051561

Value \ Scenario	Single dose	Repeated admin
Numerical Error	8e-07	6e-06

We see a match at the order of 10^{-6} on the maximum concentration in both scenarios.

2.2.5 Carvedilol

2.2.5.1 Parameters Estimation Verification

Covariates: weight, smoker status
Parameters encoded in the model are:

- Bioavailability F = 1.0
- Lag Tlag = 0
- Absorption rate Ka = 0.81
- Clearance CL = 10 + 0.434*weight + 29.9 * smoker
- Distribution volume V = 832
- Elimination rate Ke is Cl/V

Subjects:

- Subject 1: Standard (weight = 70, non-smoker)
- Subject 2: Weight=100, smoker (smoker=1)

Table 14: Parameters calibration values for subject 1, carvedilol.

Parameter	Calibrated	Expected	Calib Error
F	1.0	1.0	0.0
Tlag	0.0	0.0	0.0
Ka	0.81	0.81	0.0
Cl (subject 1)	40.379999	40.38	5e-15
V	832.0	832.0	0.0
Ke (subject 1)	0.0485336	0.04853365384615384	0.0

Table 15: Parameters calibration values for subject 2, carvedilol.

Parameter	Calibrated	Expected	Calib Error
Cl (subject 2)	83.3	83.3	0.0
Ke (subject 2)	0.100120	0.100120	0.0

Calibration matches expectations perfectly on these patients.

2.2.5.2 *Maximum Concentration Verification*

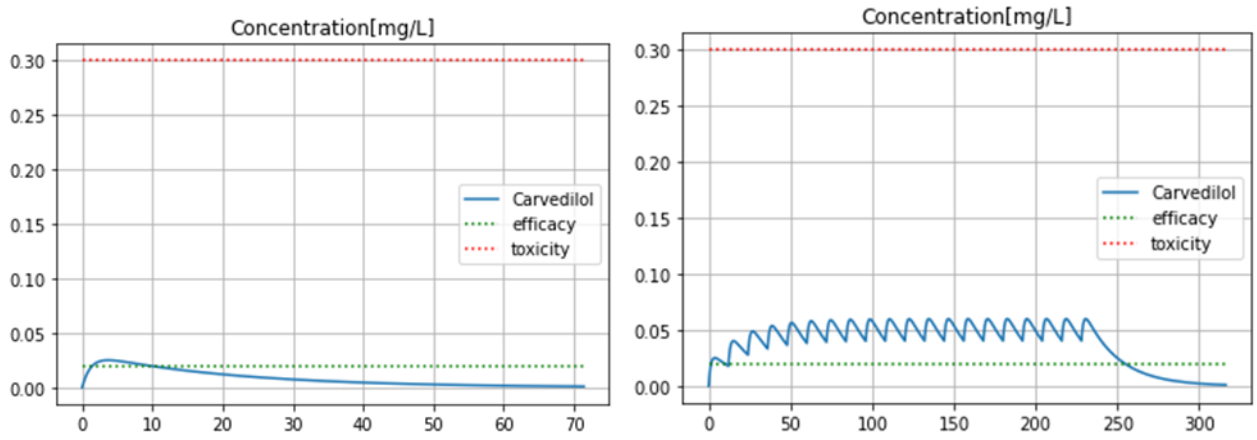

Figure 14: Numerical simulation with a patient with weight=70 and not smoker, Carvedilol is administered orally every 12 hours with a dose of 25mg, for a period of 10 days (where steady state is practically obtained).

Results on maximal concentration are shown in Table 16.

Table 16: Results of numerical vs theoretical max concentrations comparison test for carvedilol.

Value \ Scenario	Single dose	Repeated admin
Numerical max concentration	0.025107	0.059925
Theoretical max concentration	0.025113	0.059931
Numerical Error	5e-06	6e-06

We see a match at the order of 1e-06 on the maximum concentration in both scenarios.

2.2.6 Clarithromycine

2.2.6.1 *Parameters Estimation Verification*

Covariates: weight, glomerular filtration rate (GFR)
Base parameters encoded in the model are:

- Bioavailability F = 0.55
- Distribution volume V = 210
- Lag Tlag = 0.0
- Elimination half-time T12 = 3.8
- Time of maximum concentration Tmax = 1.7

Calibration step will infer Ke and Ka from numerical inversion of T12 and Tmax data. If we compute T12 and Tmax with calibrated parameters and compare with original values, we can measure the calibration error.

On subject 1, a standard patient (weight=70, GFR=100), we have the values shown in Table 17.

Table 17: Parameters calibration values for subject 1, clarithromycine.

Parameter	Calibrated	Expected	Calib Error
Ke	0.182407	/	/
Ka	1.367335	/	/
T12	3.799999	3.8	4e-16
Tmax	1.700000	1.70	3e-14

For non-standard weight or GFR, there is an additional calibration step. On subject 2, with weight = 140 and GFR = 20, we have the values shown in Table 18.

Table 18: Parameters calibration values for subject 2, clarithromycine.

Parameter	Calibrated	Expected	Calib Error
V (subject 2)	420.0	420.0	0.0
Ke (subject 2)	0.060802	0.060802	0.0

Calibration matches expectations perfectly on these patients.

2.2.6.2 Maximum Concentration Verification

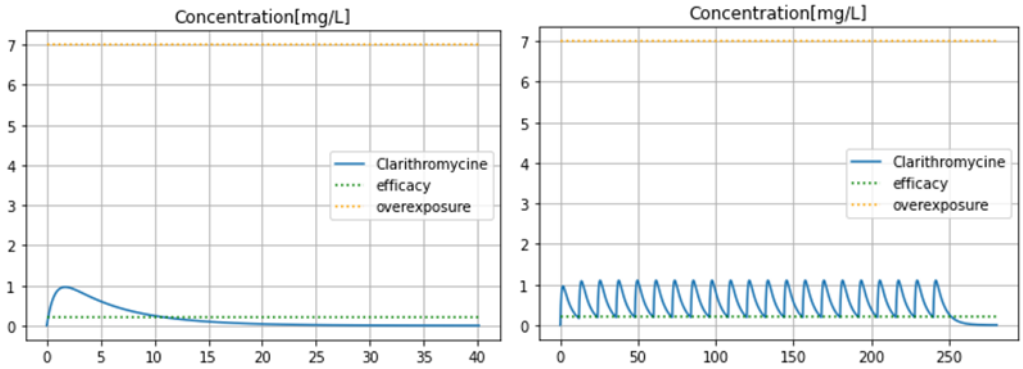

Figure 15: Numerical simulation with a patient with weight=70 and GFR=100, Clarithromycine is administered orally every 12 hours with a dose of 500mg, for a period of 20 days (where steady state is practically obtained).

Results on maximal concentration are shown in Table 19.

Table 19: Results of numerical vs theoretical max concentrations comparison test for Clarithromycine.

Value \ Scenario	Single dose	Repeated admin
Numerical max concentration	0.960148	1.101381

Value \ Scenario	Single dose	Repeated admin
Theoretical max concentration	0.960377	1.101523
Numerical Error	2e-04	1e-04

We see a match at an order on the maximum concentration in both scenarios.

2.2.7 Disopyramide

2.2.7.1 Parameters Estimation Verification

Covariates: weight, glomerular filtration rate (GFR)
For the oral route and immediate release form, base parameters encoded in the model are:

- Bioavailability F = 0.95
- Distribution volume V = 52.5
- Lag Tlag = 0.0
- Elimination half-time T12 = 6.3
- Time of maximum concentration Tmax = 1.5

Calibration step will infer Ke and Ka from numerical inversion of T12 and Tmax data. If we compute T12 and Tmax with calibrated parameters and compare with original values, we can measure the calibration error.

On subject 1, a standard patient (weight=70, GFR=90), we have values in Table 20.

Table 20: Parameters calibration values for subject 1, disopyramide.

Parameter	Calibrated	Expected	Calib Error
Ke	0.110023	/	/
Ka	2.064732	/	/
T12	6.300000	6.3	3e-15
Tmax	1.5000000	1.50	2e-14

For non-standard weight or GFR, there is an additional calibration step. On subject 2, with weight = 140 and GFR = 60, we have values in Table 21.

Table 21: Parameters calibration values for subject 2, disopyramide.

Parameter	Calibrated	Expected	Calib Error
V (subject 2)	105.0	105.0	0.0
Ke (subject 2)	0.078850	0.078850	0.0

For the oral route and controlled release form, base parameters encoded in the model are:

- Bioavailability F = 0.95
- Distribution volume V = 52.5
- Lag Tlag = 0.0
- Time of maximum concentration Tmax = 4.5

Calibration matches expectations perfectly on these patients.

2.2.7.2 Maximum Concentration Verification

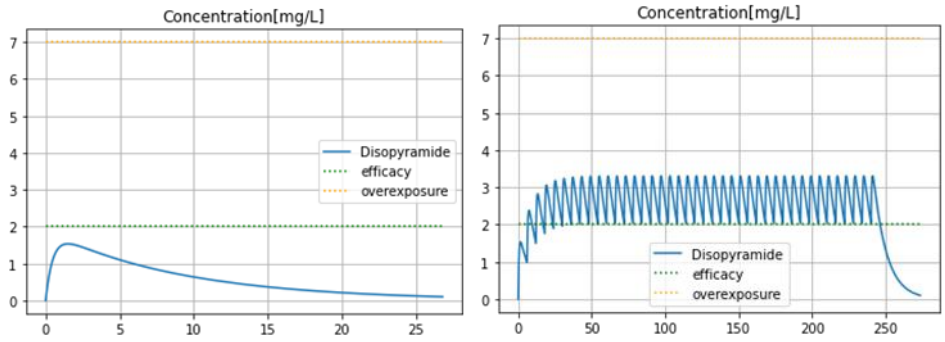

Figure 16: Numerical simulation with a patient with weight=70 and GFR=90, Disopyramide is administered orally in immediate release form every 6 hours with a dose of 100mg, for a period of 10 days (where steady state is practically obtained).

Results on maximal concentration are reported in Table 22.

Table 22: Results of numerical vs theoretical max concentrations comparison test for disopyramide.

Value \ Scenario	Single dose	Repeated admin
Numerical max concentration	1.533733	3.307138
Theoretical max concentration	1.534230	3.307674
Numerical Error	5e-04	5e-04

We see a match at the order of 1e-04 on the maximum concentration in both scenarios.

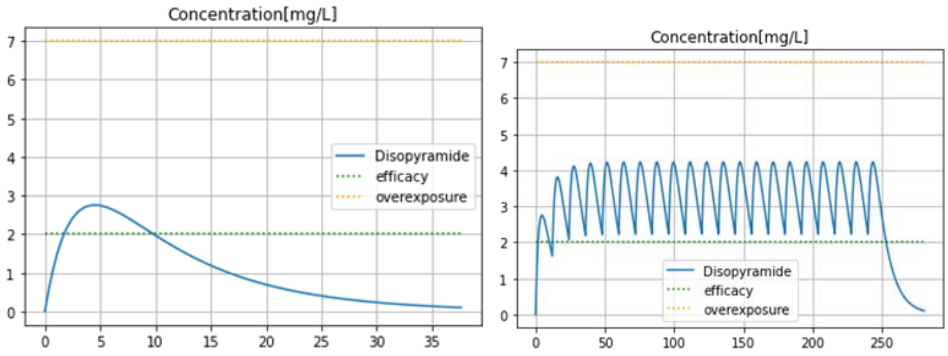

Figure 17: Numerical simulation with a patient with weight=70 and GFR=90, Disopyramide is administered orally in controlled release form every 12 hours with a dose of 250mg, for a period of 10 days (where steady-state is practically obtained).

Results on maximal concentration are reported in Table 23.

Table 23: Results of numerical vs theoretical max concentrations comparison test for Disopyramide.

Value \ Scenario	Single dose	Repeated admin
Numerical max concentration	2.754124	4.230352
Theoretical max concentration	2.757292	4.230405
Numerical Error	3e-03	5e-05

We see a match at the order of 1e-03 on the maximum concentration in the single dose scenario and 1e-05 in the repeated administration scenario.

2.2.8 Domperidone

2.2.8.1 Parameters Estimation Verification

Covariates: weight, glomerular filtration rate (GFR)
For the oral route and syrup form, base parameters encoded in the model are:

- Bioavailability F = 0.88
- Distribution volume V = 378.59
- Lag Tlag = 0.0
- Elimination half-time T12 = 8.0
- Time of maximum concentration Tmax = 0.9

Calibration step will infer Ke and Ka from numerical inversion of T12 and Tmax data. If we compute T12 and Tmax with calibrated parameters and compare with original values, we can measure the calibration error.

On subject 1, a standard patient (weight=70, GFR=100), we have values in Table 24.

Table 24: Parameters calibration values for subject 1, domperidone.

Parameter	Calibrated	Expected	Calib Error
Ke	0.086643	/	/
Ka	4.467518	/	/
T12	8.0	8.0	0.0
Tmax	0.899999	0.90	1e-15

For non-standard weight or GFR, there is an additional calibration step. On subject 2, with weight = 140 and GFR = 30, we have values in Table 25.

Table 25: Parameters calibration values for subject 2, domperidone.

Parameter	Calibrated	Expected	Calib Error
V (subject 2)	105.0	105.0	0.0
Ke (subject 2)	0.078850	0.078850	0.0

For the oral route and immediate release form, base parameters encoded in the model are:

- Bioavailability F = 0.831
- Distribution volume V = 378.59
- Lag Tlag = 0.0
- Time of maximum concentration Tmax = 1.20

On subject 1, a standard patient (weight=70, GFR=100), we have values in Table 26.

Table 26: Parameters calibration values for subject 1, domperidone.

Parameter	Calibrated	Expected	Calib Error
Ke	0.086643	/	/
Ka	3.055809	/	/
Tmax	1.199999	1.20	1e-14

For non-standard weight or GFR, there is an additional calibration step which is identical to the immediate release case before.

Calibration matches expectations perfectly on these patients.

2.2.8.2 *Maximum Concentration Verification*

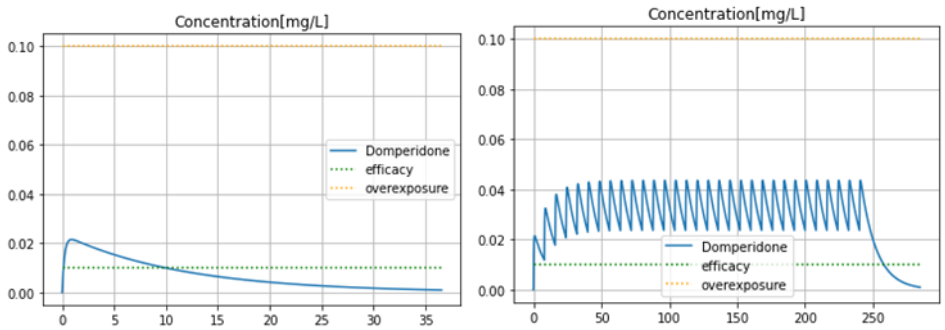

Figure 18: Numerical simulation with a patient with weight=70 and GFR=100, Domperidone is administered orally in syrup form every 8 hours with a dose of 10mg, for a period of 10 days (where steady state is practically obtained).

Results on maximal concentration are shown in Table 27.

Table 27: Results of numerical vs theoretical max concentrations comparison test for Domperidone.

Value \ Scenario	Single dose	Repeated admin
Numerical max concentration	0.021497	0.043585
Theoretical max concentration	0.021500	0.043594
Numerical Error	3e-06	9e-06

We see a match at the order of 1e-06 on the maximum concentration in both scenarios.

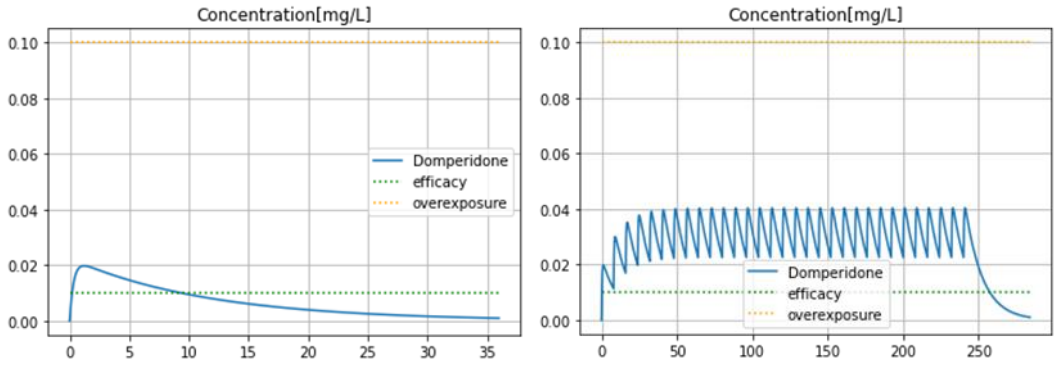

Figure 19: Numerical simulation with a patient with weight=70 and GFR=100, Disopyramide is administered orally in controlled release form every 8 hours with a dose of 10mg, for a period of 10 days (where steady state is practically obtained).

Results on maximal concentration are shown in Table 28.

Table 28: Results of numerical vs theoretical max concentrations comparison test for Domperidone.

Value \ Scenario	Single dose	Repeated admin
Numerical max concentration	0.019778	0.040366
Theoretical max concentration	0.019782	0.040373
Numerical Error	4e-06	6e-06

We see a match at the order of 1e-06 on the maximum concentration in both scenarios.

2.2.9 Droperidol

2.2.9.1 Parameters Estimation Verification

Covariates: None
Parameters encoded in the model are:

- Bioavailability F = 1.0
- Lag Tlag = 0
- Absorption rate Ka = 10.0
- Clearance CL=41.9
- Distribution volume V1 = 73.6
- Distribution volume V2 = 79.8
- Intercompartmental clearance Q = 71.5
- Elimination rate Ke is Cl/V
- Intercompartmental transfer rates are K12=Q/V1 and K21=Q/V2

Subject 1: Standard (weight = 70)

Results are shown in Table 29.

Table 29: Parameters calibration values for subject 1, droperidol.

Parameter	Calibrated	Expected	Calib Error
F	1.0	1.0	0.0
Tlag	0.0	0.0	0.0
Ka	10.0	10.0	0.0
Q	71.5	71.5	0.0
Cl	41.9	41.9	0.0
V1	73.60	73.60	0.0
V2	79.8	79.80	0.0
Ke	0.569293	0.569293	0.0
K12	0.971467	0.971467	0.0

Parameter	Calibrated	Expected	Calib Error
K21	0.8959899	0.895989	0.0

Calibration matches expectations perfectly.

2.2.9.2 Maximum Concentration Verification

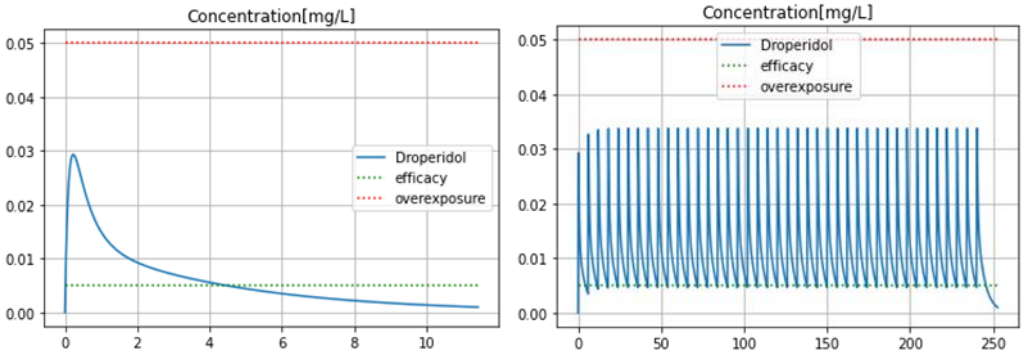

Figure 20: Numerical simulation with a patient with weight=70, Droperidol is administered in intra-muscular route every 6 hours with a dose of 3mg, for a period of 10 days (where steady state is practically obtained).

Results on maximal concentration are shown in Table 30.

Table 30: Results of numerical vs theoretical max concentrations comparison test for Droperidol.

Value \ Scenario	Single dose	Repeated admin
Numerical max concentration	0.029310	0.033755
Theoretical max concentration	0.029321	0.033755
Numerical Error	1e-05	4e-08

We see a match at the order of 1e-05 on the maximum concentration in the single dose scenario and 1e-08 in the repeated administration scenario.

2.2.10 Flecainide

2.2.10.1 Parameters Estimation Verification

Covariates: weight
For the oral route and syrup form, base parameters encoded in the model are:

- Bioavailability F = 0.90
- Distribution volume V = 581.0
- Lag Tlag = 0.0
- Elimination half-time T12 = 14.0
- Time of maximum concentration Tmax = 2.40

Calibration step will infer Ke and Ka from numerical inversion of T12 and Tmax data. If we compute T12 and Tmax with calibrated parameters and compare with original values, we can measure the calibration error.

On subject 1, a standard patient (weight=70, GFR=100), we have values in Table 31.

Table 31: Parameters calibration values for subject 1, flecainide.

Parameter	Calibrated	Expected	Calib Error
Ke	0.049510	/	/
Ka	1.459318	/	/
T12	14.0	14.0	0.0
Tmax	2.400000	2.40	5e-14

For non-standard weight, there is an additional calibration step. On subject 2, with weight = 140, we have values in Table 32.

Table 32: Parameters calibration values for subject 2, flecainide.

Parameter	Calibrated	Expected	Calib Error
V (subject 2)	1162.0	1162.0	0.0

For the oral route and immediate release form, base parameters encoded in the model are:

- Bioavailability F = 090
- Distribution volume V = 581.0
- Lag Tlag = 2.5
- Time of maximum concentration Tmax = 23.0

On subject 1, a standard patient (weight=70), we have values in Table 33.

Table 33: Parameters calibration values for subject 1, flecainide.

Parameter	Calibrated	Expected	Calib Error
Ke	0.049510	/	/
Ka	0.048057	/	/
Tmax	22.999999	23	1e-11

For non-standard weight, there is an additional calibration step which is identical to the immediate release case before.

Calibration matches expectations perfectly on these patients.

2.2.10.2 Maximum Concentration Verification

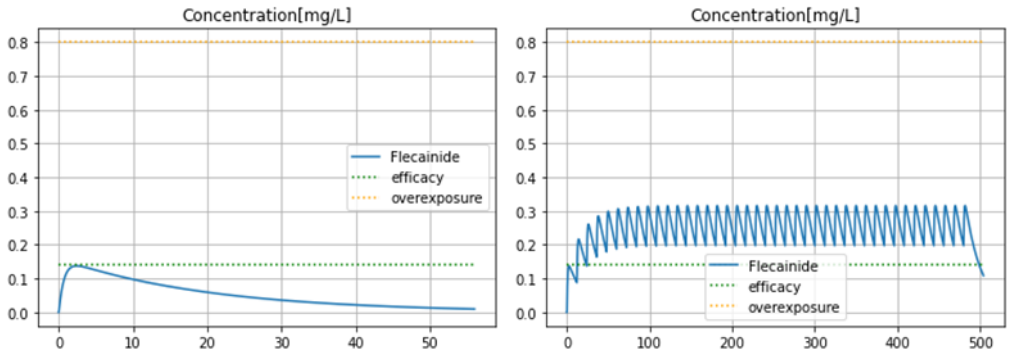

Figure 21: Numerical simulation with a patient with weight=70, Flecainide is administered orally in immediate release form every 12 hours with a dose of 100mg, for a period of 20 days (where steady state is practically obtained).

Results on maximal concentration are shown in Table 34.

Table 34: Results of numerical vs theoretical max concentrations comparison test for Flecainide.

Value \ Scenario	Single dose	Repeated admin
Numerical max concentration	0.137531	0.315845
Theoretical max concentration	0.137550	0.315845
Numerical Error	2e-05	3e-07

We see a match at the order of 1e-04 on the maximum concentration in both scenarios.

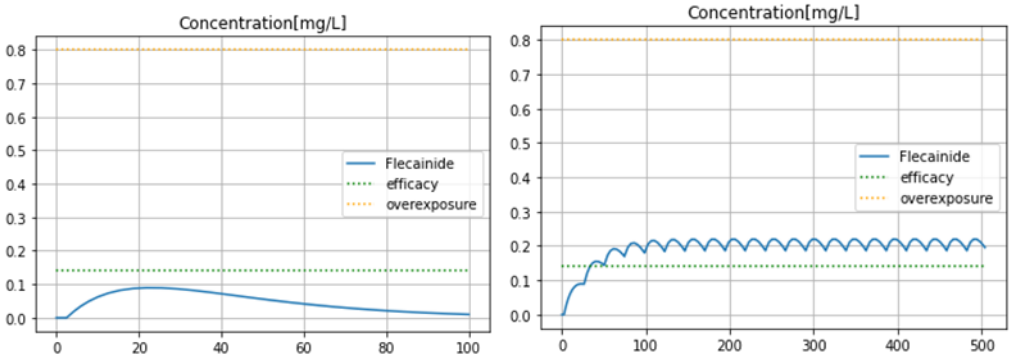

Figure 22: Numerical simulation with a patient with weight=70, Flecainide is administered orally in controlled release form every 24 hours with a dose of 200mg, for a period of 20 days (where steady state is practically obtained).

Results on maximal concentration are shown in Table 35.

Table 35: Results of numerical vs theoretical max concentrations comparison test for Flecainide.

Value \ Scenario	Single dose	Repeated admin
Numerical max concentration	0.089676	0.219461
Theoretical max concentration	0.089824	0.220423
Numerical Error	1e-04	1e-03

We see a match at the order of 1e-04 on the maximum concentration in the single dose scenario and 1e-03 in the repeated administration scenario.

2.2.11 Metronidazole

2.2.11.1 Parameters Estimation Verification

Covariates: weight
For the oral route and syrup form, base parameters encoded in the model are:

- Bioavailability F = 1.0
- Distribution volume V = 45.50
- Lag Tlag = 0.0
- Elimination half-time T12 = 9.0
- Time of maximum concentration Tmax = 1.0

Calibration step will infer Ke and Ka from numerical inversion of T12 and Tmax data. If we compute T12 and Tmax with calibrated parameters and compare with original values, we can measure the calibration error.

On subject 1, a standard patient (weight=70, GFR=100), we have values in Table 36.

Table 36: Parameters calibration values for subject 1, metronidazole.

Parameter	Calibrated	Expected	Calib Error
Ke	0.077016	/	/
Ka	4.036010	/	/
T12	9.0	9.0	0.0
Tmax	0.999999	1.0	1e-14

For non-standard weight, there is an additional calibration step. On subject 2, with weight = 140, we have values in Table 37.

Table 37: Parameters calibration values for subject 2, metronidazole.

Parameter	Calibrated	Expected	Calib Error
V (subject 2)	91.0	91.0	0.0

For the oral route and immediate release form, base parameters encoded in the model are:

- Bioavailability F = 0.70
- Distribution volume V = 45.50
- Lag Tlag = 0.0
- Time of maximum concentration Tmax = 4.0

On subject 1, a standard patient (weight=70), we have values in Table 38.

Table 38: Parameters calibration values for subject 1, metronidazole.

Parameter	Calibrated	Expected	Calib Error
Ke	0.0770163	/	/
Ka	0.583102	/	/
Tmax	4.000000	4.0	1e-13

For non-standard weight, there is an additional calibration step which is identical to the immediate release case before.

Calibration matches expectations perfectly on these patients.

2.2.11.2Maximum Concentration Verification

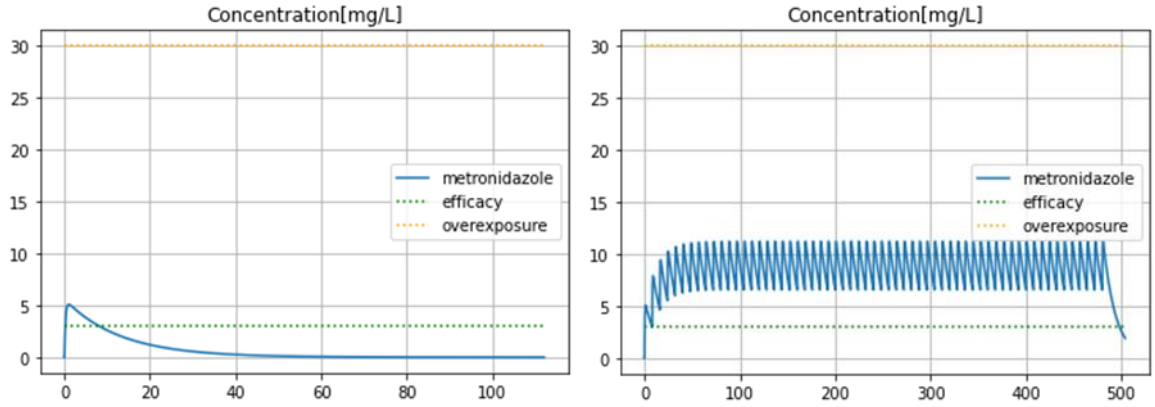

Figure 23: Numerical simulation with a patient with weight=70, Metronidazole is administered orally in tablet form every 8 hours with a dose of 250mg, for a period of 20 days (where steady state is practically obtained).

Results on maximal concentration are shown in Table 39.

Table 39: Results of numerical vs theoretical max concentrations comparison test for metronidazole.

Value \ Scenario	Single dose	Repeated admin
Numerical max concentration	5.086579	11.228237
Theoretical max concentration	5.087223	11.228255
Numerical Error	6e-04	2e-05

We see a match at the order of 1e-03 on the maximum concentration in the single dose scenario and 1e-05 in the repeated administration scenario.

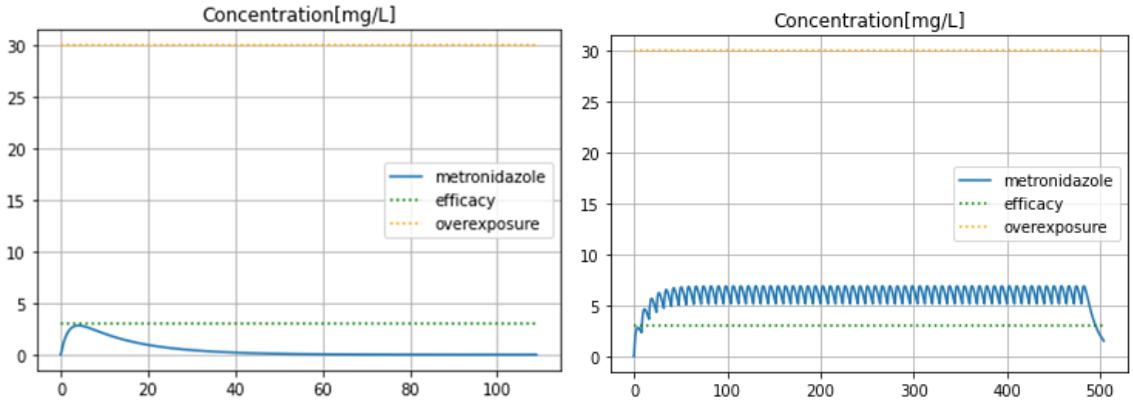

Figure 24: Numerical simulation with a patient with weight=70, Metronidazole is administered orally in solution form every 8 hours with a dose of 250mg, for a period of 20 days (where steady state is practically obtained).

Results on maximal concentration are shown in Table 40.

Table 40: Results of numerical vs theoretical max concentrations comparison test for metronidazole.

Value \ Scenario	Single dose	Repeated admin
Numerical max concentration	2.824809	6.904372
Theoretical max concentration	2.826412	6.905676
Numerical Error	2e-03	1e-03

We see a match at the order of 1e-03 on the maximum concentration in both scenarios.

2.2.12 Mexiletine

2.2.12.1 Parameters Estimation Verification

Covariates: weight
Parameters encoded in the model are:

- Bioavailability F = 1.0
- Lag Tlag = 0
- Absorption rate Ka = 3.1
- Clearance CL= 0.38*weight
- Distribution volume V = 5.3*weight
- Elimination rate Ke is Cl/V

Subjects:

- Subject 1: Standard, weight = 70
- Subject 2: Weight = 100

Results in Table 41 and Table 42.

Table 41: Parameters calibration values for subject 1, mexiletine.

Parameter	Calibrated	Expected	Calib Error
F	1.0	1.0	0.0
Tlag	0.0	0.0	0.0
Ka	3.1	3.1	0.0
Cl (subject 1)	26.6	26.6	0.0
V (subject 1)	371.0	371.0	0.
Ke (subject 1)	0.071698	0.071698	0.0

Table 42: Parameters calibration values for subject 2, mexiletine.

Parameter	Calibrated	Expected	Calib Error
Cl (subject 2)	38.0	38.0	0.0
V (subject 2)	530.0	530.0	0.0
Ke (subject 2)	0.071698	0.071698	0.0

Calibration matches expectations perfectly on these patients.

2.2.12.2 Maximum Concentration Verification

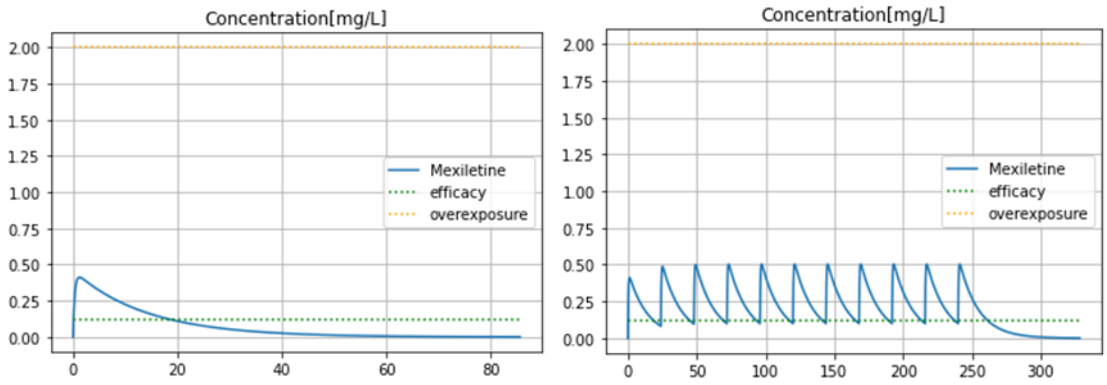

Figure 25: Numerical simulation with a patient with weight=70, Mexiletine is administered orally in immediate release form every 24 hours with a dose of 167mg, for a period of 10 days (where steady state is practically obtained).

Results on maximal concentration are shown in Table 43.

Table 43: Results of numerical vs theoretical max concentrations comparison test for mexiletine.

Value \ Scenario	Single dose	Repeated admin
Numerical max concentration	0.411726	0.503706
Theoretical max concentration	0.411729	0.503801
Numerical Error	3e-06	1e-04

We see a match at the order of 1e-06 on the maximum concentration in the single dose scenario and 1e-04 in the repeated administration scenario.

2.2.13 Nicorandil

2.2.13.1 Parameters Estimation Verification

Covariates: weight
Parameters encoded in the model are:

- Bioavailability F = 0.75
- Lag Tlag = 0
- Absorption rate Ka = 1.41
- Clearance CL= 26.3 *1.94 *power(weight/70,0.75)
- Distribution volume V1 = 18.1 *1.39 *(weight/70)
- Distribution volume V2 = 24.1 *4.06 *(weight/70)
- Intercompartmental clearance Q = 71.6 *0.519 *power(weight/70,0.75)
- Elimination rate Ke is Cl/V
- Intercompartmental transfer rates are K12=Q/V1 and K21=Q/V2

Subjects:

- Subject 1: Standard, weight = 70
- Subject 2: Weight = 100

Results are shown in Table 44 and Table 45.

Table 44: Parameters calibration values for subject 1, Nicorandil.

Parameter	Calibrated	Expected	Calib Error
F	0.75	0.75	0.0
Tlag	0.0	0.0	0.0
Ka	1.41	1.41	0.0
Cl (subject 1)	51.021999	51.022	3e-14
V1 (subject 1)	25.159000	25.159	2e-14
Ke (subject 1)	2.027982	2.027982	3e-15
Q (subject 1)	37.160399	37.1604	4e-15
V2 (subject 1)	97.845999	97.846	1e-14
K12 (subject 1)	1.477022	1.477022	2e-15
K21 (subject 1)	0.379784	0.379784	1e-16

Table 45: Parameters calibration values for subject 2, mexiletine.

Parameter	Calibrated	Expected	Calib Error
Cl (subject 2)	66.670536	66.670536	4e-14
V1 (subject 2)	35.941428	35.941428	3e-14
Ke (subject 2)	1.854977	1.85497	3e-15
Q (subject 2)	48.557559	48.557559	3e-14
V2 (subject 2)	139.78	139.78	1e-14
K12 (subject 2)	1.351019	1.351019	2e-15
K21 (subject 2^2)	0.347385	0.347385	2e-16

Calibration matches expectations perfectly on these patients.

2.2.13.2 Maximum Concentration Verification

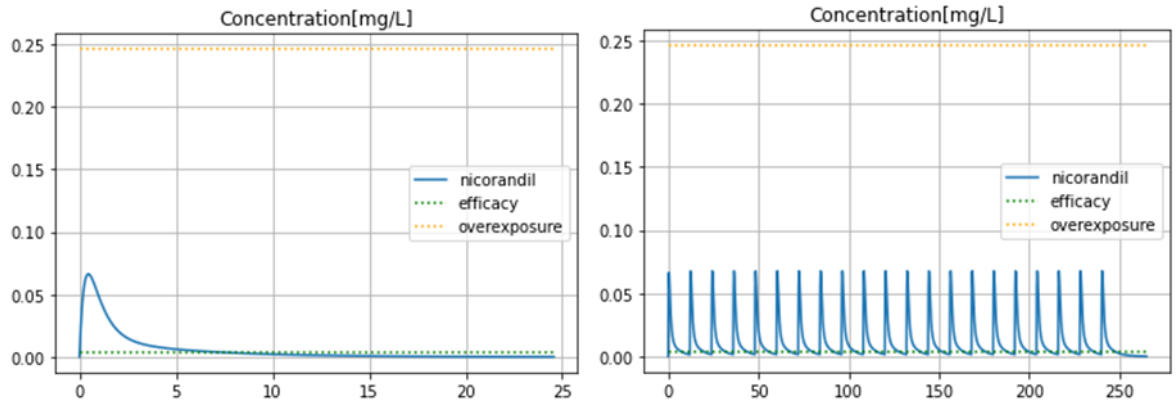

Figure 26: Numerical simulation with a patient with weight=70, Nicorandil is administered orally in immediate release form every 12hours with a dose of 10mg, for a period of 10 days (where steady state is practically obtained).

Results on maximal concentration are shown in Table 46.

Table 46: Results of numerical vs theoretical max concentrations comparison test for nicorandil.

Value \ Scenario	Single dose	Repeated admin
Numerical max concentration	0.066330	0.067574
Theoretical max concentration	0.066331	0.067707
Numerical Error	6e-07	1e-04

We see a match at the order of 1e-06 on the maximum concentration in the single dose scenario and 1e-04 in the repeated administration scenario.

2.2.14 Ondansetron

2.2.14.1 Parameters Estimation Verification

Covariates: weight, age, sex
Base parameters encoded in the model are:

- Bioavailability F = 0.55
- Distribution volume V = 140
- Lag Tlag = 0.0
- Elimination half-time T12 = 3.0
- Time of maximum concentration Tmax = 1.9

Calibration step will infer Ke and Ka from numerical inversion of T12 and Tmax data. If we compute T12 and Tmax with calibrated parameters and compare with original values, we can measure the calibration error.

On subject 1, a standard patient (weight=70, sex=male, age=40), we have values in Table 47.

Table 47: Parameters calibration values for subject 1, ondansetron.

Parameter	Calibrated	Expected	Calib Error
Ke		/	/
Ka		/	/
T12	3.0	3.0	0.0
Tmax	1.900000	1.90	1e-13

For non-standard weight, age or for females, there is an additional calibration step. On subject 2, a female with weight = 140 and age= 62, we have values in Table 48.

Table 48: Parameters calibration values for subject 2, ondansetron.

Parameter	Calibrated	Expected	Calib Error
V (subject 2)	420.0	420.0	0.0
F (subject 2)	0.6050000	0.605	1e-16
Ke (subject 2)	0.169889	0.169889	0.0

Calibration matches expectations perfectly on these patients.

2.2.14.2 Maximum Concentration Verification

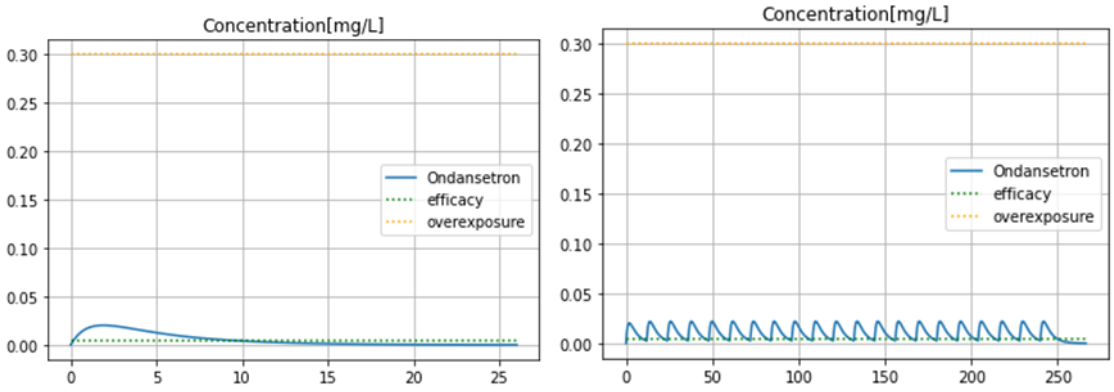

Figure 27: Numerical simulation with a patient with weight=70 and GFR=100, Ondansetron is administered orally in immediate release form every 12 hours with a dose of 8.0mg, for a period of 10 days (where steady state is practically obtained).

Results on maximal concentration are shown in Table 49.

Table 49: Results of numerical vs theoretical max concentrations comparison test for ondansetron.

Value \ Scenario	Single dose	Repeated admin
Numerical max concentration	0.020251	0.022020
Theoretical max concentration	0.020261	0.022032
Numerical Error	1e-05	1e-05

We see a match at the order of 1e-05 on the maximum concentration in both scenarios.

2.2.15 Sotalol

2.2.15.1 Parameters Estimation Verification

Covariates: weight, glomerular filtration rate (GFR)
Base parameters encoded in the model are:

- Bioavailability F = 0.80
- Distribution volume V = 84.7
- Lag Tlag = 0.0
- Elimination half-time T12 = 7.18
- Time of maximum concentration Tmax = 3.1

Calibration step will infer Ke and Ka from numerical inversion of T12 and Tmax data. If we compute T12 and Tmax with calibrated parameters and compare with original values, we can measure the calibration error.

On subject 1, a standard patient (weight=70, GFR=90), we have values in Table 50.

Table 50: Parameters calibration values for subject 1, sotalol.

Parameter	Calibrated	Expected	Calib Error
Ke	0.096538	/	/
Ka	0.763717	/	/
T12	7.179999	7.18	2e-15
Tmax	3.099999	3.10	3e-13

For non-standard weight or GFR, there is an additional calibration step. On subject 2, with weight = 140 and GFR = 30, we have values in Table 51.

Table 51: Parameters calibration values for subject 2, sotalol.

Parameter	Calibrated	Expected	Calib Error
V (subject 2)	169.4	169.4	0.0
Ke (subject 2)	0.051487	0.051487	0.0

Calibration matches expectations perfectly on these patients.

2.2.15.2Maximum Concentration Verification

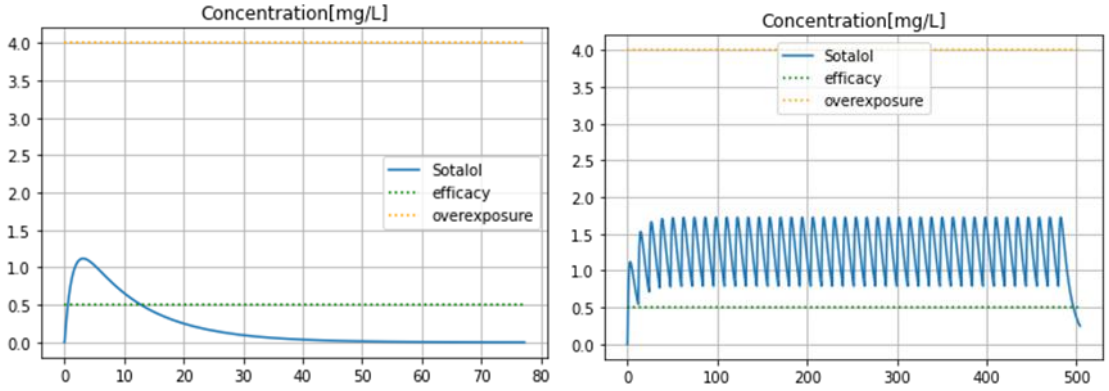

Figure 28: Numerical simulation with a patient with weight=70 and GFR=90, Sotalol is administered orally every 12 hours with a dose of 160mg, for a period of 20 days (where steady state is practically obtained).

Results on maximal concentration are shown in Table 52.

Table 52: Results of numerical vs theoretical max concentrations comparison test for sotalol.

Value \ Scenario	Single dose	Repeated admin
Numerical max concentration	1.120008	1.724555
Theoretical max concentration	1.120354	1.724586
Numerical Error	3e-04	3e-05

We see a match at the order of 1e-04 on the maximum concentration in the single dose scenario and 1e-05 in the repeated administration scenario.

2.2.16 Vandetanib

2.2.16.1 Parameters Estimation Verification

Covariates: weight, renal status
Base parameters encoded in the model are:

- Bioavailability F = 1.0
- Distribution volume V = 3876
- Lag Tlag = 0.0
- Elimination half-time T12 = 195.4
- Time of maximum concentration Tmax = 6.0

Calibration step will infer Ke and Ka from numerical inversion of T12 and Tmax data. If we compute T12 and Tmax with calibrated parameters and compare with original values, we can measure the calibration error.

On subject 1, a standard patient (weight=80.70, normal renal status), we have values in Table 53.

Table 53: Parameters calibration values for subject 1, vandetanib.

Parameter	Calibrated	Expected	Calib Error
Ke	0.003547	/	/
Ka	0.932085	/	/
T12	195.4	195.40	0.0
Tmax	5.9999999	6.0	4e-13

For non-standard weight and renal status, there is an additional calibration step. On subject 2, with weight = 100 and moderate renal impairment, we have values in Table 54.

Table 54: Parameters calibration values for subject 2, vandetanib.

Parameter	Calibrated	Expected	Calib Error
V (subject 2)	4802.973977	4802.973977	0.0
Ke (subject 2)	0.002217	0.002217	0.0

Calibration matches expectations perfectly on these patients.

2.2.16.2 Maximum Concentration Verification

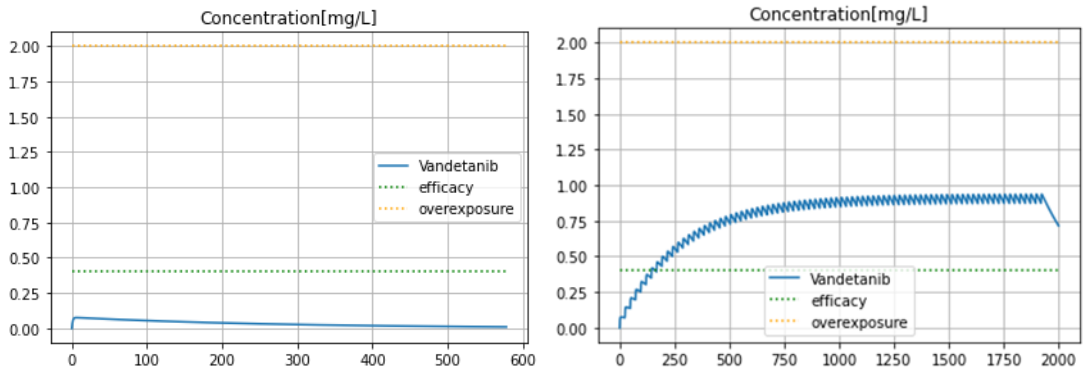

Figure 29: Numerical simulation with a patient with weight=80.70 and normal renal status, Vandetanib is administered orally every 24 hours with a dose of 300mg, for a period of 80 days (where steady state is practically obtained).

Results on maximal concentration are shown in Table 55.

Table 55: Results of numerical vs theoretical max concentrations comparison test for vandetanib.

Value \ Scenario	Single dose	Repeated admin
Numerical max concentration	0.075767	0.936377
Theoretical max concentration	0.075769	0.9373355
Numerical Error	2e-06	1e-03

We see a match at the order of 1e-06 on the maximum concentration in the single dose scenario and 1e-03 in the repeated administration scenario.

2.2.17 Cisapride (new)

2.2.17.1 Parameters estimation verification

Covariates: weight
Base parameters encoded in the model are:

- Bioavailability F = 1 if weight<=6.5, 0.45 else
- Absorption rate Ka = 2.58
- Distribution volume V = 21.9 if weight<=6.5, 2.4*weight else
- Clearance CL= 0.538*weight if weight <=6.5, 0.16635*weight else
- Lag Tlag = 0.0
- Elimination rate Ke is Cl/V

Subject 1: Standard, weight = 70
Subject 2: Weight = 5

Results:

Table 56. Parameters calibration values for subject 1, cisapride.

Parameter	Calibrated	Expected	Calib Error
F	0.45	0.45	0.
Tlag	0.0	0.0	0.
Ka	2.58	2.58	0.
Cl (subject 1)	11.6445	11.6445	0.
V (subject 1)	168.0	168.0	0.
Ke (subject 1)	0.0693125	0.0693125	0.

Table 57. Parameters calibration values for subject 2, cisapride.

Parameter	Calibrated	Expected	Calib Error
Cl (subject 2)	2.6900000000000004	2.6900000000000004	0.
V (subject 2)	21.9	21.9	0.
Ke (subject 2)	0.12283105022831053	0.12283105022831053	0.

Calibration matches expectations perfectly on these patients.

2.2.17.2Maximum concentration verification

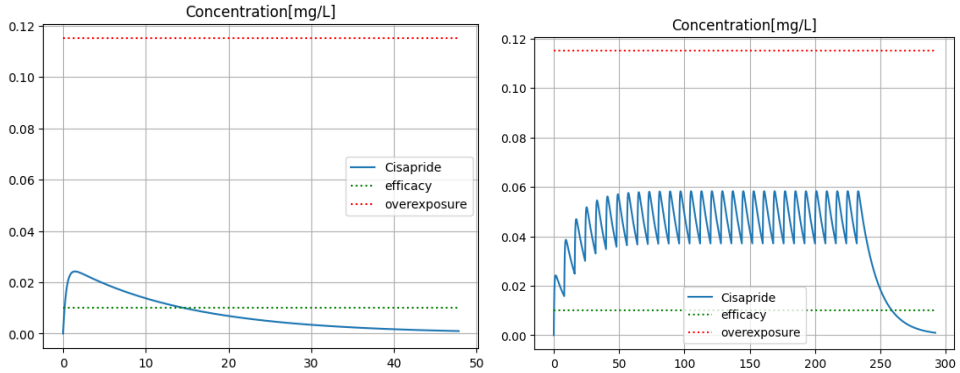

Figure 30. Numerical simulation with a patient with weight=70, Cisapride is administered orally in immediate release form every 8 hours with a dose of 10mg, for a period of 10 days (where steady state is practically obtained).

Results on maximal concentration are:

Table 58. Results of numerical vs theoretical max concentrations comparison test for cisapride.

Value \ Scenario	Single dose	Repeated admin
Numerical max concentration	0.02423948252897734	0.058305949870917105
Theoretical max concentration	0.024240298461323584	0.058309039152327165
Numerical Error	8e-07	3e-06

We see a match at the order of 1e-07 on the maximum concentration in the single dose scenario and 1e-06 in the repeated administration scenario.

2.2.18 Quinidine (new)

2.2.18.1 Parameters estimation verification

Covariates: age, height175, heart_failure, alcohol, glomular_filtratiuon_rate_50
Base parameters encoded in the model are:

- Bioavailability F = 1
- Absorption rate Ka = 0.894
- Distribution volume V = 230
- Clearance CL= `(18-0.101*age)*(1+0.156*height175)*(1-0.115*heart_failure)*(1+0.23*alcohol)*(1-0.178*glomerular_filtration_rate50)`
- Lag Tlag = 0.0
- Elimination rate Ke is Cl/V

Subject 1: Standard, (age = 40, height175 = False, alcohol = False, heart_failure = False, glomerular_filtration_rate50 = False)
Subject 2: age = 70, height175 = True, alcohol = True, heart_failure = True, glomerular_filtration_rate50 = True

Results:

Table 59. Parameters calibration values for subject 1, quinidine.

Parameter	Calibrated	Expected	Calib Error
F	1.0	1.0	0.
Tlag	0.0	0.0	0.
Ka	0.894	0.894	0.
Cl (subject 1)	13.96	13.96	0.
V (subject 1)	230	230	0.
Ke (subject 1)	0.060695652173913046	0.060695652173913046	0.

Table 60. Parameters calibration values for subject 2, quinidine.

Parameter	Calibrated	Expected	Calib Error
Cl (subject 2)	11.305719226548	11.305719226548	0.
V (subject 2)	230	230	0.
Ke (subject 2)	0.0491553009849913	0.0491553009849913	0.

Calibration matches expectations perfectly on these patients.

2.2.18.2 Maximum concentration verification

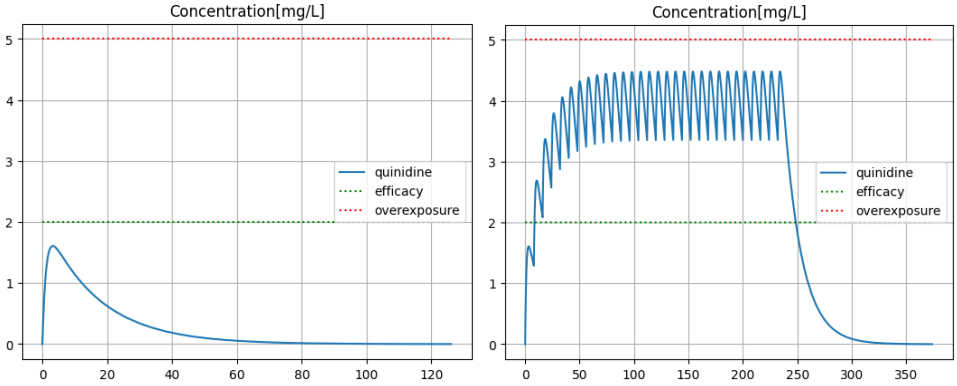

Figure 31. Numerical simulation with a patient with age = 40, height175 = False, alcohol = False, heart_failure = False, glomerular_filtration_rate50 = False, Quinidine is administered orally in immediate release form every 8 hours with a dose of 450mg, for a period of 10 days (where steady state is practically obtained).

Results on maximal concentration are:

Table 61. Results of numerical vs theoretical max concentrations comparison test for quinidine.

Value \ Scenario	Single dose	Repeated admin
Numerical max concentration	1.6076329860206504	4.481889408189059
Theoretical max concentration	1.6084130438913176	4.482588813614823
Numerical Error	7e-04	6e-04

We see a match at the order of 1e-04 on the maximum concentration in the single dose scenario and 1e-04 in the repeated administration scenario.

2.2.19 Pimozide (new)

2.2.19.1 Parameters estimation verification

Covariates: cyp2d6_poor, cyp2d6_intermediate, weight
Base parameters encoded in the model are:

- Bioavailability F = 1
- Lag Tlag = 1.14
- Absorption rate Ka = 0.68
- Clearance CL= 54.9*(1+(cyp2d6_poor*(-0.73224)))*(1+(cyp2d6_intermediate*(-0.3479)))
- Distribution volume V1 = Vc_pop*(weight/70)
- Distribution volume V2 = Vp_pop*(weight/70)
- Intercompartmental clearance Q = 69.2
- Elimination rate Ke is Cl/V1_pop
- Intercompartmental transfer rates are K12=Q/V1_pop and K21=Q/V2_pop
- V1_pop = 1240
- V2_pop = 1040

Subject 1: Standard, (cyp2d6_poor = False, cyp2d6_intermediate = False, weight = 70)
Subject 2: cyp2d6_poor = True, cyp2d6_intermediate = True, weight = 100

Results:

Table 62. Parameters calibration values for subject 1, pimozide.

Parameter	Calibrated	Expected	Calib Error
F	1.0	1.0	0.
Tlag	1.14	1.14	0.
Ka	0.68	0.68	0.
Q	69.2	69.2	0.
Cl	54.9	54.9	0.
V1	1240	1240.60	0.
V2	1040	1040	0.
Ke	0.044274193548387096	0.044274193548387096	0.
K12	0.05580645161290323	0.05580645161290323	0.
K21	0.06653846153846155	0.06653846153846155	0.

Table 63. Parameters calibration values for subject 2, pimozide.

Parameter	Calibrated	Expected	Calib Error
Q	69.2	69.2	0.
Cl	9.5858856504	9.5858856504	0.
V1	1771.4285714285716	1771.4285714285716	0.
V2	1485.7142857142858	1485.7142857142856	2.2737367544323206e-13
Ke	0.007730552943870967	0.007730552943870967	0.
K12	0.05580645161290323	0.05580645161290323	0.
K21	0.06653846153846155	0.06653846153846155	0.

Calibration matches expectations perfectly on these patients.

2.2.19.2 Maximum concentration verification

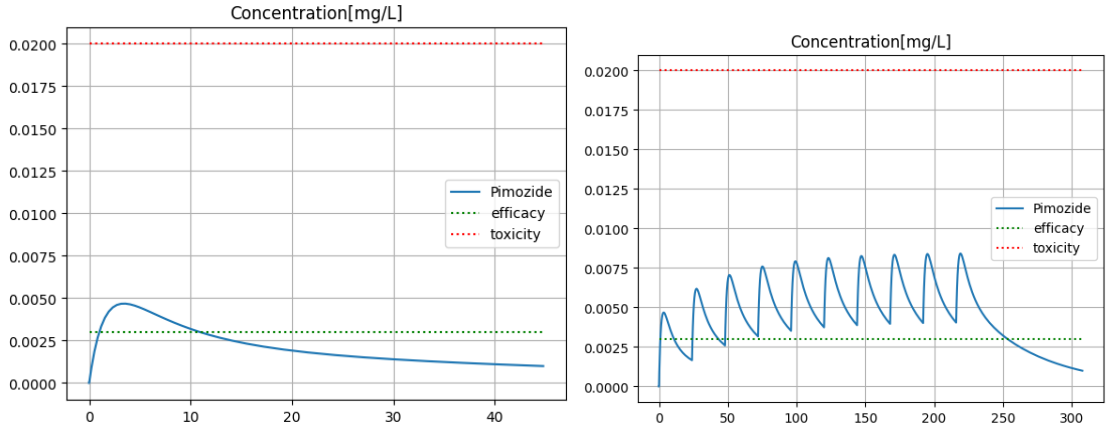

Figure 32. Numerical simulation with a patient with yp2d6_poor = False, cyp2d6_intermediate = False, weight = 70, Pimozide is administered orally in immediate release form every 24 hours with a dose of 8mg, for a period of 10 days (where steady state is practically obtained).

Results on maximal concentration are:

Table 64. Results of numerical vs theoretical max concentrations comparison test for Pimozide.

Value \ Scenario	Single dose	Repeated admin
Numerical max concentration	0.004681713859826777	0.008469479733903898
Theoretical max concentration	0.004684922922706496.004684922922706496	0.008470042097963223
Numerical Error	3e-06	5e-07

We see a match at the order of 1e-06 on the maximum concentration in the single dose scenario and 1e-07 in the repeated administration scenario.

2.2.20 Azimilide (new)

2.2.20.1 Parameters estimation verification

Covariates: weight, sex_m, smoker
Base parameters encoded in the model are:

- Bioavailability F = 1
- Absorption rate Ka = 0497
- Distribution volume V = 717+9.88*(weight-43)
- Clearance CL= .92*(weight-43)^0.208*(1+0.171*sex_m)*(1+0.155*smoker)
- Lag Tlag = 0.0
- Elimination rate Ke is Cl/V

Subject 1: Standard, (weight = 70, sex_m = True, smoker = False)
Subject 2: weight = 100, sex_m = False, smoker = True

Results:

Table 65. Parameters calibration values for subject 1, Azimilide.

Parameter	Calibrated	Expected	Calib Error
F	1.0	1.0	0.
Tlag	0.0	0.0	0.
Ka	0.497	0.497	0.
Cl (subject 1)	9.111012134175734	9.111012134175734	0.
V (subject 1)	983.76	983.76	0.
Ke (subject 1)	0.009261417555273373	0.009261417555273373	0.

Table 66. Parameters calibration values for subject 2, Azimilide.

Parameter	Calibrated	Expected	Calib Error
Cl (subject 2)	10.497600019706496	10.497600019706496	0.
V (subject 2)	1280.16	1280.16	0.
Ke (subject 2)	0.00820022498727229	0.00820022498727229	0.

Calibration matches expectations perfectly on these patients.

2.2.20.2 Maximum concentration verification

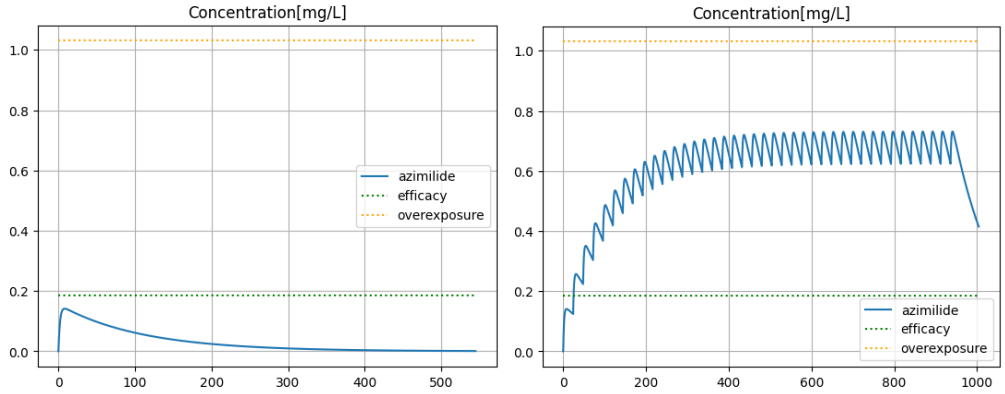

Figure 33. Numerical simulation with a patient with weight = 70, sex_m = True, smoker = False, Azimilide is administered orally in immediate release form every 24 hours with a dose of 150mg, for a period of 40 days (where steady state is practically obtained).

Results on maximal concentration are:

Table 67. Results of numerical vs theoretical max concentrations comparison test for Azimilide.

Value \ Scenario	Single dose	Repeated admin
Numerical max concentration	0.1413527658705101	0.7312231382741505
Theoretical max concentration	0.14137027860948836	0.7313798853329698
Numerical Error	1e-05	1e-04

We see a match at the order of 1e-05 on the maximum concentration in the single dose scenario and 1e-04 in the repeated administration scenario.

2.2.21 Dofetilide (new)

2.2.21.1 Parameters estimation verification

Covariates: weight, glomerular filtration rate (GFR), sex
Base parameters encoded in the model are:

- Bioavailability F = 0.9
- Distribution volume V = 210
- Lag Tlag = 0.0
- Elimination half-time T12 = 10
- Time of maximum concentration Tmax = 2.5

Calibration step will infer Ke and Ka from numerical inversion of T12 and Tmax data. If we compute T12 and Tmax with calibrated parameters and compare with original values, we can measure the calibration error.

On subject 1, a standard patient (weight=70, GFR=90, sex=male), we have the values shown in Table 68.

Results:

Table 68. Parameters calibration values for subject 1, dofetilide.

Parameter	Calibrated	Expected	Calib Error
Ke	0.06931471805599454	/	/
Ka	1.2147786874767705	/	/
T12	3.7999999999999994	3.8	4e-16
Tmax	2.50000000000003	2.5	4e-14

For non-standard weight, GFR or sex, there is an additional calibration step. On subject 2, with weight = 140, GFR = 20 and sex=female, we have the values shown in Table 69.

Table 69. Parameters calibration values for subject 2, dofetilide.

Parameter	Calibrated	Expected	Calib Error
V (subject 2)	420.0	420.0	0.0
Ke (subject 2)	0.022257726131313795	0.022257726131313802	7e-18

Calibration matches expectations perfectly on these patients.

2.2.21.2 Maximum concentration verification

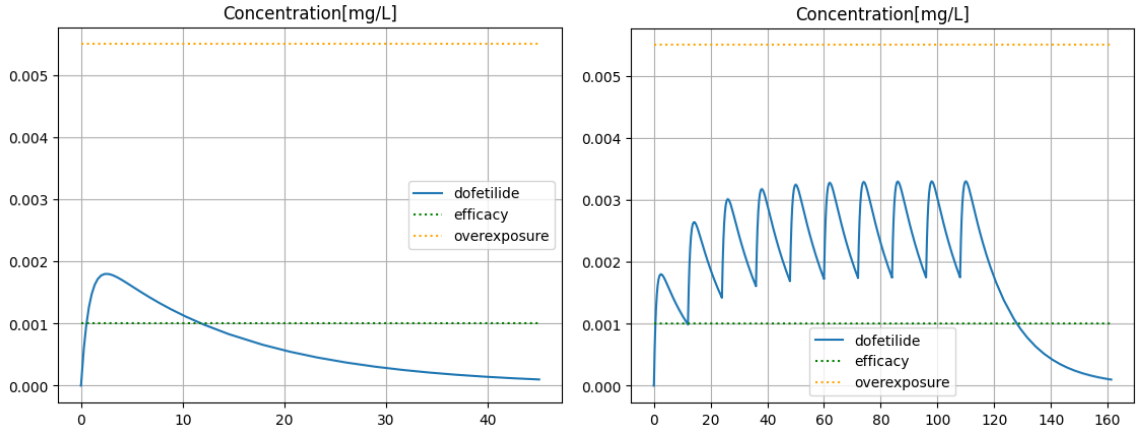

Figure 34. dofetilide is administered orally in immediate release form every 12 hours with a dose of 0.5mg, for a period of 5 days (where steady state is practically obtained).

Results on maximal concentration are shown in table 70:

Table 70. Results of numerical vs theoretical max concentrations comparison test for dofetilide.

Value \ Scenario	Single dose	Repeated admin
Numerical max concentration	0.0017993474498899193	0.0033021122506749425
Theoretical max concentration	0.0018019208898293845	0.0033030553342123636
Numerical Error	3e-06	1e-06

We see a match at the order of 3e-06 on the maximum concentration in the single dose scenario and 1e-06 in the repeated administration scenario.

2.2.22 Summary

Maximum calibration error on model parameters is at most 1e-13, which is materially negligible.

Concerning maximum concentrations, we have the values summarized in Table 71.

Table 71: Summary of maximum concentration numerical error for verified drugs.

Numerical Error on Cmax	Single dose	Repeated admin
Clozapine	1e-06	3e-06
Chlorpromazine	1e-06	4e-06
Escitalopram	9e-07	5e-06
Risperidone	8e-07	6e-06
Carvedilol	5e-06	6e-06
Clarithromycine	2e-04	1e-04

Numerical Error on Cmax	Single dose	Repeated admin
Disopyramide	5e-04 | 3e-03	5e-04 | 5e-05
Domperidone	3e-06 | 4e-06	9e-06 | 6e-06
Droperidol	1e-05	4e-08
Flecainide	2e-05 | 1e-04	3e-07 | 1e-03
Metronidazole	6e-04 | 2e-03	2e-05 | 1e-03
Mexiletine	3e-06	1e-04
Nicorandil	6e-07	1e-04
Ondansetron	1e-05	1e-05
Sotalol	3e-04	3e-05
Vandetanib	2e-06	1e-03
Cisapride	8e-07	3e-06
Quinidine	7e-04	6e-04
Pimozide	3e-06	5e-07
Azimilide	1e-05	1e-04
Dofetilide	3e-06	1e-06

On these molecules, no instability was observed and the numerical error on the quantity of interest is most of the time between 1e-03 and 1e-06. Numerical simulation of these models is accurate and robust with default error tolerances. In all cases, this numerical error is way smaller than the therapeutic range (toxicity or overexposure threshold minus the efficacy threshold). Hence, the simulation is suitable to solve drug concentration time courses and answer the Question of Interest.

2.3 Use Error

Use-Error in the PK part is managed at different levels to make sure meaningful drug concentration figures are obtained:

- Input control at the public interface simulation.
- Input control at the ExaTwin simulation request level.
- Peer-review of the Model file level and consistency checks in ExaTwin of the encoding.
- Finally, the verification itself has been reviewed guaranteeing results and conclusions.

3 Conclusion

This technical annex expands on Annex A6.1-UC3-PK which was initially included in the SimCardioTest deliverable D6.1, and reports technical details relative to the verification of the PK numerical model developed for Use Case 3 including activities performed after M30 till the end of the UC3 PK verification work. General conclusions relative to the verification of UC3 numerical model are reported in Annex A of the SimCardioTest Final Report.

4 Bibliography

[1] “SciPy Org.,” [Online]. Available: https://scipy.org/about/.

This project received funding from the European Union’s Horizon 2020 research and innovation program under grant agreement No 101016496